

# **Modeling orbital induced variations in circum-Mediterranean climate**

Modelleren van astronomisch gestuurde klimaatvariati es rondom de  
Middellandse Zee

(met een samenvatting in het Nederlands)

## **PROEFSCHRIFT**

ter verkrijging van de graad van doctor aan de Universiteit Utrecht  
op gezag van de Rector Magnificus Prof. dr. W.H. Gispen  
ingevolge het besluit van het College voor Promoties  
in het openbaar te verdedigen op  
27 september 2004 des middags te 12.45 uur

door

**Erik Tuenter**

geboren op 21 februari 1975, te Doetinchem

promotor: Prof. Dr. J.E. Meulenkamp  
Faculteit Geowetenschappen, Universiteit Utrecht  
co-promotoren: Dr. S.L. Weber  
Koninklijk Nederlands Meteorologisch Instituut (KNMI), De Bilt  
Dr. F.J. Hilgen  
Faculteit Geowetenschappen, Universiteit Utrecht

The investigations were supported by the Netherlands Council for Earth and Life Sciences (ALW) with financial aid from the Netherlands Organisation for Scientific Research (NWO). This study was part of the PIONEER project 'Late Neogene climate variability in annual to Milankovitch frequency bands. An integrated Mediterranean approach', grant awarded to Dr. F.J. Hilgen. This study was done at the Royal Dutch Meteorological Institute (KNMI) in De Bilt, the Netherlands.

# Contents

<b>1</b>	<b>Introduction and summary</b>	<b>1</b>
1.1	History of the astronomical theory of paleoclimates . . . . .	2
1.2	Orbital parameters . . . . .	4
1.2.1	Obliquity . . . . .	5
1.2.2	Eccentricity . . . . .	5
1.2.3	Precession . . . . .	6
1.2.4	Computation of the orbital parameters . . . . .	7
1.3	Insolation . . . . .	8
1.4	Geological records . . . . .	13
1.4.1	Mediterranean sapropels . . . . .	13
1.4.2	Greek pollen . . . . .	16
1.4.3	Atlantic foraminifera . . . . .	17
1.5	Paleoclimate modeling . . . . .	17
1.5.1	Experimental set-up . . . . .	17
1.5.2	Models . . . . .	19
1.5.3	Related studies in the literature . . . . .	21
1.6	Summary of the thesis . . . . .	22
<b>2</b>	<b>The response of the African summer monsoon to remote and local forcing due to precession and obliquity</b>	<b>25</b>
2.1	Introduction . . . . .	26
2.2	The model and experimental set-up . . . . .	27
2.3	Global results . . . . .	29
2.4	African summer monsoon . . . . .	34
2.5	Local and remote forcing . . . . .	39
2.6	Conclusions and discussion . . . . .	42
<b>3</b>	<b>Simulation of climate phase lags in the response to precession and obliquity forcing and the role of vegetation</b>	<b>45</b>
3.1	Introduction . . . . .	46
3.2	The model and experimental set-up . . . . .	47
3.3	Insolation . . . . .	50
3.4	Low latitudes . . . . .	52

3.5	High latitudes . . . . .	58
3.6	Conclusions and discussion . . . . .	64
<b>4</b>	<b>The influence of precession and obliquity on the Atlantic/European winter climate</b>	<b>67</b>
4.1	Introduction . . . . .	68
4.2	Model and experimental set-up . . . . .	69
4.3	The mean climatic response . . . . .	70
4.4	Changes in climatic variability . . . . .	74
4.5	Summary and conclusions . . . . .	81
<b>5</b>	<b>Coupling between orbital precession and long-term dynamics in the North Atlantic/European region</b>	<b>83</b>
5.1	Introduction . . . . .	84
5.2	Ptolemais sedimentary cycles . . . . .	85
5.3	Palynological analysis . . . . .	87
5.4	Results and discussion . . . . .	87
5.5	Concluding remarks . . . . .	92
<b>6</b>	<b>The effect of precession-induced changes in the Mediterranean freshwater budget on circulation at shallow and intermediate depth</b>	<b>93</b>
6.1	Introduction . . . . .	94
6.2	Model description . . . . .	94
6.3	Precession-induced changes in the Mediterranean freshwater budget . . . . .	96
6.4	Results . . . . .	100
6.4.1	Control experiment . . . . .	100
6.4.2	The role of runoff; Constant discharge . . . . .	101
6.4.3	The role of (P-E) over the basin . . . . .	105
6.4.4	The role of runoff; Monthly-varying discharge . . . . .	108
6.4.5	Combined precession minimum experiment . . . . .	109
6.5	Discussion . . . . .	112
6.6	Conclusions . . . . .	113
<b>7</b>	<b>Outlook and perspectives</b>	<b>115</b>
	<b>Bibliography</b>	<b>117</b>
	<b>Samenvatting</b>	<b>135</b>
	<b>Dankwoord</b>	<b>143</b>
	<b>Curriculum Vitae</b>	<b>145</b>
	<b>Publications</b>	<b>147</b>



# Chapter 1

## Introduction and summary

The climate of the Earth varies over a broad range of time-scales, from a few seconds associated with turbulence to some billions of years caused by tectonic changes. Apart from this irregular variability (quasi)periodic signals can be found in the climate system. They are mostly astronomically dictated and some are strictly periodic, e.g., the diurnal rotation and the annual revolution of the Earth. Other (quasi)periodic astronomical induced variations are related to changes in the orbital parameters: precession (date of perihelion), obliquity (tilt of the Earth's rotational axis) and eccentricity of the Earth's orbit. They describe the shape of the orbit of the Earth around the Sun and the orientation of the rotation axis of the Earth with respect to its orbital plane. Changes in the orbital parameters strongly affect the strength and the spatial and seasonal pattern of the insolation received by the Earth eventually resulting in climatic oscillations. The expression of these orbitally induced climate oscillations is found in sedimentary archives of widely different age and environment all over the world. One example are sapropels (organic-rich black layers) which are ubiquitously present in the deeper parts of the Mediterranean Sea (MS) throughout at least the last 13 million years (Ma). The proxy data related to sapropels clearly point to a precession dominated oscillation in the climate system. The paleoclimatic origin of sapropels is not fully understood. One hypothesis is that sapropels are controlled by the discharge of the river Nile which is determined by the strength of the African monsoon. When the discharge (of fresh water) is high, the salinity of the surface water will decrease resulting in a weaker thermohaline circulation in the MS. This reduces the refreshing of the deep water resulting in oxygen depletion at the bottom which could cause deposition of sapropels.

Despite their ubiquitous presence and numerous studies the paleoclimatic origin of sapropels is not fully understood. A lot of uncertainties exist of which some are addressed in this thesis by modelling studies:

1. Lourens et al. (1996, 2001) found a distinct obliquity component in the sapropel record, despite the weak obliquity induced insolation signal at low latitudes. If the hypothesis is right, i.e., the deposition of sapropels is controlled by the strength

of the boreal summer monsoon, clearly an obliquity signal should be present in the African monsoon. Therefore the first question is: **What is the orbital signal in the African monsoon? In more detail: Is there an obliquity signal in the African monsoon and, if so, what are the mechanisms?**

2. Lourens et al. (1996) determined by radiocarbon dating a lag of several thousands of years for the youngest Holocene sapropel with respect to the precession parameter. It is unclear whether this sapropel is an exception or that all sapropels are deposited with a lag with respect to the precession parameter. This results in the second question: **What is the transient response of the climate system to the orbital forcing? In more detail: Are there any phase differences between the orbital forcing and the climate response?**

3. The MS does not only receive fresh water from the south (i.e., the river Nile) but also from the northern borderlands. This could also play an important role in the deposition of sapropels. Therefore the third question is: **What is the orbital signal in the Atlantic/European climate?**

4. When the orbital signals in the runoff that enters the MS are known, it is still uncertain how the thermohaline circulation in the MS will respond. Therefore the fourth question which will be addressed is: **How do the orbital induced variations in the hydrological cycle (runoff, precipitation and evaporation) influence the thermohaline circulation of the Mediterranean Sea?**

The first three questions will be studied by global climate models. They are used for simulating the orbital signals in the circum-Mediterranean climate. Because the resolution of global models is too coarse for simulating the circulation in the MS, a high resolution regional model of the MS is used for question 4.

First a general introduction to the orbital theory is given in the first part of this chapter. A short summary of the history of the astronomical theory of paleoclimates will be given in section 1.1. In section 1.2 the orbital parameters will be described and in section 1.3 the effects of the changing orbital parameters on the insolation will be discussed. The second part of this chapter gives some background knowledge for this thesis. In section 1.4 the orbital signature in the geological records will be discussed in more detail. This is followed by a survey of the climate models and experimental set-up used in this thesis in section 1.5. Finally, a summary of each chapter of this thesis will be given in section 1.6.

## 1.1 History of the astronomical theory of paleoclimates

In this section a condensed history of the astronomical theory until about 1980 is presented. It is largely based on Paillard (2001). A more extensive description of the history of the astronomical theory can be found in Imbrie and Imbrie (1979), Imbrie

(1982) and Berger (1988).

In the beginning of the nineteenth century Agassiz (1838) was the first to rigorously promote the idea of an ice age, although several others had suggested major glacial cycles before. He stated that the erratic boulders, moraines and deeply scratched bedrocks that could be found in many places in the Alps, Scotland and North America had been caused by glaciation. Already soon afterwards, Adhémar (1842) suggested that the orbital variations of the Earth affect climate and cause these glacial cycles. His ideas were based on the known precession of the equinoxes and he suggested that the lengths of the seasons is responsible for the glaciations. When boreal winters last longer a glaciation would occur. This implied that the Northern Hemisphere (NH) would be glaciated about every 23,000 years (23 ka) and the Southern Hemisphere (SH) would be glaciated during the opposite phase of the precession cycle. He supported his ideas with the present Antarctic ice sheet on the SH and the fact that the NH is essentially not glaciated. Adhémar was the first to suggest a cyclicity in the occurrence of ice ages induced by astronomical forcing. This idea was elaborated by Croll (1875) who proposed that precession would be very important because of its influence on the seasonal insolation, with the winter insolation being critical for glaciation. Low NH winter insolation would result in larger areas covered with snow which would turn into ice sheets because of the positive albedo feedback. Furthermore, he was aware of the role of eccentricity through its modulation of precession and he also hypothesized that obliquity could play a role in the theory of the ice ages. Finally, Croll realised that the astronomical forcing is relatively small, and he tried to find some amplifying mechanisms, especially in the ocean.

After Croll there was not much interest in the glacial cycles for several decades. Renewed interest in the ice ages was caused by detailed studies of glacial deposits showing that multiple glaciations had occurred. In 1924, an alternative theory of the ice ages was formulated by Köppen and Wegener with the help of Milankovitch [95]. In contrast to Croll, they stated that low summer insolation at high northern latitudes would initiate an ice age because winter snow will survive eventually leading to the build up of an ice sheet. In 1941 Milutin Milankovitch was the first to be able to compute the radiation at the top of the atmosphere for different latitudes, taking into account the precession, eccentricity and obliquity of the Earth [132]. According to Milankovitch the cyclicity of the climate should have periods of 23 ka because of precession and 41 ka because of obliquity changes. He also stated that the summer insolation at 65°N is very critical for the forming of ice ages.

In marine sediment cores, cyclicity was first demonstrated by Emiliani (1955) in the isotopic composition of fossil shells of foraminifera. Emiliani interpreted the isotopic changes as changes in temperature. However, Shackleton (1967) and Duplessy et al. (1970) proposed that Emiliani's signal was in addition caused by ice volume changes which was confirmed by Imbrie and Kipp (1971). In the early sixties and seventies dating methods based on magnetostratigraphy and the radio-isotopes of uranium, thorium and potassium were developed. These methods made it possible to demonstrate a clear cyclicity of 100 ka in several records throughout the world [66, 23, 100]. This 100 ka cycle was in contrast with the theory of Milankovitch which predicted 23 ka and in particular 41 ka cycles. However, a careful spectral analysis

of marine records in a paper of Hays et al. (1976) revealed, besides the 100 ka cycle, also 41, 23 and 19 ka cycles. This confirmed the theory of Milankovitch. The 23 and 19 ka cycles can be explained by the splitting of the precession cycle into 23 ka and 19 ka cycles, as described in Vernekar (1972) and Berger (1977, 1978). After the landmark paper of Hays et al. (1976) numerous papers were published dealing with orbital frequencies recorded in geological records all over the world.

Not only the deep sea record became important in the seventies, also mathematical models were developed as a tool to understand climatic variations. The first models were mainly dealing with the explanation of the response of the global ice volume to insolation. In a pioneering study of this kind, Calder (1974) simply stated that below a given level of insolation the ice sheets are growing, while above this level they are shrinking. It turned out that the output is very sensible to the used parameters but for one choice of parameters the model predicts all the major terminations for the last 0.8 Ma. Weertman (1976) also modeled the fluctuations of a continental ice sheet but he used a more complex model than Calder (1974). It turned out that the model of Weertman (1976) was able to simulate the magnitude of the known fluctuations in ice sheet dimensions for the past 2 Ma. Again the output was very sensitive to the model parameters. A considerable advance in modelling complexity was made by Pollard (1978), who coupled Weertman's ice sheet model to an energy balance model of the atmosphere. Pollard's model was the first model that had two polar ice caps. The results for the ice volume for the last 150,000 years (150 ka) were reasonable, but the results prior to 150 ka before present (BP) were not very well. A more robust model was described by Imbrie and Imbrie (1980), containing a relaxation of the ice volume to the forcing. In the model the time constant for melting needed to be larger than that for accumulation to get proper results. This is contradictory to the characterisation of glacial cycles by slow accumulation and rapid melting of the ice sheets. Nevertheless, the results show a fairly good agreement with the data for the last glacial cycle but a poor agreement for earlier cycles.

From 1980 onward the increasing computer power made it possible to build more complex high-resolution models including more climate components (i.e., hydrosphere, cryosphere, biosphere, atmosphere). From the early 80's, the focus is not only on the simulation of the magnitude of ice sheets, but also on other parts of the climate system such as the ocean circulation and monsoons.

## 1.2 Orbital parameters

The parameters of the Earth's orbit are obliquity, precession and eccentricity. They describe the shape of the Earth's orbit around the Sun and the orientation of the Earth's rotational axis. Due to gravitational forces between the Earth and the Moon and between the Earth and the other planets the orbital parameters are not constant but oscillate very slowly. In this section first the orbital parameters and their oscillations will be described and after that the different methods for computing the parameters will be shortly discussed.

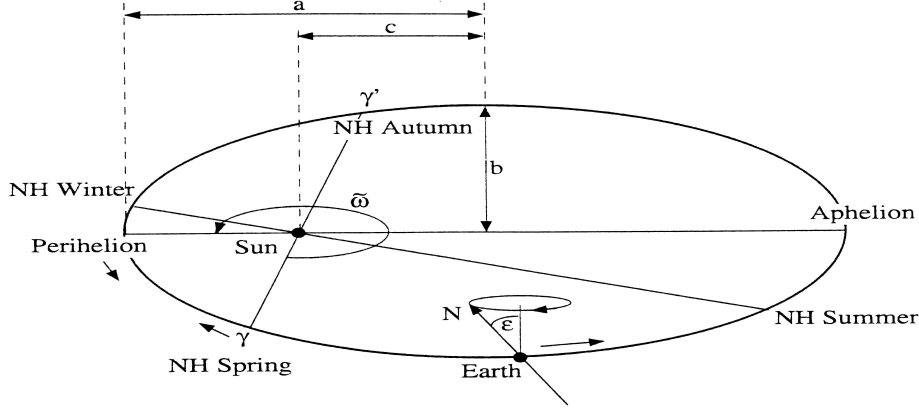


Figure 1.1: *The orbital parameters of the Earth.  $b$  is the semiminor axis. Winter and summer solstice occurs at the locations denoted by NH winter and NH summer, respectively.  $\gamma$  and  $\gamma'$  are the vernal and autumnal equinoxes, respectively. In the present day configuration the Earth is in perihelion around 3 January. This position, relative to the vernal equinox  $\gamma$ , is measured by the  $\tilde{\omega}$  angle. From Paillard (2001).*

### 1.2.1 Obliquity

The tilt, or obliquity ( $\varepsilon$ ), of the Earth is defined as the angle between the Earth's rotational axis and the normal of the orbital plane (Fig. 1.1). In other words,  $\varepsilon$  is the angle between the Earth's equatorial plane and its orbital plane. Because  $\varepsilon$  is not equal to zero, seasons exist on Earth. Furthermore, obliquity defines the locations of the polar circles and the tropics of Capricorn and Cancer. Because the Earth is not exactly a sphere, the Sun and the Moon exert a torque on its equatorial bulge resulting in a change of the obliquity. The current value is 23.45 degrees but during the last 1 Ma it varied from about 22 to 24.5 degrees (Fig. 1.2). The component with by far the largest amplitude has a period of 41 ka [13]. This period is stable for at least the last 1.5 Ma [12]. Over long time-scales it shortens going back in time due to the shortening of the Earth-Moon distance, i.e. from 41 ka (present day) to 29 ka at 500 Ma BP [11].

### 1.2.2 Eccentricity

The Earth's orbit around the Sun is an ellipse. The Sun is roughly located in one of its two foci. The eccentricity ( $e$ ) of the Earth's orbit is defined as  $e = c/a$  where  $a$  is the ellipse semi-major axis which measures the size of the ellipse and  $c$  is the distance from focus to center (Fig. 1.1). The current eccentricity is 0.017 but in the past 1 Ma the eccentricity varied from about 0.06 to almost 0, i.e., a circular orbit (Fig. 1.2). The most important period in the series expansion for eccentricity is 413 ka [13] while

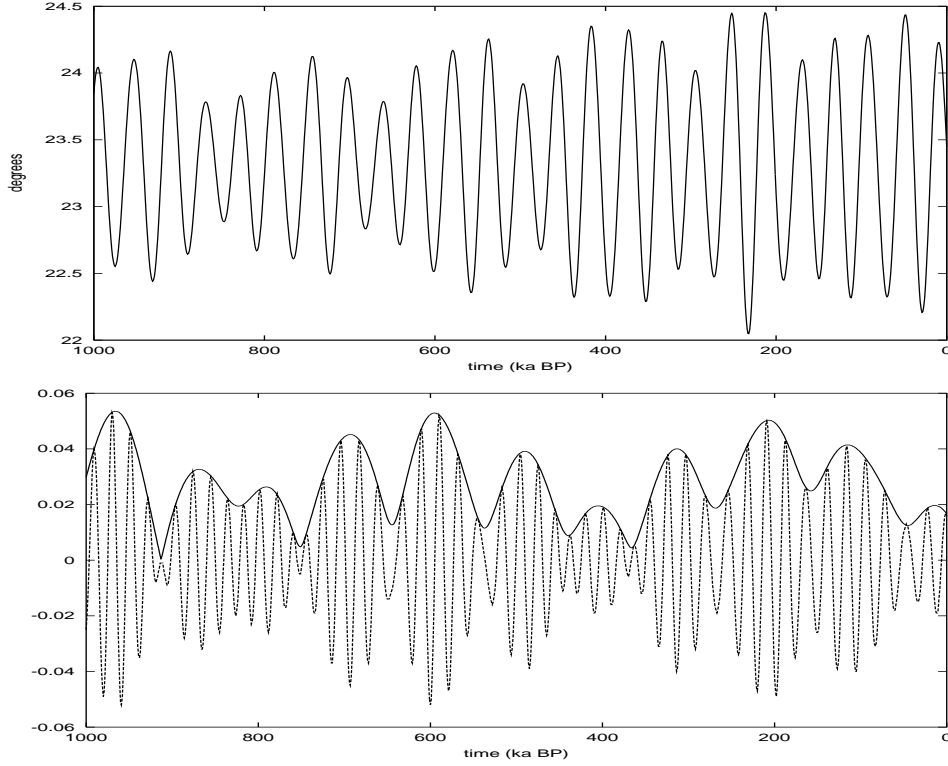


Figure 1.2: *Orbital parameters for the last 1 million years. Upper panel: obliquity (in degrees). Lower panel: eccentricity (solid line) and the precession parameter,  $e \sin(\pi + \tilde{\omega})$ , (dashed line), where  $\tilde{\omega}$  is the angle between the vernal equinox and perihelion, measured counter clockwise. The values are computed according to Berger (1978).*

the next four periods range from 95 to 131 ka which contribute to a peak which is often referred to as the 100 ka eccentricity cycle. The sixth period is 2.3 Ma which has been observed in very long geological records.

### 1.2.3 Precession

The locations along the Earth's orbit where the Sun is perpendicular to the equator at noon are called equinoxes ( $\gamma$  and  $\gamma'$  in Fig. 1.1). Then the night lasts as long as the day at all latitudes. This occurs around 21 March (vernal equinox, NH spring, Fig. 1.1) and around 21 September (autumnal equinox, NH autumn). The summer (winter) solstice is defined as the location of the Earth where the Sun is perpendicular to the tropics of Capricorn,  $23.45^\circ\text{N}$  (Cancer,  $23.45^\circ\text{S}$ ) which occurs around 21 June (21 December). In Fig. 1.1 'NH Winter' and 'NH Summer' indicate the present locations of the winter and summer solstice, respectively.

The Earth's rotational axis rotates (or precesses) around the normal to the orbital plane like a spinning top (Fig. 1.1). This rotation causes a clockwise movement of the equinoxes (as well as the solstices) along the Earth's orbit and this is called precession of the equinoxes. The quasi period of this precession of the equinoxes is 25.7 ka relative to the stars. However, for the climate, only the movement of  $\gamma$  relative to perihelion (the location of the Earth's orbit closest to the Sun) is important. This relative movement is called climatic precession and is measured by  $\tilde{\omega}$  which is the angle between vernal equinox and perihelion, measured counter clockwise (Fig. 1.1). Perihelion moves counter clockwise around the Sun with a period of about 75 ka. The combination of the perihelion movement and of the precession of the equinoxes results in a period of the climatic precession of about 20 ka.

In practice, it is usual to combine the climatic precession and eccentricity, because when eccentricity is zero, perihelion is undefined and there is no climatic effect associated with precessional changes. Therefore, in this thesis the precession parameter  $e \sin(\pi + \tilde{\omega})$  is used to compute (climatic) precession [13]. It is important to note that also the definition  $e \sin \tilde{\omega}$  is used. The latter definition only changes the sign of the precession parameter. Using the definition of Berger (1978) the precession parameter is at its minimum when summer solstice occurs at perihelion (then  $\tilde{\omega} = 90^\circ$  and  $e \sin(\pi + \tilde{\omega})$  is negative). In this thesis this configuration is called minimum precession due to the minimum value of the precession parameter. Maximum precession occurs when winter solstice is near perihelion, so that  $\tilde{\omega} = 270^\circ$  and  $e \sin(\pi + \tilde{\omega})$  is positive.

The two most important periods of the precession parameter are 23.7 and 22.4 ka while the following 3 periods are around 19 ka [13]. This results in the periods of 23 ka and 19 ka which are frequently found in geological records. These periods are about 1 ka smaller when eccentricity is at its minimum [12]. Just as for obliquity, the periods of precession shortens back in time due to shortening of the Earth-Moon distance (from 23 to 19 ka and 19 to 16 ka from present day to 500 Ma BP, Berger et al. (1992)).

### 1.2.4 Computation of the orbital parameters

The incoming insolation at a given point on Earth depends on 1) the position of the Earth in space and 2) the orientation of the Earth relative to the Sun. To calculate the position of the Earth is by far the most complex part of an astronomical solution, because the Earth's orbital motion is perturbed by all other planets of the Solar System. The first approximate solution of this problem was given by Le Verrier (1856) and it was this solution which was used by Milankovitch for his studies on the astronomical origin of the ice ages (Milankovitch, 1920,1940). A refined orbital solution was given by Bretagnon in 1974 which has been used as basis for the widely applied Ber78 [13] solution for the computation of the insolation, precession, obliquity and eccentricity parameters back to 1 Ma BP.

Laskar (1985) computed in an extensive way a new solution for the whole solar system. Subsequently, Laskar (1986, 1988) performed a numerical integration in combination with vast analytical computations to provide a much more accurate solution, La88, for the orbital evolution of the Solar System, which included also a full solution

of obliquity and precession. The precession and obliquity time series of La88 were not widely distributed, but the orbital part of La88 was used in Ber90 (Berger and Loutre, 1991) to derive another solution for precession and obliquity aimed at climate computations. In 1989, Laskar demonstrated that the behavior of the orbits of the planets are chaotic [114]. This implies that the calculations of the astronomical solution over several hundreds of millions of years are useless for especially paleoclimate studies (see also Laskar, 1999). The La88 solution was slightly improved by Laskar in 1990 [115]. A comparison between La90 and the direct numerical integration of the QTD91 solution [160] revealed, however, that the main obliquity and precession periods of the two solutions diverge with time over the past 3 Ma [117]. In the QTD91 solution, a term was introduced which describes the change in the speed of rotation of the Earth as result of tidal dissipation by the action of the Sun and Moon. If the same, present day, value is used the discrepancy with QTD91 is almost completely removed. The resulting La90 solution with tidal dissipation set to the present day value is now generally termed as the La93 solution. In this solution, also a second term can be modified. This term refers to the change in the dynamical ellipticity of the Earth, which may strongly depend on glacial-interglacial cyclicity and hence the buildup and retreat of large ice caps [153, 135, 134] and/or on long-term mantle convection processes [51]. Similar to the tidal dissipation term, a small change in the dynamical ellipticity of the Earth will change the main precession and obliquity frequencies.

The uncertain values of the tidal dissipation and dynamical ellipticity of the Earth are at present considered as the most limiting factors to obtain accurate solutions for the precession and obliquity time series of the Earth over a time span of millions of years. This is contrary to the solution for eccentricity which can be considered reliable over 10 to 20 Ma [117, 116]. At present, there exists only one possible way to test the extent of change of both parameters in the (geological) past. This test involves a statistical comparison between the obliquity-precession interference patterns of the insolation time series and those observed in geological records [121]. Lourens et al (2001) showed for instance by using an exceptional record of climate change from the eastern Mediterranean, that over the past 3 million years the decline in the speed of rotation was on average smaller than the average value obtained for the present day; this probably as result of the large ice caps that dominated Earth's climate from the Late Pliocene to the present day.

The La93 solution with present day values of tidal dissipation and dynamical ellipticity is used in chapter 5 of this thesis. This solution is used because it deals with records from the late Miocene - early Pliocene for which this solution is more accurate than the Ber78 solution. In the remainder of this thesis the Ber78 solution is used for the computation of the orbital parameters back to 1 Ma BP.

### 1.3 Insolation

When the orbital parameters are known, the insolation for any latitude and at any time of the year can be computed. The computation of the insolation described in



this section is mainly based on Berger et al. (1993) and Berger and Loutre (1994).

The total energy received by the Earth at the distance  $r$  from the Sun is equal to

$$W_E = S_a \left(\frac{a}{r}\right)^2 \pi R^2 \quad (1.1)$$

where  $S_a$  is the solar energy received by unit of time on a surface of unit area perpendicular to the Sun's rays and situated at the distance  $a$  from the Sun ( $a$  is the semi-major axis) and  $R$  is the radius of the Earth.

The insolation received by the Earth over one year is obtained by integrating equation 1.1 in time over a complete year of length  $T$ . This results in:

$$W_E^T = \frac{S_a}{\sqrt{1-e^2}} \pi R^2 T. \quad (1.2)$$

During the integration of equation 1.1 it was assumed that  $e$  is constant over one year which is reasonable since  $e$  varies between 0 and 0.07 in 100 ka [8]. The insolation received per unit of time and per unit of the Earth's surface (in J/sm<sup>2</sup> = W/m<sup>2</sup>) is obtained by dividing equation 1.2 by the Earth's surface times the length of the year ( $4\pi R^2 T$ ):

$$\overline{W}_E = \frac{S_a}{4\sqrt{1-e^2}} = \frac{S_0}{4} \quad (1.3)$$

$S_0$  is often defined as 'solar constant'. However, it is not a proper constant because it depends on the eccentricity. The current value of  $S_0$  is about 1360 W/m<sup>2</sup> [118]. Equation 1.3 shows that the global annual insolation is only a function of the solar activity through  $S_a$  and of the eccentricity through  $(1-e^2)^{-\frac{1}{2}}$ . When eccentricity increases, the global annual insolation also increases although the effect is very small, as shown in Fig. 1.3 (cf. Figs. 1.3 and 1.4).

The insolation at a given latitude and a given time received on a surface at a distance  $r$  from the Sun is given by:

$$W(\phi, \lambda, H) = S_a \left(\frac{a}{r}\right)^2 \cos z \quad (1.4)$$

where  $z$  is the solar zenith angle from the Sun:

$$\cos z = \sin \phi \sin \delta + \cos \phi \cos \delta \cos H \quad (1.5)$$

Here  $\phi$  is the latitude,  $H$  is the hour angle of the Sun which defines the time of the day and  $\delta$  is the declination of the Sun which is related to the true longitude of the Sun,  $\lambda$ , by:

$$\sin \delta = \sin \lambda \sin \varepsilon \quad (1.6)$$

Over one year,  $\lambda$  varies from 0 to 360° while  $\delta$  varies between  $-\varepsilon$  and  $+\varepsilon$ .

The Earth-Sun distance,  $r$ , is given by the ellipse equation:

$$r = \frac{a(1-e^2)}{1+e \cos \nu} \quad (1.7)$$

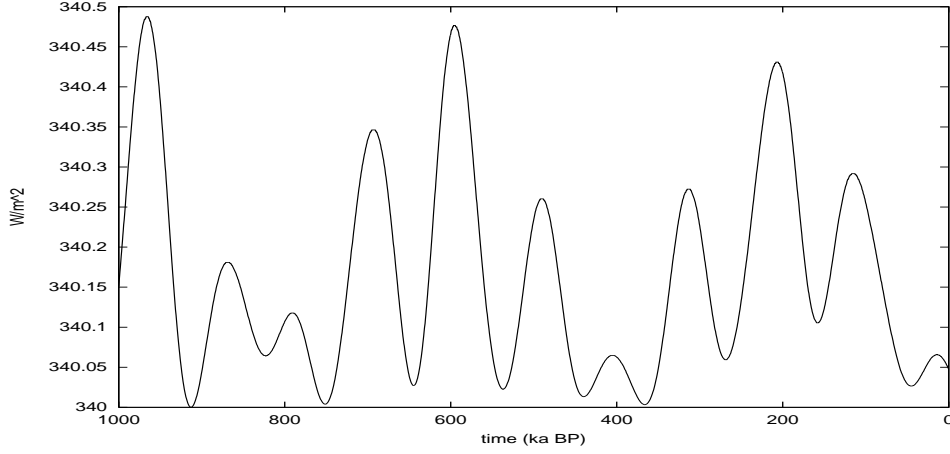


Figure 1.3: *Global annual incoming insolation at the top of the atmosphere for the last 1 Ma. The values are computed according to equation 1.3 with  $S_0 = 1360 \text{ W/m}^2$  and the eccentricity as shown in the lower panel of Fig. 1.2.*

with  $\nu$  being the true anomaly related to the true longitude of the Sun by:

$$\nu = \lambda - \tilde{\omega} \quad (1.8)$$

Combining equations 1.5-1.8 equation 1.4 can be rewritten as

$$W(\phi, \lambda, H) = S_a \frac{(1 + e \cos(\lambda - \tilde{\omega}))^2}{(1 - e^2)^2} (\sin \phi \sin \lambda \sin \varepsilon + \cos \phi \cos \delta \cos H) \quad (1.9)$$

Over one year,  $\varepsilon$ ,  $e$ , and  $\tilde{\omega}$  are assumed to be constant. Over a given day,  $\lambda$  and  $\delta$  are assumed to be constant while  $H$  varies from 0 at solar noon to 24h. The long-term behaviour of each factor in equation 1.9 is governed by a different orbital parameter: the obliquity  $\varepsilon$  drives  $\cos z$ , the precession  $\tilde{\omega}$  drives  $(1 + e \cos(\lambda - \tilde{\omega}))^2$  and the eccentricity  $e$  drives  $(1 - e^2)^{-2}$ . Note that the eccentricity appears as  $(1 - e^2)^{-2}$  while in the global annual insolation it appears as  $(1 - e^2)^{-\frac{1}{2}}$  (equation 1.3).

To illustrate the influence of precession on the insolation, the upper panel of Fig. 1.4 shows the monthly zonally averaged insolation difference between two precession extremes. Shown is the insolation during minimum precession minus the insolation during maximum precession. Obliquity is fixed to isolate the influence of precession. In NH summer the insolation is much higher during minimum precession because the NH summer is located in perihelion (nearest to the Sun, Fig. 1.1) while during maximum precession the NH summer is in aphelion (furthest away from the Sun). In NH winter the situation is reversed. Therefore, the seasonal contrast on the NH from maximum precession to minimum precession is enhanced (i.e., warmer summers and colder winter during minimum precession) while the seasonal contrast on the SH is reduced at the same time (colder summers and warmer winters during minimum precession).

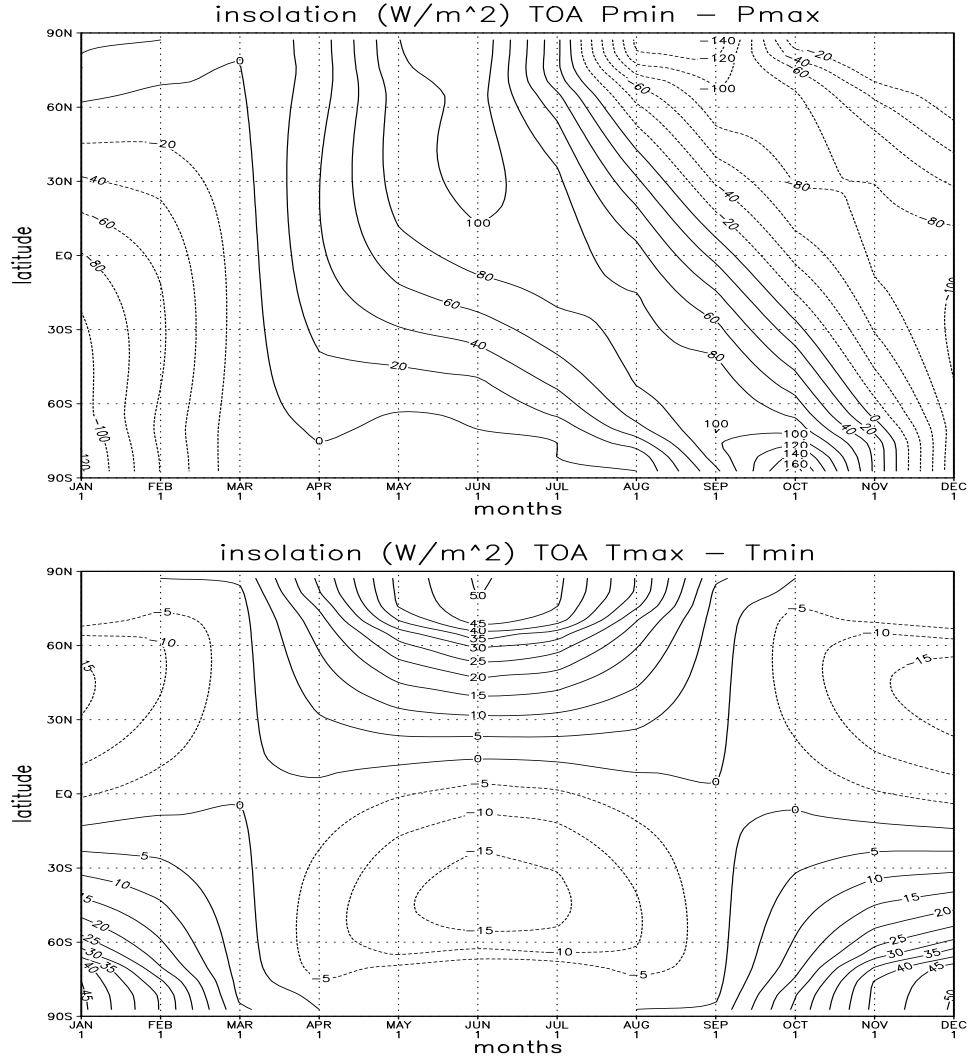


Figure 1.4: Monthly incoming insolation differences in  $W/m^2$  at the top of the atmosphere (TOA). Upper panel: minimum precession ( $\tilde{\omega} = 84^\circ$ ,  $e = 0.056$  and  $esin(\pi + \tilde{\omega}) = -0.055$ ) at 959 ka BP (Fig. 1.2) minus the insolation during maximum precession ( $\tilde{\omega} = 266.5^\circ$ ,  $e = 0.058$  and  $esin(\pi + \tilde{\omega}) = 0.058$ ) at 970 ka BP with fixed obliquity ( $22.08^\circ$ ). Contour interval is  $20 W/m^2$ . Lower panel: Maximum obliquity (or Tilt,  $\varepsilon = 24.45^\circ$ ) at 213 ka BP minus minimum obliquity ( $\varepsilon = 22.08^\circ$ ) at 232 ka BP with zero eccentricity. Contour interval is  $5 W/m^2$ .

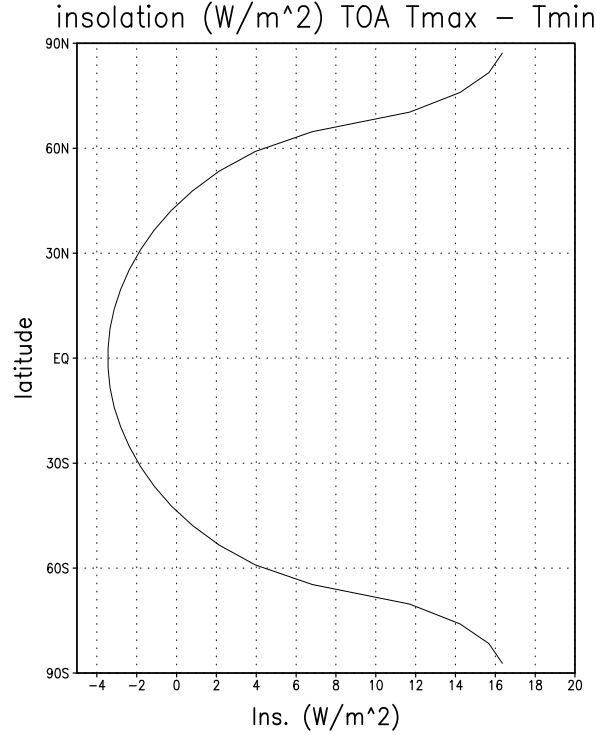


Figure 1.5: *Annual incoming insolation differences in  $W/m^2$  at the top of the atmosphere: Maximum obliquity minus minimum obliquity with zero eccentricity.*

The insolation during maximum obliquity minus the insolation during minimum obliquity is shown in Fig. 1.4. To exclude the influence of precession, the eccentricity is set to zero (i.e., a circular Earth orbit) resulting in  $e \sin(\pi + \tilde{\omega}) = 0$  for all  $\tilde{\omega}$ . When obliquity increases the tropics of Cancer and Capricorn move to the poles while the polar circles move equatorward. This results in stronger insolation on the NH and weaker insolation on the SH in NH summer during maximum obliquity. In NH winter the situation is reversed. Therefore, from low to high obliquity the seasonal contrast is enhanced on both Hemispheres and the insolation contrast between the Hemispheres is enhanced as well. In contrast to precession, obliquity influences the mean annual insolation at a certain latitude. When obliquity increases, the poles receive more energy in summer but stay in the polar night during winter. The annual mean insolation therefore increases symmetrically at the poles and consequently the annual insolation must decrease around the equator because the global annual insolation does not depend on obliquity (equation 1.3). In contrast to eccentricity changes, obliquity variations have a substantial effect of several  $W/m^2$  on the local annual insolation (cf. Figs. 1.3 and 1.5).

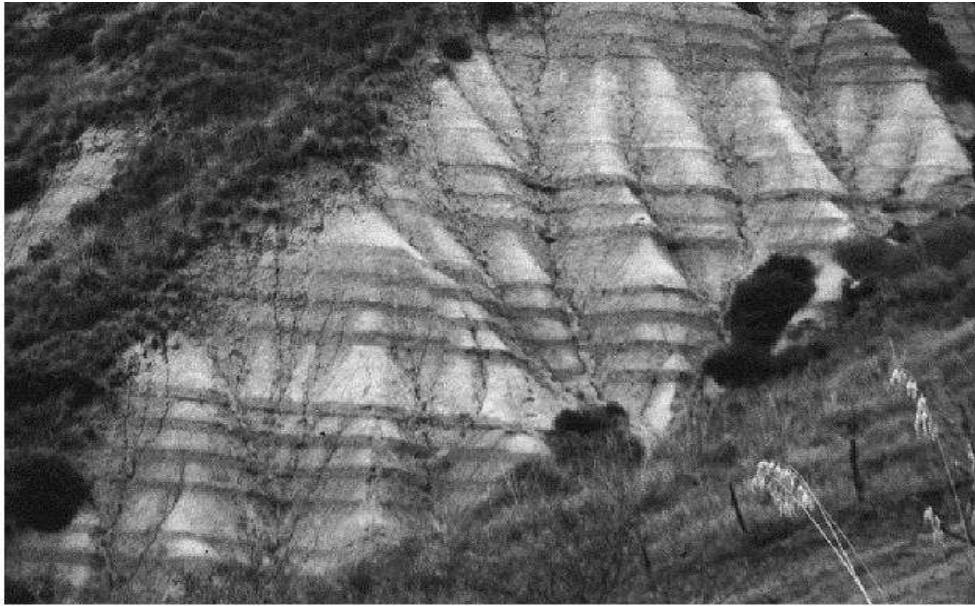


Figure 1.6: *Sapropels from the Miocene, Sicily.*

## 1.4 Geological records

In this section the most important geological records which are used for comparison with the model simulations are described. They are sapropels in the MS, foraminiferal estimates of Sea Surface Temperatures (SSTs) in the Atlantic Ocean and a pollen record from northern Greece.

### 1.4.1 Mediterranean sapropels

The first record consists of the well known record of successive sapropels in the eastern MS. Sapropels are organic-rich black layers which were deposited in the deeper parts of the MS and which are now sometimes exposed above sea level due to tectonic uplift (Fig. 1.6).

The sapropel record exhibits a robust precession (and eccentricity) signal (Fig. 1.7) which can be traced back to at least 13.5 Ma BP. This indicates that sapropels are not strongly influenced by the Quaternary ice ages. Individual sapropels correspond to strong NH summer insolation which occurs during minimum precession [165, 69] (Fig. 1.7).

An hypothesis for the mechanism of sapropel formation is the forming of oxygen-depleted deep water induced by weakening of the thermohaline circulation (Fig. 1.8). This weakening may be caused by stronger fresh water discharge from the river Nile

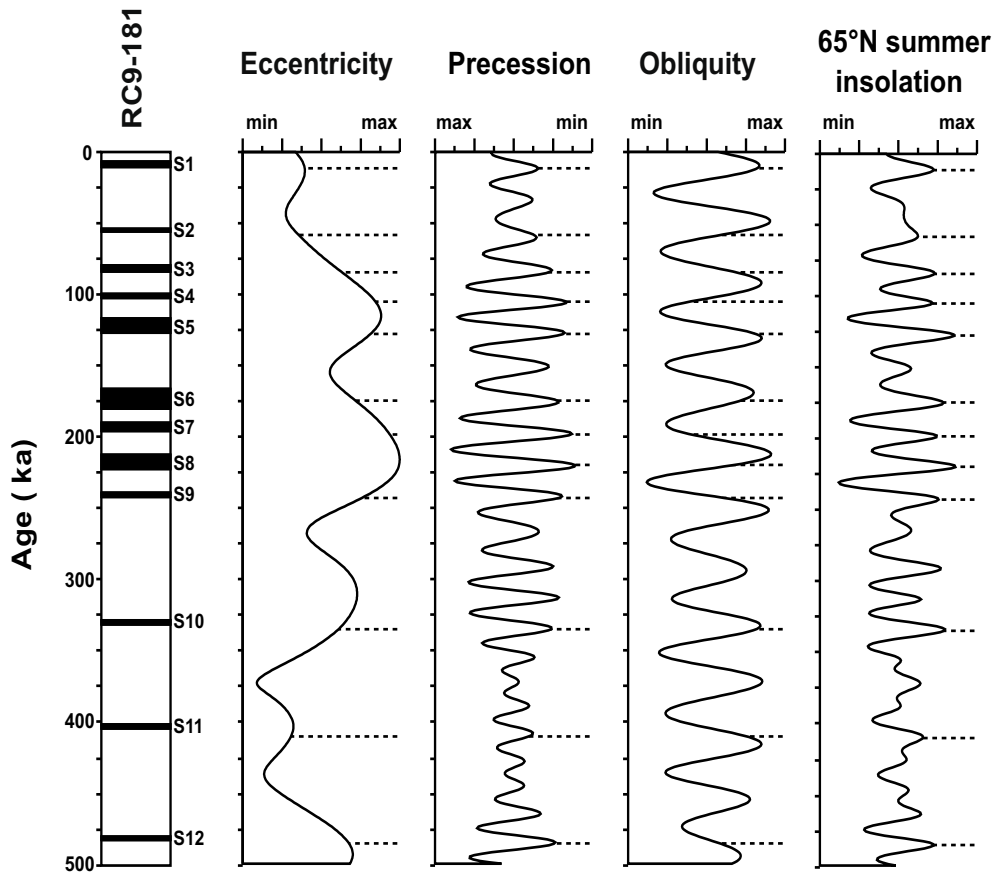


Figure 1.7: *Astronomical phase-relationships for the late Pleistocene sapropel record of a core from the Eastern MS (left panel) MS based on astronomical tuning to 65°N summer insolation maximum. Also shown are the eccentricity, precession parameter and the obliquity for the last 500 ka. The right picture shows the 21 May to 21 July insolation at 65°N. The orbital parameters are computed according to the solution of La93 solution.*

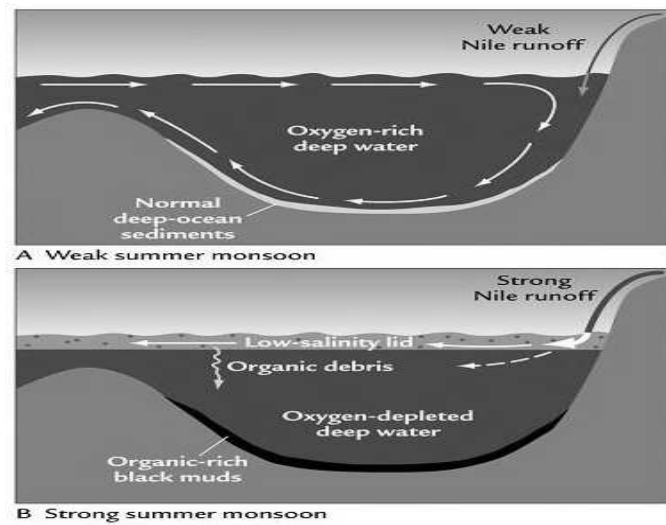


Figure 1.8: *Simplified Mediterranean circulation. A) Present day situation: Salty surface water chilled by cold air in winter sinks and carries dissolved oxygen to deeper layers. B) During minimum precession increased discharge from the river Nile could create a low-density surface-water lid that inhibited sinking of surface water and caused the deep ocean to lose its oxygen and deposit organic-rich black muds. From Ruddiman (2001).*

which reduces the surface water density thereby suppressing deep water formation. This process reduces or even eliminates the refreshing of deep waters, resulting in oxygen depletion at the bottom. Indeed, Rossignol-Strick (1983) showed that a sapropel is formed every time when the African summer monsoon is very strong. This intensification always occurs at times of strong NH summer insolation (i.e., during minimum precession). This strong insolation leads to an enhanced temperature contrast between land and ocean which leads, in turn, to a larger land-ocean pressure difference and thus to an intensified monsoonal flow. The high discharge of the river Nile associated with strong monsoons could result in the deposition of Mediterranean sapropels [166]. At the same time the marine productivity may have increased due to the enhanced nutrient input by the rivers. This contributes to the reduction of oxygen levels at the bottom as well.

Although they are ubiquitously present and show a distinct cyclicity, a lot of uncertainties about sapropels still exist. Some are addressed in this thesis:

1. Lourens et al. (1996, 2001) found alternating thick/thin sapropels in the MS reflecting a distinct influence of obliquity whereby thick/thin sapropels correspond to maximum/minimum obliquity (Fig. 1.7). Clearly, an obliquity signal should be present in the African monsoon if the sapropels are controlled by variations in the Nile discharge. This obliquity influence is in apparent contrast with the weak obliquity

signal in the insolation at low latitudes (Fig. 1.4). In chapter 2 the orbital signal in the African monsoon is studied.

2. Lourens et al. (1996) determined by radiocarbon dating a lag of several thousands of years for the youngest Holocene sapropel (S1, Fig. 1.7) with respect to the precession parameter. Because the other sapropels are too old for radiocarbon dating, it is uncertain whether this sapropel is an exception or whether all sapropels are deposited with a lag. In the latter case there should be a lag in the response of the circum Mediterranean climate with respect to the precession parameter. In chapter 3 the transient response of the climate system to the orbital forcing is studied to detect any leads or lags between the orbital forcing and the climate response.

3. The influence from the northern borderlands on the MS is unclear. The effects of increased rainfall in the northern borderlands (and over the MS) could also be important for sapropel formation [173, 37]. Although the runoff from the north might be smaller than from the river Nile, it enters the MS near or at the locations of deep water formation (the current deep water formation sites are the Gulf of Lyon, the Adriatic Sea and the Aegean Sea, see e.g., Josey (2003)). Furthermore, in contrast to the runoff from the river Nile, it mainly enters the MS in the cold season, i.e., the season when deep water is formed. Therefore, the runoff from the northern borderlands could be more effective in affecting the deep water formation than runoff from the south. However, the orbital influence (i.e. precession and obliquity) on the European/Mediterranean climate is not clear. In chapter 4 climate model results are presented with the aim to obtain a better understanding of the orbital influence on the European climate.

4. It is not clear how the thermohaline circulation in the MS will respond to changes in the precipitation over the MS basin and in the runoff (both from the north and south). Furthermore, as stated above, the response of the deep water formation to variations in the runoff from the north could be very different than to runoff from the south. In chapter 6, an ocean model of the MS is used to study the response of the thermohaline circulation to variations in the runoff and precipitation.

### 1.4.2 Greek pollen

In chapter 5 of this thesis a pollen record from northern Greece for the Late Miocene - early Pliocene is described. The results show a clear precession signal pointing to wetter conditions in southern Europe in NH winter during minimum precession compared to maximum precession. At present day the most important sources for NH winter precipitation in southern Europe are precipitation-laden cyclones forming over the MS and originating from the Atlantic Ocean. The latter are mainly controlled by the North Atlantic Oscillation (NAO). The NAO is associated with a large-scale net displacement of air between the Azores high (a high pressure system over the subtropical Atlantic Ocean) and the Icelandic low (a low pressure region near Iceland) [74]. An enhanced pressure gradient, or high NAO-index (i.e. stronger than normal Azores high and deeper than normal Icelandic low) leads to more northeast oriented transport of moist Atlantic air into Europe. This results in wetter conditions in northern Europe and drier conditions in the Mediterranean region [74, 75]. Con-



versely, a weak NAO-index causes a more southern trajectory of the cyclones, leading to wet conditions in the Mediterranean region. The cyclones forming over the MS occur mainly in NH autumn and are caused by the difference between the low surface air temperatures and the high Mediterranean SSTs leading to atmospheric convection and growth of cyclones (i.e. cyclogenesis). The model results of chapter 4 are used to propose possible mechanisms for the enhanced precipitation during minimum precession in southern Europe.

### 1.4.3 Atlantic foraminifera

During the analysis of the transient climate response to the orbital forcing described in chapter 3, it turned out that the thermohaline circulation in the Atlantic Ocean showed a distinct lag with respect to the precession parameter. To compare this with sedimentary data the results of Imbrie et al. (1992) are used. They showed from foraminiferal estimates that in the Quaternary the tropical Atlantic cold-season SSTs lag the precession parameter by about 3 ka, while at high latitudes Atlantic SSTs lag the precession parameter by about 6 ka. For obliquity the lag at low latitudes is quite ambiguous while at high latitudes it is about 10 ka.

In this thesis the behaviour of the Atlantic thermohaline circulation is also studied, although it does not directly affect the MS. However, the response of the thermohaline circulation in the Atlantic Ocean and in the MS to orbital forcing could be very similar. A similar mechanism that caused the Atlantic lag could also be responsible for the lag of the youngest Holocene sapropel found by Lourens et al. (1996).

## 1.5 Paleoclimate modeling

Climate models can be very useful to get a better understanding of past climates. Next to paleoclimatic data, model simulations can give insight in past climates and in mechanisms leading to climate changes.

In this section first the experimental set-ups used in this thesis are discussed. Then the models are described and finally some relevant literature will be discussed.

### 1.5.1 Experimental set-up

In general there are two kinds of paleoclimate simulations with models: 'snapshots' of specific times in the past and transient experiments. In addition, the simulations can be as realistic as possible or they can be idealised. Snapshot experiments are performed by specifying the insolation and boundary conditions like tracegas concentration, orography etc. for a specific time in the past. Realistic snapshot experiments use all prevailing radiation forcing terms and boundary conditions at that time. An advantage is that the results can be directly compared to paleoclimatic data. A disadvantage is the difficulty to determine the cause of any climate response. In an idealised snapshot experiment only one forcing term or boundary condition is changed

while the remaining forcing terms and boundary conditions are kept fixed (this kind of experiment is also called sensitivity experiment). In this way the climate response must be related to that particular forcing or boundary condition. However, it is not straightforward to compare the results of an idealised snapshot experiments to paleoclimatic data.

In transient experiments the forcing and/or boundary conditions change during the simulation. Again only one forcing or boundary condition can be changed (idealised) or everything can be changed together according to prevailing conditions (realistic). A transient experiment gives information about phase differences between the climate response and the forcing. However, most transient simulations to study the orbital influence on the climate are, in general, more time consuming than snapshots experiments. Therefore it is not possible to use a very complex model because the simulation time would be too long.

An objective of the studies described in this thesis is to investigate the separate influence of obliquity and precession on the climate system. In chapter 2 and 4 this is done by idealised snapshot experiments whereby either the precession parameter or obliquity was changed. For the precession signal, simulations with variable precession values are performed with fixed obliquity. In the same way, the obliquity signal is isolated by varying the obliquity while the precession parameter is fixed. In all simulations the boundary conditions (like vegetation, orography and the concentration of trace gases) are kept constant at present day values. In particular, the size and location of the present day ice sheets are kept constant throughout the simulations. The reason for this is that the formation of sapropels is fairly independent of (Quaternary) ice ages and the associated waxing and waning of ice sheets [121].

In chapter 3 the transient response of the climate system to orbital forcing is discussed. This is done by idealised transient experiments. As in chapter 2 and 4 either the obliquity or precession is changed but now the orbital parameter changes in time. In this way it is possible to study the phase difference between the climate response and the orbital forcing. Again fixed present day boundary conditions were used. In additional transient experiments, again either obliquity or precession was changed but now a vegetation model was included (the other boundary conditions were still kept fixed at present day values). This makes it possible to study the role of vegetation in the transient climate response to orbital forcing.

In chapter 6 the response of the MS to hydrological (i.e., precipitation, evaporation and runoff) changes are studied. The hydrological changes were obtained from snapshot simulations described in chapter 2. The response of the MS to these changes are studied by sensitivity experiments whereby one component of the hydrological cycle (for instance, the discharge of the river Nile) is changed while the other boundary conditions and the forcing are kept fixed.

When the precession parameter varies (like in the simulations described in chapters 2-4 of this thesis) the length of the seasons also varies. According to Kepler's law, the number of days between equinoxes and solstices is proportional to the area covered between the astronomical positions. In order to define a calendar for the simulations, a reference date must be arbitrarily chosen. In most model studies the date of the vernal equinox is used as a reference. However, because of the the different length of

the seasons, the insolation patterns in two different simulations are in phase around vernal equinox but they are not in phase around the solstices and the autumnal equinox. A way to overcome this is the use of angular definitions of months, i.e., the elliptical orbit is divided in 12 regular  $30^\circ$  increments, starting from the vernal equinox [87]. Insolation patterns are then automatically phased for any value of the precession parameter since equinoxes and solstices are  $90^\circ$  apart from each other. As a counterpart, the length of the angular months are not the same. However, Joussaume and Braconnot (1997) showed that the error in the insolation differences introduced by using angular months is much smaller than the error introduced by phase shifts.

In the simulations described in this thesis the definition of the calendar is similar to the definitions used in most studies, i.e. the vernal equinox is fixed at March 21 at noon and the months are defined following the present day calendar. Using a present day calendar introduces an error in the phase of the seasons. During minimum precession boreal summer (located at perihelion) is shorter than boreal summer during maximum precession (located at aphelion) because the orbital speed is larger at perihelion. In Joussaume and Braconnot (1997) it is shown that using a present day calendar and fixed vernal equinox introduces the largest error in the insolation at high latitudes in autumn. The autumnal averages of climatic parameters like temperature and precipitation are biased towards the NH winter season in the minimum precession run (when NH summer is short). Therefore, using a present day calendar might introduce errors, especially in chapter 4 of this thesis where the orbital influence on the European climate in NH autumn/winter is simulated. However, the objective of this thesis is to study the mechanisms of the orbital influence in (circum)Mediterranean climate rather than to study very realistic climates. The use of a present day calendar might give rise to errors in the amplitude of monthly climatic parameters but the mechanisms will not be affected. Furthermore, using a present day calendar makes it possible to compare the results obtained in this thesis to other model studies because nearly all studies use a present day calendar.

### 1.5.2 Models

A broad range of numerical climate models exist which differ both in complexity and configuration. Concerning complexity, three types of models are distinguished: Simple Energy Balance Models (EBMs), more complex Earth system Models of Intermediate Complexity (EMICs) and very complex General Circulation Models (GCMs). In general EBMs only simulate the temperature response to changes in the forcing. Sometimes EBMs are zero-dimensional and sometimes they have latitudinal and/or longitudinal dimension. In the latter case very basic parameterisations are used for heat transport by the atmospheric circulation. EBMs are very fast which makes them very suitable for long (paleo)climate runs [141, 175]. EMICs [33] are often more complete than EBMs, i.e., they contain more advanced parameterisations or they explicitly resolve the hydrological cycle and circulation. Due to the extended computations they are slower than EBMs. However, they are still relatively fast because of the coarse resolution and the simplified parameterisations which make them also suitable for long runs. Finally, GCMs have high resolution and they are

very complex, i.e., they explicitly resolve the circulation and hydrological cycle and they use sophisticated parameterisations of subgrid scale processes like radiation and cloud formation. This makes them suitable for detailed studies of the climate but they are too slow for very long runs.

Next to the complexity, the configuration of climate models also varies. The main parts of a climate model are the atmosphere and the ocean which are mostly coupled. Sometimes a model consists of only an atmosphere model (with a prescribed ocean) or only an ocean model (with a prescribed atmosphere). The ocean/atmosphere configuration can be extended by other climate components, like a sea ice model, an ice sheet model and/or a vegetation model.

In chapter 2 a global coupled 3-dimensional EMIC was used for sensitivity experiments to study the orbital signal in the monsoons. An EMIC instead of a GCM was used because a lot of experiments are performed. The atmospheric component is ECBilt [143] which is coupled to a flat-bottom ocean model with a thermodynamic sea ice model. Because ECBilt was developed for studying processes at mid- and high latitudes (e.g., Selten et al. (1999)) it is based on the quasi-geostrophic equations. However, ageostrophic components are included. Due to these ageostrophic components both the strength and the spatial pattern of the mean annual cycle of the African summer monsoon are simulated quite well compared to observations (i.e., NCEP/NCAR reanalysis [90]). Weber (2001) and Weber et al. (2004) compared the sensitivity of monsoonal precipitation in the model to insolation changes with other models [88, 17] and concluded that ECBilt is in the middle range for the African monsoon.

In chapter 3, the coupled model of intermediate complexity CLIMBER-2.3 (for CLIMate and BiosphERe, Petoukhov et al. (2000)) is used for the very long (130 ka) transient runs. CLIMBER consists of an atmosphere model, an ocean model with a thermodynamic sea ice model and a land/vegetation model. CLIMBER instead of ECBilt is used because it is much faster (with ECBilt it would take too much simulation time). This is mainly caused by its coarse resolution. CLIMBER does not resolve synoptic timescales and the vertical structure of temperature and humidity are prescribed. The ocean model [180] describes the zonally averaged temperature, salinity, and velocity for three separate basins (Atlantic, Indian and Pacific oceans) which are connected by the Southern Ocean. The terrestrial vegetation model which is also used in the experiments is VECODE (VEgetation COntinuous DEscription, Brovkin et al. (1997)) which computes the fraction of the potential vegetation (i.e., grass, trees and bare soil). It has been shown that CLIMBER-2.3 is successful in simulating both cold climates [55] and warm climates [54, 99].

For the snapshot experiments to study the orbital signal in the Atlantic/European sector described in chapter 4, again the (slightly improved) atmospheric model ECBilt is used but now it is coupled to the ocean/sea ice model CLIO [59]. CLIO is a primitive equation, 3-dimensional free-surface ocean GCM coupled to a thermodynamic sea ice model. The main reason for the use of the (slower) ECBilt-CLIO compared to CLIMBER used in chapter 3 is the fact that CLIMBER does not resolve synoptic timescales while this is the most important mechanism for precipitation in Europe. The reason for performing new simulations with ECBilt-CLIO instead of

using the results of ECBilt coupled to another ocean model as described in chapter 2 is that ECBilt-CLIO has a thermodynamic-dynamic sea ice model which give better results for sea ice and the thermohaline circulation in the Atlantic ocean is simulated better in ECBilt-CLIO. Both the Atlantic thermohaline circulation and sea ice can be very important for the climate in Europe.

The model used in chapter 6 is a regional model of the MS (i.e., the atmospheric forcing has to be prescribed). The reason for using this model is that the models used in chapter 2-4 have a too coarse resolution to resolve important processes in the MS. The model is a primitive equation model featuring a free surface. It has a horizontal resolution of  $1/4 \times 1/4$  degrees and comprises 19 horizontal levels the majority of which is concentrated in the upper few hundred meters in order to resolve the mixed layer and thermocline. The model includes a small segment of the Atlantic Ocean in order to simulate the exchange at the Strait of Gibraltar. In this "Atlantic box" temperature and salinity are relaxed to prescribed Atlantic values. When atmospheric forcing is prescribed, the model proves to be unable to simulate the complete thermohaline circulation, especially deep-water formation [127].

### 1.5.3 Related studies in the literature

In numerous model studies snapshot experiments for simulating the climate response to Milankovitch forcing have been performed. Certain times in the past are of most interest like the last interglacial (125 ka BP, e.g. Harrison et al., 1995, Kubatzki et al., 2000 and Loutre and Berger, 2003), the glacial inception (116 ka BP, e.g. Yoshimori et al., 2002, Vettoretti et al., 2003 and Meissner et al., 2003), the last glacial maximum (18 ka BP, e.g. Kitoh et al., 2001, Kagayama et al., 2001 and Shin et al., 2003), the early Holocene (Kutzbach and Gallimore, 1988 and Mitchell et al., 1988) and the mid-Holocene (6 ka BP, e.g. Hewitt and Mitchell, 1998 and Mikolajewicz et al., 2003). Long transient climate simulations are rare because of the high computational costs (e.g., Berger et al., 1998, Claussen et al., 2003, Jackson and Broccoli, 2003).

The studies mentioned above used a combined precession and obliquity signal. In this thesis these signals are separated because the main objective is to study the climate response to the separate signals. The method of separate obliquity and precession signals used in this thesis is not unique. Suarez and Held (1979), Short and Mengel (1986), Harvey (1989) and Short et al. (1991) used an EBM to investigate the obliquity and/or precession signal in the climate system. With a two-dimensional EBM Short et al. (1991) studied the obliquity and precession signal in the atmospheric surface temperature. Over mid-latitudinal land areas they found a linear temperature response to both obliquity and precession. At tropical latitudes the response was more complex. In chapter 2 the results of ECBilt are compared to the results of Short et al. (1991).

Using an AGCM (Atmospheric GCM), Oglesby and Park (1989) and Park and Oglesby (1990, 1991) studied the effects of obliquity and precession on the Mid-Cretaceous (100 Ma BP). Although the geography and topography were very different from the present day, the results show that some basic features are similar, in particular the simulation of an obliquity signal at low latitudes, as described in Chapter

2.

Prell and Kutzbach (1987) found with an AGCM in permanent July mode both an obliquity and a precession signal in the African monsoon. In addition to this study a more extensive set of orbital parameters was used and the seasonal cycle was taken into account in chapter 2. For high latitudes, Kutzbach et al. (1991) and Gallimore and Kutzbach (1995) performed simulations with an AGCM to investigate the sensitivity of snow and sea ice to orbitally-caused insolation changes. Gallimore and Kutzbach (1995) showed that in their model the influence of obliquity was much stronger than the influence of precession on NH sea ice. Their results are compared with the results of ECBilt-CLIO in chapter 4. Finally, Braconnot and Marti (2004) showed with a coupled ocean-atmosphere model that precession strongly influences the surface temperature and salinity of the Indian Ocean due to changes in the hydrological cycle over the basin (precipitation, evaporation and river runoff).

Transient simulations to investigate possible leads/lags between the climate response and the orbital forcing as described in chapter 3 are very rare due to the high computational costs. One exception is a study with an EBM of Short and Mengel (1986), who obtained a lag of 2-3 ka for the maximum summer temperature over the northern African continent with respect to the precession parameter. At high northern latitudes the lag over land was less than 1 ka. Crucifix and Loutre (2002) and Crucifix et al. (2002) performed transient simulations whereby they studied the relative importance of the separate obliquity and precession signal. However, focus was not on phase differences between the climate response and the orbital forcing.

## 1.6 Summary of the thesis

In the beginning of this chapter the central questions studied in this thesis are given. The first question is addressed in **chapter 2**. With the global climate model ECBilt several time-slice experiments are performed to study the isolated precession and obliquity signal in the African summer monsoon. The results show that both signals influence the monsoon and they consist of similar features: During minimum precession and maximum obliquity the precipitation intensifies and the precipitation maximum moves further to the north than during maximum precession and minimum obliquity, respectively. It turns out that the response of the African summer monsoon to orbital induced insolation forcing can be divided into a response to insolation forcing at high northern latitudes (i.e., remote influence) and a response to insolation forcing at low latitudes (i.e., local influence). The local influence consists of an increased temperature contrast between land and ocean and an associated enhanced low-level monsoonal flow during summers with high insolation. The remote influence consists of two mechanisms: 1. Increased summer insolation at high latitudes causes a deepening of the convergence zone over southern Asia resulting in stronger winds from the Atlantic Ocean into southern North Africa and 2. warmer air at high latitudes caused by the strong insolation is able to contain more water vapour. This moister air penetrates from high latitudes southward into the northern monsoon region and causes more precipitation. Both the obliquity and the precession signal contain the

remote influence. The local influence only applies to the precession signal because the obliquity signal barely effects the insolation at low latitudes. This chapter has been published in *Global and Planetary Change* [188].

The main objective of **chapter 3** is to examine leads and lags in the response of the climate system to separate obliquity and precession induced insolation changes (question 2). This is done by performing long (130 ka) transient simulations with a coupled model of intermediate complexity, CLIMBER-2. The focus is on internal feedbacks which may give rise to leads/lags in the climate system. The version used of CLIMBER-2 includes a vegetation model but no ice sheet model. The results show that leads and lags occur in the response of the African/Asian monsoon, temperatures at high northern latitudes and the Atlantic thermohaline circulation. For the monsoon the response shows leads in May and June and lags for August and September with respect to the precession parameter in the simulation with fixed vegetation. Including interactive vegetation results in a shortening of the leads and lags due to the albedo feedback. However, both for fixed and interactive vegetation the monthly phase differences cancel out resulting in no phase differences between the annual precipitation and the precession parameter. For obliquity no lags were found between the monthly or annual precipitation and the obliquity parameter. At high latitudes, the lags of the surface air temperatures (SAT) over land in late winter/early spring are about 1 ka and 5 ka compared to the precession parameter for fixed and interactive vegetation, respectively. The lag of the SSTs is about 10 ka (they are out of phase by 180 degrees) in both simulations. For obliquity both the SAT and the SSTs are out of phase by 180 degrees compared to the obliquity parameter for fixed and interactive vegetation (the lag being 20 ka). Finally, the precessional lag for high-latitude SAT in late winter/early spring induces an annual lag of several thousand years in the Atlantic thermohaline circulation by changing the strength of the convection which occurs in winter. For obliquity no lag is found for the annual Atlantic thermohaline circulation. The first conclusion of chapter 3 is that vegetation feedbacks can cause lags in the response of monthly climate parameters for precession. So, ice sheets are not necessary for the creation of lags. The second conclusion is that an annual lag is only possible when an internal process (like the Atlantic thermohaline circulation) acts as a filter for certain seasons. This chapter is under review for publication in *Climate Dynamics* [190].

Question 3 is studied in **chapter 4**. In this chapter the separate obliquity and precession signal in the Atlantic/European climate is studied with a global coupled climate model of intermediate complexity (ECBilt-CLIO). Focus is on changes in the climatic variability and the mean climate in the cold season. Changes in the climatic variability are most pronounced over the convection sites in the northern Atlantic Ocean, where the atmospheric flow triggers sudden expansions in sea-ice coverage over the northern convection site, lasting 10-50 yrs in the control run. This results in reduced convection and, with a lag of about 30 years, decreased Atlantic thermohaline circulation. During maximum precession and minimum obliquity stronger events of longer duration were found while during minimum precession and maximum obliquity no events were simulated. Summer insolation was found to determine the strength and duration of the events. The mean climatic state to orbital forcing shows an earlier

winter state during minimum precession compared to maximum precession, resulting in a NAO-like atmospheric circulation and enhanced precipitation in northern Europe in autumn. In southern Europe a different mechanism influences precipitation in autumn, namely the strong land-sea temperature contrast in the Mediterranean Sea region during minimum precession and maximum obliquity (compared to maximum precession and minimum obliquity, respectively), which results in enhanced precipitation. This chapter is in preparation for publication [189].

**Chapter 5** describes a late Miocene - early Pliocene pollen record from northern Greece. Late Miocene - early Pliocene vegetation in the Eastern Mediterranean primarily responds to strong fluctuations in growing-season soil moisture variability induced by precipitation availability in winter. The pollen record reveals a clear precession signal with stronger precipitation during minimum precession compared to maximum precession. Based on the results obtained in chapter 4, it is proposed that two mechanisms can cause the enhanced precipitation in southern Europe during minimum precession. The first mechanism involves enhanced cyclogenesis over the Mediterranean Sea during precession minima resulting from enhanced air-sea temperature contrast in autumn. The second mechanism is a eastward displacement of the Icelandic low and a weaker and westward displacement of the Azores high in late winter/early spring during minimum precession compared to maximum precession. This implies prevailing southern trajectories of winter cyclones, leading to increased rainfall in the Mediterranean borderlands. It is most likely that the first mechanism is much stronger than the second mechanism. This chapter has been submitted to *Global and Planetary Change* [93].

**Chapter 6** deals with question 4. In this chapter the consequences of the precession-induced changes in the hydrological cycle for the circulation of the Mediterranean Sea at shallow and intermediate depths are investigated. Changes in runoff, precipitation and evaporation, as found in chapter 2 of this thesis, are used to modify the forcing of a regional ocean model for the Mediterranean Sea. The adjustment of forcing is carried out parameter by parameter in order to perform a sensitivity analysis. It is shown that the precession-induced increase in net precipitation over the Mediterranean Sea itself is of equal or greater importance than the increase in runoff from the bordering continents. The direct influence of enhanced discharge from the Nile is restricted to the Levantine coast, away from the sites of deep-water formation. Increased winter runoff from the north, which enters the sea through the Rhône, Po, and also via the Black Sea, is shown to affect the sites of deep water formation more effectively. This chapter is in preparation for publication [127].

**Chapter 7** presents the main conclusions of this thesis and an outlook to further research.



## Chapter 2

# The response of the African summer monsoon to remote and local forcing due to precession and obliquity

### Abstract\*

In this chapter we examine the orbital signal in Earth's climate with a coupled model of intermediate complexity (ECBilt). The orbital influence on climate is studied by isolating the obliquity and precession signal in several time-slice experiments. Focus is on monsoonal systems with emphasis on the African summer monsoon. The model shows that both the precession and the obliquity signal in the African summer monsoon consists of an intensified precipitation maximum and further northward extension during minimum precession and maximum obliquity than during maximum precession and minimum obliquity. In contrast to obliquity, precession also influences the seasonal timing of the occurrence of the maximum precipitation. The response of the African monsoon to orbital induced insolation forcing can be divided into a response to insolation forcing at high northern latitudes and a response to insolation forcing at low latitudes, whereby the former dominates. The results also indicate that the amplitude of the precipitation response to obliquity depends on precession, while the precipitation response to precession is independent of obliquity. Our model experiments provides an explanation for the precession and obliquity signals in sedimentary records of the Mediterranean (e.g., Lourens et al. 1996; 2001), through monsoon-induced variations in Nile river outflow and northern Africa aridity.

---

\*This chapter has been published as: Tuenter, E., S.L. Weber, F.J. Hilgen and L.J. Lourens (2003). The response of the African summer monsoon to remote and local forcing due to precession and obliquity. *Global and Planetary Change*, 36: 219-235. [188]

## 2.1 Introduction

The deposition of successive sapropels (organic-rich black layers) in the eastern Mediterranean Sea has been related to astronomical forcing of the climate. Individual sapropels are correlated with strong Northern Hemisphere (NH) summer insolation which is associated with minimum peaks in the orbital precession index [165, 69]. The orbital precession index is defined as  $e \sin(\pi + \tilde{\omega})$  where  $e$  is the eccentricity of the Earth orbit and  $\tilde{\omega}$  is the longitude of the perihelion. Rossignol-Strick (1983) first showed that a sapropel is formed every time that the boreal summer insolation produces an African monsoon index above a certain threshold (i.e., a strong African monsoon). A higher insolation leads to an enhanced temperature contrast between land and ocean which leads, in its turn, to a larger land-ocean pressure difference and thus to an intensified low-level monsoonal flow. The heavy discharge of the river Nile which is associated with strong monsoons, could result in the forming of Mediterranean sapropels.

Tropical insolation is precession dominated. Besides the sapropels, this is also reflected in other paleoclimatic data showing strong precessional components in the boreal summer monsoons. Examples are records of abundance of planktic foraminifera from the Arabian Sea indicating coastal upwelling strength which is related to the strength of the southwest Indian monsoon surface wind fields [158], or the occurrence of eolian freshwater diatoms in equatorial Atlantic deep-sea sediments, indicating periods of aridity in tropical Africa [156].

However, Lourens et al. (1996; 2001) found alternating thick/thin sapropels in the Mediterranean Sea reflecting a pronounced *obliquity* component, whereby thick (thin) sapropels correspond to obliquity maxima (minima). This suggests that apart from a precessional component, also an obliquity signal is present in the strength of the African monsoon.

Several model studies found clear orbital signals in the monsoonal systems. A large number of these studies simulate a combined precession and obliquity signal, where precession dominates obliquity effects. For example, model simulations show that on the NH the summer monsoon circulation strengthened after the Last Glacial Maximum ( $\sim 18,000$  years Before Present (18 ka BP)), attaining its maximum in the early Holocene ( $\sim 9$  ka BP) and then weakening to its modern-day strength [108]. This signal coincides with the NH summer insolation which also increased after 18 ka BP with a maximum at 9 ka BP. Other studies confirmed the enhanced monsoonal strength at 9 ka BP [102, 106]. Just a few studies separate the precession and obliquity signal and most of these studies use an Energy Balance Model (EBM) [182, 64, 175]. However, these studies only give an indirect indication of obliquity and precession signals in the monsoon by signals in the tropical temperature [175].

Both a precession and an obliquity signal in the African monsoon has been found using several generic radiation pattern with an AGCM (Atmospheric General Circulation Model) in permanent July mode [159], a result which seems to be confirmed by the sedimentary analysis of Lourens et al. (1996; 2001). Remarkably, the largest insolation amplitude which is associated with obliquity is found at high latitudes.

Concerning the response of the monsoons to obliquity and precession, a number of problems remain: What is the physical mechanism with which the obliquity signal

can manifest itself in the African monsoon strength? Or, alternatively, are changes of monsoon intensity caused by solar radiation at high latitudes, at low latitudes or at a combination of latitudes? Do orbital variations influence the spatial pattern and timing of the monsoons? Finally, does the sensitivity of the monsoons to precession and obliquity depend on the background climatic state, or, alternatively, the prevailing orbital configuration?

To address these questions, we examined both the obliquity and precession signal in the climate with focus on the African summer monsoon using a model of intermediate complexity (ECBilt). As opposed to Prell and Kutzbach (1987), we examine the orbital influences on the seasonal cycle of the African monsoon and we use a more extensive set of orbital parameters. Furthermore, we distinguish the orbital influences originating from higher latitudes and from lower latitudes.

The model and experimental set-up used for the simulations are described in section 2. Section 3 gives some global results concerning orbital influences on temperature, precipitation and circulation while in section 4 the African monsoon will be discussed. Section 5 presents additional experiments providing some insights into the mechanisms of the African monsoon. The study is concluded and discussed in section 6.

## 2.2 The model and experimental set-up

ECBilt [143] is a global fully coupled atmosphere/ocean/sea-ice climate model of intermediate complexity. The horizontal resolution is about 500 km in mid-latitudes for both the ocean and the atmosphere (spectral T21 for the atmosphere). The vertical resolution is 3 layers for the atmosphere and 12 layers for the ocean. The time step for the atmosphere is 4 hours and for the ocean one day. No flux corrections are used. The dynamics of the atmosphere is based on quasi-geostrophic equations but ageostrophic components are included as a (diagnostically computed) time- and spatially varying potential vorticity forcing. Due to the ageostrophic forcing the Hadley circulation is simulated qualitatively correct but it is still too weak. The land surface scheme consists of a bucket model for the soil moisture and a thermodynamic snow model. The ocean has a flat bottom and the dynamics are based on primitive equations. Finally, the sea-ice model is a thermodynamic model with no ice dynamics.

The model is very suitable for performing several (sensitivity) simulations and for long paleoclimate simulations due to its computational efficiency [207, 194]. Compared to observations, the present day mean climate is simulated reasonably well. In particular, both the strength and spatial pattern of the mean annual cycle of the African summer monsoon precipitation are simulated quite well compared to the NCEP/NCAR reanalysis [90]. For example, the precipitation averaged over the monsoon region ( $15^{\circ}\text{W}$ - $30^{\circ}\text{E}$ ,  $0$ - $20^{\circ}\text{N}$ ) shows a maximum in August in ECBilt ( $\sim 5.4$  mm/day) and in the NCEP/NCAR reanalysis ( $\sim 4.8$  mm/day). The annual variability is underestimated in the model which is mainly due to the quasi-geostrophic equations. However, in the present study only the mean pattern and strength of the monsoon are studied. Weber (2001) compared a simulation for 6 ka BP performed by

ECBilt with experiments performed by models within the Paleo Modeling Intercomparison Project (PMIP). This comparison puts ECBilt in the middle (for the African monsoon) to lower (for the Asian monsoon) range of the PMIP results concerning the sensitivity of monsoonal precipitation to insolation changes [88, 19].

In order to investigate the obliquity and the precession signal in the climate, 6 sensitivity experiments with different orbital configurations have been performed:

1. Minimum precession with minimum obliquity or tilt (P-T-)
2. Maximum precession with minimum obliquity (P+T-)
3. Minimum precession with maximum obliquity (P-T+)
4. Maximum precession with maximum obliquity (P+T+)
5. Circular Earth orbit (i.e. eccentricity = 0) with minimum obliquity (P0T-)
6. Circular Earth orbit with maximum obliquity (P0T+)

We took extreme values of the orbital parameters occurring in the last 1,000,000 years (1 Ma). The values of these orbital parameters and the corresponding insolation were calculated by the method of Berger (1978), see Table 2.1 for a survey. Extreme values of the precession index  $e \sin(\pi + \tilde{\omega})$  rather than extreme values of  $\sin(\pi + \tilde{\omega})$  are considered, because precession is modulated by eccentricity. Therefore it is necessary to include eccentricity. We use the terms 'minimum' and 'maximum' precession referring to the minimum and maximum values of  $e \sin(\pi + \tilde{\omega})$ , respectively. Note from Table 2.1 that the eccentricities of the maximum and minimum precession are not equal. However, the difference is very small, which consequently also applies to the difference in global mean annual insolation. For each experiment the model was

Orbital					
Parameter	Tilt (deg)	$e \sin(\pi + \tilde{\omega})$	$e$	$\tilde{\omega}$ (deg)	occurrence (ka BP)
P+		0.058	0.058	273.50	970
P-		-0.055	0.056	95.96	959
T+	24.45				213
T-	22.08				232
P0		0.00	0.00	-	-

Table 2.1: *Orbital parameters used for the 6 sensitivity experiments. P+, P-, T+ and T- are maximum precession, minimum precession, maximum tilt and minimum tilt, respectively. A precession maximum (minimum) means winter (summer) solstice in perihelion. The tilt is defined as the angle between the ecliptic and the equator,  $e$  is the eccentricity of the orbit of the Earth and  $\tilde{\omega}$  is the angle between the vernal equinox and perihelion (measured counter clockwise). P0 is the simulation with a circular Earth orbit. The time of occurrence is given in 1000 years Before Present.*

run for a period of 500 years, with present day conditions as initial state. The first 400 years of the simulation were regarded as a spin-up period. After 400 years the upper and mid-layers of the ocean were in equilibrium. The deep layers still showed trends. These deep-ocean trends are comparable in amplitude to those found in the

control run. The only forcing is the insolation changes due to the orbital parameters which were kept constant during the simulations. All other boundary conditions (like orography, concentration of trace gases and surface characteristics (e.g. albedo, roughness)) were kept to present day values.

We will primarily consider four 'basic' experiments: the precession signal with a minimum obliquity and the obliquity signal with a circular Earth orbit. The latter is used to examine the obliquity signal because during a circular Earth orbit there is no influence of precession (i.e.,  $e \sin(\pi + \tilde{\omega}) = 0$  for each  $\tilde{\omega}$ ). The other experiments will be discussed when there are significant differences with the basic precession and obliquity experiments.

## 2.3 Global results

In this section we present the global differences between minimum and maximum precession, and minimum and maximum obliquities in DJF (December-January-February) and JJA (June-July-August). The results are averaged over the last 100 years of the 500-year simulations. A local, two-sided Student's t-test is used to determine statistical significance.

Fig. 2.1a shows the incoming insolation differences at the top of the atmosphere caused by precession changes. In boreal spring and summer the minimum precession insolation is much larger than the maximum precession insolation, with the largest differences in the NH. This is caused by the summer solstice in perihelion. In boreal winter the maximum precession insolation is larger with the largest differences on the Southern Hemisphere (SH). This means that precession enhances the seasonality on the NH and weakens it on the SH.

Insolation changes caused by obliquity show a very clear asymmetrical pattern with respect to the equator with more (less) boreal summer (winter) insolation during maximum obliquity on the NH (Fig. 2.1b). This figure also shows that the insolation at low latitudes is barely influenced by obliquity and that obliquity enhances the contrast between the hemispheres during summer and winter.

Figs. 2.2a-d show that in DJF and JJA the obliquity and precession induced differences of the surface air temperature (SAT) are largest over the landmasses and smallest over the oceans. The latter is caused by the damping effects of the oceans due to their large thermal inertia. In general, the SAT-response is proportional to the forcing. The positive precession and obliquity signal over the Labrador Sea in DJF is related to sea-ice effects. The relatively small SAT-response over the tropical regions in JJA (even negative for obliquity, Fig. 2.2d) is related to the monsoon response, which will be discussed below.

Changes in SAT, precipitation and circulation due to changes in precession are similar whether obliquity is set to maximum values (i.e. P-T- and P+T-) or to minimum values (P-T+ and P+T+). This also applies to the obliquity signal when precession is set to maximum values (i.e. P+T+ and P+T-) or to a circular Earth orbit (i.e. P0T+ and P0T-). However, over the NH landmasses in JJA the SAT-response to the obliquity signal during minimum precession is much larger (not shown), although the

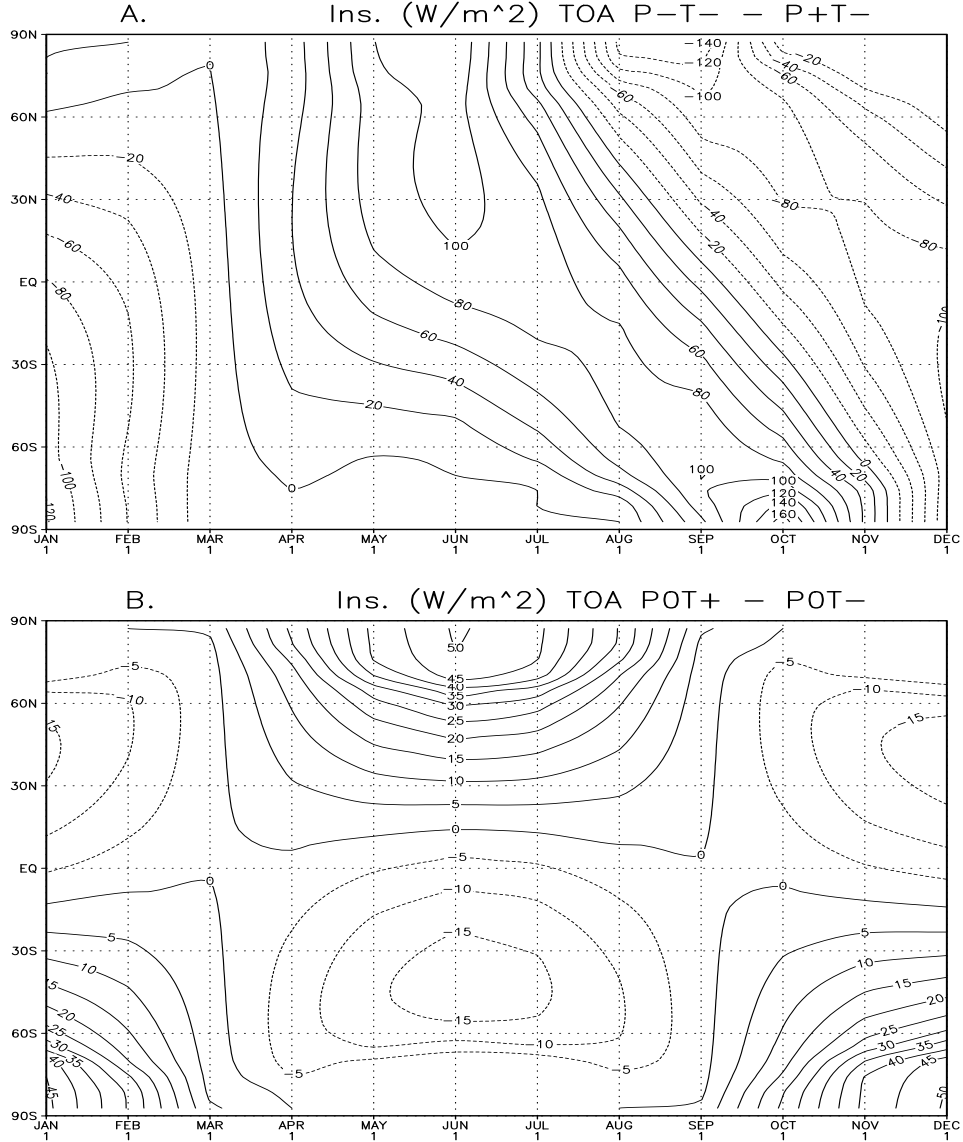


Figure 2.1: Monthly incoming insolation differences in  $\text{W/m}^2$  at the top of the atmosphere. See Table 2.1 for an explanation of the symbols. Fig. a: Minimum precession minus maximum precession. Contour interval is  $20 \text{ W/m}^2$ . Fig. b: Maximum obliquity minus minimum obliquity. Contour interval is  $5 \text{ W/m}^2$ .

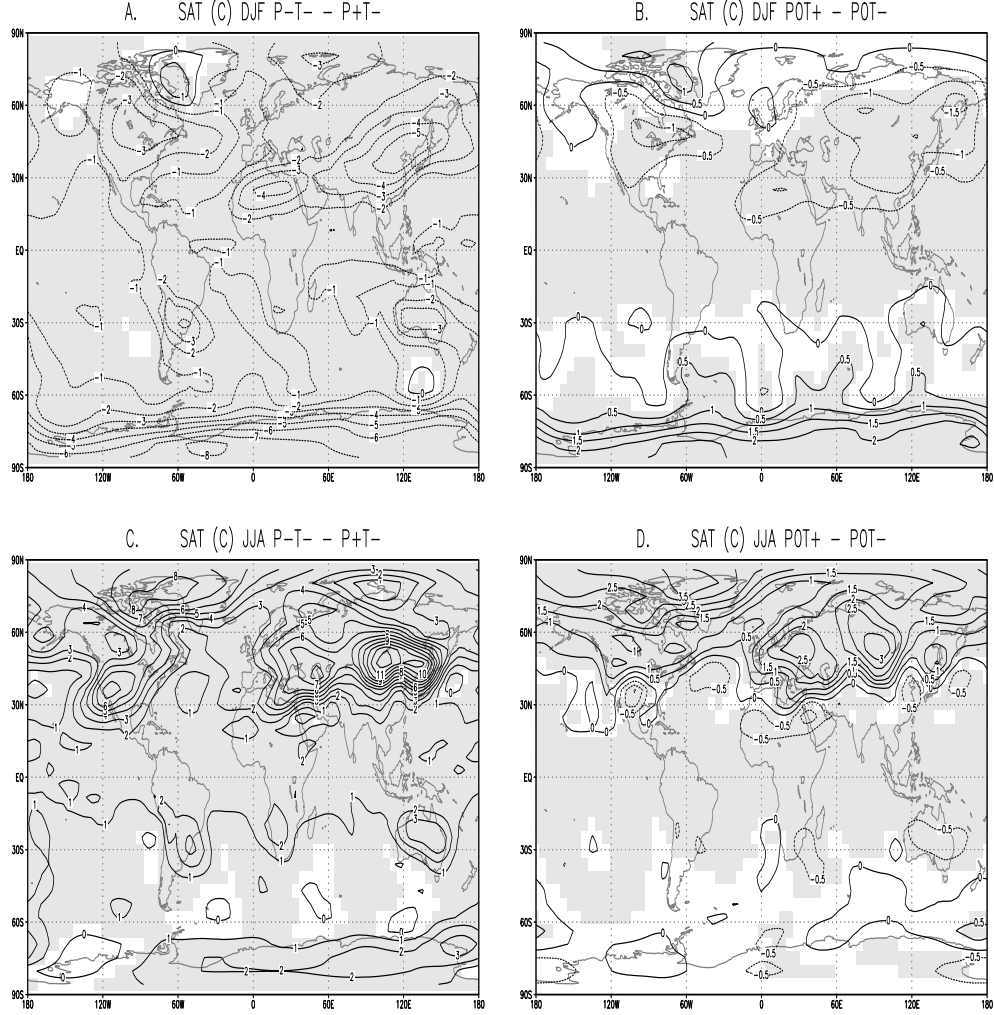


Figure 2.2: Seasonal differences of the surface air temperature (SAT) in degrees Celsius. See Table 2.1 for an explanation of the symbols. Fig. a: December-January-February (DJF) precession signal; Fig. b: Obliquity signal for DJF; Fig. c: June-July-August (JJA) precession signal; Fig. d: Obliquity signal for JJA. Shaded areas are significant at the 99% level, calculated by a local, two-sided Student's *t*-test. Contour interval is 1°C for Figs. a and c, and 0.5°C for Figs. b and d.

insolation differences are very similar compared to the other obliquity experiments. The pattern of the obliquity induced SAT-differences during minimum precession is similar to the pattern shown in Fig. 2.2d but the maximum differences are about 4-5°C over central Asia and over Europe and 3°C over North America. This can be explained by strong evaporation in late spring and early summer due to the relatively high temperatures during minimum precession, causing very low soil moisture in summer. Therefore, the additional insolation due to a maximum obliquity only heats the atmosphere, rather than both increasing the evaporation and heating the atmosphere.

Both precession and obliquity results show that the temperature response to insolation changes is linear in ECBilt, except for certain regions like the Labrador Sea and the tropics. Apart from these regions, the temperature response of ECBilt is consistent with the response of an EBM using similar orbital parameters [175].

In JJA the precession signal in the precipitation shows a much stronger Asian and African monsoon during minimum precession (Fig. 2.3a). Also over eastern North America and over northern South America the precipitation is stronger during minimum precession. The increased precipitation over the monsoon regions is at the expense of the precipitation over the oceans. The obliquity signal (Fig. 2.3b) consists of an intensified African and Asian monsoon and stronger precipitation over eastern North America during maximum obliquity, while over northern South America the response is negative. Heating (cooling) of land relative to the ocean apparently causes stronger (weaker) monsoonal circulation and associated precipitation. The enhanced African monsoon causes the relatively weak or negative signal in the SAT (Figs. 2.3 c-d) because the shortwave radiation is used for enhanced evaporation instead of heating the atmosphere.

In DJF the precession signal in the precipitation (Fig. 2.3c) consists of more precipitation over the (subtropical) oceans and less precipitation over the SH monsoon regions during minimum precession. A strong precession signal in the South American monsoon was also found in paleoclimatic data [124, 4]. Contrary to precession, obliquity hardly influences the SH monsoons (cf. Figs. 2.3c-d). Apparently, obliquity induced insolation differences are too small to influence austral summer monsoonal precipitation.

As with SAT, the obliquity signal in JJA precipitation is different for minimum precession compared to a circular Earth orbit and maximum precession. The response in the African and Asian monsoon is smaller than in the other experiments. This feature will be discussed further in section 4 where we focus on the African monsoon.

Prell and Kutzbach (1987) used an AGCM to compute the sensitivity of the African and Asian monsoon to changes in the NH insolation in (a perpetual) July. They found a sensitivity of 5 for the African monsoon to obliquity and precession induced NH insolation forcing, i.e. a 1% increase in NH solar radiation produces a 5% increase in equatorial North African precipitation. This sensitivity coefficient is comparable to that found in ECBilt.



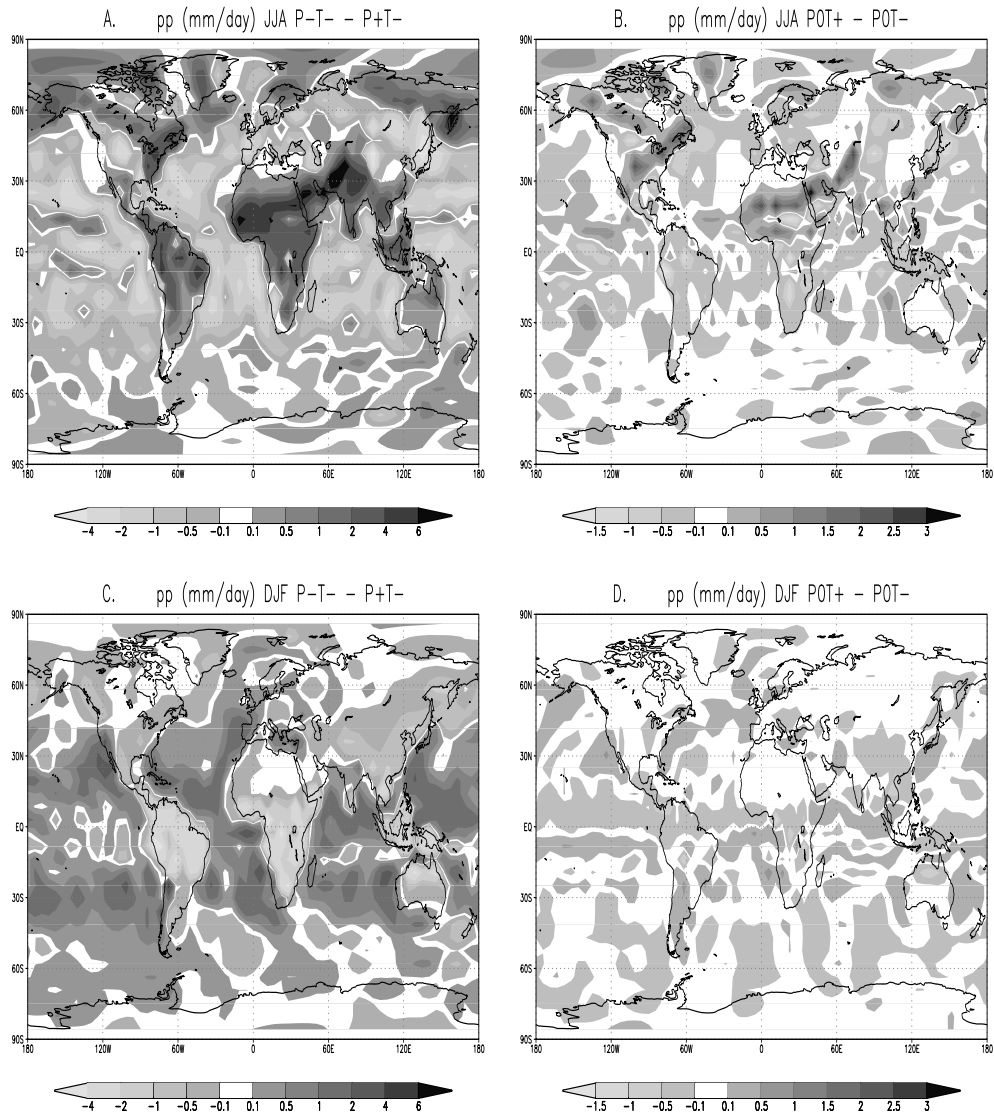


Figure 2.3: Same as Figs. 2.2a-d but now for the precipitation in mm/day. The 99% significance level is approximately at +0.1 and -0.1 mm/day for all figures.

## 2.4 African summer monsoon

The precession induced zonal mean precipitation differences over North Africa (i.e., zonally averaged over land gridboxes between 10°W and 40°E) show a much stronger maximum during minimum precession compared to maximum precession (i.e., 9 mm/day vs. ~6 mm/day, Figs. 2.4a/b), with a further northward extension of the precipitation during minimum precession. Fig. 2.4c shows that the precession induced differences are largest around 20°N and that the largest differences occur 1-2 months after the maximum difference in insolation (Fig. 2.1a). Comparing precession simulations with a minimum precession, a circular Earth orbit and a maximum precession (Figs. 2.4a, 2.4e and 2.4b, respectively) reveals that the maximum precipitation shifts from July-August, to August and August-September.

In general, obliquity induced precipitation differences (Figs. 2.4d/e) show the same pattern as precession. During maximum obliquity the precipitation extends slightly further northward and its maximum is stronger and located further south with respect to minimum obliquity. The latitudinal displacement of the maximum explains the tripole structure seen in Fig. 2.3b (see also Fig. 2.4f). Unlike precession the obliquity signal does not change the time of occurrence of the maximum precipitation. This also applies to other parameters (e.g., temperature, specific humidity and low-level circulation). The difference pattern (Fig. 2.4f) shows the largest difference around 20°N and 8°N and it occurs 1-2 months after the maximum difference of the insolation (Fig. 2.1b).

In order to explain the simulated obliquity and precession signal in the African monsoon, we have examined the specific and relative humidity, surface temperature fields and the large-scale circulation (velocity potential, low-level winds and moisture transport). The vertically averaged specific humidity is larger for minimum precession with the maximum difference north of 20°N (Fig. 2.5a), while the relative humidity is also increased (Fig. 2.5c). The increased specific humidity is mainly due to increased temperatures (Fig. 2.2c) but the increased relative humidity indicates that temperature does not explain the total specific humidity response. The obliquity signal consists of increased specific humidity north of 20°N during maximum obliquity (Fig. 2.5b), with the temperature either lower or slightly higher over that region (Fig. 2.2d), resulting in increased relative humidity (Fig. 2.5d). Fig. 2.6a shows the JJA wind vector during minimum precession, together with the difference in wind amplitude between minimum and maximum precession. The precession forcing does not significantly change the direction of the wind. The westerly winds around 15°N over southern north Africa and the tropical Atlantic Ocean are much stronger during minimum precession. This is consistent with an intensified convergence region (centered at 30°N, 80°E; Tibet) and the associated stronger zonal gradient in the velocity potential. The enhanced westerlies transport much more moisture to the African continent which leads to enhanced precipitation. The zonally averaged zonal component of the wind over northwestern Africa (10W-15E, not shown) reveals that the maximum wind occurs in June/July during minimum precession and in July/August during maximum precession. This is consistent with the timing of the maximum strength of the convergence centre over Tibet. Over the Sahara the northeastern/eastern winds

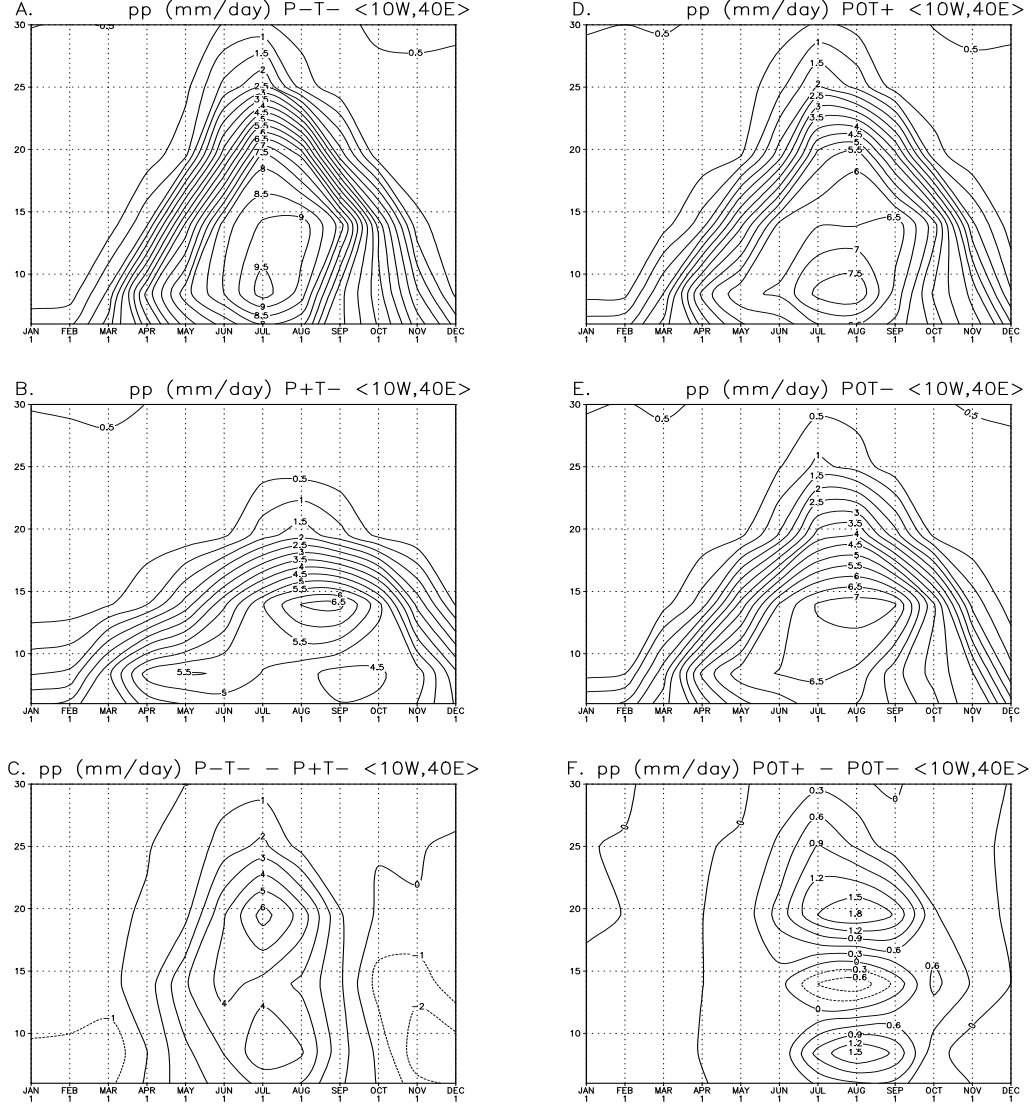


Figure 2.4: Zonally averaged ( $10^{\circ}$  W- $40^{\circ}$  E) precipitation (in mm/day) as a function of latitude and month. Fig. a: Minimum precession with minimum obliquity; Fig. b: Maximum precession with minimum obliquity; Fig. c: Difference between Figs. a and b, i.e., the response to the precession forcing; Fig. d: Circular Earth orbit with maximum obliquity; Fig. e: Circular Earth orbit with minimum obliquity; Fig. f: Difference between Figs. d and e, i.e. the response to the obliquity forcing.

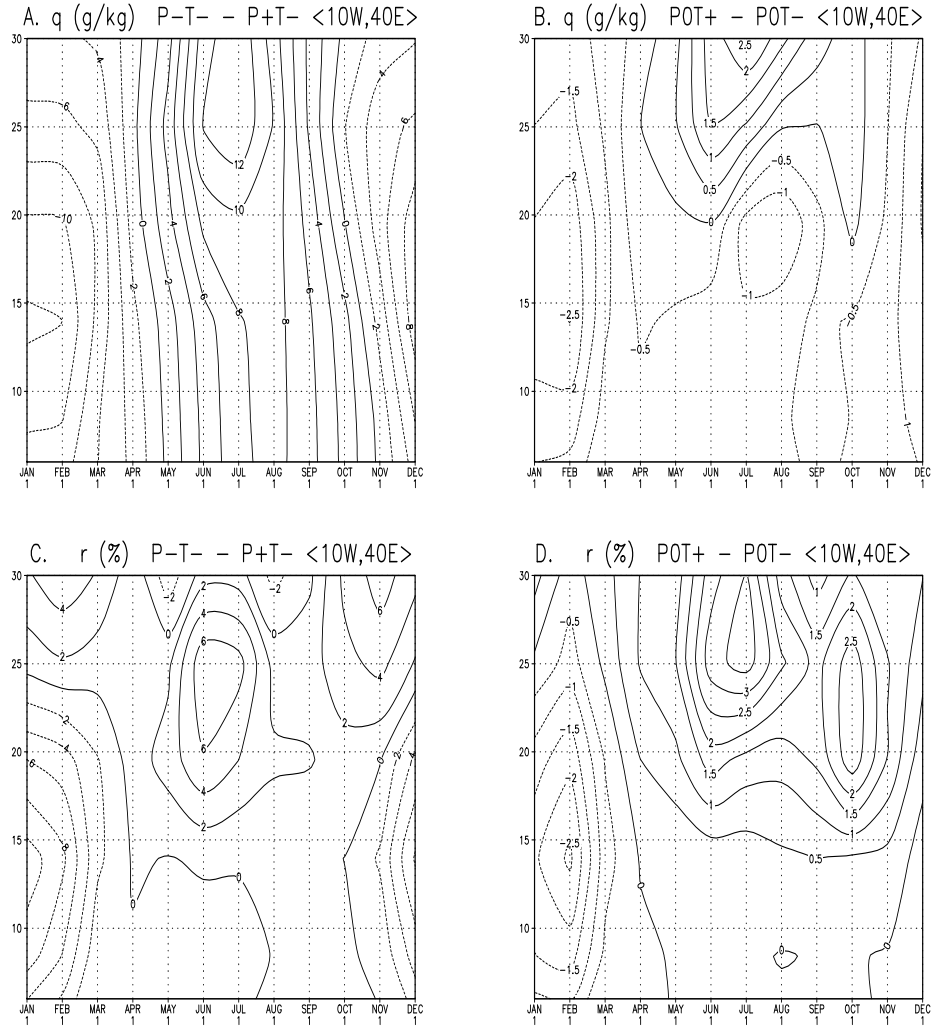


Figure 2.5: Same as Fig. 2.4 but now the response of the specific humidity (g/kg) to a: the precession forcing and b: the obliquity forcing. The response of the relative humidity (in %) to c: the precession forcing and d: the obliquity forcing.

are comparable or even weaker during minimum precession (Fig. 2.6a). However, the transport of moisture to the south by these weaker winds is still larger due to the large increase in specific humidity (Fig. 2.5a). Over the Atlantic Ocean the winds associated with the Azores High (AH) are stronger during minimum precession, related to a slightly stronger AH ( $\sim 1$  hPa). However, the wind over the African continent is not strongly influenced by changes in the AH.

The response of the wind to the obliquity signal (Fig. 2.6b) consists of enhanced westerlies around  $15^\circ\text{N}$  during maximum obliquity. Again, the direction of the wind has not significantly changed. Over the northern Sahara the wind during maximum obliquity is slightly weaker than during minimum obliquity. However, there is still an enhanced transport of moisture into the northern monsoon region due to the increased specific humidity (Fig. 2.5b). This enhanced moisture transport causes the increased precipitation over the northern monsoon region during maximum obliquity (Fig. 2.4f). Due to a northward displacement of the AH, the wind is stronger (weaker) over the northern (southern) region of the AH during maximum obliquity (Fig. 2.6b). As noted earlier in section 3, the obliquity signal with minimum precession differs

$P_{addit}$	South of $30^\circ\text{N}$ : Circular Earth orbit and maximum obliquity North of $30^\circ\text{N}$ : Minimum precession and maximum obliquity
$P_{remote}$	Remote precession signal (north of $30^\circ\text{N}$ ), i.e. $P_{addit}$ minus $P_{0T+}$
$P_{local}$	Local precession signal (south of $30^\circ\text{N}$ ), i.e. $P_{-T+}$ minus $P_{addit}$
$T_{addit30}$	South of $30^\circ\text{N}$ : Circular Earth orbit and minimum obliquity North of $30^\circ\text{N}$ : Circular Earth orbit and maximum obliquity
$T_{addit50}$	South of $50^\circ\text{N}$ : Circular Earth orbit and minimum obliquity North of $50^\circ\text{N}$ : Circular Earth orbit and maximum obliquity
$T_{remote30}$	Remote obliquity signal (north of $30^\circ\text{N}$ ), i.e. $T_{addit30}$ minus $P_{0T-}$
$T_{remote50}$	Remote obliquity signal (north of $50^\circ\text{N}$ ), i.e. $T_{addit50}$ minus $P_{0T-}$

Table 2.2: *Orbital configurations used for the additional experiments.  $P_{addit}$  is the additional precession simulation.  $T_{addit30}$  and  $T_{addit50}$  are additional obliquity simulations.*

in some aspects from those with a circular Earth orbit and maximum precession. The obliquity-related JJA precipitation signal over Africa is smaller for a minimum precession than in the other experiments. In particular, around  $20^\circ\text{N}$  the differences are about 1.5 to 2 mm/day while south of  $20^\circ\text{N}$  the differences are absent. This can be understood as follows. For minimum precession the obliquity forcing is added to a strong insolation in early summer. This results in low soil moisture in summer and a relatively large signal in SAT. At the same time, the rising branch of the large-scale circulation cell over the African-Asian continent becomes relatively dry and latent heating is reduced. This results in a relatively weak signal in the velocity potential over Asia and a weak response in the zonal wind over northern Africa. Therefore, the precipitation signal is very weak in the southern and central monsoon region. The northern branch is not affected, as the pattern and amplitude of the specific humidity response is similar to that found in the basic experiment. For a circular Earth orbit

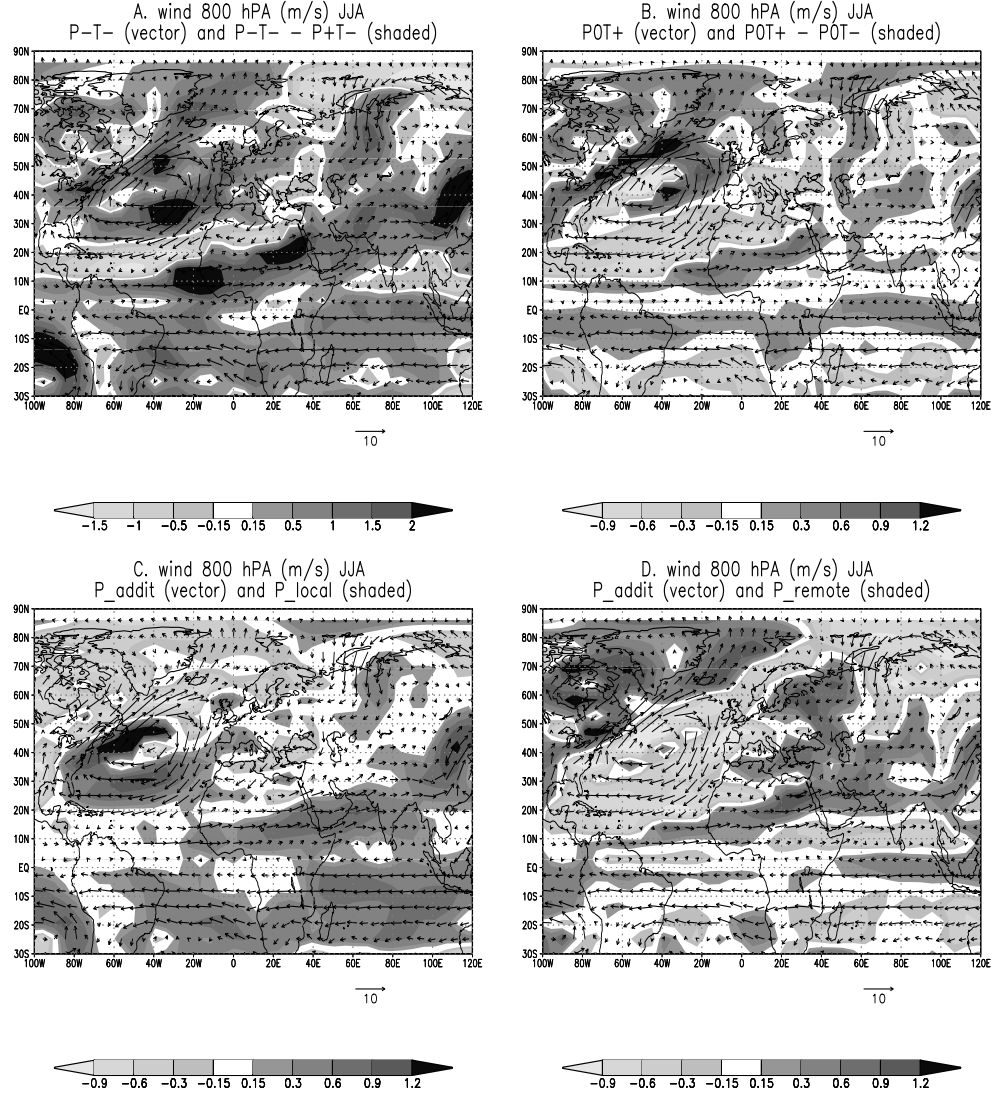


Figure 2.6: *Fig. a: The wind vector in JJA (m/s) at 800 hPa (arrows) during minimum precession together with the difference (minimum precession minus maximum precession) in wind amplitude (m/s, shaded). Fig. b: Same as Fig. a but now for maximum obliquity (wind vector; arrows) and the maximum obliquity minus minimum obliquity difference (shaded). Fig. c: Wind vector for the additional precession simulation (see Table 2.2) and the wind amplitude response to the local precession signal (shaded, see Table 2.2). Fig. d: Wind vector is similar to Fig. c together with the wind amplitude response to the remote precession signal (shaded, see Table 2.2). See also the text for more information. The 99% significance level is approximately at +0.15 and -0.15 m/s for all figures. Note that the scale in Fig. a differs from Figs. b-d.*

and maximum precession the obliquity forcing is added to a smaller insolation. In these cases the humidity supply for the large-scale circulation is not limited.

## 2.5 Local and remote forcing

The obliquity and precession signals in the simulated African summer monsoon give rise to the question whether changes of monsoon intensity are caused by solar radiation changes at high latitudes, at low latitudes, or at a combination of latitudes. In order to examine this issue further, additional simulations have been performed. First we separate the precession signal into a remote effect (i.e., due to the influence of insolation changes north of  $30^\circ\text{N}$ ) and a local effect (i.e., due to the influence of insolation changes south of  $30^\circ\text{N}$ ). The local precession signal ' $P_{local}$ ' and the remote precession signal ' $P_{remote}$ ' can be obtained by subtracting an additional experiment ' $P_{addit}$ ' and earlier defined precession experiments, see Table 2.2. The additional experiment uses an insolation forcing with a minimum precession north of  $30^\circ\text{N}$  and a circular Earth orbit south of  $30^\circ\text{N}$ , with a maximum obliquity at all latitudes. This set-up does not separate the influence of insolation changes over North Africa ( $0$ - $30^\circ\text{N}$ ) and over the Southern Hemisphere. However, in ECBilt there is a very small transport of air across the equator (see, for example Fig. 2.6a) which is mainly due to the quasi-geostrophic approximation. Therefore, in ECBilt insolation changes in the Southern Hemisphere barely influence the African monsoon. The pattern of the insolation forcing for both the remote and the local signal can be derived from Fig. 2.1a, but the amplitude of the difference is about 50% smaller.

The pattern and amplitude of the precipitation differences induced by the remote forcing (Fig. 2.7a) is similar to the obliquity induced differences (Fig. 2.4f) except that the differences occur 1-2 months earlier. Furthermore, precipitation maxima occur in July during the additional precession simulation and in August during the circular Earth orbit simulation (not shown). The remote influence is most important at subtropical latitudes ( $20^\circ\text{N}$ - $30^\circ\text{N}$ ). The largest differences caused by the local precession forcing are located around  $15^\circ\text{N}$  (Fig. 2.7b). The local forcing does not change the timing of the precipitation maxima, which occur both in July (not shown). Comparing the local and remote influence, it can be concluded that the relative importance of each depends strongly on latitude. The total difference pattern of the precipitation (i.e., local + remote forcings, not shown) is similar to the pattern shown in Fig. 2.4c, except that the amplitude is about 50% smaller in agreement with the insolation differences. The response of the specific humidity to the remote precession signal (not shown) consists of increased specific humidity ( $\sim 4$  g/kg) over latitudes around  $25^\circ\text{N}$ , similar to the obliquity signal (Fig. 2.5b). The relative humidity is higher (Fig. 2.7c), while the temperature is slightly increased (not shown). Examining the vertically-averaged moisture transport reveals that the remote signal induces a stronger southward moisture transport into northern Africa resulting in higher specific and relative humidities over northern Africa. The local precession signal in the specific humidity consists of higher values over the entire monsoon region. However, this increase is fully explained by higher temperatures. The relative humidity is even

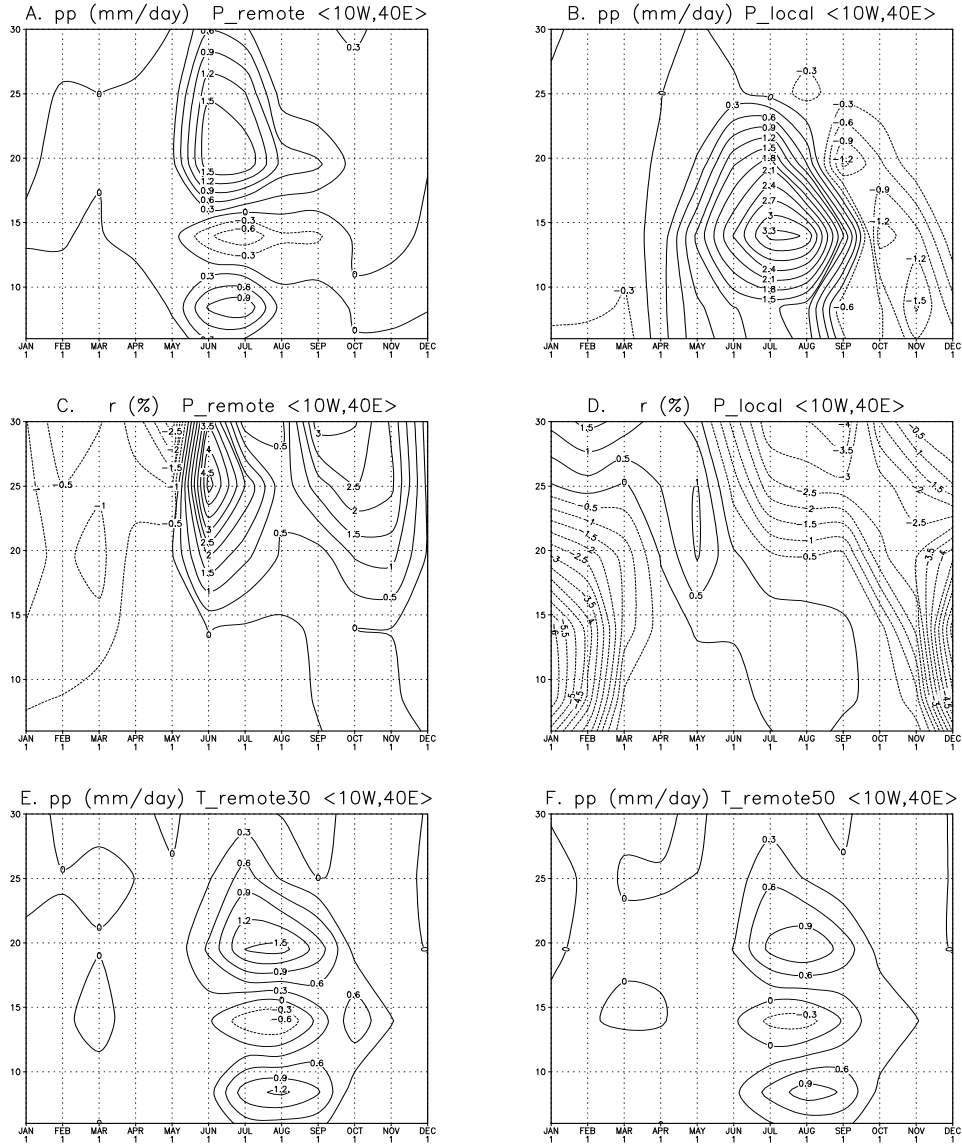


Figure 2.7: Same as Fig. 2.4 but now the response of the precipitation (mm/day) to a: the remote precession signal and b: the local precession signal. The response of the relative humidity (in %) to c: the remote precession signal and d: the local precession signal. The response of the precipitation (mm/day) to e: the remote obliquity response (north of 30°N) and f: the remote obliquity response (north of 50°N). See for more information the text and Table 2.2.



lower (Fig. 2.7d).

Figs. 2.6c and 2.6d show that in JJA the enhanced westerlies from the Atlantic Ocean into Africa is a local (Fig. 2.6c) as well as a remote signal (Fig. 2.6d). It is not possible to strictly separate the remote and local signal in the large-scale circulation. However, there are some distinctive features. The remotely induced wind response is located further northward and extends into the Asian landmass, while the local signal is restricted to the area south of  $30^\circ\text{N}$ . The remote signal is primarily due to the deepening of the large-scale convergence over Asia, while the local signal is a combination of enhanced convergence and the increased heating contrast between the African continent and the adjacent Atlantic Ocean. The zonally-averaged zonal wind over northwestern Africa ( $10^\circ\text{W}$ - $15^\circ\text{E}$ , not shown) shows a temporal shift in the wind maxima in  $P_{remote}$  (in June during the additional run and in July during the simulation with the circular Earth orbit) while there is no sign of a shift in  $P_{local}$  (both in June). The wind maxima in  $P_{remote}$  are concurrent with maxima in the strength of the Asian convergence centre. During minimum precession the insolation at high northern latitudes rapidly decreases after its maximum in June, while the maximum precession insolation decreases more slowly (not shown). This results in higher insolation during maximum precession with respect to minimum precession at high latitudes in August-September (Fig. 2.1a), causing a shift in the timing of maximum strength of the Asian convergence zone. This, in turn, shifts the timing of the monsoonal circulation and the associated precipitation. Obliquity changes do not change the seasonal pattern of insolation (Fig. 2.1b) and therefore no obliquity induced temporal shift in the precipitation is found.

From this additional experiment it follows that the precession signal in precipitation can be separated in a remote and a local signal. The remote precession signal is very similar to the total obliquity signal (cf. Figs. 2.7a and 2.4f). The earlier occurrence of the precipitation maximum for minimum precession is found to be a remote signal.

From the results described above it can be concluded that the obliquity signal in the African monsoon originates from insolation changes at mid- to high latitudes. In order to confirm this hypothesis, we performed an additional obliquity simulation,  $T_{addit30}$ , see Table 2.2. From this experiment we obtain the response to the obliquity induced insolation forcing north of  $30^\circ\text{N}$  ( $T_{remote30}$ , see Table 2.2). Any effects of the (small amplitude) obliquity forcing at low latitudes are turned off in this additional experiment. The results (Fig. 2.7e) reveal that the remote forcing north of  $30^\circ\text{N}$  accounts for 80-90% of the total signal (cf. Figs. 2.7e and 2.4f). To emphasize the role of high latitudes, we repeated this experiment with obliquity forcing restricted to latitudes north of  $50^\circ\text{N}$  ( $T_{addit50}$  and  $T_{remote50}$ , see Table 2.2). The results (Fig. 2.7f) show that obliquity forcing north of  $50^\circ\text{N}$  explains still 60-70% of the total signal (cf. Figs. 2.7f and 2.4f). This is partly caused by the insolation induced increased temperature at high latitudes, resulting in increased specific humidity. This moisture is transported southwards to lower latitudes. A second mechanism for transporting the obliquity signal from high latitudes to lower latitudes is the insolation induced pressure change at high latitudes. This influences the large-scale circulation and the pressure over central Asia, resulting in a stronger large-scale convergence.

## 2.6 Conclusions and discussion

The present study shows that the African summer monsoon is influenced both by obliquity and precession. During either maximum obliquity or minimum precession the monsoonal precipitation is enhanced and the precipitation extends further northward than during minimum obliquity and maximum precession, respectively. Both the obliquity and the precession signal consist of remote influences (i.e., insolation changes north of  $30^{\circ}\text{N}$ ), while the precession signal also consists of a local signal (i.e., insolation changes south of  $30^{\circ}\text{N}$ ). The influence of obliquity and the remote influence of precession on African precipitation can be traced back to similar mechanisms. One of the remote mechanisms is stronger wind from the Atlantic Ocean into southern north Africa forced by a deepening of the convergence zone over southern Asia resulting from an increase of summer insolation at high latitudes. Another remote mechanism is penetration of moist air from high latitudes southwards into the northern monsoon region. This is related to the increased ability of the atmosphere to contain water vapour due to the higher temperatures at high latitudes. An additional (local) mechanism of the precession signal is the stronger heating contrast between North Africa and the adjacent Atlantic Ocean which also enhances the low-level monsoonal circulation, bringing relatively moist air to the African continent. Concluding, changes in the monsoon intensity are caused by solar radiation changes at high and at low latitudes.

The time of occurrence of the maximum monsoonal precipitation is influenced by precession but not by obliquity. The insolation maximum shifts through the summer months due to precession, which results in shifts in the maximum strength of the Asian convergence zone and the associated westerlies over northern Africa. Thus, the timing of the precession signal in the African monsoon is primarily a remote effect.

It was found that the precession signal in the African monsoon does not depend on obliquity, while the amplitude of the obliquity signal depends on the prevailing precession. In particular, in the model the obliquity signal is weaker during minimum precession than during maximum precession and a circular Earth orbit. It is a challenge for paleoclimatic studies whether this dependence can also be found in paleoclimatic data, especially for large eccentricity values.

Some important mechanisms for the African summer monsoon are not taken into account in ECBilt. For example, several Holocene studies for 6 ka BP found that the mutual interaction between vegetation and the atmosphere amplifies the response of the hydrological cycle [101, 24, 54, 20]. Including this mechanism would cause an enhanced sensitivity of the African summer monsoon to obliquity and precession compared to the present results. Another caveat is the use of a simple bucket model, which could cause the dependence of the obliquity signal on the prevailing precession. The very low Asian soil moisture in summer during minimum precession is probably at least in part due to the high sensitivity of the bucket model to temperature changes. Further research with a GCM with a more advanced soil moisture scheme and higher spatial resolution is needed to clarify this point.

The stronger northward extension of the monsoonal precipitation during minimum precession and maximum obliquity consists of only one latitudinal model grid-

point. However, this northward shift has also been found in several generally higher-resolution simulations for 6 ka BP [17], and to a stronger extent for 126 ka BP [43]. The orbital induced northward shift of the African monsoon thus seems to be a realistic feature, which would be enhanced when vegetation is taken into account (e.g., Kutzbach et al., 1996).

Park and Oglesby (1991) performed several runs with an AGCM to study the obliquity and precession influences for the Mid-Cretaceous (100 Ma BP). Although a direct comparison with our results is difficult due to the different geography and topography, some basic features are similar. They noted that the precession signal for most model variables and model regions is stronger than the obliquity signal, even at high latitudes. However, they also found a significant obliquity signal in the hydrological cycle (evaporation minus precipitation) over the equatorial South Atlantic and proto-West Africa (centered around 10°S and 40°W) in a perpetual July. This signal is caused by the circulation changes associated with the impact of obliquity on the southern wintertime pressure maximum.

The results of the present model study are consistent with paleoclimatic data [156, 121]. These studies found a strong precessional component in the strength of the African monsoon. In addition, the obliquity signal found in the present simulations provides an explanation for the obliquity-related signals in the sedimentary records of the Mediterranean (e.g., Lourens et al., 1996; 2001), through monsoon-induced variations in Nile river outflow and northern Africa aridity.

We have shown that remote forcing (precession and obliquity) and local forcing (precession) both affect the strength of the African summer monsoon. As the phasing of precession does not depend on the latitude, this validates the use of the traditional 65°N Milankovitch insolation curve as a target for tuning sedimentary cycles in the Mediterranean. It is interesting that we find an obliquity signal in the African summer monsoon without the (amplifying) role of glacial ice sheets. This is in agreement with the presence of obliquity signals in the Mediterranean sedimentary records of early Pliocene age [121] and late Miocene age [70] which are formed well before the onset of the late Pliocene and Pleistocene glacial cycles.



## Chapter 3

# Simulation of climate phase lags in the response to precession and obliquity forcing and the role of vegetation

### Abstract\*

Long (130,000 years) transient simulations with a coupled model of intermediate complexity (CLIMBER-2) have been performed. The main objective of the study is to examine leads and lags in the response of the climate system to separate obliquity and precession induced insolation changes. Focus is on the role of internal feedbacks in the coupled atmosphere/ocean/sea-ice/vegetation system. No interactive ice sheets were used. The results show that leads and lags occur in the response of the African/Asian monsoon, temperatures at high latitudes and the Atlantic thermohaline circulation. For the monsoon, leads and lags of the monthly precipitation with respect to the precession parameter were found which are strongly modified by vegetation. In contrast, no lag was observed for the annual precipitation. At high latitudes during late winter/early spring a vegetation induced lag with respect to the precession parameter was found for surface air temperatures. Again, no annual lag was detected. The lag in the *monthly* surface air temperatures induces a lag in the *annual* overturning in the Atlantic Ocean by changing the strength of the deep convection. The lag is several thousand years. The obliquity-related forcing does not give rise to lags in the climate system. We conclude that lags in monthly climatic variables, which are due to vegetation feedbacks, can result in an annual lag when a climatic process (like deep water formation) acts as a filter for certain months.

---

\*This chapter is under review for publication in *Climate Dynamics* as: Tuenter, E., S.L. Weber, F.J. Hilgen, L.J. Lourens and A. Ganopolski, (2004). Simulation of climate phase lags in the response to precession and obliquity forcing and the role of vegetation. [190]

### 3.1 Introduction

It is generally accepted that changes in the orbital parameters (i.e. eccentricity, precession and obliquity) and the associated changes in insolation strongly influence the climate on Earth. Paleoclimatic data often indicate leads and/or lags of the climatic response with respect to the orbital parameters. Imbrie et al. (1989) showed that the tropical Atlantic cold-season Sea Surface Temperature (SST) lag the precession parameter by about 45 degrees (3000 years (3 ka)), while at high latitudes Atlantic SST lags the precession parameter by about 100 degrees (6 ka). For obliquity the lag at low latitudes is quite ambiguous while at high latitudes it is about 90 degrees (10 ka). Clemens et al. (1991) observed a lag of about 7-8 ka for precession and no significant lead/lag for obliquity in several proxies for the strength of the Indian monsoon. Finally, Lourens et al. (1996) obtained a lag of several thousands of years for the youngest Holocene Mediterranean sapropel with respect to the precession parameter, which might be an indication of a lag of the African summer monsoon.

In general, lags of the climate system with respect to the orbital parameters are ascribed to the long response time-scale associated with the growth and decay of ice sheets. Imbrie et al. (1992) showed that in the Pleistocene the global ice volume lags both the precession and the obliquity parameter by about 90 degrees (5 ka for precession and 10 ka for obliquity). However, the inferred lag of 3 ka for the pre-Pleistocene sapropel record with respect to the precession parameter may point to feedbacks independent of glacial cycles (Lourens et al., 1996).

Due to high computational costs orbital induced leads/lags have rarely been the subject of model simulations. In a study with an energy balance model (EBM), Short and Mengel (1986) obtained a lag of 2-3 ka for the maximum summer temperature over the northern African continent with respect to the precession parameter. At high northern latitudes the lag over land was less than 1 ka.

The main objective of the present study is to investigate whether the climate system can lead/lag the orbital forcing without the long response time of ice sheets. For this purpose a coupled climate model of intermediate complexity, CLIMBER-2 [154] without an ice sheet model is used. Our approach is to study the separate obliquity and precession signal together with the combined signal. This method has already been used by other model studies (e.g., Prell and Kutzbach, 1987; Short et al., 1991; Gallimore and Kutzbach, 1995 and in chapter 2 of this thesis). Several other model studies have found that vegetation significantly influences the equilibrium response of the climate system to the orbital forcing both at low latitudes (e.g., Kutzbach et al., 1996; Claussen and Gayler, 1997 and Doherty et al., 2000) and at high latitudes (e.g. Foley et al., 1994; Ganopolski et al. 1998 and Wyputta and McAvaney, 2001). It is our hypothesis that vegetation could also influence leads/lags of the climate system to the orbital forcing. To study this, we performed simulations with and without an interactive vegetation model. Because the influence of vegetation is most pronounced at high and low latitudes, we will focus on low Northern Hemisphere (NH) latitudes with emphasis on the African/Asian monsoon and on high NH latitudes with emphasis on the Atlantic/European climate.

The model and experimental set-up are described in section 2. In section 3 the

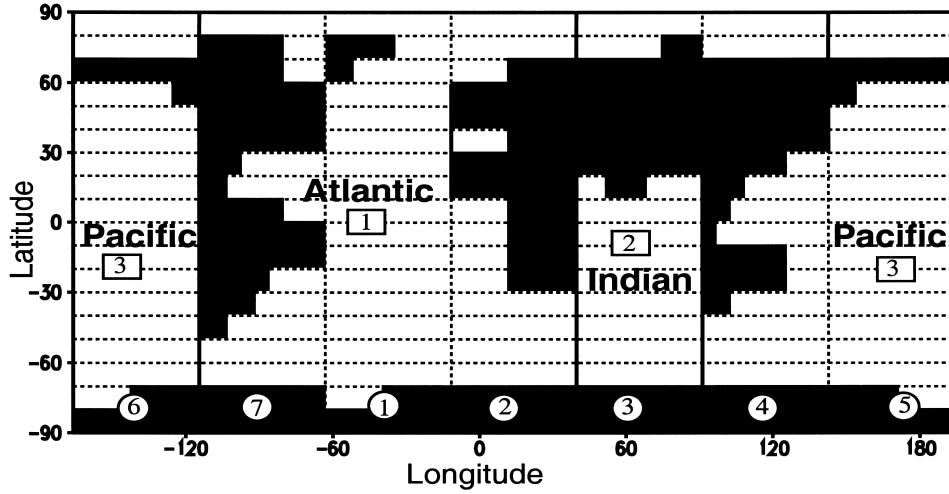


Figure 3.1: Representation of the Earth geography in CLIMBER-2.3. Horizontal dashed lines separate grid cells for the atmospheric grid (the latitudinal resolution for the ocean is  $2.5^\circ$ ). Vertical dashed lines show only atmospheric grid cells. Atmospheric sectors are numbered in the circles. Black area indicates only the relative fractions of land and ocean in the atmospheric grid cells. Solid vertical lines show the partition between the three ocean basins.

relation between the orbital parameters and the insolation will be explained. The response of the climate system to orbital forcing at low latitudes will be given in section 4, while in section 5 the response at high latitudes will be discussed. In section 6 the study is concluded and discussed.

## 3.2 The model and experimental set-up

We use the coupled model of intermediate complexity CLIMBER-2 (for CLIMate and BiosphERE, version 3, Petoukhov et al. (2000)), which is very suitable for long (paleo)simulations due to its fast turnaround time. The model consists of an atmosphere model, an ocean/sea-ice model and a land/vegetation model. This version of the model contains no ice sheet model. No flux adjustments are used.

The atmospheric model is a 2.5-dimensional statistical-dynamical model with a resolution of  $10^\circ$  in latitude and approximately  $51^\circ$  in longitude (Fig. 3.1). The model does not resolve synoptic timescales but uses statistical characteristics associated with ensemble-means of the system. The vertical structure of temperature and humidity is prescribed. These vertical profiles are used for the computation of the 3-dimensional fields of the atmospheric circulation and the radiative fluxes. The vertical resolution for the circulation, temperature and humidity is 10 levels and for the long-wave radiation 16 levels. The time step is one day.

Exp.	Tilt (degrees)	Precession	Eccentricity	Vegetation
P	Fixed (22.08)	Variable (Fig. 3.2)	Variable (Fig. 3.2)	Fixed (PD)
T	Variable (Fig. 3.2)	Fixed (0.0)	Fixed (0.0)	Fixed (PD)
PT	Variable (Fig. 3.2)	Variable (Fig. 3.2)	Variable (Fig. 3.2)	Fixed (PD)
PV	Fixed (22.08)	Variable (Fig. 3.2)	Variable (Fig. 3.2)	Interactive
TV	Variable (Fig. 3.2)	Fixed (0.0)	Fixed (0.0)	Interactive
PTV	Variable (Fig. 3.2)	Variable (Fig. 3.2)	Variable (Fig. 3.2)	Interactive

Table 3.1: *Orbital configuration and vegetation used for the 6 transient experiments. P is the precession experiment with fixed vegetation, T is the obliquity (Tilt) experiment with fixed vegetation and PT is the combined precession and obliquity experiment with fixed vegetation. PV, TV, and PTV are the precession, obliquity and combined experiments with interactive vegetation, respectively. PD stands for Present Day. The tilt is defined as the angle between the ecliptic and the equator. Precession is defined as  $e \sin(\pi + \tilde{\omega})$  with  $e$  the eccentricity of the orbit of the Earth and  $\tilde{\omega}$  is the angle between the vernal equinox and perihelion (measured counter clockwise).*

The terrestrial vegetation model is VECODE (VEgetation COntinuous DEscription, Brovkin et al. (1997)). The model computes the fraction of the potential vegetation (i.e., grass, trees and bare soil). This is a continuous function of the annual sum of positive day-temperatures and the annual precipitation. There is no lag in the response of the vegetation to the climate because at the end of each model year new fractions are computed which are used for the following year. The computed vegetation changes affect the land-surface albedo and the hydrological cycle. The time step of VECODE is one year.

The ocean model is based on the model of Stocker et al. (1992) and describes the zonally averaged temperature, salinity and velocity for three separate basins (Atlantic, Indian and Pacific oceans, Fig. 1). The three basins are connected by the Southern Ocean through which mass, heat and salt are exchanged. The latitudinal resolution is  $2.5^\circ$  and the vertical resolution is 20 unequal levels. The time step is 5 days. The ocean model includes a simple thermo-dynamic sea-ice model which computes the sea-ice fraction and thickness for each grid box, with a simple treatment of advection and diffusion of sea-ice.

Results of CLIMBER-2 compare favorably with data of the present day climate [154]. Results of sensitivity experiments (like changes in  $\text{CO}_2$ , vegetation cover and solar irradiance) performed with CLIMBER-2 agree reasonably well with results of more comprehensive models [56]. The model is successful in simulating cold climates [55], while Ganopolski et al. (1998a) and Kubatzki et al. (2000) have shown that the model is also able to simulate warm periods like the mid-Holocene and the last interglacial maximum (6 ka and 125 ka Before Present (ka BP)), respectively. Finally, the model has been used for transient simulations of the (African) monsoon with good agreement with paleoclimatic data [31].

With CLIMBER-2 we performed 3 different transient simulations for the interval from 280 to 150 ka BP, one for the precession signal, one for the obliquity signal



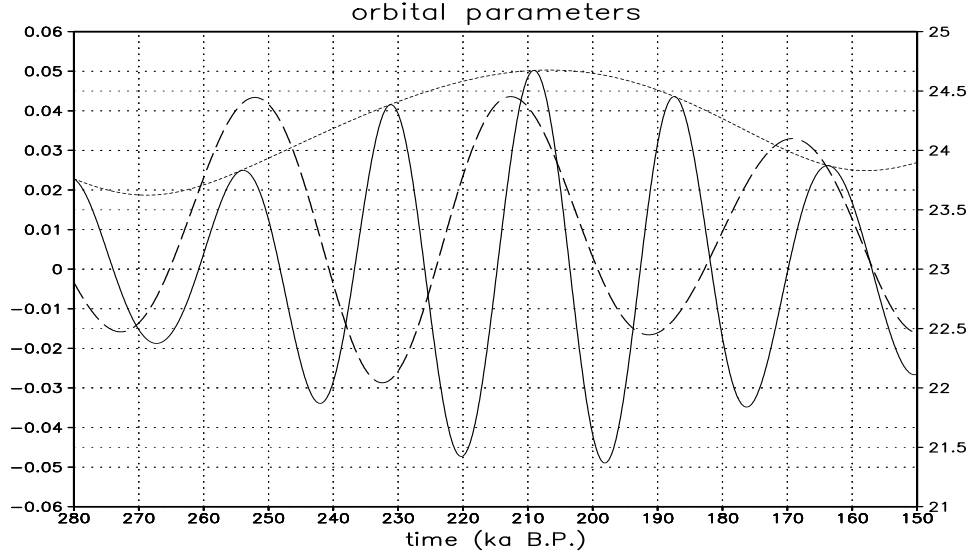


Figure 3.2: *Orbital parameters for the period 280-150 ka BP: Eccentricity (short dashed), the precession parameter (solid) and obliquity (long dashed). The left vertical axis displays the values for eccentricity and the precession parameter. The right axis shows the values for obliquity (in degrees). The horizontal axis displays time (in 1000 years Before Present).*

and one for the combined signal. The orbital parameters used in this study were computed with the method described in Berger (1978). For the precession signal (P) the eccentricity and precession are shown in Fig. 2 while obliquity (or tilt) was fixed at a minimum value (i.e., 22.08 degrees), see also Table 3.1. The precession index is defined as  $e \sin(\pi + \tilde{\omega})$  with  $e$  the eccentricity of the Earth's orbit and  $\tilde{\omega}$  the angle between the vernal equinox and perihelion (measured counter clockwise). From the definition of the precession parameter it can be derived that it is necessary to let the eccentricity vary because eccentricity modulates precession. We will use the terms 'minimum' and 'maximum' precession referring to the minimum and maximum values of  $e \sin(\pi + \tilde{\omega})$ , respectively. We used the minimum obliquity of the epoch for the precession simulation because the same value was already used in equilibrium experiments described in chapter 2 of this thesis. In that paper it was shown that the climate response to the precession forcing does not depend on the prevailing obliquity.

The climatic response to the obliquity signal (T) was studied by varying the tilt and using a circular Earth orbit (i.e., eccentricity=0), see Fig. 3.2 and Table 3.1. A circular Earth orbit is used because in this configuration there is no influence of precession ( $e \sin(\pi + \tilde{\omega}) = 0$  for each  $\tilde{\omega}$ ). It is useful to eliminate the precession signal because in equilibrium experiments it is found that the response of the climate to the obliquity forcing could depend on the prevailing precession (chapter 2 of this thesis). The third simulation combines the precession and obliquity signal (PT, Table 3.1) by varying both the obliquity parameter and the precession parameter. The 280-150 ka

BP interval was selected because it contains a rather extreme eccentricity cycle (but not the most extreme cycle of the last 1 million years) and the most extreme obliquity oscillations of the last 1 million years. It should be noted that our objective is to study phase differences between the climate system and the separate orbital signals without the influence of interactive ice sheets, rather than to perform a realistic simulation of this time interval.

All three experiments described above have been carried out with the coupled atmosphere-ocean model and with the atmosphere-ocean-vegetation model. In the simulations with the atmosphere-ocean model the vegetation was prescribed according to observed present day coverage and was kept constant during the simulations. The results of the simulations with the atmosphere-ocean-vegetation model will be denoted as PV, TV and PTV for the precession, obliquity and combined simulations, respectively (Table 3.1).

For all 6 simulations the boundary conditions like orography, land-sea configuration, ice sheets and concentration of trace gasses were kept constant. For the initial state present day conditions were used for all simulations. The results will be shown as averages over 100 years as the periods of the oscillations of the orbital parameters are much larger than 100 years. The lags and leads are computed by maximising the linear correlation.

### 3.3 Insolation

In this section the general relation between the orbital parameters and the insolation is discussed. Furthermore, it is shown that the lag of the climate response to insolation within the seasonal cycle can cause a lead or lag in time with respect to the orbital parameters.

During minimum precession summer solstice occurs nearest to the Sun and winter solstice occurs furthest away from the Sun while this is reversed during maximum precession. This results in increased insolation during boreal summer and decreased insolation during boreal winter for all NH latitudes during minimum precession with respect to maximum precession (Fig. 3.3). The maximum insolation shifts in time with respect to the precession parameter: For January to May it leads the precession parameter; for June there is virtually no lead or lag while it lags the precession parameter for July to December. At low latitudes the Sun passes overhead twice. For instance, at  $15^\circ\text{N}$  the Sun passes overhead  $\sim 6$  weeks before and after summer solstice. This results in two insolation maxima during maximum precession, one in April and one in August. It is obvious that during minimum precession the Sun also passes overhead twice. However, because summer solstice occurs in perihelion there is only one insolation maximum which occurs in June. When spring (autumn) equinox occurs in perihelion the monthly insolation also consists of only one maximum in April (August). Precession does not influence the annual insolation at all latitudes. Eccentricity changes cause changes in the annual insolation, but the signal is very small (about  $0.2 \text{ W/m}^2$  between minimum and maximum eccentricity).

Changes in obliquity cause stronger seasonality on the NH with stronger inso-

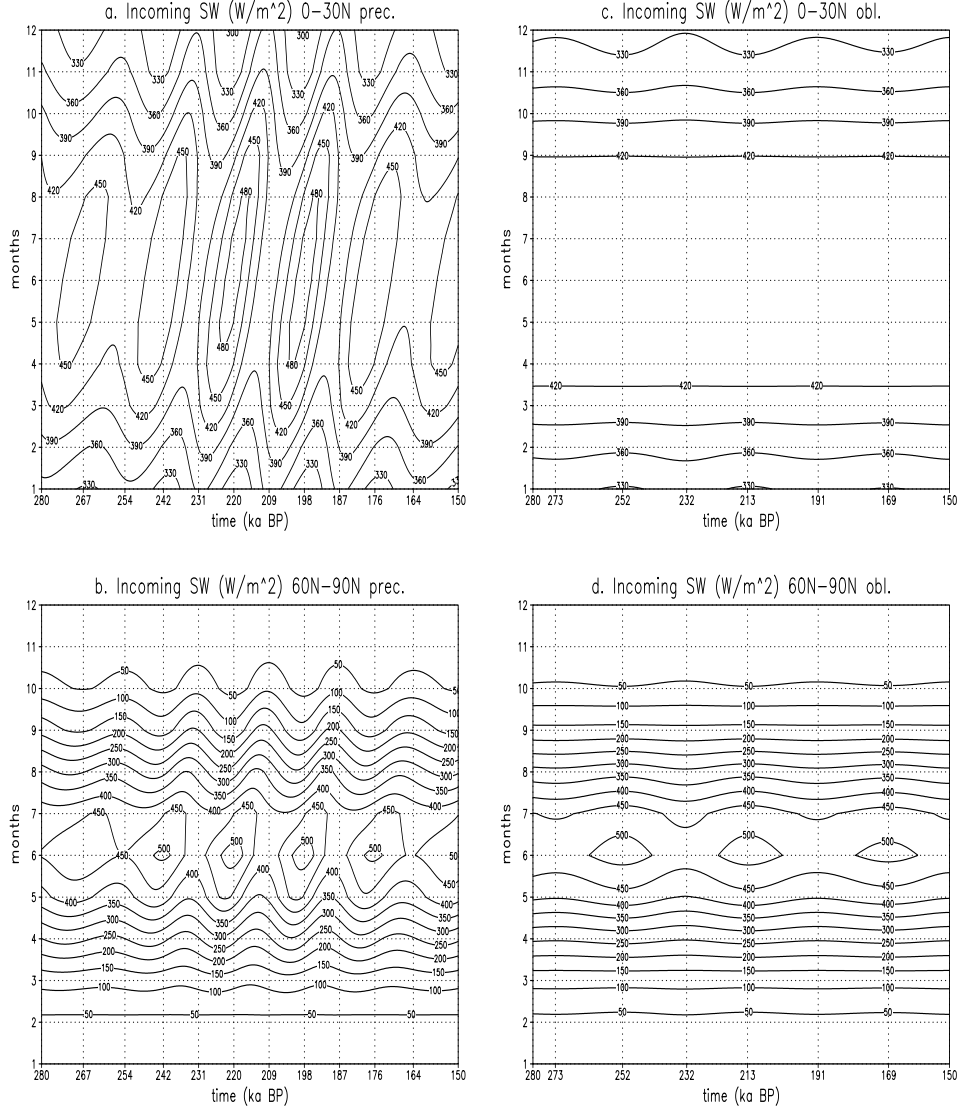


Figure 3.3: Monthly incoming shortwave radiation (in  $W/m^2$ ) for a) the precession signal averaged over 0–30° N, b) the precession signal averaged over 60° N–90° N, c) the obliquity signal averaged over 0–30° N and d) the obliquity signal averaged over 60° N–90° N. Horizontal axis displays the time (in 1000 years Before Present). On the horizontal axis the years are given when minimum and maximum precession (in a and b) and maximum and minimum obliquity occur (in c and d) occur, see also Fig. 3.2. The vertical axis displays the months. Contour interval is 30  $W/m^2$  for a and c and 50  $W/m^2$  for b and d.

lation during summer and weaker insolation during winter going from minimum to maximum obliquity. At high northern latitudes the obliquity signal in summer insolation is much stronger than in winter insolation due to the polar night (Fig. 3.3). At low latitudes the obliquity signal is negligible in summer while in winter the obliquity signal consists of slightly weaker insolation during maximum obliquity compared to minimum obliquity (Fig. 3.3). These seasonal signals result in an annual signal with stronger insolation at high latitudes and weaker insolation at low latitudes during maximum obliquity. In other words, in contrast to precession, obliquity induces changes in the annual meridional insolation gradient.

The response of the climate to insolation changes within a year can be translated into a lead/lag in time. To illustrate this the relation between the absorbed insolation at mid-latitudes for the precession experiment with fixed vegetation (P) in the summer months and the precession parameter is shown in Fig. 3.4a. The phase of the precession parameter and the insolation are nearly similar for June while the insolation in July lags the precession parameter by about 1800 years (i.e., the period of precession ( $\sim 21$  ka) divided by 12 months). The insolation in August lags the precession parameter by about 3600 years. In general, the response of the surface air temperature (SAT) over land lags the insolation by about 1 month. In time this means that, for example, the phase of the SAT in August is similar to the phase of the insolation in July (Fig. 3.4b). Therefore, the SAT in August lags the precession parameter by about 1800 years. For similar reasons the SAT in July is in phase with the precession parameter while the SAT in June leads the precession parameter. Over the oceans, the SAT generally lags the insolation by about 2 months within a year. This results in no phase difference between the SAT in August and the precession parameter and a lead of about 1800 (3600) years for the SAT in July (June) with respect to the precession parameter (Fig. 3.4c). It is obvious that for obliquity the SAT over land also lags the insolation with one month while the lag over the ocean is about two months. However, the phases for the insolation in June, July, August and other months are the same, i.e., they are either in phase or exactly out of phase with the obliquity parameter (Fig. 3.4d). This results in no phase differences between the obliquity parameter and the SAT both over land and over the oceans (not shown).

We have chosen to illustrate the general mechanism by summer temperatures at mid-latitudes without the role of vegetation because this is the most simple example. In the remaining part of this paper we will see that this simple picture can be strongly disturbed by changes in vegetation and/or albedo due to sea-ice and snow responses.

### 3.4 Low latitudes

In experiment P the strength of the African/Asian monsoon is strongly influenced by precession with stronger precipitation during minimum precession and weaker precipitation during maximum precession (Fig. 3.5a). The African and Asian monsoon are combined because in the model they generally respond in the same way to the orbital forcing. Besides the strength, precession also controls the length of the monsoon season: During minimum precession the monsoon season starts approximately one month

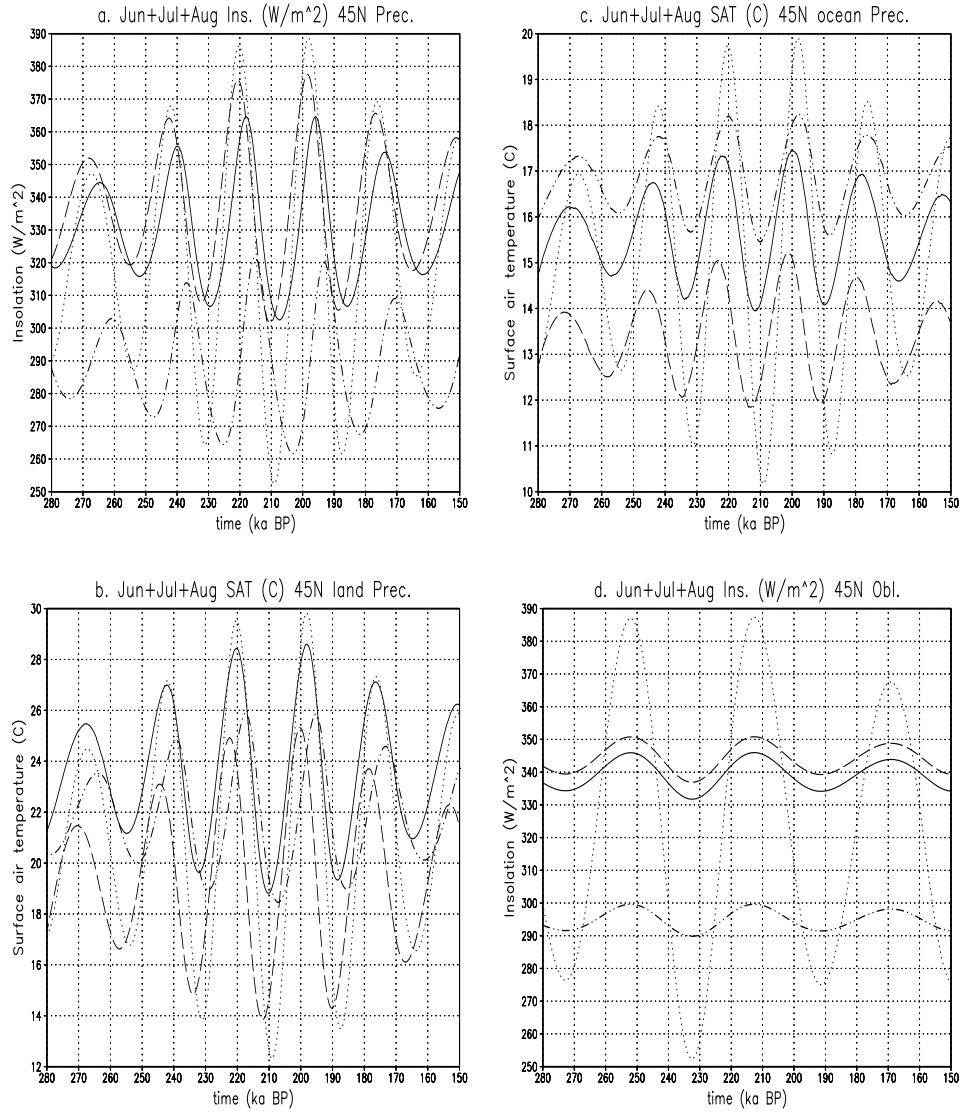


Figure 3.4: a) Net incoming solar flux at the top of the atmosphere in  $\text{W/m}^2$ ; b) Zonally averaged surface air temperature (SAT, in  $^{\circ}\text{C}$ ) over land; c) Zonally averaged SAT ( $^{\circ}\text{C}$ ) over the oceans and d) Net incoming solar flux at the top of the atmosphere in  $\text{W/m}^2$ . The parameters are plotted in all figures for June (dashed line), July (solid line) and August (dashed-dotted line) for the latitudinal belt  $40^{\circ}\text{N}$ - $50^{\circ}\text{N}$  (Fig. 3.1). Figs. a-c are results from experiment P and Fig. d shows results for experiment T. For easy comparison of the phases, in Figs. a-c the precession parameter multiplied by -1 is plotted (dotted line, arbitrary scale) and in Fig. d the obliquity parameter is plotted (dotted line, arbitrary scale). Horizontal axis displays time (in 1000 years Before Present).

earlier and ends one month later than during maximum precession (Fig. 3.5a). The pattern of the precipitation closely follows the insolation pattern taking into account a lag of about one month (cf. Figs. 3.3a and 3.5a). One consequence is that during minimum precession the maximum precipitation occurs in July, i.e., one month after the maximum insolation. The one month lag of the precipitation with respect to the insolation translates into a lead of the precipitation with respect to the precession parameter of 3600 years and 2200 years for May and June, respectively; virtually no lead in July (500 years); and a lag for August and September (1900 and 4700 years, respectively). For the annual mean, the monthly leads and lags (as well as the amplitudes) cancel out resulting in no phase difference between the precession parameter and the annual monsoonal precipitation (Fig. 3.6a). The influence of eccentricity solely consists of a modulation of the precession signal.

With interactive vegetation (PV) the precession signal is much stronger compared to experiment P and the monsoon season is extended (Fig. 3.5b). Both differences are induced by albedo lowering and a stronger local hydrological cycle induced by the larger tree fraction during minimum precession (Fig. 3.7a). The lower albedo induces an earlier warming of the land, so that the onset of the monsoon occurs about 1 month earlier. In autumn vegetation tends to prolong the monsoon season which is probably caused by the enhanced local moisture recycling. The amplification of the monsoon response by vegetation and the extension of the monsoon season were also found in time-slice experiments (e.g., Broström et al., 1998 and Doherty et al., 2000).

The monthly phase differences between precipitation and the precession parameter are smaller in experiment PV than in experiment P (Figs. 3.5a-b). In experiment PV the phase differences are 2600, 1600 and 400 years lead for May, June and July, respectively; and 1200 and 3200 years lag for August and September, respectively. This is caused by the albedo signal. In the model, the albedo of snow free areas is only a function of vegetation cover which is in the tropics mainly determined by the annual precipitation. Because the annual precipitation is in phase with the precession parameter (Fig. 3.6) the albedo signal also is in phase with the precession parameter. The combined insolation and albedo signal cause the smaller leads and lags between the monthly precipitation and the precession parameter.

Despite the very weak obliquity induced insolation signal at low latitudes, there is an obliquity signal in the monsoonal precipitation consisting of stronger (weaker) precipitation during maximum (minimum) obliquity (Fig. 3.5c). This can be explained by the obliquity induced insolation forcing at high to mid-latitudes (chapter 2 of this thesis). As for precession, the precipitation in the obliquity experiments also lags the insolation within a year by one month. However, as explained in the previous section this does not result in leads/lags between the obliquity parameter and the monthly (and annual) precipitation (Figs. 3.5c and 3.6a).

Adding interactive vegetation to the obliquity experiment results in a more than doubling of the signal (Fig. 3.5d). This is due to an alternating increase of the tree fraction and the desert fraction (Fig. 3.7b). As for precession, this changes the albedo and the strength of the local hydrological cycle. Furthermore, the monsoon season also lasts two months longer for TV than for T. In experiment TV compared to experiment T the duration of the wetter periods (i.e. positive anomalies compared

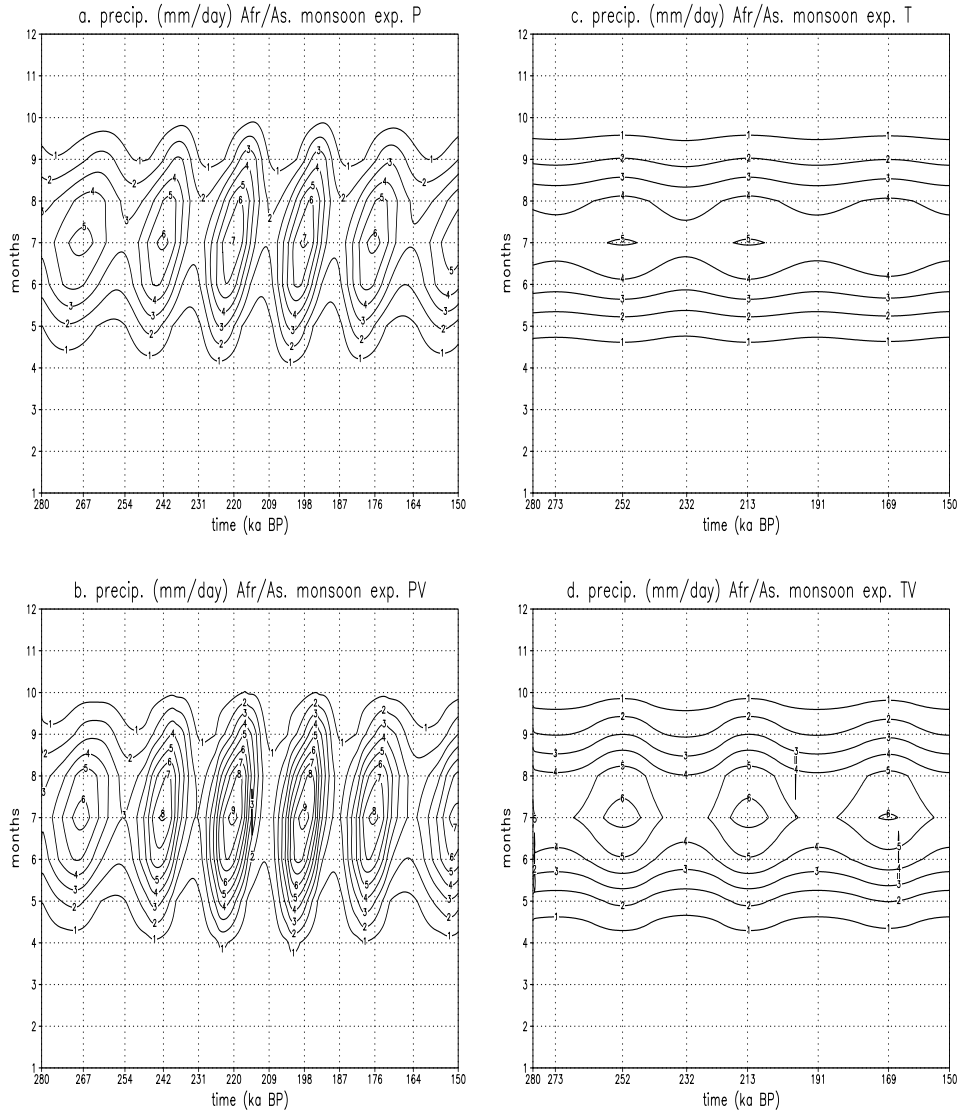


Figure 3.5: *Precipitation for the African/Asian monsoon (in mm/day) for a) experiment P; b) experiment PV; c) experiment T and d) experiment TV (see Table 3.1). The African/Asian monsoon is defined as the average precipitation over the grid boxes ( $10^{\circ}\text{N}$ - $20^{\circ}\text{N}$ , atmospheric sector 2) and ( $20^{\circ}\text{N}$ - $30^{\circ}\text{N}$ , atmospheric sector 3), see Fig. 3.1. Contour interval is 1 mm/day. Horizontal axis labeling as in Fig. 3.3.*

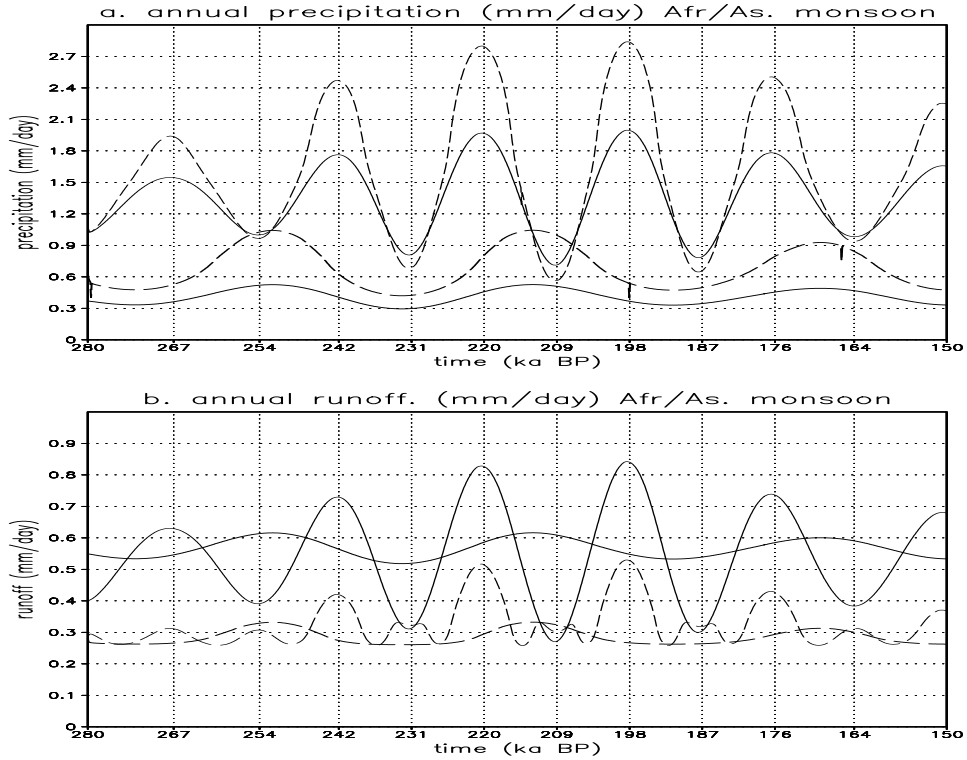


Figure 3.6: *a) Annual precipitation (in mm/day) and b) annual runoff (in mm/day) for the African/Asian monsoon for experiment P (thin solid line), experiment PV (thin dashed line), experiment T (thick solid line) and experiment TV (thick dashed line), see Table 3.1. For plotting purposes 1 mm/day has been subtracted for both obliquity experiments in Fig. a. The African/Asian monsoon is defined as in Fig. 3.5. Horizontal axis labeling as in Fig. 3.3a.*

to the mean precipitation over the whole period) are shorter while the duration of the dryer periods increases by several thousands of years. This is caused by the pattern of the tree fraction (Fig. 3.7b). During dry periods the tree fraction decreases and then remains near zero because it can not become negative. This introduces an asymmetrical pattern around a long term mean for the tree fraction. This causes the asymmetrical pattern for the length of wet and dry periods.

The precipitation response to both obliquity and precession for the Sahara (20°N-30°N, atmospheric sector 2 (Fig. 3.1)) shows the same features as the African/Asian monsoon (not shown). A difference is that the enhancement of the signal in the experiments PV and TV is not dominated by trees, but by grass. During dry periods (i.e., during maximum precession and minimum obliquity) the Sahara is a desert while during wet periods (minimum precession and maximum obliquity) the Sahara is partly



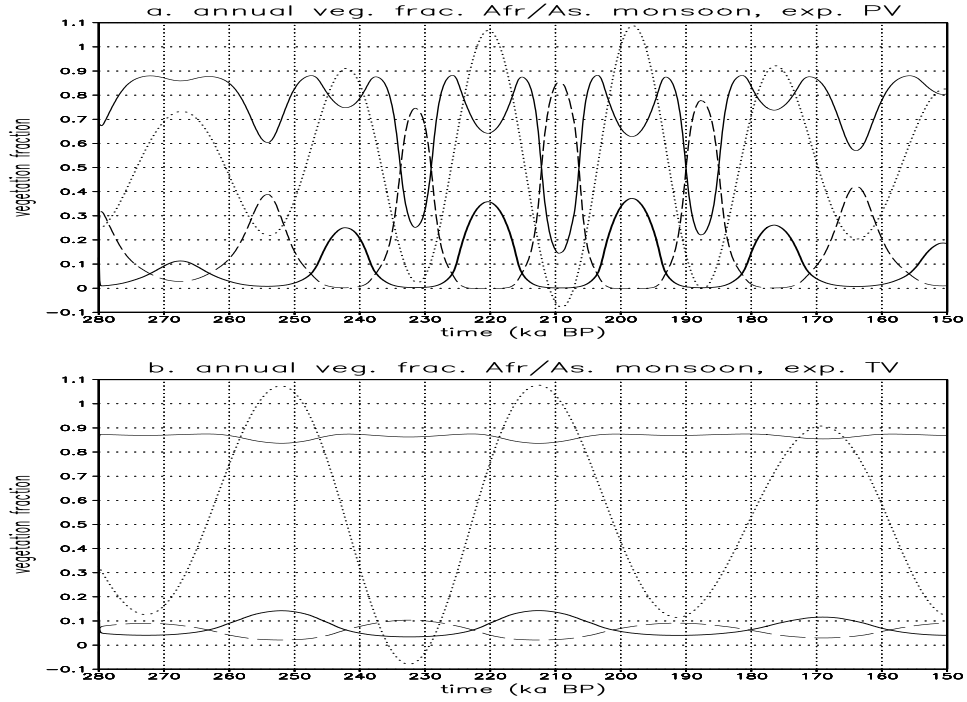


Figure 3.7: Annual tree fraction (thick solid line), grass fraction (thin solid line) and bare soil (i.e., desert) fraction (dashed line) for a) experiment PV and b) experiment TV (see table 3.1) for the African/Asian monsoon. The African/Asian monsoon is defined as in Fig. 3.5. For easy comparison of the phases, in Fig. a the precession parameter multiplied by -1 is plotted (dotted line, arbitrary scale) and in Fig. b the obliquity parameter is plotted (dotted line, arbitrary scale). For comparison, the vegetation fractions for experiments P and T are 0.18 (trees), 0.81 (grass) and 0.01 (desert). Horizontal axis labeling as in Fig. 3.3a. for a and Fig. 3.3c for b.

covered with grass (about 70% for precession and about 50% for obliquity). Contrary to the central monsoon region, albedo changes are more important for the Sahara than changes in the hydrological cycle because the conversion grass-desert strongly changes the albedo while it has a minor effect on the strength of the hydrological cycle as was also found by Brovkin et al. (1998). The obliquity and precession induced monthly patterns of the runoff from the African/Asian monsoon are very similar to the precipitation patterns shown in Figs. 3.5a-d. However, despite the stronger precipitation the annual runoff is weaker in the experiments PV and TV than in P and T, respectively (Fig. 3.6). This can be explained by the enhanced evaporation in the vegetation experiments. Consequently, more water is recirculated in the region and is not available for runoff.

For the monsoon the combined signal PT is a quasi-linear combination of P and

T (i.e., the sum of the anomalies of the experiments P and T is very close to the anomalies of experiment PT). Some differences are found between the sum of the separate signals and experiment PTV. When maximum obliquity and maximum precession prevail at the same time the precipitation anomalies in experiment PTV are more negative than the sum of the separate anomalies. This is caused by the tree fraction which is lower in experiment PTV than the sum of experiments PV and TV.

With reference to a model simulation of tropical climate phase lag between the maximum summer temperature and the precession parameter [176], we also describe the precession signal in the tropical SAT in experiment P. Within a year the SAT follows the insolation forcing with a lag of one month leading to a maximum temperature in July during minimum precession (Fig. 3.8). During maximum precession the SAT shows two maxima reflecting the first and second overhead passage of the Sun at  $15^{\circ}\text{N}$  (see previous section). The second maximum is weaker than the first, which is mainly due to the negative feedback of the monsoonal precipitation on the SAT. It has been hypothesized that monsoon precipitation would follow the local temperature signal so that runoff to the Mediterranean Sea would lag the precession parameter [121]. However, in the present model experiment we observed a one-month lag of maximum precipitation with respect to the precession parameter consistent with the large-scale insolation forcing rather than the local forcing. This implies that the responses of local precipitation and SAT to the precession induced insolation forcing are not similar. This can be even more strongly observed in experiment PV where the SAT does not increase after May due to the strong monsoonal feedback (not shown).

### 3.5 High latitudes

In this section the orbital influence on the temperature at high latitudes and the Atlantic thermohaline circulation will be discussed.

#### Air temperature

Fig. 3.9a shows the precession induced anomalies in monthly SAT over land for January-April (JFMA). For later use non-standard season definitions are discussed. However, the temperatures for the conventional seasons respond in a very similar manner. In experiment P the SAT lags the seasonal insolation by about 1 month, which results in leads/lag in time with respect to the precession parameter as explained before. The annual signal of the SAT for  $0-60^{\circ}\text{N}$  (not shown) responds linearly to the small (eccentricity induced) annual insolation. At high latitudes the annual SAT anomalies are relatively large (about  $\pm 0.5^{\circ}\text{C}$  for minimum/maximum precession, respectively) which is caused by albedo changes induced by snow. There is no lag between the annual SAT and the precession parameter. The most important difference between experiments P and PV is the phase of the signal over  $50^{\circ}\text{N}-80^{\circ}\text{N}$  and to a lesser degree over  $20^{\circ}\text{N}-30^{\circ}\text{N}$  in JFMA (Figs. 3.9a-b). These phase differences between P and PV are caused by albedo changes induced by changes in the vegeta-

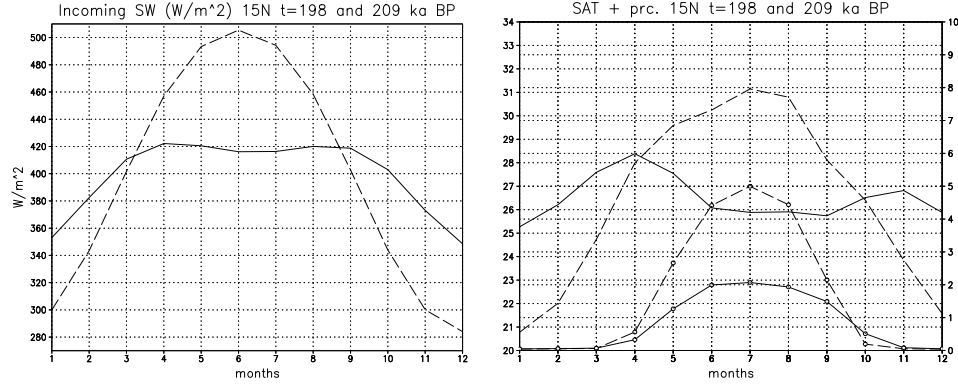


Figure 3.8: *Left panel: Monthly incoming shortwave radiation (in  $W/m^2$ ) at the top of the atmosphere for  $15^\circ N$  at 198 ka BP, i.e. during minimum precession (dashed line) and at 209 ka BP, i.e. during maximum precession (solid line). Right panel: Monthly surface air temperature (in  $^\circ C$  left axis) at 198 ka BP (dashed line) and at 209 ka BP (solid line) and precipitation (in mm/day, right axis) at 198 ka BP (dashed line with open circles) and at 209 ka BP (solid line with open circles). For the right panel the values are from experiment P and for gridbox ( $10^\circ N$ - $20^\circ N$ , atmospheric sector 2, see Fig. 3.1). Horizontal axes display the months.*

tion cover. During minimum precession the warm summers (and the increased annual precipitation) promote the growth of trees at the expense of the grass fraction over  $50^\circ N$ - $80^\circ N$ . We also see a northward displacement of the tree line (not shown). While in JFMA the snow fractions differ only slightly between the experiments P and PV, the tree fraction is larger in the area covered by snow in experiment PV than in experiment P. This induces a lower albedo and consequently higher SAT in experiment PV. After minimum precession the tree fraction gradually decreases. Consequently, in boreal winter less snow is covered by trees causing an increase of the albedo for PV. This lowers the temperature resulting in the occurrence of the lowest temperatures some thousands of years later than in experiment P (Figs. 3.9a-b). This implies that at high latitudes the lag of the SAT in JFMA in experiment PV with respect to the precession parameter is about 5 ka. For MJJA (not shown) the amplitude of the SAT signal is higher in experiment PV than in experiment P due to the positive vegetation-albedo feedback. The annual SAT signal in experiment PV (not shown) is relatively large, taken into account that the annual insolation signal is very small. This large signal is a reflection of the strong summer SAT signal which is not compensated in the other seasons. There is no lag between the annual SAT and the precession parameter.

The seasonal SAT over land in experiments T and TV shows no leads/lags with respect to the obliquity parameter except at high latitudes where the SAT signal is opposite to the insolation. Therefore the SAT at high latitudes is out of phase with the obliquity parameter (i.e., a 20 ka lag). This is related to the SST signal, see below.

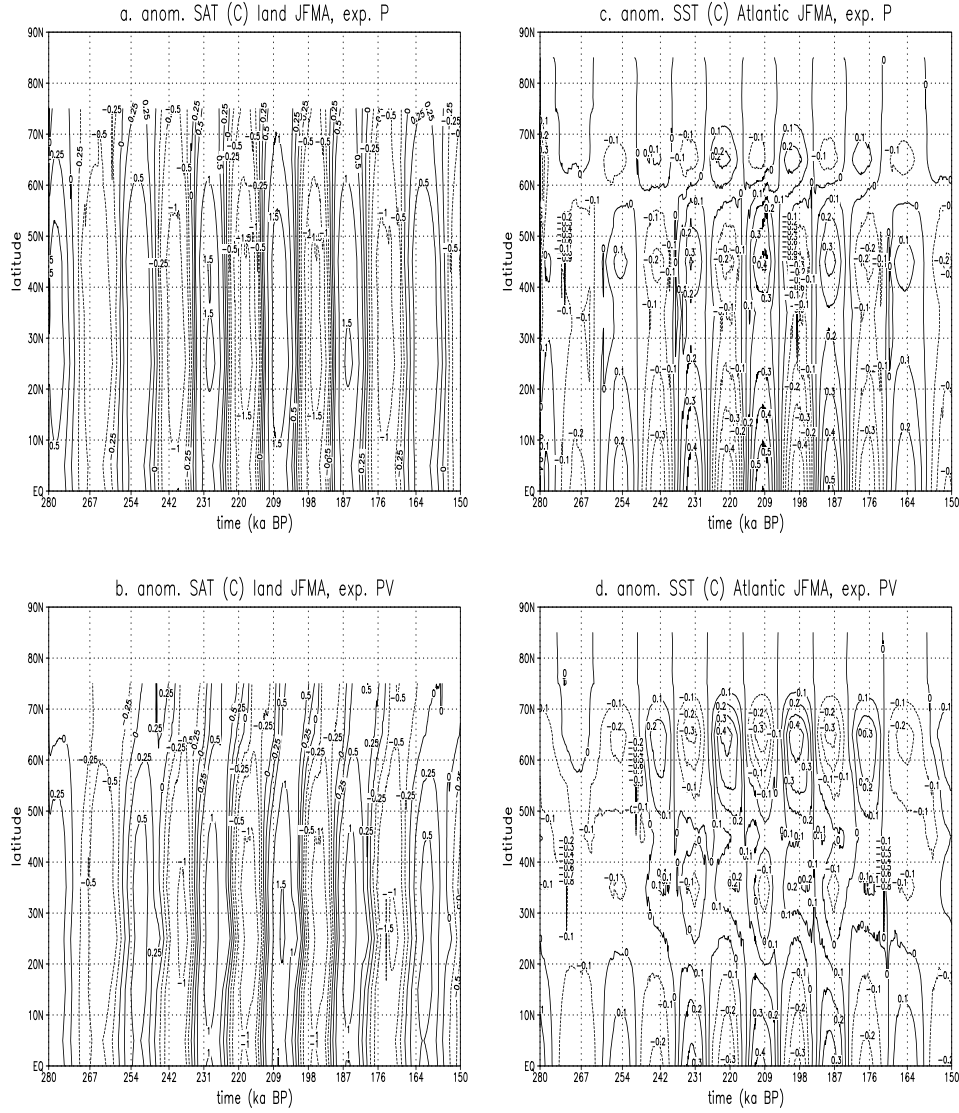


Figure 3.9: Anomalous January-April surface air temperatures ( $^{\circ}\text{C}$ ), zonally averaged over land for a) experiment P and b) experiment PV. Anomalous January-April sea surface temperatures ( $^{\circ}\text{C}$ ) for the Atlantic basin in atmospheric sector 1 (Fig. 3.1) averaged over January to April for c) experiment P and d) experiment PV (see Table 3.1). The anomalies are computed with respect to the January-April values averaged over the whole period (280-150 ka BP). For a) and b) contour lines are plotted for  $0^{\circ}\text{C}$ ,  $\pm 0.25^{\circ}\text{C}$ ,  $\pm 0.5^{\circ}\text{C}$ ,  $\pm 1^{\circ}\text{C}$ ,  $\pm 1.5^{\circ}\text{C}$  and  $\pm 2.0^{\circ}\text{C}$ . Contour interval for c) and d) is  $0.1^{\circ}\text{C}$ . Negative anomalies are dashed. The vertical axis displays latitude. Horizontal axis labeling as in Fig. 3.5a.

The annual SAT responds linearly to the annual insolation with no phase differences with respect to the obliquity parameter.

The combined SAT signal in experiment PT is a linear combination of experiments P and T for all seasons and all latitudes. Comparing experiment PTV to the sum of PV and TV reveals some small differences for mid- and high latitudes during maximum obliquity. This is mainly related to sea-ice effects, as the anomalous amount of sea-ice coverage in PTV is not exactly similar to the sum of PV and TV.

### Sea surface temperature

In experiment P the Atlantic SST from 0-60°N in JFMA (Fig. 3.9c) responds linearly to the insolation forcing (with a lag of 3-4 months), resulting in virtually no lag with respect to the precession parameter. From 60°N-70°N the SST signal is opposite to the insolation signal which is caused by sea-ice. In summer the water is strongly warmed by the strong insolation during minimum precession (not shown). This results in relatively high SST during autumn and winter and in less sea-ice. For 70°N-90°N this effect is negligible because here the Atlantic Ocean is almost completely covered with sea-ice. The annual signal consists of positive (negative) SST anomalies ( $\sim 0.4^\circ\text{C}$ ) over 50°N-90°N during minimum (maximum) precession and no signal over the other latitudes. For minimum precession this is a reflection of the summer heating which is not fully compensated by the cooling in winter. No lag is found between the precession parameter and the annual SST.

In experiment PV at mid-latitudes the JFMA SST signal is small while from 60°N-70°N the signal is stronger than in experiment P (Figs. 3.9c-d). The latter is a result of the stronger sea-ice signal induced by the stronger SST signal in summer, which can be associated with the stronger SAT signal in experiment PV compared to experiment P. The pattern of the annual signal in experiment PV is similar to experiment P but the amplitude is about twice as large, which is caused by the stronger summer signal in experiment PV.

The obliquity induced seasonal SST signal in experiment T and TV show the same features as for precession (not shown). In particular, the JFMA SST signal over 60°N-70°N is opposite to the insolation. Just as for precession, this is induced by less sea-ice during maximum obliquity caused by the strong summer heating. The annual SST signal consists of higher SST at mid- and high latitudes during maximum obliquity, consistent with the annual insolation signal. No lag between the obliquity parameter and the annual SST were found.

The combined precession and obliquity SST signals (PT and PTV) show the same features as for SAT: For fixed vegetation the combined signal is a linear combination of the separate signals while in experiment PTV during maximum obliquity some small non-linear behaviour is found which is mainly induced by sea-ice.

### Atlantic thermohaline circulation

The strength of the Atlantic THC and the meridional density gradient between the South Atlantic and the sinking region in the North Atlantic are closely tied together.

Hughes and Weaver (1994) found an almost linear relationship between the strength of the Atlantic overturning and the difference between the density of the northern sinking branch and the density at the boundary of the South Atlantic ( $30^{\circ}\text{S}$ ). They proposed that the latter latitude is not very strict ( $1.75^{\circ}\text{N}$  gave an equally good result), which was confirmed by Rahmstorf (1996).

The maximum of the annual Atlantic meridional mass transport for the precession experiments P and PV is shown in Fig. 3.10a. During minimum precession the overturning is stronger than during maximum precession in experiment P. In experiment PV the overturning lags the precession parameter for some thousands of years. The changes in the (vertically averaged) annual density gradient between the northern Atlantic ( $50^{\circ}\text{N}$ - $65^{\circ}\text{N}$ ) and the Southern Atlantic ( $20^{\circ}\text{S}$  to the equator) for experiments P and PV (not shown) are consistent with the changes in the overturning strength. In order to find the cause for the changed annual meridional density gradient we first examined whether the precession induced annual meridional insolation gradient and/or the annual freshwater forcing could cause these changes. The meridional insolation gradient is close to zero because precession does not influence the annual insolation. The contribution of the annual freshwater forcing (not shown) to the buoyancy forcing is even smaller than the contribution of the insolation forcing. Both forcings do not show a phase difference between the experiments P and PV from which we conclude that they do not cause the precession induced changes in the Atlantic THC.

Next we examined winter convection in the North Atlantic ocean. Convection is strongest in the model in the months JFMA, when temperatures over the American continent are very low and cold air is transported by the westerly circulation from the continent to the Atlantic Ocean. This induces a strong cooling and an associated strong convection in the northern Atlantic Ocean. In experiment PV the SAT signal over America in JFMA lags the precession parameter (Fig. 3.11). This results in a displacement of the strongest convection and the associated strongest overturning some thousands of years after minimum precession.

Fig. 3.10b shows the THC response in the experiments T and TV consisting of stronger (weaker) overturning during minimum (maximum) obliquity. The obliquity induced THC signal can be explained by changes in the Atlantic meridional density gradient. During maximum obliquity the stronger insolation at high latitudes warms the water (i.e., the density decreases) while the weaker insolation at low latitudes induces cooler water (i.e., higher density). This results in a weaker meridional density gradient (not shown) and consequently a weaker overturning. The obliquity induced differences of the winter convection in the northern Atlantic are about four times smaller (with stronger convection during maximum obliquity) than the precession induced differences. The obliquity induced freshwater forcing of the North Atlantic (not shown) counteracts the thermal signal, but is negligible compared to the thermal forcing.

Both experiments PT and PTV are a linear combination of the separate experiments. Consequently, the amplitude of the combined signal is mainly an obliquity signal (especially for PTV), while a precession induced phase difference is found between experiments PT and PTV.

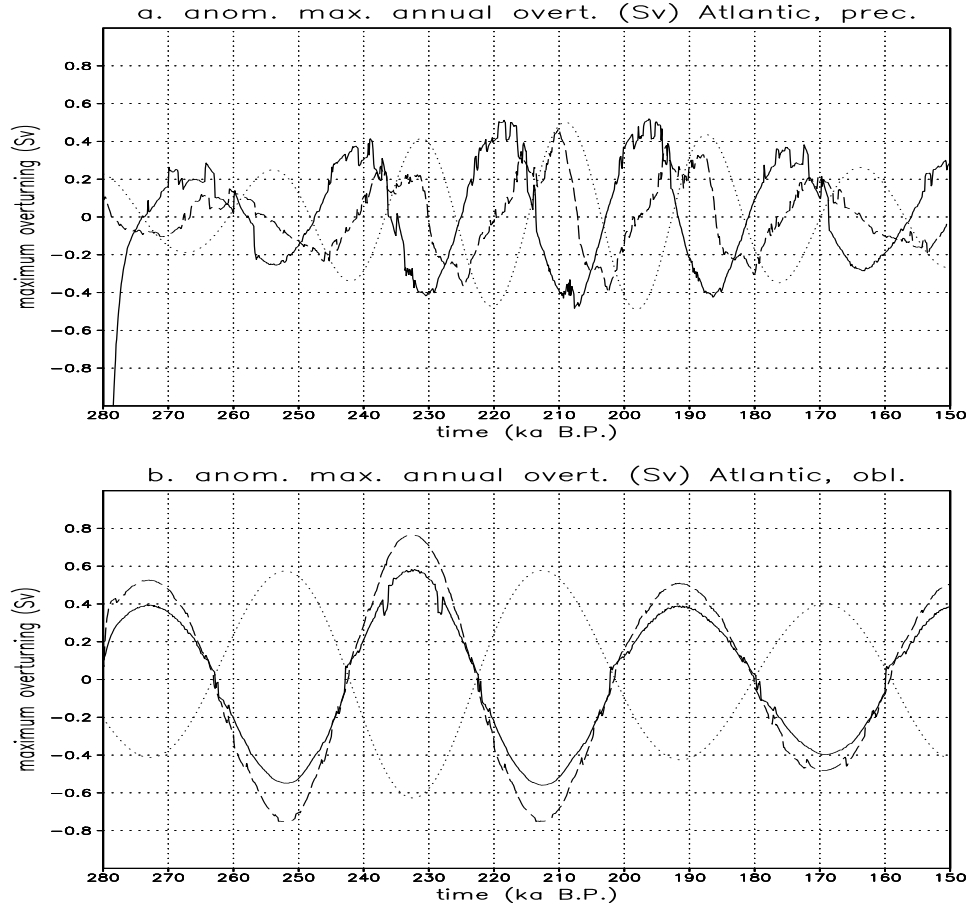


Figure 3.10: Maximum of the annual meridional mass transport (in Sverdrups =  $10^6$   $m^3/s$ ) in the Atlantic Ocean for a) experiment P (solid line) and experiment PV (dashed line) and b) experiment T (solid line) and experiment TV (dashed line), see Table 3.1. For comparison of the phases, the absolute precession parameter multiplied by 10 (in Fig. a) and the anomalous obliquity parameter divided by 2 (in Fig. b) are plotted (both dotted lines). The anomalies are computed with respect to the values averaged over the whole period (280-150 ka BP). The horizontal axis displays time (in 1000 years Before Present).

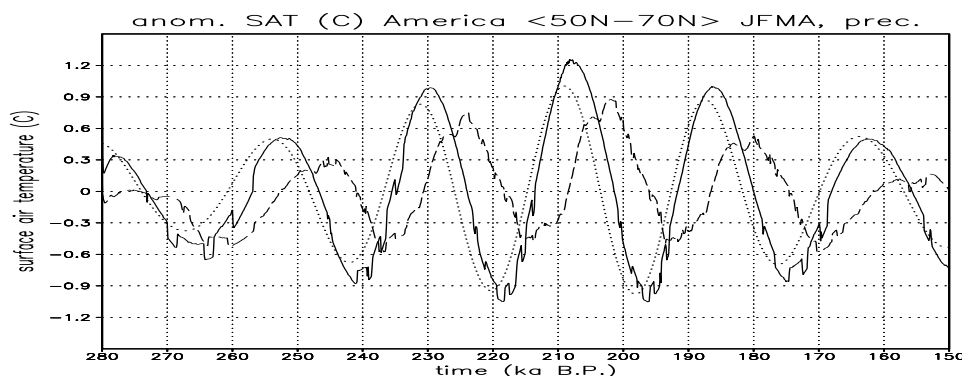


Figure 3.11: Anomalous surface air temperature (SAT, in  $^{\circ}\text{C}$ ) averaged over the grid boxes ( $50^{\circ}\text{N}$ – $70^{\circ}\text{N}$ , atmospheric sector 7, see Fig. 3.1) for January–April for experiment P (solid line) and experiment PV (dashed line), see Table 1. For comparison of the phases, the absolute precession parameter multiplied by 20 is plotted (dotted line). The anomalies are computed with respect to the values averaged over the whole period (280–150 ka BP). The horizontal axis displays time (in 1000 years Before Present).

### 3.6 Conclusions and discussion

In this paper we investigated whether a lead and/or lag can exist between the orbital forcing and the response of the climate system to this forcing without using interactive ice sheets. In order to study the influence of vegetation we performed experiments with a coupled atmosphere-ocean model and an atmosphere-ocean-vegetation model. Our approach was to study the response to the separate obliquity and precession forcing.

For precession there are phase differences between the monthly insolation and the precession parameter. In general, this translates the lag of the climate response to the insolation within a year into a lead/lag between the climate response and the precession parameter in time. For example, the insolation in July lags the precession parameter by about 2 ka. The SAT over land in August responds to the insolation in July and consequently the SAT in August lags the precession parameter by 2 ka. For obliquity the insolation in all months show no phase difference with the obliquity parameter. Therefore the lag of the climate response within a year does not result in a phase difference with respect to the obliquity parameter in time. In this study we have showed that this simple mechanism can be strongly modified by vegetation (at high and low latitudes) and/or albedo changes induced by sea-ice and snow (at high latitudes).

At low latitudes the response of the monsoon system leads the precession parameter in May and June and lags it in August and September. Including interactive vegetation strongly shortens the leads and lags due to the albedo feedback. However, both for fixed and interactive vegetation the monthly phase differences (and amplitudes) cancel out resulting in no phase differences between the annual precipi-



tation and the precession parameter. For obliquity no lags were found between the monthly or annual precipitation and the obliquity parameter. There is a lengthening of the periods with weak monsoons (i.e., during minimum obliquity) and a shortening of the periods with relatively strong monsoons (i.e., during maximum obliquity) in experiment TV compared to experiment T.

SAT and SST at low and mid-latitudes follow insolation closely with a lag of 1-2 months and 3-4 months, respectively. This implies leads and lags with respect to the precession parameter and no leads/lags with respect to the obliquity parameter. North of  $60^{\circ}\text{N}$  the response is more complex due to vegetation, snow and sea-ice albedo feedbacks. For example, the lag of the SAT in JFMA is about 1 ka and 5 ka in experiment P and experiment PV compared to the precession parameter, respectively, while in both precession experiments the SST is out of phase by 180 degrees (10 ka). In experiment T and TV both the SAT and the SST is out of phase by 180 degrees (20 ka) compared to the obliquity parameter.

Finally, the Atlantic THC was found to be stronger during minimum precession than during maximum precession in experiment P while the THC lags the precession parameter by several thousands of years. in experiment PV. Maxima are caused by cold winters over the continent which induce enhanced convection and a stronger THC. The precession induced lag which is found in the surface air temperature also results in a lag of the THC in experiment PV with respect to the precession parameter. The obliquity signal consists of a stronger (weaker) THC during minimum (maximum) obliquity. However, in contrast to precession, this signal is induced by a stronger (weaker) annual insolation gradient during minimum (maximum) obliquity. Anomalies in the Atlantic THC are larger in the obliquity driven experiments than in the precession driven experiments. This is consistent with results of Brickman et al. (1999) who showed that the energy in the obliquity frequency is larger than in the precession frequency, using the same ocean model (but another atmosphere model).

To summarize, in addition to the general mechanism for obtaining leads and lags for the climate response to the precession signal, we found a strong influence of vegetation and sea-ice. The strength of the African/Asian monsoon exhibits monthly leads and lags with respect to the precession parameter which are modified by vegetation. For the annual precipitation there was no lead or lag. At high latitudes the monthly leads/lags of SAT and SST with respect to the precession parameter are strongly influenced by vegetation and sea-ice. Sea-ice also introduces phase differences of SAT and SST with respect to the obliquity parameter in late winter/early spring. Only in the Atlantic THC we found an *annual* lag in the precession experiment with interactive vegetation. No annual lag is found unless an internal process acts as a filter for certain seasons.

In paleoclimatic data, Imbrie et al. (1992) found lags in the northern Atlantic SST with respect to both the precession and the obliquity parameter for the Pleistocene. We have shown that in the Atlantic Ocean lags with respect to the precession parameter can occur due to changes in the timing of the seasonal cycle (in experiment PV) or due to sea-ice (in experiments P and PV as well as in experiments T and TV). Similar mechanisms might be responsible for the lags found in the paleoclimatic data. The present model results confirm that the SST signal results from

complex interactions between insolation, vegetation coverage, air temperatures, sea-ice, convection and the ocean circulation. The simplicity of CLIMBER-2 (e.g., a 2-dimensional Atlantic basin, simple sea-ice model) hinders a direct comparison of the computed leads/lags to those observed in paleoclimatic data. Furthermore, ice sheet dynamics could introduce leads/lags in data which are not taken into account in the present study.

Clemens et al. (1991) observed a lag of about 7-8 ka for the precession signal in marine proxies in the Arabian Sea. These proxies are direct indicators for the upwelling of cold water and thus indirect indicators for the strength of the summer monsoon winds. In our study no lag between the strength of the monsoon and the precession parameter was found. However, Braconnot and Marti (2004) showed with a coupled ocean-atmosphere model that the Indian ocean is sensitive to the precession induced timing of the maximum summer insolation (in early summer or in late summer). The surface temperature and, in particular, the surface salinity of the Indian Ocean strongly depends on the timing of the insolation forcing. Consequently, the circulation of the Indian Ocean also depends on this. This might be an explanation for the lag found by Clemens et al. (1991). For obliquity, Clemens et al. (1991) found no significant lag which is consistent with our simulation of the monsoon.

Lourens et al. (1996) inferred a constant lag of 3 ka between sapropel formation in the Mediterranean Sea with respect to the precession parameter, based on the age of the youngest Holocene sapropel. The formation of sapropels is associated with a weakening of the thermohaline circulation and a decrease of the deep water formation in the Mediterranean basin. Both the rate of the deep water formation and the strength of the thermohaline circulation are influenced by changes in the surface buoyancy forcing, such as changes in cold air outbreaks from the European continent or changes in the runoff from the river Nile. Following the latter scenario, the time lag for the sapropels was related to the  $\sim 3$  ka time lag of the maximum summer temperature in northern Africa with respect to the precession parameter. Such a lag was obtained in Short and Mengel (1986), who suggested that the maximum summer temperature is an indication for the moisture availability to the monsoon area during the rainy season. In the present study it is shown that the maximum in local summer temperature can indeed lag the precession parameter, but that the precipitation responds to the large-scale forcing. Consequently, the annual runoff from the African monsoon is in phase with the precession parameter. Therefore, it is unlikely that the lag in the sapropel record is caused by lags in the African monsoon. We hypothesize that this lag in the sapropel record can be explained by cold air outbreaks or winter runoff from the European continent. A similar mechanism as found in the Atlantic THC might apply to the Mediterranean deep water formation. Model studies with a high resolution Mediterranean basin forced by regional atmospheric model output, are needed to test this hypothesis.

## Chapter 4

# The influence of precession and obliquity on the Atlantic/European winter climate

### Abstract\*

In this chapter the separate obliquity and precession signal in the Atlantic/European climate is studied with a global coupled climate model of intermediate complexity (ECBilt-CLIO). Focus is on changes in the climatic variability and the mean climate in the cold season. Changes in the climatic variability are most pronounced over the convection sites in the northern Atlantic Ocean, where the atmospheric flow triggers sudden expansions in sea-ice coverage over the northern convection site, lasting 10-50 yrs in the control run. This results in reduced convection and, with a lag of about 30 years, decreased Atlantic thermohaline circulation. During maximum precession and minimum obliquity stronger events of longer duration were found while during minimum precession and maximum obliquity no events were simulated. Summer insolation was found to determine the strength and duration of the events. The mean climatic state to orbital forcing shows an earlier winter state during minimum precession compared to maximum precession, resulting in a NAO-like atmospheric circulation and enhanced precipitation in northern Europe in autumn. In southern Europe a different mechanism influences precipitation in autumn, namely the strong land-sea temperature contrast in the Mediterranean Sea region during minimum precession and maximum obliquity (compared to maximum precession and minimum obliquity, respectively), which results in enhanced precipitation.

---

\*This chapter is in preparation for publication as: Tüenter, E., S.L. Weber, F.J. Hilgen and L.J. Lourens (2004). The influence of precession and obliquity on the Atlantic/European winter climate [189]

## 4.1 Introduction

The deposition of successive sapropels (organic-rich, black layers) in the deep eastern Mediterranean Sea (MS) exhibits a distinct precession related signal. Individual sapropels are deposited during minimum precession, i.e., when summer solstice occurs at perihelion [165, 69]. In addition, Lourens et al. (1996, 2001) found an obliquity signal in the sapropel record with thicker sapropels during increased obliquity. Sapropel deposition is generally thought to be associated with the strength of the African monsoon, which can influence the ThermoHaline Circulation (THC) in the MS through variations in discharges of the river Nile. Precession as well as obliquity signals have indeed been found in the African summer monsoon in simulations with a General Circulation Model (GCM) as described in chapter 2 of this thesis.

Runoff from the northern borderlands which enters the MS could also play an important role in the formation of sapropels [173, 37]. In contrast to the runoff from the river Nile, the runoff from the north is high in the cold season when deep water is formed. Besides, part of the run-off from the north enters the MS near or at the locations of deep water formation (i.e., the Gulf of Lyon, the Adriatic Sea and the Aegean Sea [86]). For this reason, runoff from the north could be more effective in changing the convection strength than the Nile discharge. Therefore, orbital signals in the hydrological cycle at mid- and high latitudes could also affect the formation of sapropels.

A few model studies have investigated the influence of orbital parameter changes on the northern high-latitude climate. For example, Mitchell et al. (1988) and Kutzbach and Gallimore (1988) performed simulations for 9000 years Before Present (9 ka BP), when NH summer insolation was stronger and NH winter insolation was weaker than at present. They found a reduction in the extent and thickness of Atlantic sea-ice in summer, autumn and early winter while the Arctic sea-ice was thinner throughout the year compared to present. The reduced sea-ice coverage results in higher temperatures at northern high latitudes in autumn and winter. Montoya et al. (2000) also found reduced NH sea-ice cover throughout the year in a simulation of the last interglacial (125 ka BP), a period with more extreme orbital conditions than at 9 ka BP. These simulations use a combined obliquity and precession forcing whereby precession dominates the insolation signal, even at high latitudes. Kutzbach et al. (1991) and Gallimore and Kutzbach (1995) separated the influence of obliquity and precession on the climate at high latitudes. They concluded that obliquity has a larger impact on NH sea-ice than precession, with again summer insolation dominating the annual signal in sea-ice cover.

The purpose of the present study is to investigate the influence of the separate obliquity and precession forcing on the Atlantic/European climate with a coupled atmosphere/ocean/sea-ice model. Focus is on the climatic response in the cold season in order to examine the potential influence of the European climate on the formation of sapropels in the MS. Furthermore, we will describe the mean climatic response as well as changes in climatic variability.

## 4.2 Model and experimental set-up

The global climate model to be used consists of the atmospheric component ECBilt and the ocean/sea-ice component CLIO. The atmospheric component ECBilt2 [169] is a global spectral quasi-geostrophic model truncated at T21. There are 3 layers in the vertical. ECBilt has simple parameterisations for the diabatic heating due to radiative fluxes, the release of latent heat and the exchange of sensible heat with the surface. The model contains a full hydrological cycle which is closed over land by a bucket model for soil moisture.

The ocean/sea-ice model is CLIO [59], a primitive equation, free-surface ocean general circulation model with a thermodynamic-dynamic sea-ice model. The horizontal resolution is  $3^\circ \times 3^\circ$  and it has 20 unevenly spaced vertical levels. The ocean model has a relatively sophisticated parameterization of vertical mixing [58]. The three-layer sea-ice model takes into account sensible and latent heat storage in the snow-ice system. It simulates the changes of snow and ice thickness in response to surface and bottom heat fluxes. sea-ice is considered to behave as a viscous-plastic continuum. Use of a thermodynamic-dynamic sea-ice model can result in very different sea-ice patterns compared to a thermodynamic sea-ice model (see e.g. Vavrus (1999) and Holland et al. (2001)).

There is no local flux correction in ECBilt-CLIO. However, the model overestimates the precipitation over the Atlantic and Arctic oceans and underestimates the precipitation over the North Pacific [143]. Therefore the precipitation is artificially reduced by 10% over the Atlantic basin and 50% over the Arctic basin. The corresponding water is redistributed homogeneously over the North Pacific. A comparison of model climatology with observations can be found in Goosse et al. (2000).

We adopt the same experimental set-up as used in chapter 2 of this thesis, see also Prell and Kutzbach (1987) and Short et al. (1991). The precession and obliquity signals are separated by performing two experiments with extreme values of one parameter while the other parameter is kept fixed (Table 4.1). The terms 'minimum' and 'maximum' precession are used to refer to the minimum and maximum value of the precession parameter  $e \sin(\pi + \tilde{\omega})$ . Note from Table 4.1 that the eccentricities of the maximum and minimum precession are slightly different. The eccentricities used to examine the obliquity signal have a small non-zero value, because a zero eccentricity caused numerical instabilities in the model. An eccentricity of 0.001 (and present day  $\tilde{\omega}$ ) induces a small precession signal in the simulations for obliquity. However, this signal is negligible compared to the obliquity induced insolation signal.

The initial state for all simulations is the present day state. The only forcing is the insolation change due to the orbital parameters, which were kept constant during the simulations. All other boundary conditions like ice sheets, vegetation and concentration of trace gases were kept to present day values. All experiments were run for 500 yrs. The mean response, which is discussed in section 3, is defined as the average over the last 100 yrs. In order to examine changes in climatic variability, the P-T- and P0T+ experiments were continued for another 500 yrs and the control run, P+T- and P0T- experiments for another 1500 yrs.

Simulation	Tilt (deg)	$e \sin(\pi + \tilde{\omega})$	$e$	$\tilde{\omega}$ (deg)
P+T-	22.08	0.058	0.058	273.50
P-T-	22.08	-0.055	0.056	95.96
P0T+	24.45	0.0013	0.0010	257.96
P0T-	22.08	0.0013	0.0010	257.96
PD	23.45	0.017	0.017	257.96

Table 4.1: *Orbital parameters used for the 5 experiments. P+, P-, T+ and T- refer to maximum precession, minimum precession, maximum tilt (or obliquity) and minimum tilt, respectively. PD stands for present day (i.e, the control run). A precession maximum (minimum) means winter (summer) solstice in perihelion. The tilt is defined as the angle between the ecliptic and the equator,  $e$  is the eccentricity of the orbit of the Earth and  $\tilde{\omega}$  is the angle between the vernal equinox and perihelion (measured counter clockwise). The extreme parameter values occurred during the last 1 million years (Berger, 1978).*

### 4.3 The mean climatic response

The precession and obliquity induced signals in Surface Air Temperature (SAT) primarily reflect the insolation forcing, in agreement with earlier results described in chapter 2 of this thesis. However, in the transition seasons September-October-November (SON) and March-April-May (MAM), when the forcing is relatively weak (Fig. 4.1), internal feedbacks strongly modify the response. This is evident at high northern latitudes, where the sea-ice albedo feedback plays an important role. As a result, when *summer* insolation is high SON temperatures are high over the land adjacent to the oceans (Fig. 4.2). A similar result holds for MAM temperatures (not shown). This is related to the response in sea-ice fraction in the Atlantic and Arctic oceans. The largest signals in the sea-ice fraction (Fig. 4.3) occur in summer with much less sea-ice during minimum precession and maximum obliquity, when summers are relatively warm (compare Fig. 4.1). The obliquity signal is comparable to the precession signal but with a smaller amplitude. Between 60°N and 80°N the sea-ice coverage is reduced during the whole year which is not in agreement with the insolation forcing. The strong summer insolation forcing results in enhanced summer melt and high Sea Surface Temperatures (SSTs), which persist throughout the winter northward of about 45°N (Fig. 4.3). The thermal inertia of the ocean surface layer thus reduces sea-ice growth during the cold season, especially at the margins of the permanent sea-ice cover. A reduced sea-ice fraction (lower albedo) in turn favours high SAT over the surrounding land mass. From the equator to about 45°N the SST response is in agreement with the insolation forcing, taking into account a lag of about two months (Fig. 4.3). In addition to the sea-ice feedback, there is a small effect in SON of atmospheric circulation changes on temperatures over Europe. The geopotential height for the 800 hPa level (from now on gh800) shows large differences between minimum and maximum precession (Fig. 4.4). During maximum precession the gh800 pattern is dominated by the Azores High (AH), which is located around

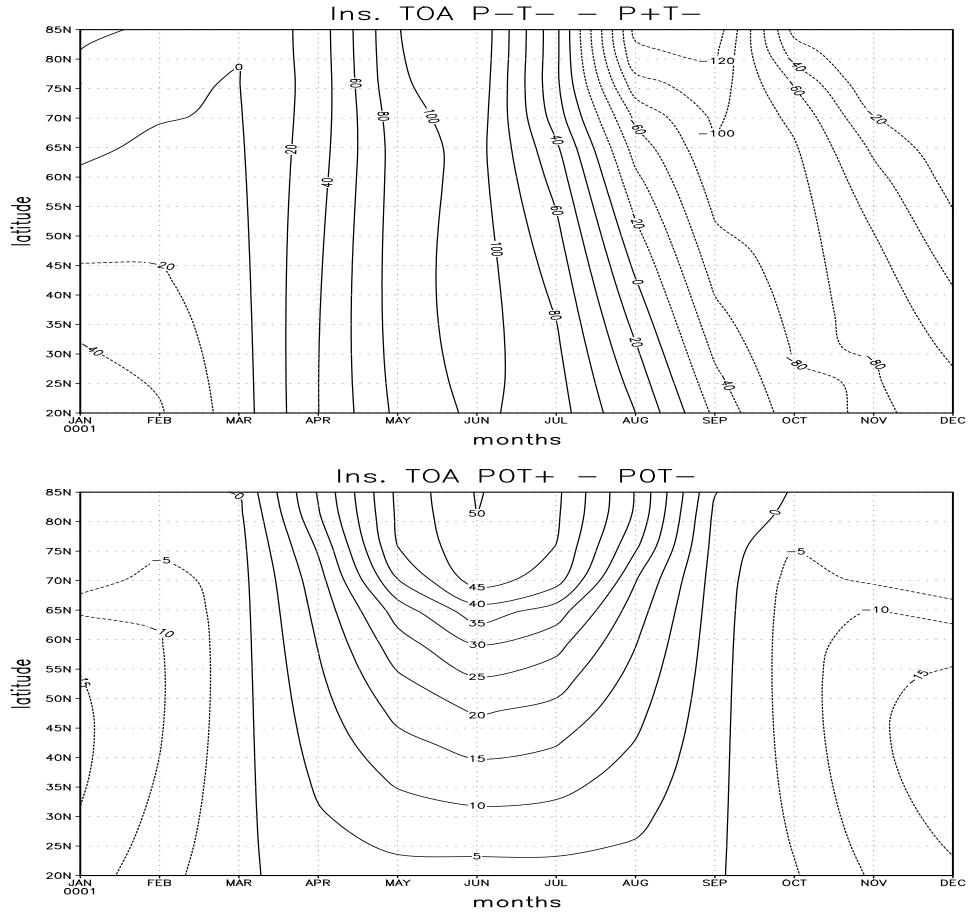


Figure 4.1: Monthly incoming insolation differences (in  $\text{W/m}^2$ ) at the top of the atmosphere (TOA) for the orbital configurations used in this study. Top panel: Minimum precession minus maximum precession, contour interval is  $20 \text{ W/m}^2$ . Bottom panel: Maximum obliquity minus minimum obliquity, contour interval is  $5 \text{ W/m}^2$ .

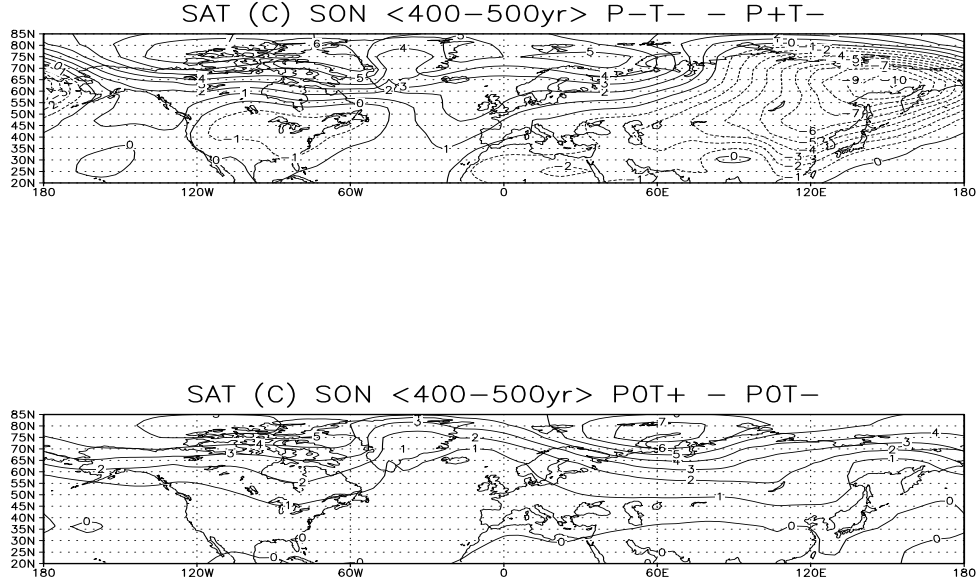


Figure 4.2: *Difference of the Surface Air Temperature for September-October-November in °C. Top panel: Minimum precession minus maximum precession, bottom panel: Maximum obliquity minus minimum obliquity. The values are averages of model years 400-500. Contour interval is 1°C.*

45°N. This implies that summer conditions still prevail. During minimum precession the gh800 pattern already turns into a winter state, with low pressure north of 50°N and the AH located around 35°N. This is a direct result of the increased seasonal contrast during minimum precession, compared to maximum precession, with decreased SAT over land in SON while the air overlying the Atlantic ocean is still warm. The earlier winter conditions result in a higher NAO-index in SON during minimum precession compared to maximum precession. This favours a stronger inflow of warm air from the Atlantic Ocean into northern Europe resulting in relative high temperatures over northern Europe and low temperatures over southern Europe [74]. In December-January-February (DJF) the strength of the Icelandic Low (IL) is not influenced by precession, but its centre is located more eastward during minimum precession compared to maximum precession (Fig. 4.4). The AH is weaker and located more westward, causing a slightly lower NAO index. In MAM the precession signal in the gh800 is very small. The obliquity signal in the Atlantic gh800 is negligible in



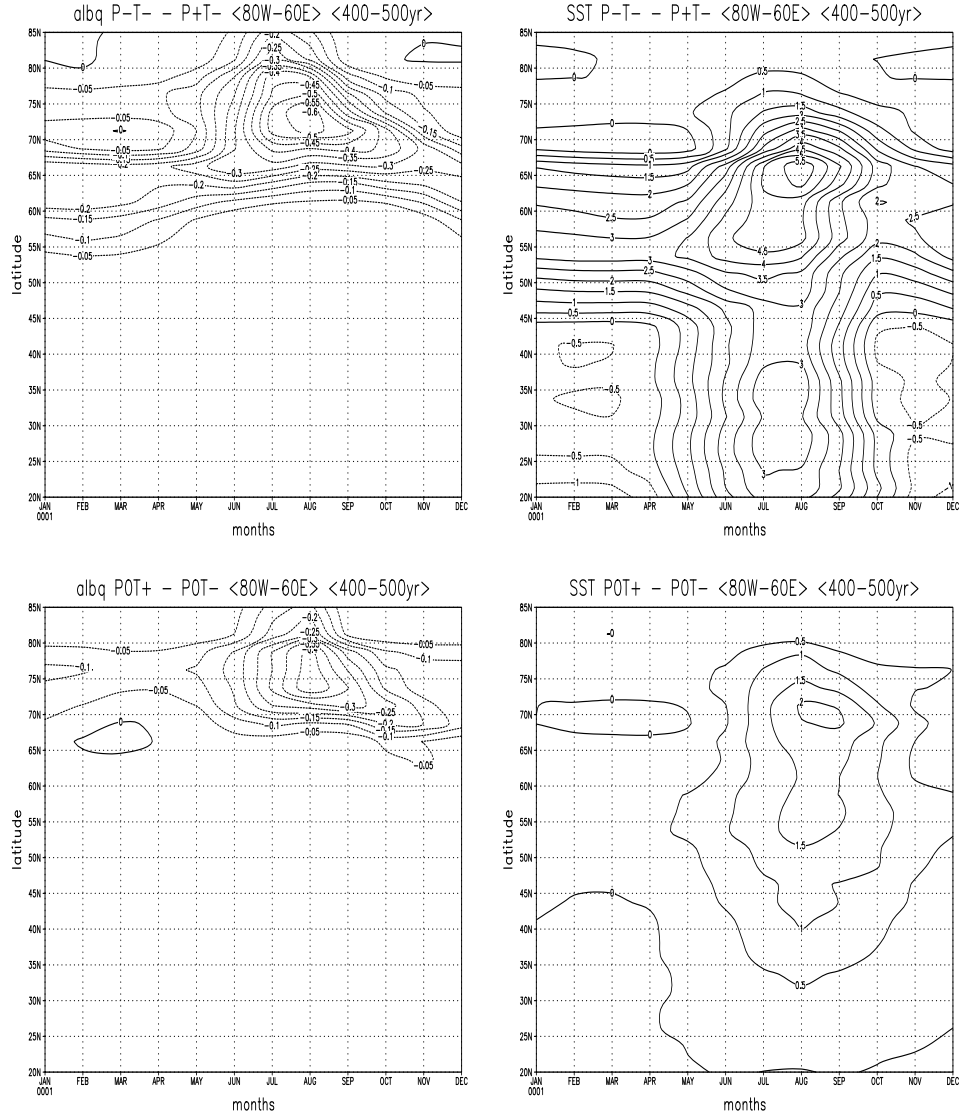


Figure 4.3: Zonally averaged ( $80^{\circ}\text{W}$ - $60^{\circ}\text{E}$ ) sea-ice fraction (left panels) and sea surface temperatures (in  $^{\circ}\text{C}$ , right panels) as a function of latitude and month (horizontal axis). Top panels: minimum precession minus maximum precession. Bottom panels: Maximum obliquity minus minimum obliquity. The values are averages of model years 400-500. Contour intervals are 0.05 for the left panels and  $1^{\circ}\text{C}$  for the right panels.

both SON and DJF (not shown). A higher NAO-index would be expected to result in a wetter northern Europe and a somewhat dryer southern Europe [74]. Indeed, over northern Europe SON precipitation is stronger during minimum precession, but the difference is small (Fig. 4.5). However, over southern Europe the precipitation signal is opposite to the signal deduced from the NAO-index. This indicates that the relation between the NAO-index and precipitation over southern Europe is weak in the model. Furthermore, a stronger mechanism plays a role in southern Europe as the SST of the MS stay high in SON after the warm summer during minimum precession. At the same time land temperatures decrease, especially over the Asian landmass (Fig. 4.2). High SST combined with low air temperatures favours atmospheric convection causing stronger precipitation during minimum precession than during maximum precession. A similar signal is visible over the Atlantic ocean. Over the MS, the signal is especially strong over the eastern part and over the adjacent land. The weaker obliquity forcing also gives rise to enhanced SON precipitation over the eastern MS during maximum obliquity compared to minimum obliquity (Fig. 4.5). The obliquity and precession signal in the evaporation over the MS have the same sign as the precipitation response but the differences are smaller, resulting in a net increase of the surface freshwater forcing. In the other seasons both the precession and obliquity signals in the precipitation over Europe and the Atlantic Ocean are inhomogeneous and small (not shown).

## 4.4 Changes in climatic variability

In a few small area's changes in climatic variability (measured by the standard deviation) are more pronounced than changes in the mean state (averaged over 100 years). They are the convection sites in the Labrador Sea and in the Greenland-Iceland-Norway (GIN) sea. As they affect the large-scale oceanic circulation, this aspect will be now discussed in detail. Sea-ice coverage over the northern GIN sea exhibits several short irregular events with a much higher coverage than normal in the 500-yr control run. These events last 10-50 yr (Fig. 4.6). Similar events have been described by Goosse et al. (2003) in a control run with an earlier version of the ECBilt-Clio model. They seem to be triggered by a random fluctuation in the atmospheric flow which induces a reduction in the southward advection of sea-ice into the Atlantic Ocean. This results in a local increase in sea-ice cover. Due to the isolating effect of sea-ice, this causes less winter cooling of the ocean surface by the atmosphere, reduced deep-water formation and a decrease in the Atlantic THC (Fig. 4.6). In the experiments with minimum precession and maximum obliquity the ice cover in the GIN sea is stable, i.e., there are no events during 500 years. In contrast to this, the experiments with maximum precession and minimum obliquity exhibit larger events which also last much longer than in the control run. The stable experiments were continued for another 500 yrs, while unstable experiments and the control run were continued for another 1500 yrs. The changes in variability were found to be robust over the full 1000/2000 yr period. In addition to the strong, persistent events there are similar events as in the control run, e.g. around model yrs 1100 and 1750 in

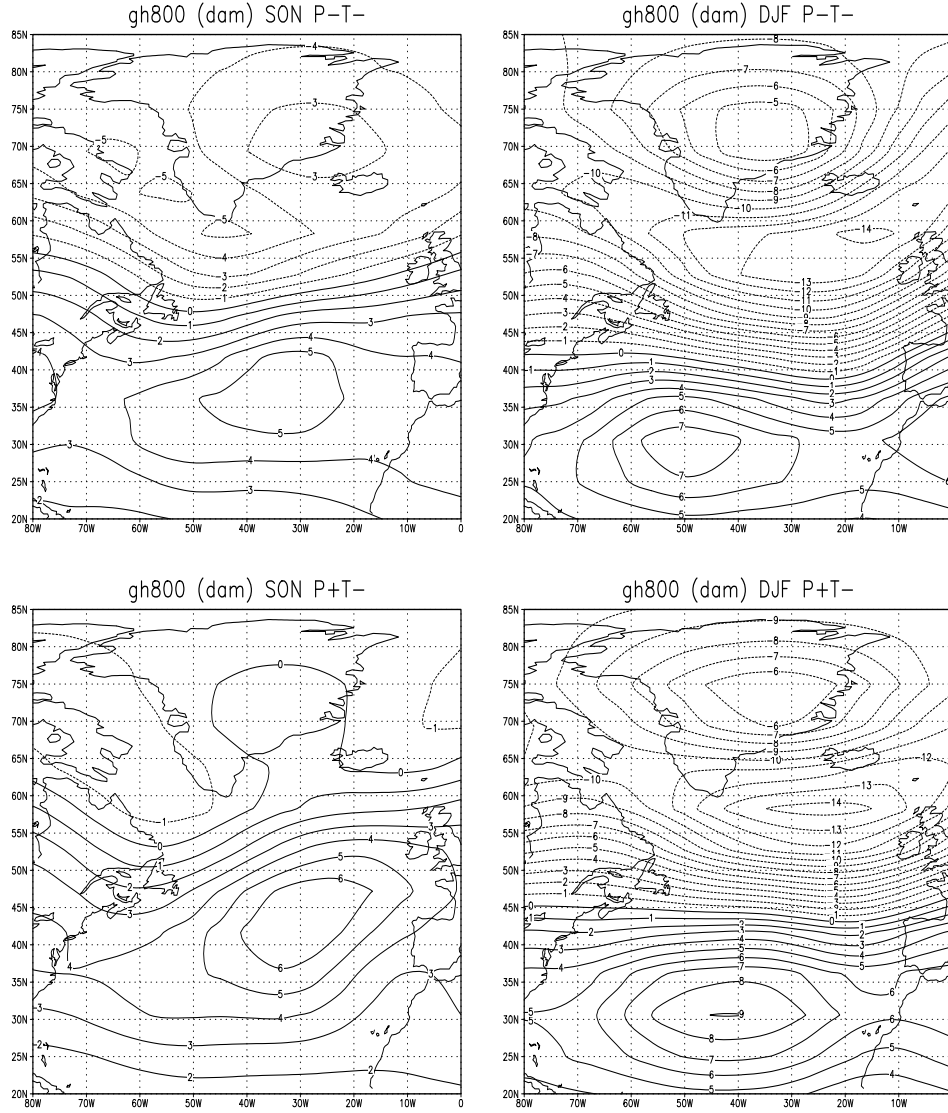


Figure 4.4: Deviations of the geopotential height of the 800 hPa level (in decameters) with respect to a standard level: September-October-November (SON) for minimum precession (top left panel), SON for maximum precession (bottom left panel), December-January-February (DJF) for minimum precession (top right panel) and DJF for maximum precession (bottom right panel). The values are averages of model years 400-500. Contour interval is 1 dam.

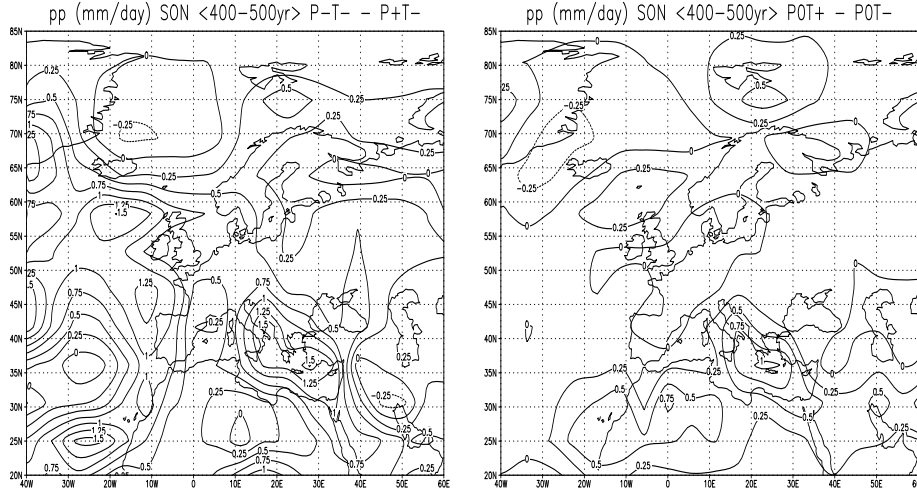


Figure 4.5: *Difference of the precipitation (in mm/day) for September-October-November. Left panel: Minimum precession minus maximum precession, right panel: Maximum obliquity minus minimum obliquity. The values are averages of model years 400-500. Contour interval is 0.25 mm/day.*

the run with maximum precession and around yrs 1350 and 1950 in the run with minimum obliquity (Fig. 4.6).

In all experiments convection responds to the changes in sea-ice fraction during an event, whereby increased sea-ice coverage results in reduced convection. Comparing the convective layer depths in DJF reveals that during an event the convection is less deep in the Labrador Sea and in the northern GIN sea, while it is stronger in the southern GIN sea (Fig. 4.7). Overall, deep-water formation is reduced resulting in a weakening of the THC, see Fig. 4.6. The smaller events cause a weakening of the THC by about 5 Sv (Sverdrups), while for the larger and more persistent events the weakening is stronger (about 10 Sv). The THC response lags the GIN sea convection and the sea-ice fraction by about 30 years.

The sea-ice fraction over the convection area in the Labrador Sea shows similar events as observed in the northern GIN sea (Fig. 4.6). However, the events in the Labrador Sea start about 30 years later compared to the northern GIN sea. This indicates that changes in the sea-ice fraction in the Labrador Sea (and the associated convection changes) result from THC changes. When the THC is reduced, the heat transport to the Labrador Sea is weaker resulting in more sea-ice. During periods with no events and in the stable experiments (i.e, minimum precession and maximum obliquity) the sea-ice fraction in the Labrador Sea is small. Only during maximum precession the sea-ice fraction increases to about 0.7 after a spin-up period and remains in that state.

To summarize, the sea-ice fraction over the convection area in the northern GIN sea shows short irregular events with more sea-ice in the control run, during maximum

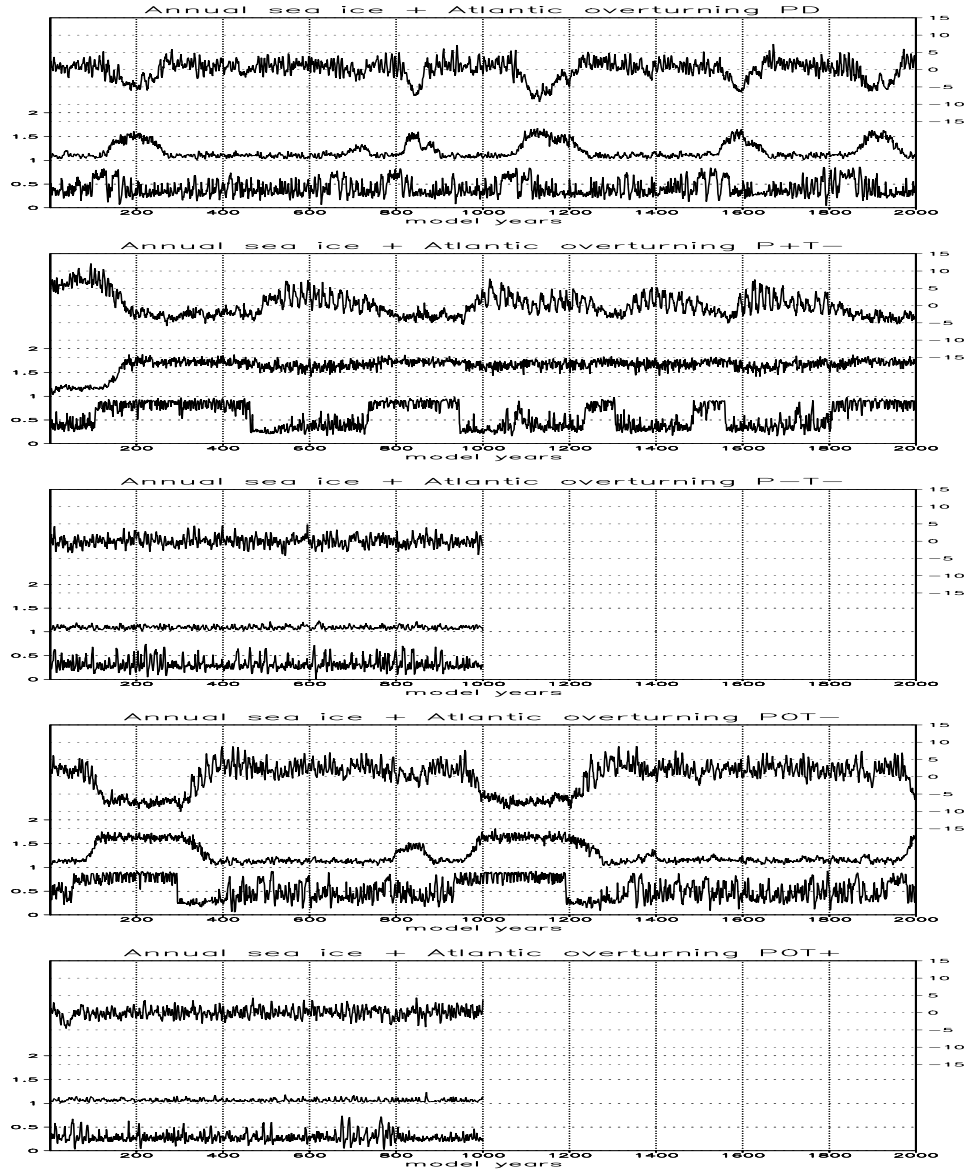


Figure 4.6: Annual sea-ice coverage (left axis) for the northern GIN Sea ( $0-20^{\circ}\text{E}; 70^{\circ}\text{N}-80^{\circ}\text{N}$ , lowest line) and for the Labrador Sea ( $65^{\circ}\text{W}-55^{\circ}\text{W}; 60^{\circ}\text{N}-70^{\circ}\text{N}$ , middle line) and the anomalous annual maximum streamfunction in the Atlantic Ocean (in Sverdrups, upper line, right axis) for the control run (top panel), maximum precession (second panel), minimum precession (third panel), minimum obliquity (fourth panel) and maximum obliquity (fifth panel). For plotting reasons 1 has been added to the sea-ice coverage in the Labrador Sea. The anomalies for the streamfunction are computed with respect to the mean of the whole experiment.

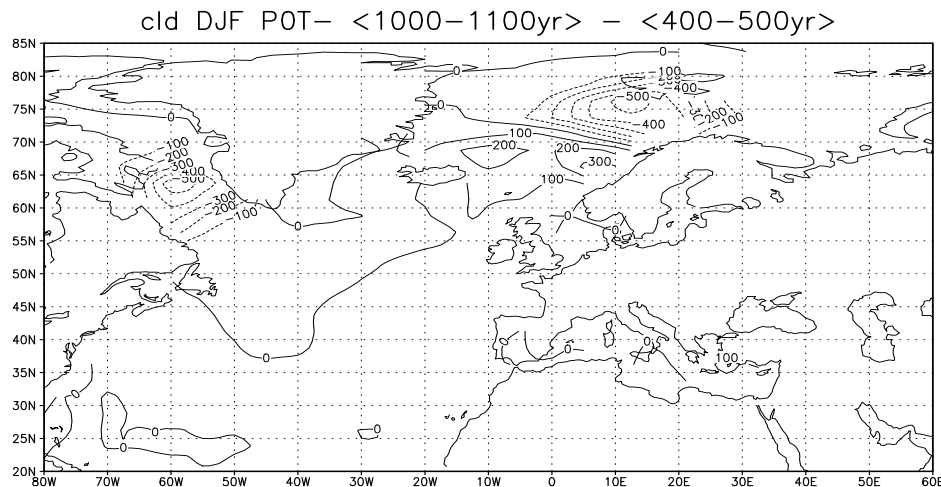


Figure 4.7: *December-January-February convective layer depth (meter) averaged over model year 1000-1100 minus the average over model year 400-500 for the minimum obliquity experiment. Contour interval is 100 m.*

precession and during minimum obliquity. In addition, during maximum precession and minimum obliquity longer and stronger events are simulated. During minimum precession and maximum obliquity neither short nor long events are found. The increased sea-ice coverage during an event strongly weakens the convection resulting in a weaker THC some 30 years later. The sea-ice fraction over the convection area in the Labrador Sea also exhibits similar events, but they are a response to changes in the THC. Therefore, in the remaining only the mechanism for the events in the northern GIN sea will be studied.

The first question that arises is how the events are initiated and what mechanism ends them. In the control run the trigger of an event seems to be an atmospheric circulation characterised by negative geopotential height anomalies over Greenland and positive ones over the GIN and Barents seas [61]. This atmospheric anomaly is associated with anomalous northward winds in the northern GIN and Barents seas and thus a reduction in the climatological southward advection of sea-ice into the Atlantic Ocean. This induces an increase of the sea-ice extent over the northern convection site in the GIN sea. A positive feedback between the surface conditions (increased sea-ice cover and reduced heat release from the ocean to the atmosphere) and the atmospheric circulation reinforces the initial atmospheric anomaly. In the present study the same atmospheric trigger is found. For example, analysis of the beginning of the event around model year 1042 in the control run (Fig. 4.6) shows that the sea-ice coverage starts to increase strongly at the end of model year 1041. At the same time, the gh800 field reveals a pattern of negative anomalies over Greenland and positive anomalies over the GIN and Barents seas (Fig. 4.8). The coincidence of these two random anomalies results in a continued increase of sea-ice coverage in the beginning of model year 1042 (not shown). The trigger for ending an event is a

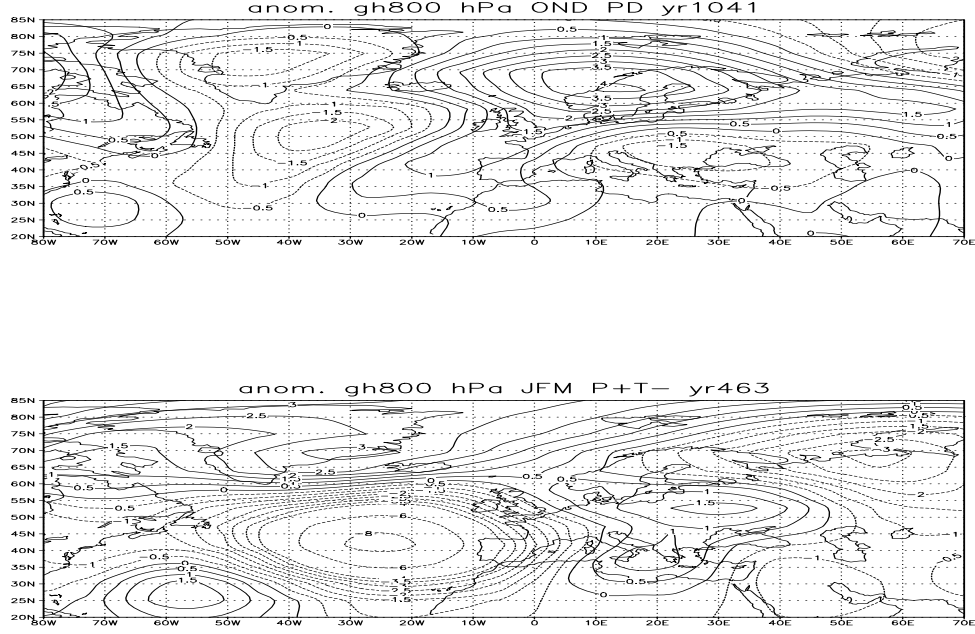


Figure 4.8: *Top panel: Anomalous geopotential height (decameter) for October-November-December in model year 1041 of the control run with respect to the October-November-December average of the model years 400-500. Bottom panel: Anomalous geopotential height (decameter) for January-February-March in model year 463 of the maximum precession experiment with respect to the January-February-March average of the model years 400-500.*

period with an opposite gh800 pattern, i.e., positive anomalies over Greenland and negative anomalies over the GIN and Barents seas. This pattern favours southward advection of sea-ice into the Atlantic Ocean resulting in reduced sea-ice coverage over the northern GIN sea. An example is shown in Fig. 4.8. This pattern, which occurs in the beginning of year 463 in the maximum precession run, leads to a strong decrease in sea-ice fraction over the northern GIN sea in spring of the same year. The second question arising from the present study is why the frequency of occurrence, strength and duration of the events changes in response to the insolation forcing. We note here that the events tend to start in winter, while the insolation forcing is strongest in summer. In order to answer this question, the probability density function (PDF) of the monthly sea-ice fraction over the northern GIN sea during periods with almost no events is computed for 3 different experiments (Fig. 4.9). Summer

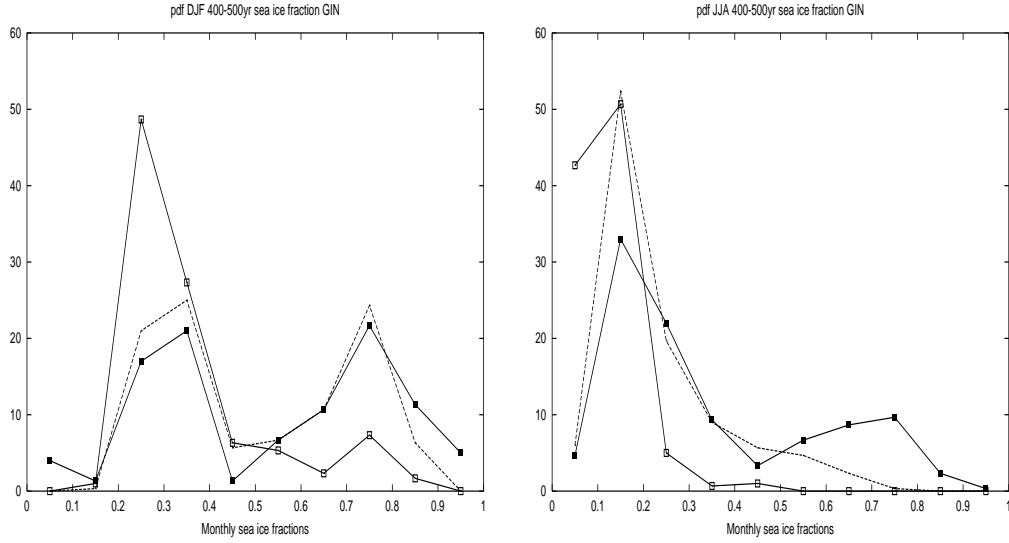


Figure 4.9: *Probability density function of the monthly sea-ice fraction over the northern GIN sea ( $70^{\circ}$  N- $80^{\circ}$  N; $0-20^{\circ}$  E) for the model years 400-500 for maximum obliquity (open squares), minimum obliquity (closed squares) and the control run (dashed line) for December, January and February (left panel) and June, July and August (right panel). The vertical axis displays percentages.*

and winter months are considered separately. The largest differences are found to occur in summer. For example, many summers are almost ice-free during maximum obliquity and only a few summers occur with sea-ice fractions larger than 0.2. During minimum obliquity about 60% of the summers have sea-ice fractions higher than 0.2, sometimes even reaching 0.8. This is a direct result of the stronger summer insolation during maximum obliquity compared to minimum obliquity (Fig. 4.1). The differences between the winter PDFs are smaller, but the summer signal clearly influences the winter signal. This was already evident in the mean signal (compare Fig. 4.3). The PDFs for winter and summer give two reasons why during maximum obliquity no events occur. Firstly, the chance that the atmosphere triggers the beginning of an event in winter during maximum obliquity is small because many years have small sea-ice fractions in winter. This diminishes the chance that a suitable state of the atmosphere coincides with a high sea-ice fraction. Second, even when the atmosphere triggers an event in winter, only a small amount of sea-ice can survive in summer due to the strong insolation. This suppresses the development of an event. In contrast, during minimum obliquity the chance that the atmosphere triggers the beginning of an event in winter is larger and a large amount of sea-ice can survive in summer. This favours the development of an event. A similar reasoning as for obliquity also applies to precession. The duration of events seems to be determined by the maximum sea-ice fractions. During winters with very high sea-ice fractions (minimum obliquity and maximum precession) an event can be triggered which is stronger than the (short) events in the control run (Fig. 4.6). In order to stop a strong event, a very strong



atmospheric trigger is necessary. This strong atmospheric trigger occurs less often than a weaker trigger. Therefore, a strong event is likely to last longer.

## 4.5 Summary and conclusions

We have investigated the influence of precession and obliquity on winter climate in the Atlantic/European sector. It turns out that over the convection sites in the northern Atlantic Ocean changes in climatic variability are more pronounced than the differences between the mean climatic states. In the control run the atmospheric flow triggers sudden expansions in sea-ice coverage over the convection sites, which last 10-50 yrs. Stronger events of longer duration were simulated in the experiments with minimum obliquity and maximum precession, while no events were found in the experiments with minimum precession and maximum obliquity. During such events convection is reduced and the THC decreases, lagging sea-ice and convection by about 30 yrs. Summer insolation was found to determine the strength and duration of the events. Atmospheric temperatures and precipitation are lower during an event, but this is only discernible at latitudes north of about 50°N. Therefore they do not influence the freshwater budget over the MS.

In the response of the mean climatic state to orbital forcing sea-ice feedbacks are found to play an important role. Sea-ice coverage decreases in autumn during periods when summer insolation is high, consistent with earlier studies [133, 103, 53]. This results in relatively high autumn temperatures at high northern latitudes. During minimum precession the winter season starts early, resulting in a NAO-like atmospheric circulation and enhanced precipitation in northern Europe. In southern Europe a different mechanism influences precipitation in autumn, namely the strong land-sea temperature contrast in the MS region during minimum precession and maximum obliquity (compared to maximum precession and minimum obliquity, respectively), which results in enhanced precipitation.

In the present study the strongest orbital signal in the hydrological cycle consists of stronger precipitation around and over the MS in autumn. This is in agreement with higher lake levels in southern Europe at 6 ka BP deduced from paleoclimatic data [214, 29]. It is also consistent with precession signals found in a pollen record for the late Miocene - Early Pliocene in Greece, as described in chapter 5 of this thesis. This record indicates that precipitation in the cold season is stronger during minimum precession compared to maximum precession. The orbital-induced precipitation signal over Southern Europe can be important for the deposition of sapropels in the MS. In chapter 6 of this thesis we examine whether increased (autumn) precipitation over the MS can influence the surface salinity as effectively as increased (summer) discharges of the river Nile.



## Chapter 5

# Coupling between orbital precession and long-term dynamics in the North Atlantic/European region

### Abstract\*

Late Miocene - early Pliocene lake sediments from northern Greece exhibit a distinctive lithologic cyclicity. This cyclicity is accurately calibrated against calculated changes in the past distribution of incoming solar radiation dominated by the 21.7 ka average periodicity of precession. The pollen record from these cycles reveals significant changes in vegetation that are primarily caused by precession-controlled fluctuations in precipitation. At present, variations in rainfall during the winter in the East Mediterranean borderlands are related to 1) meridional shifts of the trajectories of precipitation-laden cyclones that are associated with the North Atlantic Oscillation and 2) the formation of cyclones originating from the Mediterranean Sea. We propose that both the North Atlantic teleconnection and the forming of Mediterranean cyclones are responsible for the reconstructed long-term precipitation variations in southern Europe.

---

\*This chapter has been submitted for publication to *Global and Planetary Change* as: Kloosterboer-van Hove, M.L., H. Visscher, J. Steenbrink and E. Tuenter, (2004). Coupling between orbital precession and long-term dynamics in the North Atlantic/European region [93]. The author of this thesis wrote parts of the introduction and discussion and compared the results from this chapter to the results described in chapter 4 of this thesis.

## 5.1 Introduction

Complementary to modeling exercises [104, 105, 159], many geochemical and biological data firmly substantiate that long-term variation in the intensity of the monsoon systems over Asia and Africa is controlled by the changing distribution of solar energy, dictated by the 19 ka and 23 ka cycles of orbital precession [35, 167, 163]. By contrast, it is still uncertain to what extent other dominant modes of climate variability are affected by precession-controlled changes in insolation. For southern Europe, there are two important mechanisms for winter precipitation in the present day climate: The atmospheric circulation pattern known as the North Atlantic Oscillation (NAO) and the precipitation-laden cyclones originating from the Mediterranean Sea. To corroborate the hypothesis of a coupling between insolation and these mechanisms, we document the distinctive response of late Miocene-early Pliocene vegetation of southern Europe to precession-controlled changes in precipitation.

The NAO is associated with a large-scale net displacement of air between the Azores high (a high-pressure system over the subtropical Atlantic Ocean) and the Icelandic low (a low pressure region near Iceland and the Arctic) [74]. The migration of the mid-latitude North Atlantic storm tracks, where wintertime precipitation-laden cyclones are most frequently observed, is related to the pressure difference between this Azores high and Icelandic low [74, 75, 146]. An enhanced pressure gradient (positive NAO; stronger than normal Azores high and deeper than normal Icelandic low) is leading to a more northeast oriented transport of moist Atlantic air into Europe. This results in wetter conditions in northern Europe and drier conditions in the Mediterranean region [74, 75, 144, 187]. Conversely, under a weak pressure gradient, cyclones undertake a more southern trajectory, promoting relatively wet Mediterranean conditions. Precipitation data from Turkey, together with records of Tigris-Euphrates streamflow volumes, demonstrate that NAO-activity extends well into the East Mediterranean borderlands [42]. In addition to instrumental and historical records [85, 97], tree rings [36] and polar ice accumulation rates [3] reveal decade-to-century-scale variation in NAO-activity. Another source for winter precipitation in southern Europe is the development of cyclonic disturbances originating in the Mediterranean Sea by means of air-sea temperature contrast. This cyclogenesis is stronger when the sea surface temperature is high [151] leading to heavier rain events [3]. The developed cyclones are strongly affected by local orography and/or low-level baroclinicity over the northern Mediterranean coast [151]. We propose that, if we extend this short-term behavior to a precessional timescale, long-term prevalence of either southern or northern cyclone trajectories could be associated with orbitally forced variation in insolation.

Marine sedimentation in the Eastern Mediterranean region has been continuous throughout the last 10 million years and exceptionally sensitive to precession-induced environmental change [70, 98, 121, 170]. Most conspicuous within precession-controlled marine deposits are dark organic-rich marls, generally known as sapropels. Scenarios for the formation of sapropels and related sediments strongly rely on geochemical and biological evidence of periodically enhanced freshwater influx into the Mediterranean basin [38, 177]. A precession-related increase of river discharge is

largely attributed to intensified monsoonal precipitation in the low-latitude highlands of eastern Africa, resulting in increased streamflow of the Nile River (e.g. Rossignol-Strick, 1985; Rohling and Hilgen, 1991), although an effect of increased rainfall in the Mediterranean borderlands is not excluded (e.g. Shaw and Evans, 1984; Cramp et al., 1988). This implies that precession signals in the Mediterranean marine sedimentary record are for the larger part induced by secondary effects of precipitation variability in areas well outside the Mediterranean region. Any assumptions of long-term influence of precession on the Mediterranean climate itself needs to be supported by time-series data on proxy environmental variables that directly reflect changes in regional temperature and/or precipitation in the Mediterranean. Because of its sensitivity to environmental change, land vegetation can provide the necessary accurate records of long-term climate variability.

Orbitally forced frequencies have already been detected in prolonged pollen sequences from Quaternary lake deposits in Greece [136]. Their research indicates that at least during interglacial periods, changes in vegetation indicate a clear relation between precession and precipitation. However, during glacial periods this connection is less conclusive. In order to eliminate disturbing effects of glacial-interglacial climate dynamics on regional vegetation composition, an unambiguous assessment of the influence of precession on the Mediterranean climate must be performed on the basis of palynological data from a time-interval preceding the onset of Northern Hemisphere glaciation, approximately 2.75 million years ago. Such data are available from late Miocene-early Pliocene deposits of the Ptolemais basin in northern Greece.

## 5.2 Ptolemais sedimentary cycles

The Ptolemais basin (Fig. 5.1) is a fault-controlled intramontane depression 600 meter above sea level, flanked by mountain ranges of approximately 2000 meter height. Continuous sedimentation has resulted in the accumulation of a 500-600 meter thick succession of late Miocene to early Pleistocene lake sediments with intercalated lignites and fluvial deposits [152, 129, 196, 179].

Well-exposed in a series of open-pit lignite mines, late Miocene-early Pliocene sediments exhibit a distinctive cyclicity [196, 179, 178] where organic-rich and carbonate-rich deposits alternate in a regular pattern. This lithologic cyclicity is the result of lake-level fluctuations. [179, 92]. Organic-rich facies (ranging from lignitic marls to massive lignite seams) correspond to lowstand conditions with concomitant development of fringing swamp environments, while the carbonate-rich lithologies reflect relatively raised lake-levels [92]. Accurate age control, based on detailed magnetostratigraphic analysis and  $^{40}\text{Ar}/^{39}\text{Ar}$  dating of nine intercalated volcanic ash layers, demonstrates the precessional forcing of the sedimentary cycles [196, 179, 178].

Here we focus on the palynological record of seven consecutive cycles in the upper part of the Komnina Formation, exposed in the Tomea Eksi lignite mine (Fig. 5.1). Individual cycles are approximately 5 meter thick and consist of dark brown lignites, followed by grey/green clay-rich marls, and passing upward into beige carbonate-rich marls (Fig. 5.2). These cycles have been selected for palynological analysis because of

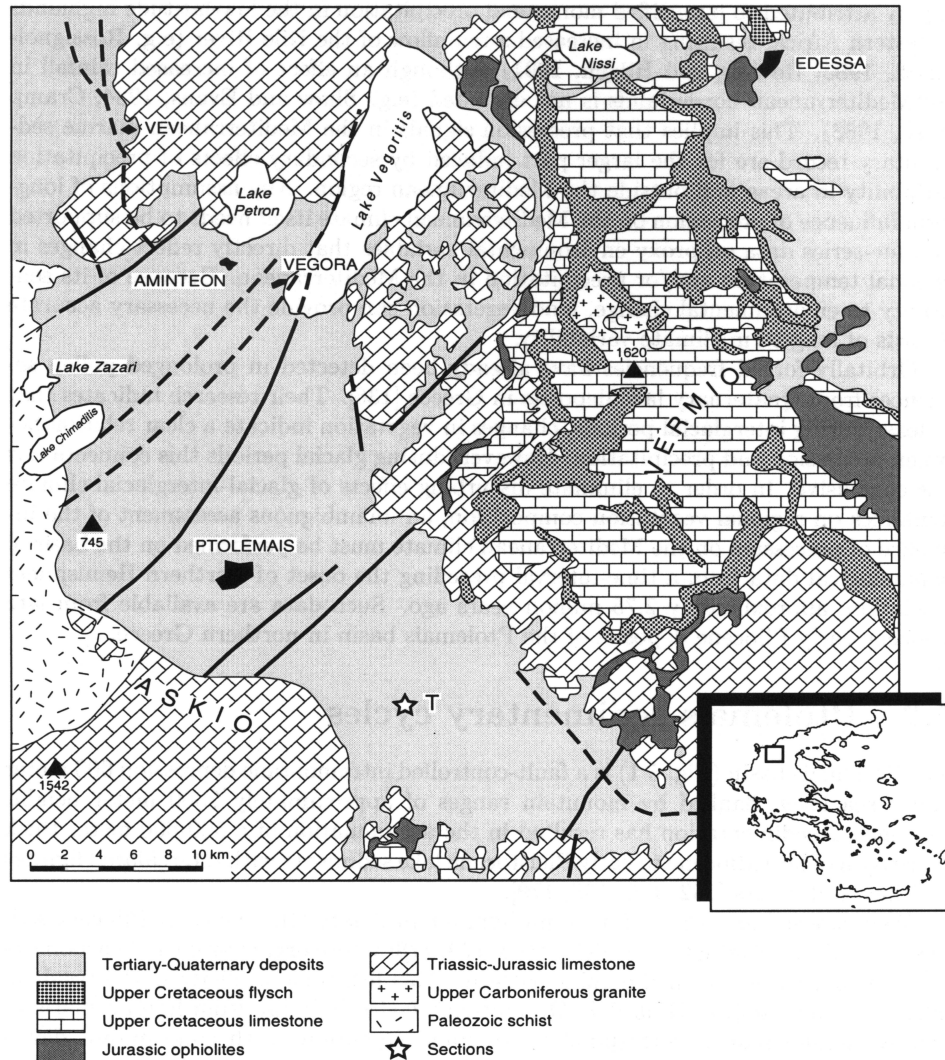


Figure 5.1: Geological sketch map of the Ptolemais Basin ( $40^{\circ}\text{N}31$ ,  $21^{\circ}\text{E}41$ ) with T the location of the Tomea Eksi section (modified after Papakonstantiou, 1979).

their high accumulation rate (average 25 cm kyr<sup>-1</sup>), minimizing effects of bioturbation in the ecological interpretation of successive pollen assemblages. [152, 129, 196, 179].

### 5.3 Palynological analysis

To detect orbitally controlled changes in vegetation in the selected time-interval, 52 samples were taken with a maximum spacing of 85 cm. This adds up to at least 5 samples per sedimentary cycle. Pollen samples were prepared using slightly modified [92] standard procedures [48]. It is at present generally accepted that morphological characteristics of most late Miocene and Pliocene pollen types can directly be related to extant genera and families. This correlation potential is a sound basis for floristic analysis of the assemblages and the recognition of similarities with modern vegetation types.

### 5.4 Results and discussion

A pollen-percentage diagram for selected plant categories is presented in Fig. 5.3. In general, the taxonomic composition of the mountainside flora is remarkably similar to that of modern vegetation communities characteristic of elevated terrain in the East Mediterranean region [199, 16, 198]. Consequently, climatic interpretation of the palynological data can largely benefit from analyses of the relation between East Mediterranean vegetation changes and Quaternary climate variability [199, 16, 198, 197, 210, 191, 52, 44]. A few significant floristic differences, however, are indicated by the presence of *Tsuga* and *Cathaya*. In Europe, these conifer taxa became extinct as a result of Pleistocene cooling. Changes in the amount of wetland elements, mainly Cyperaceae and some Taxodiaceae and ferns, are largely a reflection of lake-level fluctuations.

By accepting a distinctive altitudinal zonation comparable to modern Eastern Mediterranean mountain forests, changes in relative abundance of dominant pollen-types are likely to document range-expansion or range-contraction of communities along elevational gradients. Shifts in the forest zones can be a response to changes in precipitation and/or temperature. In the Ptolemais Basin the changes in vegetation do not point to significant changes in temperature. Equable winter temperatures throughout the different phases in the precession cycles are constrained by the continuous presence of evergreen *Quercus* and *Cedrus*. On the slopes winter temperatures must have remained above 0°C as *Quercus* cannot withstand prolonged periods with temperatures <-5°C [109]. Higher up in the mountains continual winter averages may have reached below 0°C as supported by the record of *Cedrus* [198]. At present, forests including *Cedrus* occur in areas with cool moist winters, with abundant snow in areas above 1000m [198]. Thus precipitation must have been the most important drive for changes in the late Neogene vegetation in Ptolemais. Quaternary pollen data from the East-Mediterranean uplands [16, 192, 193] support this view that moisture is the critical climatic variable

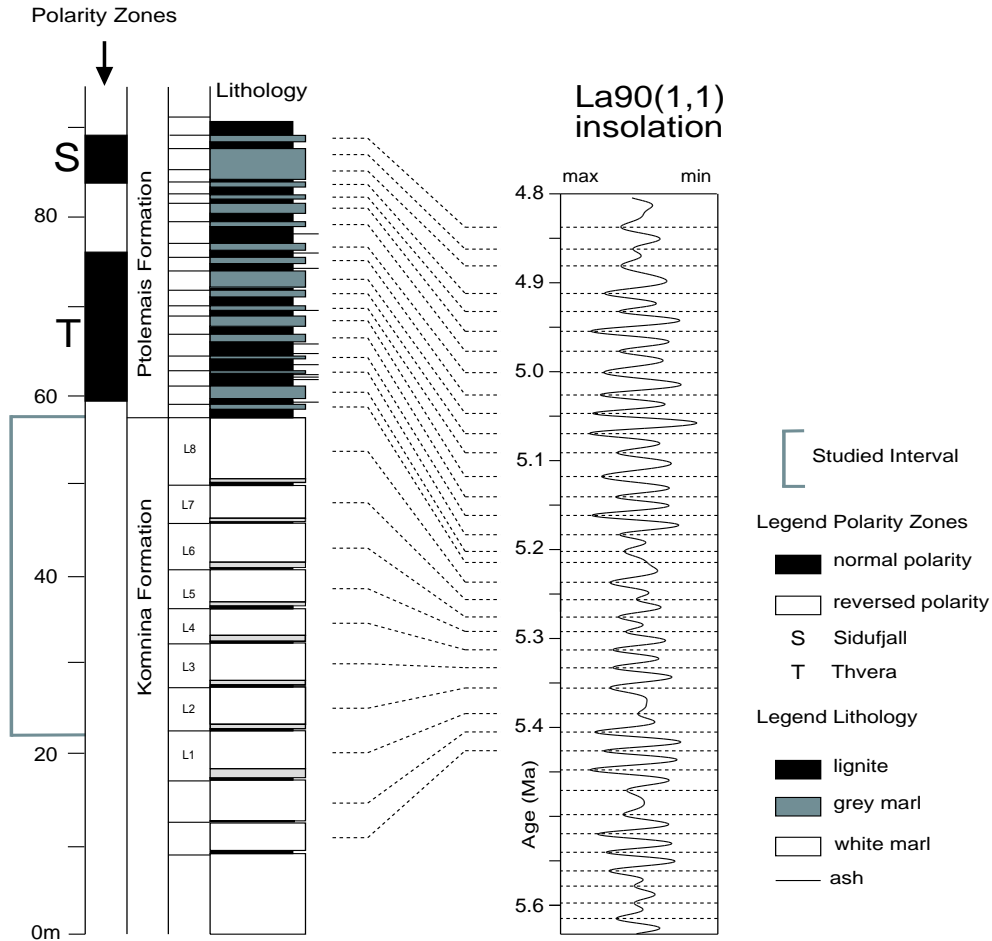


Figure 5.2: Magnetic polarity, lithology and stratigraphic classification of the upper part of the Komnina and the lower part of the Ptolemais Formation. Magnetic polarity and stratigraphic members are indicated to the left of the sedimentary cycle numbers. In the polarity column black (white) indicates normal (reversed) polarity. T and S indicate the Thvera and Sidufjall Subchrons [196]. The studied section is correlated to the 65°N summer insolation curve [115] after Steenbrink (2001). As the succession spans the period from 5.44 Ma to 5.23 Ma it also includes the Miocene-Pliocene boundary, which has been astronomically dated at 5.333 Ma [121]. There is no indication for any change or break in the vegetation succession at this boundary.



Although details may differ between cycles, the allochthonous pollen sequence reveals a consistent pattern of recurrent vegetation change from open communities to forests. In each precession cycle three phases can be recognized:

1) Pollen spectra from the organic-rich deposits reflect open vegetation periods with relatively dry climatic conditions. Mountainside vegetation is predominantly steppe-like, with *Ephedra*, Chenopodiaceae, Asteraceae and other drought-tolerant herbs capable of surviving under strongly seasonal rainfall conditions. Although growing-season soil moisture deficit probably remained a limiting factor to tree growth, subordinate but consistent (possibly long-distance) input of arboreal pollen still indicates the presence of moisture-demanding montane conifer populations, notably of *Pinus* and *Cedrus*. 2) Pronounced changes in the pollen spectra from the clay-rich marls provide evidence for increased humidity. Changing environmental conditions at lower and middle altitudes are apparent from the development of transitional open woodland, reflected by the records of a variety of deciduous trees, *Juniperus*, evergreen *Quercus* and Poaceae. Notably the spread of deciduous trees indicates enhanced soil moisture, resulting from increased orographic precipitation supply. At higher elevations, *Cedrus* and *Pinus* are the principal constituents of montane conifer forests. 3) The pollen record of the carbonate-rich marls indicates progressive humidity increase with the widespread formation of closed forests. Analogous to Holocene pollen records from the East-Mediterranean uplands [16, 197], a marked spread of *Pinus* at the expense of *Cedrus* points to increased rainfall at higher elevations. Increased humidity can also be responsible for a downslope expansion of coniferous vegetation into the mid-altitude forests, resulting in a decline of *Quercus*. Among montane conifer genera, *Tsuga* is the least resistant to summer drought, and its growth is restricted to regions where soil moisture is available throughout the growing season. [49]. Also the presence of *Cathaya* indicates wet conditions, judging from its modern endemic occurrence in medium-high mountains of south-central China [49].

The change from open steppe like vegetation, to a transitional open woodland to a closed forest with predominantly *Pinus*, *Cathaya* and *Tsuga* reflects changes in moisture availability throughout a precession cycle. In the reconstruction of Quaternary vegetation responses in the East-Mediterranean region, phases of orbitally forced precipitation increase are specifically defined in terms of abundant *summer* precipitation [136]. Such phases would imply a weakening of the seasonality of precipitation relative to present day conditions. The palynological data from Ptolemais, however, do not corroborate this assumption as there are no floristic indications of upland taxa that would require intensified summer rainfall. In early Pliocene palynological records from the West-Mediterranean region, the presence of wetland vegetation with abundant *Taxodium* has also been interpreted in terms of rainy summers, despite the coeval occurrence of a variety of typical Mediterranean sclerophyllous taxa [183]. However, although *Taxodium* and associated wetland elements require year-round high soil moisture levels, this does not necessarily translate into high summer precipitation [186]. In more recent reviews of the West-Mediterranean records the concept of rainy summers is no longer maintained (e.g. Suc, 1995). At present, winter snow is the prominent source of soil moisture in spring, as in the Mediterranean dry periods already begin in May. Rejuvenation of modern *Cedrus* forests, for ex-

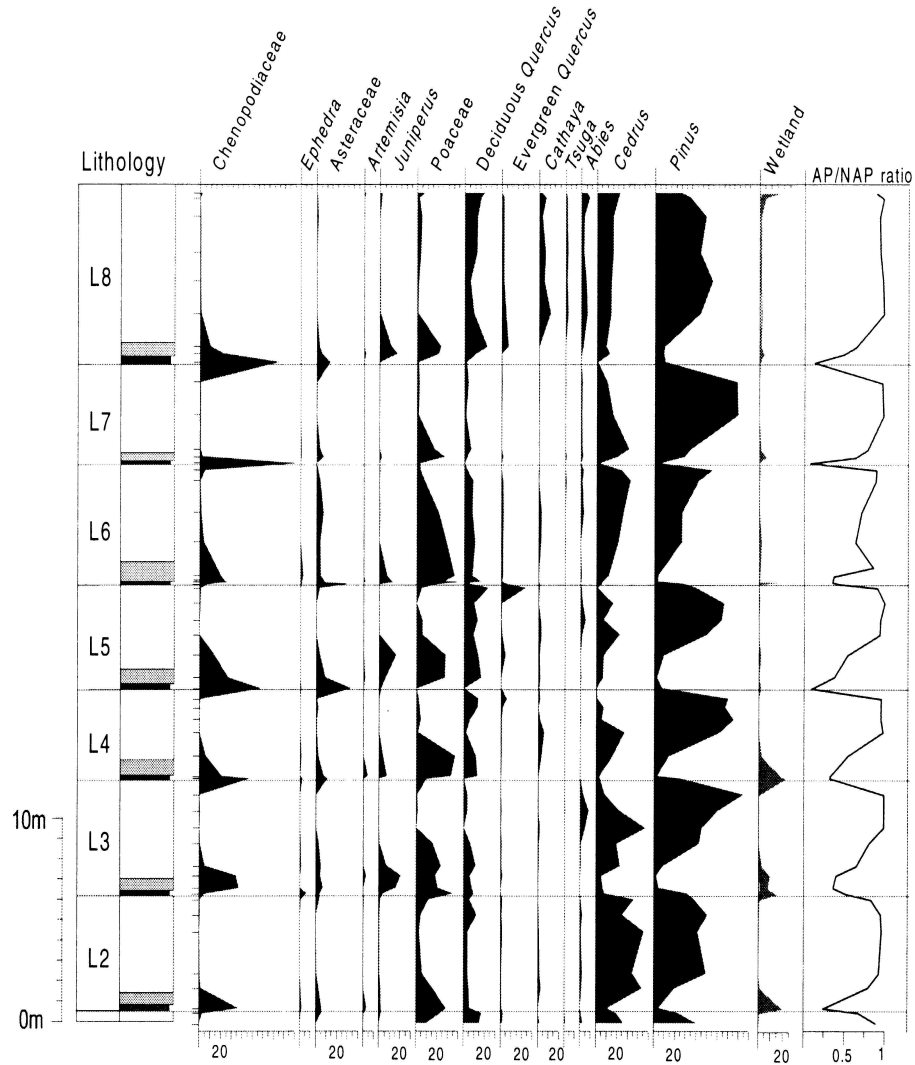


Figure 5.3: Pollen diagram representing percentages (calculated on a pollen sum consisting of the allochthonous pollen, excluding wetland elements) of selected vegetational elements. The wetland elements consist of *Cyperaceae* (mainly), *Taxodium* and some ferns. The lithology (black = organic rich marl, grey = organic rich-clayish marl, white = organic poor marl) and cycle numbers are given on the left. AP/NAP ratio = (regional arboreal pollen)/(regional arboreal pollen + regional non-arboreal pollen).

ample, would be impossible without water supply from snowmelt [49]. Analogous to these current Mediterranean conditions, the growing-season of the late Miocene-early Pliocene mountainside vegetation is confined to the spring, and the vegetation primarily responded to strong fluctuations in growing-season soil moisture, rather than direct rainfall.

The magnitude of the inferred relative changes in orographic precipitation is difficult to estimate. Minimum precipitation rates may be constrained by *Cedrus*. In the East-Mediterranean mountains, *Cedrus* forests nowadays occur in areas with a high annual (mainly winter) precipitation of 1000-1500 mm [49]. Maximum precipitation can be in the order of 2000 mm, as indicated by the occurrence of *Tsuga*. At present, nearest occurrences of this genus are in monsoon-influenced forests of the Himalayas, where annual precipitation can exceed 2000 mm. Based on our record we can thus assume fluctuations in the order of minimal 500 mm. Such changes in precipitation could readily account for the closed-basin lake-level variation observed in the lignite-marl cycles of the Ptolemais Formation.

The Ptolemais pollen record shows that late Miocene-early Pliocene vegetation in the East Mediterranean region primarily responded to strong fluctuations in growing-season soil moisture variability induced by precipitation availability in winter. Associated temperature fluctuations are less obvious. Such is in agreement with time-series data on Mediterranean sea-surface temperature, inferred from  $\delta^{18}\text{O}$  values and biological temperature proxies [162, 120, 203]. Analogous to Quaternary vegetation responses [210, 191, 136, 52, 44], phases with enhanced precipitation can be associated with precession minima, corresponding to periods of elevated summer insolation and reduced winter insolation. This association is confirmed by the preferred phase relation deduced from the correlation of the Ptolemais cycles to the computed insolation curve [196, 179], where carbonate-rich intervals correspond to precession minima and organic-rich layers to precession maxima.

Sofar, changes in precipitation were coupled to the monsoon, which was proven to be affected by precession (e.g. Rossignol-Strick, 1983;1985). This coupling can only pertain when precipitation during summer is considered. However, in the absence of compelling evidence for increased summer precipitation, we propose an alternative scenario of periodic changes in winter precipitation to account for the orbital frequencies in the early Pliocene vegetation development. Historical climate data from Turkey indicate that variation in orographic winter precipitation in the East-Mediterranean borderlands is largely associated with the atmospheric circulation pattern known as the North Atlantic Oscillation (NAO) [42]. In a Quaternary perspective, there is increasing evidence that also century-to-millennial scale climatic events in the North Atlantic sector reflect a sun-climate relationship [72, 119, 125, 185, 195]. The pervasive  $\sim 1.5$  ka climate cycle expressed in glacial Dansgaard-Oeschger cycles as well as recurrent Holocene cooling events [15] has already been explicitly associated with the NAO [57]. It is conceivable that, also in the Neogene, a North Atlantic climatic teleconnection has been responsible for changes in the intensity of wintertime rain-bearing westerly winds. During a precession minimum, prolonged predominance of weak North Atlantic pressure gradients would result in prevailing southern trajectories of winter cyclones, leading to increased rainfall in the Mediterranean borderlands.

A precession maximum would promote reduced moisture transport.

Model simulations as described in chapter 4 of this thesis indicate two different mechanisms for stronger precipitation in southern Europe during precession minima. The first mechanism involves a slightly weaker Icelandic low and Azores high in late winter/early spring. This implies a lower NAO-index during a precession minimum, which results in prevailing southern trajectories of winter cyclones, leading to increased rainfall in the Mediterranean borderlands. The weaker Icelandic low is mainly caused by more sea ice cover and lower sea surface temperatures in the North Atlantic during a precession minimum. This relationship between sea ice cover/sea surface temperatures and the strength of the Icelandic low is also found in other model studies (e.g., Haywood et al., 2000). The second mechanism involves enhanced cyclogenesis over the Mediterranean Sea during precession minima resulting from enhanced air-sea temperature contrast in autumn. The air temperature quickly decreases due to the weaker autumn insolation, whereas the sea temperature reacts more slowly and remains warm after the strong summer insolation. This results in an enhanced air-sea temperature contrast promoting the growth of cyclonic disturbances resulting in stronger precipitation during precession minima.

The occurrence of sapropels in the Mediterranean basin is confined to precession minima (e.g. Hilgen et al., 1995; Krijgsman et al., 1995). Our research indicates that not only enhanced monsoonal activity in summer, but also increases in winter precipitation in southern Europe, could have played an important role in sapropel formation. Considering the continual 10 million year record of sapropels and related marine sediments [70, 98, 121, 170], climatic consequences of glacial-interglacial fluctuations in southern Europe have not interrupted the proposed coupling between orbital precession and long-term atmosphere dynamics.

## 5.5 Concluding remarks

In contrast to the dynamics of the monsoon, the orbital influence on the atmosphere dynamics in the North Atlantic/European region are imperfectly understood. Despite the scale difference, our analysis of long-term climatic cyclicity corroborates the role of insolation on atmospheric circulation in the North Atlantic/European sector, and may thus contribute to a better understanding of contemporary NAO behavior and other causes for precipitation variability in southern Europe.

## Chapter 6

# The effect of precession-induced changes in the Mediterranean freshwater budget on circulation at shallow and intermediate depth

### Abstract\*

In this chapter the consequences of the precession-induced changes in the hydrological cycle for the circulation of the Mediterranean Sea at shallow and intermediate depths are investigated. Changes in runoff, precipitation and evaporation, as found in chapter 2 of this thesis, are used to modify the forcing of a regional ocean model for the Mediterranean Sea. The adjustment of forcing is carried out parameter by parameter in order to perform a sensitivity analysis. It is shown that the precession-induced increase in net precipitation over the Mediterranean Sea itself is of equal or greater importance than the increase in runoff from the bordering continents. The direct influence of enhanced discharge from the Nile is restricted to the Levantine coast, away from the sites of deep-water formation. Increased winter runoff from the north, which enters the sea through the Rhône, Po, and also via the Black Sea, is shown to affect the sites of deep water formation more effectively.

---

\*This chapter is in preparation for publication as: Meijer, P. Th. and E. Tuenter, (2004). The effect of precession-induced changes in the Mediterranean freshwater budget on circulation at shallow and intermediate depth [127]. The author of this thesis wrote parts of the introduction, prepared data for the forcing of the simulations and was involved in the analyses of the results.

## 6.1 Introduction

In chapter 2 of this thesis the orbital signals in the climate over and around the Mediterranean Sea were simulated. In this chapter we investigated how these signals affect the properties and circulation of the Mediterranean Sea. It is important to study these effects because it is thought that sapropels are formed due to weakening of the thermohaline circulation. In particular changes in the freshwater budget are considered relevant because of their effect on winter mixing and thus on the formation of intermediate and deep waters. An increase in the amount of freshwater input is expected to decrease sea surface salinity which may result in a more stable (less unstable) stratification in the regions of intermediate and deep mixing. The resolution of the climate model used in chapter 2 (ECBilt) is too coarse to resolve the circulation in the Mediterranean Sea. Therefore, the model predictions of orbitally-induced changes in the atmosphere are here used to force a regional high-resolution ocean general circulation model of the Mediterranean Sea. Because of their low resolution the atmospheric fields predicted by ECBilt cannot be used to force the ocean model directly. Instead, we take a present day climatology as a reference and adjust this to precession minimum conditions using the difference between the ECBilt experiment for the present day and the ECBilt run for precession minimum. This adjustment to precession minimum conditions is done parameter by parameter in order to achieve a sensitivity analysis. For each experiment we will examine changes in sea surface salinity in February which is when intermediate and deep convection is known to take place. At present, intermediate water formation takes place between Crete and Cyprus. Deep water formation occurs in the Gulf of Lions in the western sub-basin (WMed) and in the southern Adriatic Sea in the eastern sub-basin (EMed).

The processes responsible for sapropel formation in the Mediterranean Sea have been addressed from the venture point of ocean modelling before [140, 181]. Our work differs from these earlier studies in the sense that we explore the consequences of a new dedicated series of climate model experiments. Moreover, in the above-mentioned studies, the net flux of freshwater through the sea surface (precipitation minus evaporation) is replaced by a relaxation to prescribed sea surface salinity. Situations with a freshwater budget different from today were then examined by modifying the assigned surface salinity field. In contrast, our ocean model is fully forced by (interactive) fluxes which allows, for example, to directly apply the precession-induced change in precipitation as a surface boundary condition. Recently, Myers (2002) studied the effect of reductions in net evaporation starting from a model driven by fluxes that were derived from a previous relaxation experiment.

## 6.2 Model description

Our ocean general circulation model is the Mediterranean version of "MOMA" which is used in a set-up similar to that of Meijer et al. (2004) in their study of the effects of paleogeography. MOMA is due to David Webb (e.g., Webb, 1996) and is based on the Modular Ocean Model [145]. The Mediterranean version of MOMA

has been developed at The University of Edinburgh (see Haines and Wu (1998) for an overview) and is made available to the community in the context of the MedNet project (<http://www.met.ed.ac.uk/mednet>). The MedNet-MOMA is a primitive equation model that features a free surface. The model has a horizontal resolution of  $1/4 \times 1/4$  degrees and comprises 19 horizontal levels the majority of which is concentrated in the upper few hundred meters in order to resolve the mixed layer and thermocline. The model includes a small segment of the Atlantic Ocean in order to be able to simulate the exchange at the Strait of Gibraltar. In this "Atlantic box", temperature and salinity are relaxed to prescribed Atlantic values. An interactive scheme is used to compute the net fluxes of freshwater, heat, and momentum (i.e., winds) on the basis of a set of prescribed atmospheric parameters and the modeled sea surface temperatures. The atmospheric parameters consist of monthly averaged fields. Precipitation is imposed independent of sea surface temperature and is - in the control experiment that will serve as a reference - taken from Jaeger (1976). The control experiment features annually averaged discharge of the major rivers and Black Sea. The corresponding values are, Ebro:  $550 \text{ m}^3/\text{s}$ , Rhône:  $1700 \text{ m}^3/\text{s}$ , Po:  $1550 \text{ m}^3/\text{s}$ , and Black Sea:  $6000 \text{ m}^3/\text{s}$  [215]. For the Nile we use a value of  $2854 \text{ m}^3/\text{s}$  which is an estimate of the discharge that existed prior to damming and extraction of water for irrigation [14, 84]. For a complete description of the model the reader is referred to Meijer et al. (2004). Differences between the set-up used here and that described by Meijer et al. (2004) are: (1) here the initial conditions are the full 3D fields of temperature and salinity (rather than horizontally-averaged fields), (2) discharge from the Nile is adjusted to 'pre-Aswan' conditions (see above), and (3) the atmospheric fields are not modified over the central Mediterranean Sea.

In general, ocean models developed for the Mediterranean Sea are not capable of simulating the full thermohaline circulation. Unfortunately, this proves true also for the model we use [126]. One reason for this problem is the fact that deep water formation, as it occurs at present in the Mediterranean Sea, may be considered the last in a chain of processes. Being able to simulate the last step, the sinking of waters to the seafloor due to winter cooling, requires that all previous steps (notably: intermediate water formation and dispersal of that intermediate water) are also captured well. Moreover, deep convection in the Mediterranean occurs at small spatial scale and during short periods of time. The inclusion of precipitation as a surface boundary condition - even though essential given our objectives - is known not to improve model performance. Precipitation at present is notoriously ill-constrained and this is why most models resort to using relaxation to sea surface salinity instead.

In view of the previous we will focus our attention in this study to changes in the circulation and water properties in the upper few hundreds of meters, i.e. at shallow and intermediate levels. At these levels a steady state is generally reached in less than 10 years; the results shown in this chapter are taken from year 15 of each experiment. Table 6.1 gives an overview of all experiments. To adjust precipitation and evaporation to precession minimum conditions we consider the basin average of the changes found with the ECBilt runs. In other words, the adjustment is uniform across the entire sea surface. This may be considered a first approximation, motivated in particular by the coarse resolution of the modeled atmospheric fields. All ECBilt-

Description	Figure(s)
control experiment	6.3, 6.4, and 6.5
50% increase in annual mean discharge from south	6.6
50% increase in annual mean discharge from north	6.7
P-E (over basin) adjusted to precession minimum	6.8
control experiment with monthly-varying discharge	6.9
variable discharge from north adjusted to precession min.	not shown
variable discharge of Nile adjusted to precession min.	6.10
variable discharge of all rivers and P-E adjusted to prec. min.	6.11 and 6.12

Table 6.1: *Overview of model experiments.*

derived variables are monthly averages averaged over the last 100 years of integration.

### 6.3 Precession-induced changes in the Mediterranean freshwater budget

#### ECBilt control run compared to Mediterranean climatology

Before considering the changes in the freshwater budget found with ECBilt for precession minimum conditions we compare the predicted present day precipitation and evaporation with available other estimates. This section may thus be considered an evaluation of the accuracy of ECBilt specifically regarding the Mediterranean Sea.

As explained above we will limit ourselves at this stage to monthly mean and basin-averaged values of precipitation and evaporation. In ECBilt the Mediterranean Sea consists of 9 grid cells, each measuring about  $5.5^\circ$  by  $5.5^\circ$ . The surface freshwater fluxes are shown in Fig. 6.1 expressed in mm per day. Material for comparison is from a variety of sources (see figure caption for details). Fig. 6.1 confirms something that was already concluded from the global scale model evaluation namely that ECBilt tends to underestimate precipitation. The model-predicted precipitation is close to the CMAP estimates for November through January but is lower for the rest of the year and ECBilt also gives less precipitation than the Jaeger (1976) and Legates/MSU datasets. It may be noted in passing that the latter two datasets deviate significantly during autumn and winter. A significant difference is also present between the estimates of evaporation based on the Budyko (1963) and the Kondo (1975) scheme. In its turn, ECBilt-predicted evaporation deviates from these two estimates in that it shows a much stronger seasonal variation: the spring/summer low is below that found with the Kondo (1975) scheme while the winter high is above that derived with the Budyko (1963) coefficients.

#### Precession-induced changes in runoff

To be able to calculate runoff from the bordering continents into the Mediterranean Sea, drainage basins were assigned, based roughly on the present day situation. Only



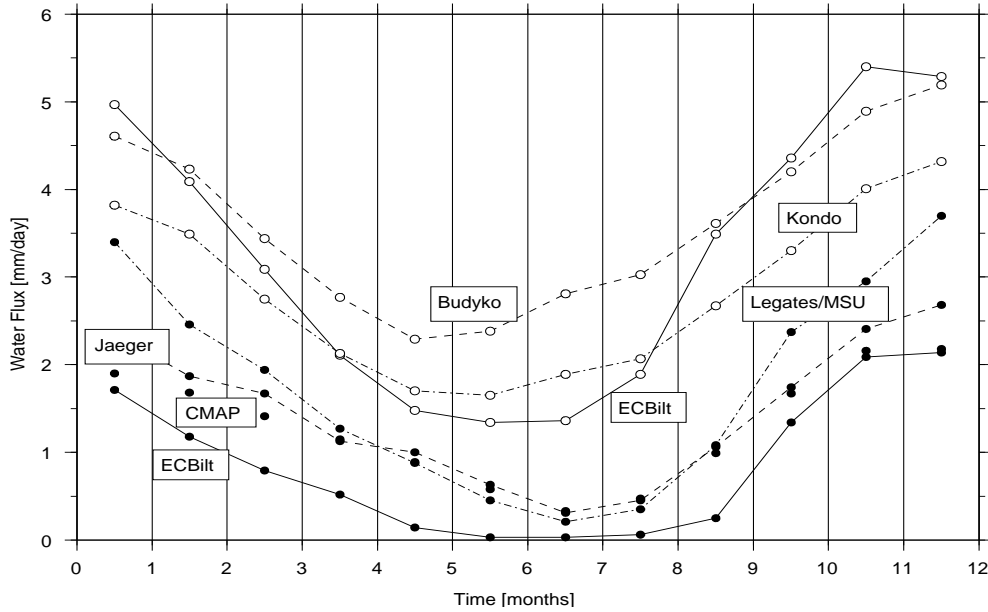


Figure 6.1: Precipitation and evaporation over the Mediterranean Sea as calculated with ECBilt for the present day, compared to other available estimates. Closed circles: precipitation, open circles: evaporation. The vertical axis gives the absolute value of the basin-averaged water flux in mm/day. Key to precipitation, continuous line: ECBilt; no line: CMAP; dashed line: Jaeger (1976); dash-dotted line: Legates/MSU. Key to evaporation, continuous line: ECBilt; dashed line: using Budyko (1963) scheme; dash-dotted line: using Kondo (1975) scheme. The precipitation climatology due to Jaeger (1976) is based on rain gauge measurements (resolution  $5^\circ$  longitude by  $2.5^\circ$  latitude). Two datasets obtained by merging gauge measurements, satellite observations, and model results are used: the Legates/MSU climatology (Wallace, Mitchell, and Lau, Joint Institute for the Study of the Atmosphere and Ocean, <http://tao.atmos.washington.edu>) and CMAP (CPC Merged Analysis of Precipitation, Xie and Arkin (1997)). Both datasets have a resolution of  $2.5^\circ$  in longitude and latitude. For evaporation we show two estimates derived by Gerasimos Korres of Athens University and made available in the context of the Mediterranean Forecasting System Pilot Project (<http://www.oc.phys.uoa.gr/mfspp>). Fields are based on a climatology obtained by averaging of European Centre for Medium-Range Weather Forecasts re-analysis data for Jan 1979 - Dec 1993 and have a resolution of  $1^\circ \times 1^\circ$ . (Korres and Lascaratos (2003) give details of the data processing). Evaporation was calculated using either the Budyko (1963) or Kondo (1975) bulk aerodynamic scheme.

two basins were considered: one that drains into the Mediterranean Sea from the north and one that comprises all water entering from the south. Fig. 6.2a shows the monthly averaged runoff values thus found, both for the present day experiment and for the precession minimum run. Runoff values are given in normalised fashion by dividing the monthly values of runoff from the south by the annual mean of that runoff found with the control experiment and likewise for runoff from the north. It is these normalised values that will be used in the ocean experiments. Absolute values of the changes in runoff are shown in Fig. 6.2c where they are expressed in terms of an equivalent basin-wide change in sea level (the volume of runoff entering per unit of time is divided by the surface area of the Mediterranean Sea). This allows for direct comparison with the surface freshwater fluxes, precipitation and evaporation (see below). Fig. 6.2a shows that runoff from the south is less than average during February - May and greater than average in summer, i.e. July - September. In contrast, during roughly the same period, June - September, runoff from the north is predicted by ECBilt to be very small. Runoff from the north is above average in the period November - March. The precession minimum experiment predicts an overall increase of runoff from both the south and the north; annual mean values increase by a factor 1.20 and 1.07, respectively. These increases occur at different times of the year, however. Runoff from the south increases in May - September, while runoff from the north is higher in October - March.

### Precession-induced changes in P-E

Fig. 6.2b summarizes the ECBilt-derived changes in monthly-mean precipitation (P) and evaporation (E) over the Mediterranean Sea that we find going from the present day to precession minimum conditions (the change in P-E is repeated in Fig. 6.2c). Changes in precipitation are small from April - August and reach a maximum in October, i.e. it is in October that precipitation in the precession minimum run reaches its greatest excess over precipitation in the present day run. During the period March - July evaporation in the precession minimum run is less than in the present day experiment: the difference corresponds to a flux of water into the sea (positive sign in Fig. 6.2b). The period of maximum increase of precipitation (autumn and winter) coincides with a maximum increase in evaporation (the largest negative values in the figure). During most of the year the net freshwater flux into the sea (P-E) is greater at precession minimum than it is at present. The net flux is less during August - October.

Fig. 6.2c shows all changes in the freshwater budget expressed in the same units which demonstrates that the precession-induced changes in runoff and P-E are of comparable order. The maximum increase in runoff amounts to 0.3-0.4 mm/yr, net freshwater flux is maximally higher by 0.5-0.6 mm/yr.

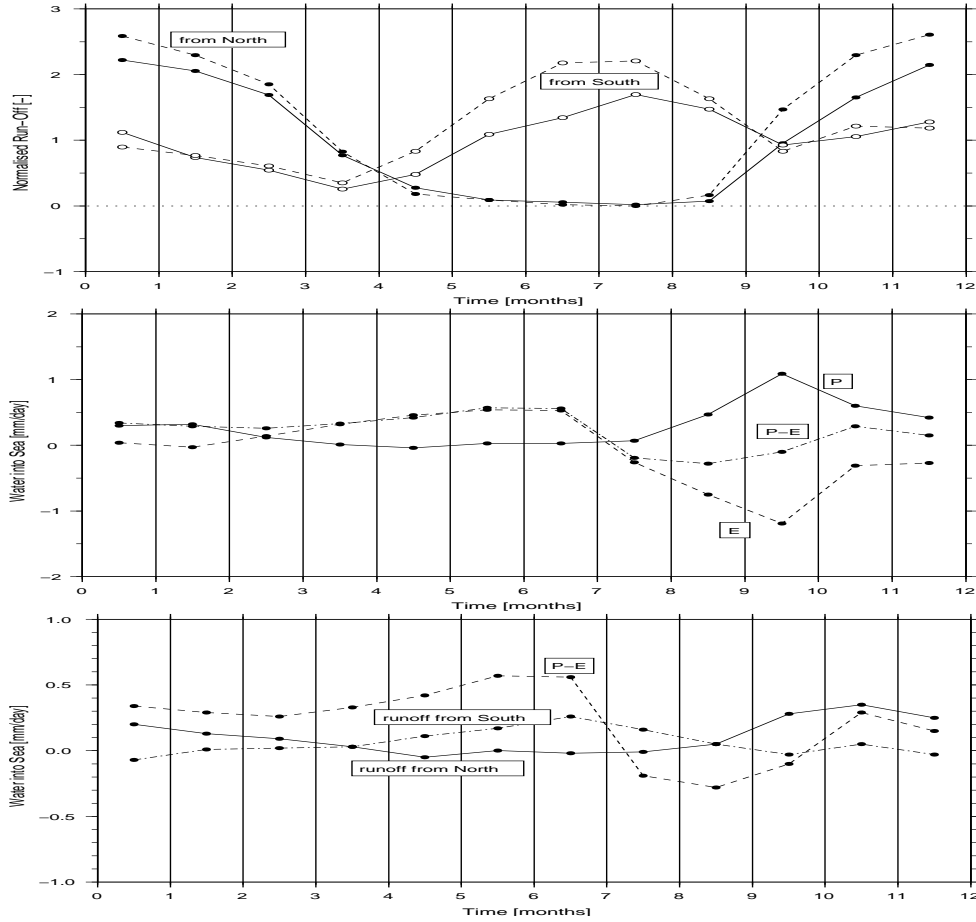


Figure 6.2: a) Monthly runoff into the Mediterranean basin from the north (closed circles) and south (open circles) as calculated with ECBilt for a present day control run (continuous lines) and for precession minimum (dashed lines). Values have been divided by the corresponding annual mean of the ECBilt control experiment. b) Change in precipitation ( $P$ , continuous line), evaporation ( $E$ , dashed line), and  $P-E$  (dash-dotted line) from present day control to precession minimum: shown is precession minimum minus control. Precipitation is taken positive (i.e., the vertical axis gives the flux of water into the sea). c) Absolute magnitudes of the changes in the three components of the freshwater budget. As before, changes are defined as precession minimum minus control. Changes in runoff have been divided by basin area to obtain an equivalent surface flux. Continuous line: runoff from north; dash-dotted line: runoff from south; dashed line:  $P-E$ .

## 6.4 Results

### 6.4.1 Control experiment

Notwithstanding the above-mentioned differences in set-up, the control experiment was found to behave in a similar way as the control experiment of Meijer et al. (2004) in many respects. For results in terms of average properties such as kinetic energy, average temperature, and average salinity the reader is referred to Meijer et al. (2004). Here we will discuss the annual mean surface circulation and then concentrate on those aspects of the control run that are pertinent to establishing the effects of precession.

The mean surface flow (30 m depth) during year 15 is shown in Fig. 6.3. In an overall sense, the model-predicted surface flow is in fair correspondence with the observed pattern (see, for example, Pinardi and Masetti, 2000). At the Strait of Gibraltar there occurs inflow of water from the Atlantic ocean. This 'Atlantic current' can be followed through the Sicily Strait, all the way into the easternmost Levantine basin. Here the flow turns back westwards around the island of Cyprus. In the northern part of the western Mediterranean we find the model representation of the Gulf of Lions gyre. The Tyrrhenian Sea is occupied by a northward flow branching off from the Atlantic current. In the northern Ionian basin and to the southeast of Crete weak cyclonic gyres are developed while to the south of the Atlantic current, in the southern Ionian basin, we observe an anti-cyclonic gyre. It must be noted that some gyres are averaged-out in this annual mean flow field. A mismatch between model and observation concerns the location of the Atlantic inflow in the western Mediterranean Sea. In contrast to what the model predicts this flow is observed to stay south of the Balearic islands. At the surface (5 m depth) the salinity pattern calculated for mid February of year 15 clearly shows the relatively fresh inflow of Atlantic water, in the western Mediterranean as well as in the eastern Mediterranean (Fig. 6.4a). The result of net evaporation is obvious in the raised salinity of the EMed. In particular the discharge from the Po, Black Sea, and Nile is expressed by locally reduced salinities. The modeled sea surface salinity differs from the observed field in the northward shifted Atlantic inflow and in its high salinity in the southern Ionian basin. Fig. 6.4b illustrates the distribution of mixed layer depth in the control experiment. In addition, this figure shows at which locations the properties of the mixed layer match that of Levantine Intermediate Water (LIW) as defined by Lascaratos et al. (1993): temperature between 15-16°C and salinity between 38.95-39.05 psu. Depths to about 500 meter (locally deeper) are reached in the EMed at longitudes between Crete and Cyprus, in the southern Aegean Sea, in the Ionian Sea off Calabria, and in the northern WMed. In correspondence with observations, water of LIW properties is predicted to occur between Crete and Cyprus. In addition the model shows water of these characteristics to exist south and west of mainland Greece and in the southern Ionian sea. In February, the mixed layer is deepest in a general sense, i.e. across the whole basin. By mid March (not shown) a shallow surface layer has been reinstated in many parts of the basin but in particular to the west of Crete and off Calabria the mixed layer reaches greater depths than in February (up to 1500 meter).

So as to visualise the simulated thermohaline circulation we show in Fig. 6.5

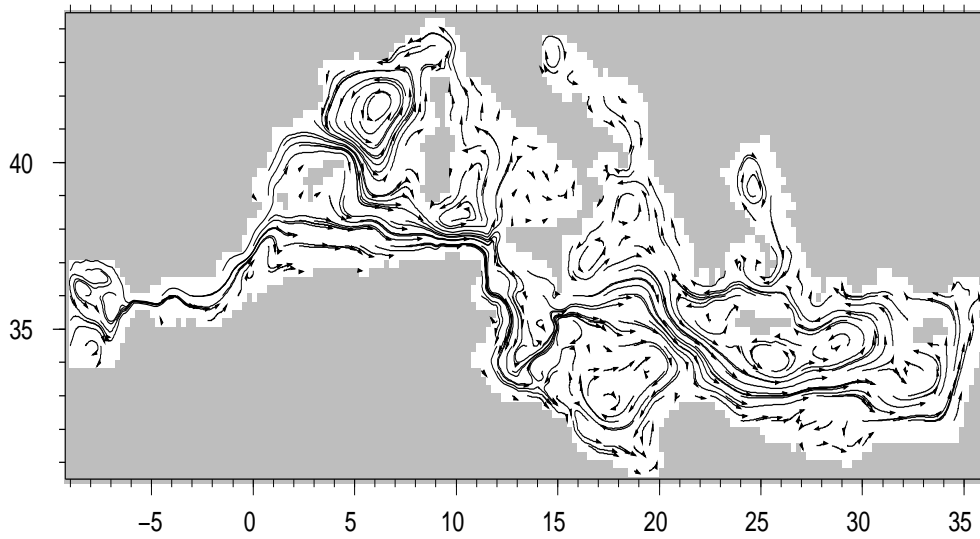


Figure 6.3: *Trajectories of annual mean surface flow (30 m depth) for the control experiment. Shown are the paths particles would travel in 60 days keeping the annual mean velocity field constant.*

the mean zonal overturning stream function for year 15. This stream function was calculated on the basis of the annual mean velocity field following the definition of Stratford et al. (2000). At each longitude and depth, velocities are integrated in the meridional direction thus obscuring any north-south variation that may be present. The resulting graph is potentially as misleading as it is revealing and must be interpreted with caution. Note in particular the central portion of Fig. 6.5 where flow in the eastern Tyrrhenian Sea is combined with flow in the northernmost Adriatic and to the south of Sicily. The reason for this being of course that these areas share the same longitude. Notwithstanding these distortions the figure clearly demonstrates the presence of overall eastward transport at the surface in both basins and a westward return flow at intermediate depth. The latter is displaced downwards in the area west of Crete due to the outflow of dense water from the southern Aegean Sea. Also demonstrated very clearly by Fig. 6.5 is the failure of our ocean model to simulate circulation at depths below the intermediate return flow.

#### 6.4.2 The role of runoff; Constant discharge

At precession minimum, ECBilt predicts an increase in runoff from the south and north by, respectively, a factor 1.20 and 1.07. Here we deliberately take an overestimate of this increase and examine, river by river, the effect on circulation of an increase in discharge by 50%. In this we first concentrate on rivers draining the African continent. Fig. 6.6 shows the change in surface salinity for February. It must be emphasized that, as yet, we consider the case of constant discharge; the effects of

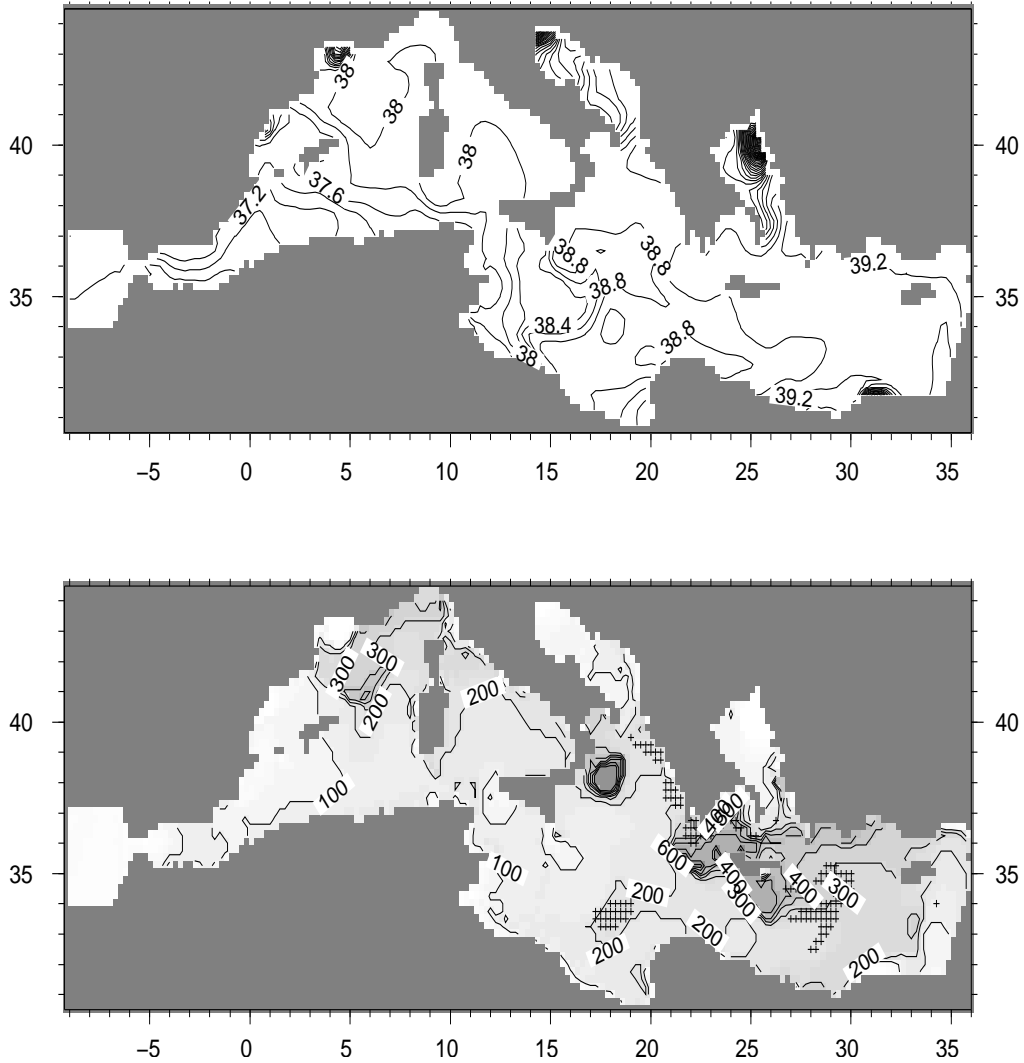


Figure 6.4: a) Sea surface salinity field computed for February of year 15 of the control experiment. Contour interval is 0.2 psu. b) Distribution of mixed layer depth for February of year 15 of the control experiment. Contour interval is 100 meter. Small crosses denote cells where the salinity and temperature of the mixed layer match those of Levantine Intermediate Water as defined by Lascaratos et al. (1993). A shading is added to clarify the pattern of mixed layer depth: darker grey corresponds to deeper mixing.

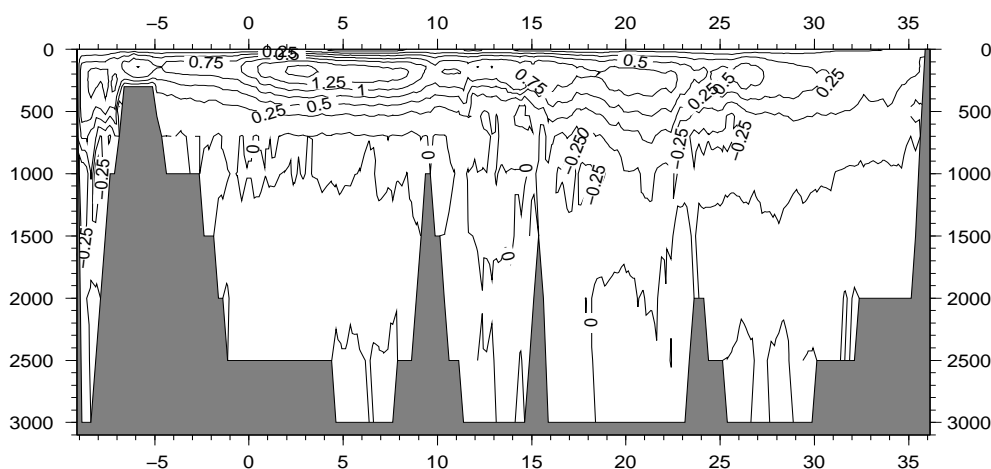


Figure 6.5: Zonal overturning streamfunction calculated on the basis of the annual mean velocity field of year 15 of the control run. Contour interval is 0.25 Sv. At each longitude the most deeply situated seafloor is indicated. Transport is along streamlines to the right when going from high to low values of the streamfunction.

introducing a monthly variation is discussed below.

Increasing the discharge from the Nile (Fig. 6.6a) results in a lowering of salinity along the coast of the easternmost basin which is where the Nile water is being carried as part of the Atlantic current. The zone of reduced salinity can be traced into the southern Aegean Sea and even beyond the strait between Crete and mainland Greece. In the Ionian Sea we find more areas of lower salinity but also areas where the salinity has increased; here salinity differences with respect to the control experiment build a complex pattern. Of particular interest is the finding that salinity changes are relatively small in the area between Crete and Cyprus where we know formation of Levantine Intermediate Water takes place. When the climate over Africa was wetter than at present, significant amounts of runoff from the continent may have entered the sea through other rivers than the Nile. The discovery of old river channels, now buried below desert sands, supports this suggestion. Figs. 6.6b and c show the consequences of 50% of the pre-Aswan Nile discharge flowing in from points to the west of the Nile. In the first case water enters at the Gulf of Syrte, in the second case it flows in from the Gabes depression of Tunisia. Both experiments show a decrease in salinity in the vicinity of the river mouth and a combination of salinity reduction and increase in the northern Ionian Sea. For both experiments it holds true that effects on salinity are subdued in the eastern part of the Mediterranean Sea.

On close inspection, when studying changes in the surface flow pattern as well, it follows that the complex mix of negative and positive salinity changes in the Ionian Sea is mostly related to small changes in the current pattern. For example, the area of increased salinity to the west of Crete, best seen in Fig. 6.6a but present in the other experiments as well, proves due to a small southward shift in the northern

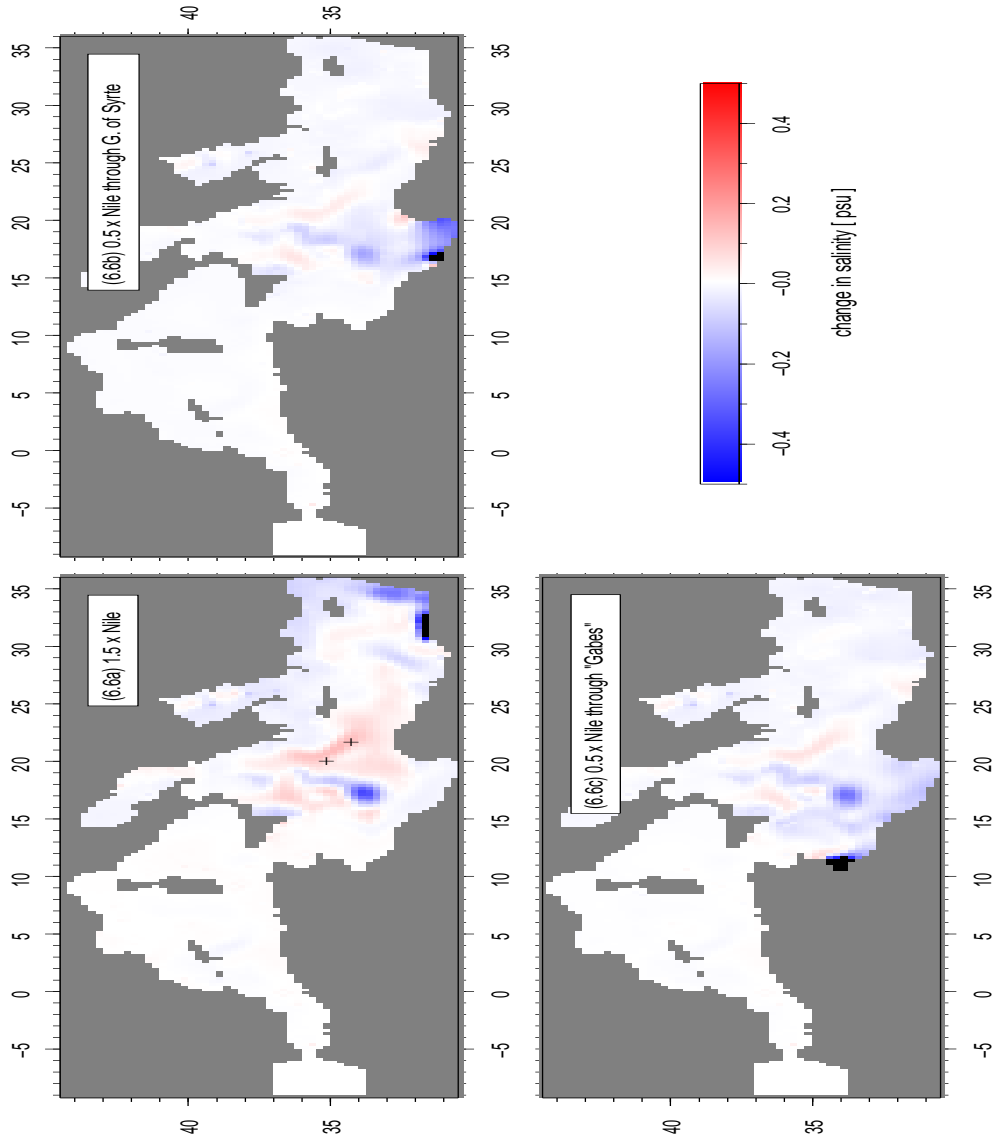


Figure 6.6: Change in sea surface salinity in February due to increase in discharge from the Nile and alternative points at the southern coast. Reference is the control experiment. a) Pre-Aswan Nile discharge increased with 50%. b) 50% of pre-Aswan Nile discharge flowing in through Gulf of Syrte. c) 50% of pre-Aswan Nile flowing in through Gabes depression. Areas with the largest positive differences are indicated with '+'. Over the other areas the differences are either positive but very small or negative.



boundary of the Atlantic current. Places that used to be touched by the relatively fresh Atlantic current are now occupied by saltier adjacent waters. Likewise, the pronounced salinity decrease in the middle of the southern Ionian Sea is related to a further eastward reach of a relatively fresh current that branches off from the Atlantic current.

The response of mixed layer depth to increased runoff from the south is similar for all three cases considered (not shown): in parts of the EMed where the control experiment shows mixing to extend down to intermediate levels (Fig. 6.4b), the depth reached by mixing is reduced due to the addition of extra discharge. These reductions in depth are most widespread for the case of extra discharge from the Nile. In this case the maximum decrease between Crete and Cyprus is 160 meter. Although reductions in mixing depth clearly coincide with reductions in surface salinity the reverse is not necessarily true. For example, the significant reductions in salinity that occur at the points where the extra runoff enters the basin have no corresponding expression in mixed layer depth: these locations are always characterised by stably stratified waters. In particular for the case of increased Nile discharge we also find small areas where the depth of mixing increases; these areas coincide with areas of increased surface salinity. Mixing depth in the WMed is found to be unaffected.

One month later, by mid March, the patterns of changes in sea surface salinity and mixed layer depth are similar to those found for mid February and results are not shown here. In particular everywhere to the west of Crete the differences (negative and positive) are of slightly greater magnitude. This difference between March and February proves present in all our experiments and from this point onwards we will only describe the results obtained for February.

In the same fashion that we handled extra runoff from the south we now study the effect of increased runoff from the north. The northern rivers Po, Rhône, Ebro, and also the net inflow from the Black Sea are separately increased by 50%. As was the case for rivers from the south, the effect on surface salinity (Fig. 6.7) is often twofold: a reduction of salinity in the vicinity of the river mouth, directly related to the addition of freshwater, and a more complex expression further away, associated with changes in the current pattern. As shown by Fig. 6.7a extra discharge from the Black Sea has a pronounced effect. Salinity is reduced in the northern Aegean Sea but also, via the westward flow through the strait between Crete and mainland Greece, in the Adriatic Sea. This is relevant knowing that the southern Adriatic Sea is the site of deep water formation for the EMed. Further to the south, in the Ionian Sea, we find a complex response that is similar to that found for increased Nile discharge (compare Figs. 6.7a and 6.6a). Increased discharge from the Rhône and Po has a direct effect on the salinity in the areas of deep water formation. Although our model does not allow us to assess the consequences for deep water formation it does show the depth of mixing in the Gulf of Lions to be reduced (not illustrated).

### 6.4.3 The role of (P-E) over the basin

Again taking the control experiment with annual mean discharge as a starting point, we now investigate the effect of adjusting the flux of freshwater (P-E) through the sea

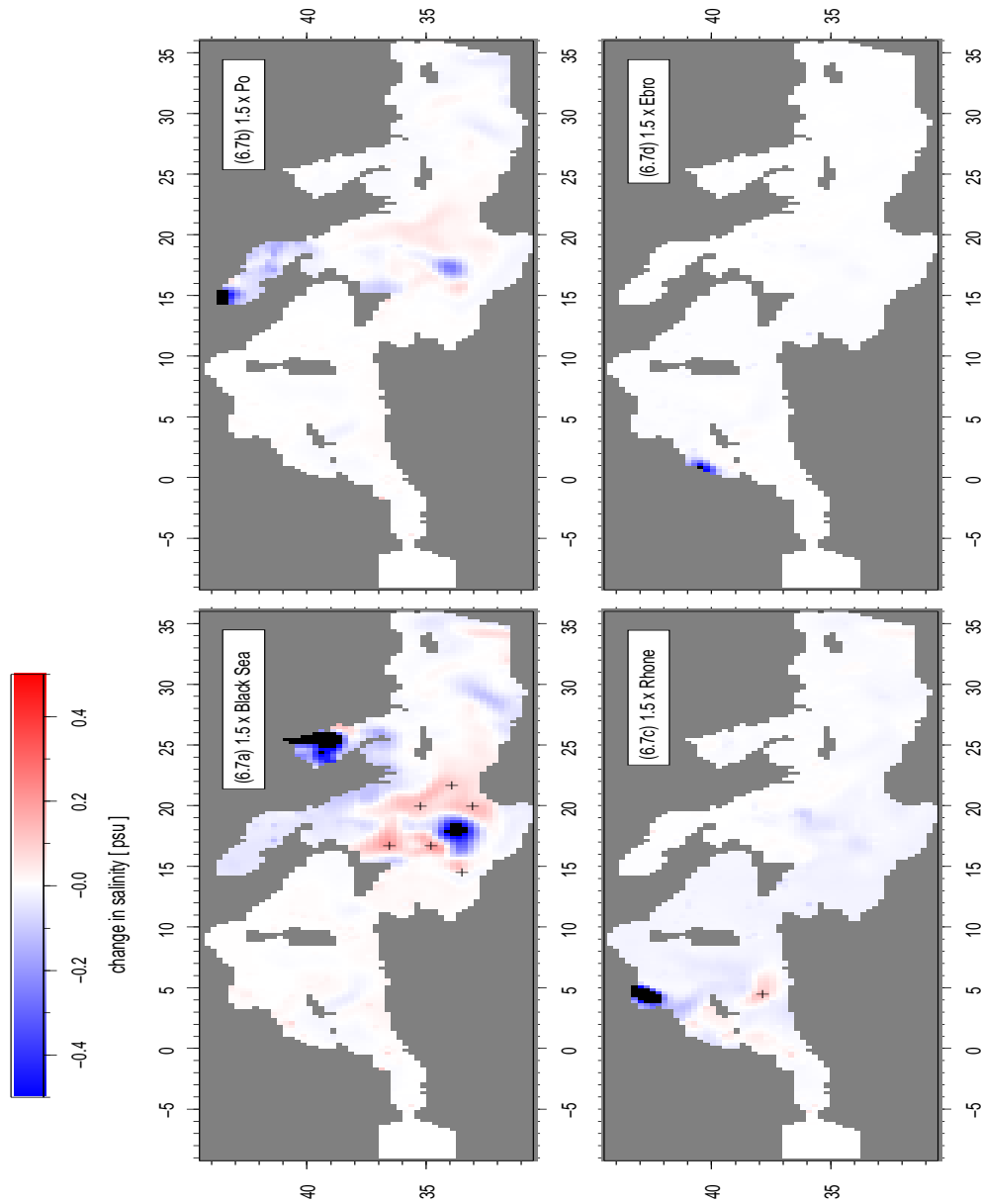


Figure 6.7: *Change in sea surface salinity in February due to 50% increase in discharge from northern Rivers and Black Sea. Reference is the control experiment. a) Black Sea. b) Po river. c) Rhône river. (d) Ebro river. Areas with the largest positive differences are indicated with '+'. Over the other areas the differences are either positive but very small or negative.*

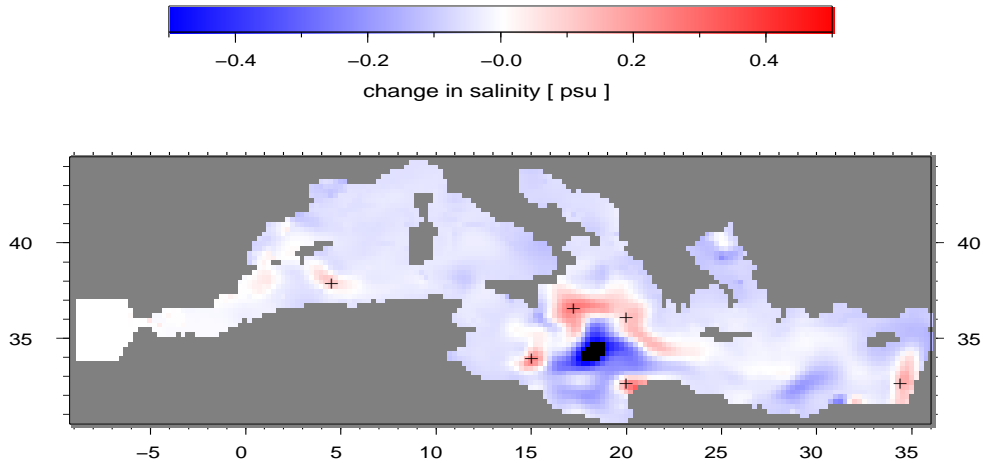


Figure 6.8: *Change in sea surface salinity in February due to precession- induced change in P-E over the Mediterranean Sea. Reference is the control experiment. Note that the scale is the same as in Figures 6.6 and 6.7. Areas with the largest positive differences are indicated with '+'.* Over the other areas the differences are either positive but very small or negative.

surface to precession minimum conditions. Fig. 6.8 gives the resulting changes in sea surface salinity. In February, as during the three preceding months, the adjustment to precession minimum amounts to an addition of (fresh) water to the sea surface. This is expressed in a widespread reduction of sea surface salinity. The pronounced salinity increase in the central Ionian Sea - very similar to that found to be associated with an increase in discharge from some of the rivers - is again related to induced changes in the current pattern. In this particular case the salinity increase appears to be related to a southward shift of the Atlantic current in conjunction with a fresher outflow from both the Aegean Sea and Adriatic Sea. The tongue-shaped zone of increased salinity along the southern Levantine coast reflects the disappearance of a tongue of relatively low salinity water which is present in this location in the control experiment (see Fig. 6.4a). This low salinity tongue is placed there during the preceding month and originates from the outflow of the Nile. Changes in the evolution of currents apparently prevent this emplacement from happening in the experiment with modified surface fluxes. Apart from some areas that remain stably stratified, parts of the basin that witness a decrease in surface salinity show a corresponding decrease in mixed layer depth and vice-versa. Between Crete and Cyprus the maximum decrease in mixed layer depth amounts to 200 meter. Even though the adjustment of P-E is done in a uniform way across the entire basin, the response of surface salinity (and mixed layer depth) is clearly not uniform. In general, changes due to the adjustment of P-E are of equal or greater magnitude than changes we found to be associated with a 50% increase in discharge from the Nile or the other rivers and Black Sea.

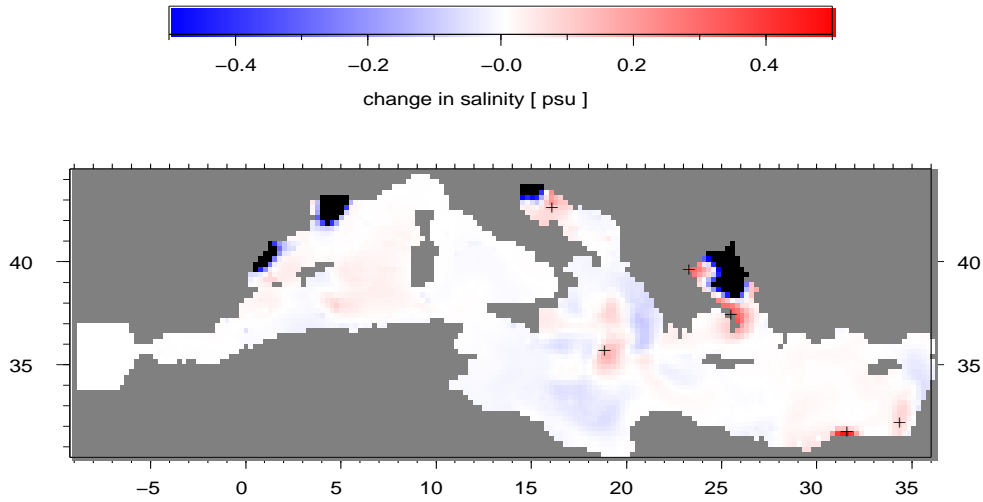


Figure 6.9: *Change in sea surface salinity in February associated with monthly-varying discharge from all rivers and Black Sea. Reference is the control experiment (with annual mean discharge). Areas with the largest positive differences are indicated with '+'.* Over the other areas the differences are either positive but very small or negative.

#### 6.4.4 The role of runoff; Monthly-varying discharge

Up to this point we have considered the case of constant discharge, i.e. a perpetual annual mean value was included. Here we examine the effect of making the discharge monthly variable by first modifying the control experiment to this extent. The size of the imposed monthly variation is that found for continental runoff in the ECBilt control run. For example, Nile discharge through the year follows the ECBilt 'runoff from the south' signal. To be precise, for each month we computed the "runoff from south" relative to the annual mean (the 'normalised runoff' of Fig. 6.2a). In the ocean model the monthly factors thus found are multiplied with the annual mean discharge values used so far. This results in a distribution of discharge through the year without changing the total annual amount. The effects of variable discharge are here shown for the case that rivers from the north (including the Black Sea) as well as the Nile are made monthly-varying (Fig. 6.9). The possibility of runoff from the south entering at other points than the Nile is ignored. The various rivers have been considered separately as well which demonstrates that the effect of the Nile is restricted to the southeastern Levantine while all changes in the rest of the basin are due to the Black Sea and the northern rivers. In the case of the Nile the effect of monthly-varying discharge proves mainly restricted to changes of the salinity in the path of the outflow along the Levantine coast. During February discharge from the Nile is less than average (Fig. 6.2a) and we observe a consequent increase in salinity of the waters right at the river mouth. In the northeastern Levantine basin, to the east of Cyprus, we find waters that are relatively fresh: these were formed at the

river mouth in summer and have been moved to this location during the intervening period.

During winter, runoff from the north is greater than average which results in a strong decrease of salinities in the vicinity of the entry points of the northern rivers and Black Sea. Elsewhere in the basin we find smaller salinity changes that are in general due to (1) changes in discharge during preceding months and (2) changes in the current pattern. The increase of winter discharge from the Rhône results in a decrease in the depth of mixing in the Gulf of Lions.

During winter at precession minimum, runoff from the north is increased (Fig. 6.2a). Therefore, for the month of February, the changes found by adjusting the monthly-variable discharge from the north to precession minimum conditions are qualitatively the same as the changes obtained for increased *annual mean* discharge. Note that, in the case of variable discharge, the 'change' is with respect to the control experiment modified to also include variable discharge (previous section). The results are not shown. In the vicinity of the river mouths we find the expected reduction of salinity and the Ionian Sea is again the site of a more complex far-field expression. The fact that the increase in discharge is now less than the 50% taken earlier is most clearly expressed in the changes related to Po and Black Sea: the corresponding zones of reduced salinity extend less far southwards.

The situation is different for the Nile. During February the discharge at precession minimum is essentially equal to that found for the present day (Fig. 6.2a). The effect on surface salinity in February (Fig. 6.10) is therefore much smaller than for the case when a constant discharge was increased by 50%. Slightly east of the center of the river mouth we find a small salinity increase. This water was formed at the river mouth during the preceding month when discharge at precession minimum was less than that at present (Fig. 6.2a). The plume of relatively fresh water off the southern Levantine coast was formed during the preceding summer (when discharge is higher at precession minimum, see Fig. 6.2a) and has been advected to this location. The fresher summer waters can not be traced beyond the northeastern Levantine.

#### 6.4.5 Combined precession minimum experiment

In our final experiment we adjust to precession minimum conditions the monthly-varying discharge from all rivers and the Black Sea, as well as the freshwater flux through the sea surface. As a reference we take the control experiment modified to include monthly-varying discharge. The resulting changes in surface salinity, shown in Fig. 6.11, are clearly a combination of the effects of each individual adjusted parameter. The salinity change may be summarized as an overall decrease due mostly to freshwater added through the surface (greater net precipitation), superimposed on which we find strong salinity reductions associated with increased runoff from the north and a combination of (strong) salinity decrease and increase in the Ionian Sea, reflecting induced changes in the current pattern. The depth of mixing has been reduced in much of the eastern Mediterranean with maximum reductions occurring in the southern Aegean Sea and to the south of Crete. The maximum reduction in the area of intermediate water formation between Crete and Cyprus is 280 meter.

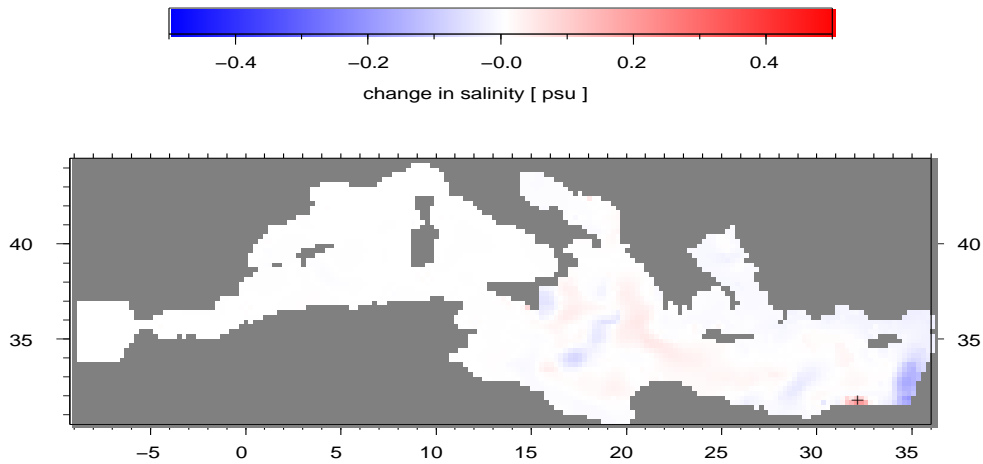


Figure 6.10: *Change in sea surface salinity in February due to adjustment of monthly-varying discharge from Nile to precession minimum. Reference is the control experiment modified to include monthly-varying Nile. Discharge from the northern rivers and Black Sea is kept constant. Areas with the largest positive differences are indicated with '+'. Over the other areas the differences are either positive but very small or negative.*

For this full precession minimum experiment we also compute the zonal overturning streamfunction (Fig. 6.12). The change with respect to the streamfunction computed for the control experiment (Fig. 6.5) is restricted to a small decrease in the intensity of the surface/intermediate depth cell. These small differences are due mainly to the adjustment to precession minimum conditions; the effect of distributing discharge over the year can be shown to have a negligible effect on the streamfunction. In the context of this combined experiment it must be pointed out that our way of implementing changes in discharge - by multiplying discharge in the control run with the normalised changes of Fig. 6.2a - leads to an increase in water input through all rivers and Black Sea that is less than the total increase in runoff. On an annual basis, the imposed increase in discharge from the Nile accounts for 35% of the change in runoff from the south and the increase in the discharge of the northern rivers and Black Sea taken together, is equal to 65% of the change in runoff from the north. The combined experiment has been repeated with discharge adjusted so that all of the increase in runoff is accounted for. In this case, changes in salinity near the river mouths are more pronounced than shown in Fig. 6.12 but the overall pattern is very similar. The intensity of overturning is reduced somewhat more.

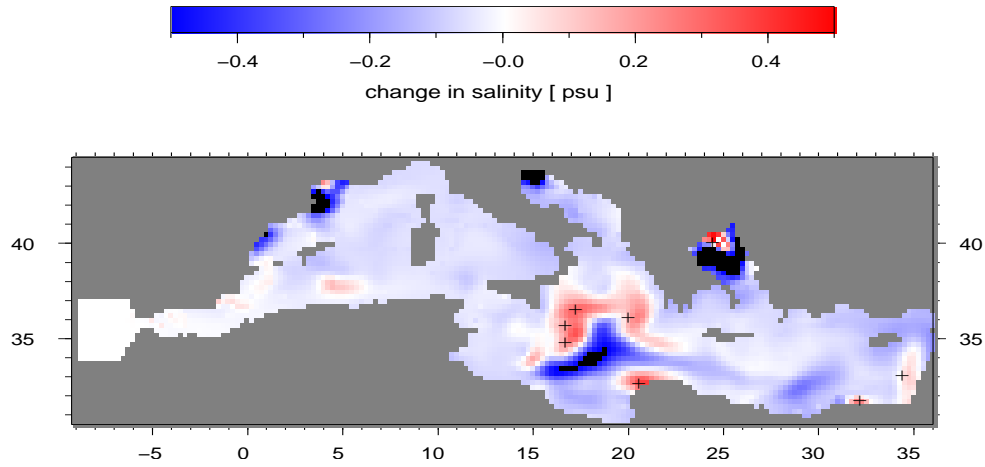


Figure 6.11: Change in sea surface salinity in February calculated for a combined precession minimum experiment. Monthly-varying discharge from all rivers and Black Sea, as well as P-E over the basin, are adjusted to precession minimum. Reference is the control experiment modified to include monthly-varying discharge. Areas with the largest positive differences are indicated with '+'. Over the other areas the differences are either positive but very small or negative.

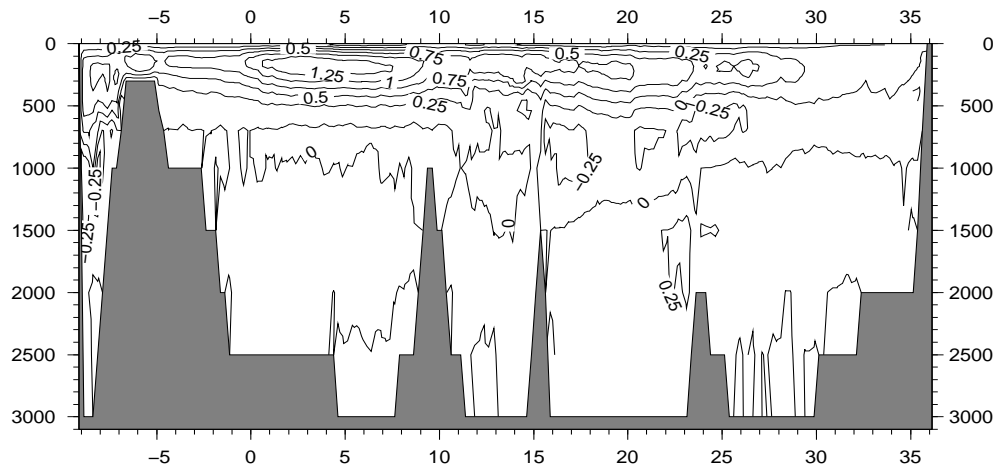


Figure 6.12: Zonal overturning streamfunction for combined precession minimum experiment (mean of year 15). Contour interval is 0.25 Sv. See caption to Fig. 6.5 for more explanation.

## 6.5 Discussion

### Implications

The work described in this chapter is a first attempt to elucidate the implications for Mediterranean circulation of the precession-induced changes in climate that are the subject of previous chapters. The model experiments provide valuable insight despite several uncertainties and limitations. In terms of magnitude of the corresponding water fluxes, the change in net precipitation over the basin itself is of the same order as the induced changes in runoff from the bordering continents. Whereas an increase in runoff from Africa is often considered crucial for sapropel formation, the associated amount of extra water is actually less than that due to net precipitation over the Mediterranean Sea itself. The effect of extra discharge from the Nile on sea surface salinity is also smaller than that of the change in net precipitation. The direct influence of the extra discharge does not extend beyond the northeastern Levantine. The limitations inherent to our model set-up do not allow us to examine the effects on deep-water formation explicitly. Nevertheless, from the way they affect sea surface salinity and mixing to intermediate levels, the discharge from the Rhône and Po rivers seems to play an important role in controlling deep water ventilation in the western and eastern sub-basin, respectively. We find that salinity reductions associated with an increase in net outflow from the Black Sea may extend to the southern Adriatic Sea and thus also affect deep water formation taking place there. Not only the location, but also the timing of the changes in discharge is important. Precession-induced increase in runoff from the north occurs in fall and winter and this extra water reduces the salinity, and hence density, of the surface waters at the sites of deep water formation in February and March which is when deep water formation is taking place.

### Uncertainties

In setting up our ocean model we chose for a realistic flux-driven coupling between the ocean and the atmosphere. This choice went at the expense of the capability of the model to simulate the full thermohaline circulation and prompted us to focus on shallow and intermediate depth levels. A pertinent question is whether the lack of deep water formation in our model perhaps influences the results that we obtain for shallower levels. An answer to this question is hard to give until we are able to compare our present results with those obtained with a "complete" model. For example, one might argue that the Mediterranean Sea should ultimately see a salinity change at all levels in response to a "wetter" climate. It remains uncertain, however, whether and how this would affect the results for shallow and intermediate depth.

### Comparison to previous studies

The issue of sapropel formation in the Mediterranean Sea was previously studied with an ocean circulation model by Myers et al. (1998) and Myers (2002). In the first of these studies a relaxation to an imposed sea surface salinity field is used



as boundary condition for salinity instead of a prescribed flux of freshwater. The circulation associated with the formation of the most recent sapropel,  $S_1$ , deposited between about 9 and 6 ka, was then modeled by adjusting present day sea surface salinities to conditions reconstructed for this time interval. This adjustment entails a typical reduction in surface salinity of 3 psu. The circulation patterns computed by Myers et al. (1998) were combined with a nutrient cycling model by Stratford et al. (2000). Here we note that the reduction in surface salinity considered by Myers et al. (1998) and Stratford et al. (2000) is significantly larger than any salinity changes we find: salinity reductions are less than 1 psu in our combined precession minimum experiment except at some river mouths at times of large discharge (Fig. 6.11). This holds true also when the total change in ECBilt-derived runoff is distributed over the different river points.

More recently, Myers (2002) presented a series of actual flux-forced model experiments. Myers (2002) started from an experiment driven by fluxes that were diagnosed from a relaxation experiment that is capable of simulating the complete thermohaline circulation and examined (1) the effect of uniform reductions in net evaporation (see also the closely related paper by Myers and Haines, 2002) and (2) the effect of increase in Nile discharge. The author finds that an increase in net precipitation by 20% or greater leads to stagnant deep waters, i.e., a precondition for sapropel formation. The amount of freshwater we added in our combined precession minimum experiment corresponds to an increase in the net precipitation with respect to the control run by 23% and, in view of the results of Myers (2002), may thus be considered sufficiently large to bring deep ventilation to a standstill. However, Myers (2002) also points out that, in order to reduce sea surface salinity to the levels associated with sapropel  $S_1$ , a much larger increase of net precipitation would be required (60-80%). This is consistent with the above-mentioned result that our combined precession minimum run produces salinity reductions less than the 3 psu inferred for the  $S_1$ . It would thus appear that the precession-induced increase in net precipitation over the basin and in runoff from the bordering continents is not enough to match the reduction in sea surface salinity thought to be associated with the most recent sapropel. In this respect it is important to keep in mind that climate models in general, and ECBilt in particular, are known to underestimate changes in precipitation [208].

## 6.6 Conclusions

In this chapter we have used a regional model for the circulation of the Mediterranean Sea to investigate the consequences of precession-induced changes in the freshwater budget. Our analysis allows us to draw the following conclusions:

- Increasing the amount of freshwater input leads to the expected reductions in (surface) salinity but also causes - via changes in the circulation pattern - some areas to witness a salinity increase.
- The effects of the change in P-E over the basin on sea surface salinity and mixing depth are of equal or greater importance than the effects of increased discharge

from the main rivers.

- The change in freshwater budget associated with precession minimum gives rise to only slightly reduced transport of the surface/intermediate depth circulation cell.
- Precession-induced increase in discharge from Rhône, Po, but also from Black Sea, may be expected to affect deep water formation.

## Chapter 7

# Outlook and perspectives

The main scientific aim of this thesis was to understand the mechanisms behind the cyclic deposition of sapropels in the Mediterranean Sea. Although productivity has played an additional role, it is generally assumed that sapropel formation is related to bottom water oxygen depletion induced by a weakening of the thermohaline circulation. This weakening may be caused by a stronger fresh water discharge entering the Mediterranean Sea. The scientific objectives relate to two fundamental questions: Firstly, how can the observed obliquity and precession signal in the sapropel record be explained? Secondly, can the observed lag of the youngest Holocene sapropel with respect to the precession parameter be explained by a lag in the response of (circum)Mediterranean climate to the precession forcing? In order to answer these questions, global climate models and a regional model of the Mediterranean Sea have been used.

The first question was addressed in chapters 2 and 4. In chapter 2 the climatic influence from the south (i.e. from the African summer monsoon) on the Mediterranean Sea was studied. It turned out that the African monsoon is influenced by precession as well as by obliquity with a stronger monsoon during minimum precession and maximum obliquity as compared to maximum precession and minimum obliquity, respectively. These signals in the African monsoon are in agreement with the signals in the sapropel record. In chapter 4 it was found that the influence from the north mainly consists of stronger precipitation over and near the Mediterranean Sea in autumn during minimum precession and maximum obliquity as compared to maximum precession and minimum obliquity, respectively. These signals are also in agreement with the sapropel record. In addition, the simulated precession signal is consistent with the precession signal found in a pollen record from northern Greece as described in chapter 5. From chapters 2 and 4 it can be concluded that the orbital signals in the sapropel record may originate from climatic influences from the north as well as from the south. However, in chapter 6 it was shown that increased (net) precipitation over the Mediterranean Sea decreases the salinity more effectively than increased discharge from the river Nile. The latter only decreases the salinity in the easternmost part of the Mediterranean Sea, away from the sites of deep-water forma-

tion. Therefore, it is hypothesized that sapropel formation is stronger influenced by (autumn) precipitation over and alongside the Mediterranean basin than by discharge from the river Nile.

The second question was addressed in chapter 3. It turned out that the lag observed for the youngest Holocene sapropel with respect to the precession parameter is not likely to be caused by the discharge from the river Nile because it does not show up in transient simulations of the African monsoon. However, a different mechanism is proposed based on a lag of some thousands of years which was simulated in the Atlantic thermohaline circulation. This lag was driven by temperature and only appeared when interactive vegetation was included. A similar mechanism could also apply to the thermohaline circulation in the Mediterranean Sea and thus explain the observed lag. On the other hand, it can not be excluded that the youngest Holocene sapropel is rather an exception compared to the older sapropels, i.e., the older sapropels could be in phase with the precession parameter. In fact, the formation of the youngest sapropel could have been influenced by processes associated with the termination of the last ice age, in particular the interruption of the last deglaciation by a return to cold climate conditions during the Younger Dryas.

Although the simulations described in this thesis already give some insight in the mechanisms underlying orbital signals in the (circum)Mediterranean climate, further research is needed. In chapters 2-4 changes in ice sheets were neglected. Even though the Mediterranean sapropel record does not appear to be strongly influenced by glacial cyclicity during the Pleistocene [121], it is obvious that ice sheets play an important role in climate change, especially at mid- and high latitudes. Therefore it would be useful to repeat the simulations described in chapters 2-4 of this thesis with an ice sheet model. In general, it would also be useful to repeat the simulations with more sophisticated and higher resolution models containing interactive vegetation. For the African summer monsoon more information about the spatial distribution and amplitude of the orbital signals would be obtained. It would be even more important to repeat the simulations for the northern borderlands as described in chapter 4 with a regional (atmosphere) model. A regional model better resolves the small scale processes associated with precipitation at mid- and high latitudes. The application of higher resolution models would also facilitate the off-line coupling to a Mediterranean Sea circulation model. An improved version of such a model which resolves deep-water formation would enable us to eventually close the link between orbital forcing and sapropel formation.

# Bibliography

- [1] J. Adhémar. Révolutions de la Mer: Déluges Périodiques, 1842. Carilian-Goeury et V. Dalmont, Paris.
- [2] L. Agassiz. Upon glaciers, moraines, and erratic blocks: Address delivered at the opening of the Helvetic Natural History Society at Neuchatel. *New Philosophy Journal Edinburgh*, 24: 864–883, 1838.
- [3] C. Appenzeller, T.F. Stocker, and M. Anklin. North Atlantic Oscillation dynamics recorded in Greenland ice cores. *Science*, 282: 446–449, 1998.
- [4] P. A. Baker, C.A. Rigsby, G.O. Seltzer, S.C. Fritz, T.K. Lowenstein, N.P. Bacher, and C. Veliz. Tropical climate changes at millennial and orbital timescales on the Bolivian Altiplano. *Nature*, 409: 698–701, 2001.
- [5] A. Berger. Support for the astronomical theory of climatic change. *Nature*, 269: 44–45, 1977.
- [6] A. Berger. Milankovitch theory and climate. *Review of Geophysics*, 26 (4): 624–657, 1988.
- [7] A. Berger and M. F. Loutre. Insolation values for the climate of the last 10 million years. *Quaternary Science Reviews*, 10: 297–317, 1991.
- [8] A. Berger and M. F. Loutre. Precession, eccentricity, obliquity, insolation and paleoclimates. In J.-C. Duplessy and M.-T. Spyridakis, editors, *Long-Term Climatic Variations*, volume I22, pages 107–151. Springer-Verlag Berlin Heidelberg, 1994.
- [9] A. Berger, M.F. Loutre, and C. Tricot. Insolation and earth’s orbital periods. *Journal of Geophysical Research*, 98 (D6): 10,341–10,362, 1993.
- [10] A. Berger, M.F. Loutre, and H. Gallée. Sensitivity of the LLN climate model to the astronomical and CO<sub>2</sub> forcings over the last 200 ky. *Climate Dynamics*, 14: 615–629, 1998.
- [11] A. Berger, M.F. Loutre, and J. Laskar. Stability of the astronomical frequencies Over the Earth’s history for paleoclimate studies. *Science*, 255: 560–565, 1992.

- [12] A. Berger, M.F. Loutre, and J.L. Mélice. Instability of the astronomical periods from 1.5 Myr to 0.5 Myr AP. *Paleoclimates*, 2 (4): 239–280, 1998.
- [13] A. L. Berger. Long-term variations of daily insolation and Quaternary climatic changes. *Journal of the Atmospheric Sciences*, 35: 2362–2367, 1978.
- [14] J.-P. Bethoux. Paleooceanographic changes in the Mediterranean Sea in the last 20000 years. *Oceanologica Acta*, 7: 43–48, 1984.
- [15] G. Bond, W. Showers, M. Cheseby, R. Lotti, P. Almasi, P. deMenocal, P. Priore, H. Cullen, I. Hajdas, and G. Bonani. A pervasive millennial scale cycle in North Atlantic Holocene and glacial climates. *Science*, 278: 1257–1266, 1997.
- [16] S. Bottema. *Late Quaternary vegetation history of northwestern Greece*. PhD thesis, Groningen, 1974. 190 pp.
- [17] P. Braconnot, M.-F. Loutre, B. Dong, S. Joussaume, P. Valdes, and PMIP participating groups. How the simulated change in monsoon at 6 ka BP is related to the simulation of the modern climate: results from the Paleoclimate Modeling Intercomparison Project. *Climate Dynamics*, 19: 107–121, 2002.
- [18] P. Braconnot and O. Marti. Impact of precession on monsoon characteristics from coupled ocean atmosphere experiments. *In preparation*, 2004.
- [19] P. Braconnot, S. Harrison, C.D. Hewitt, A. Kitoh, B. Otto-Bliesner, and S.L. Weber. Results of the PMIP working group on coupled ocean-atmosphere simulations for 6 ka BP. *To appear in 'Past Climate variability through Europe and Africa.*, Proceedings of the PAGES-PEP3 conference, 27-31 August 2001, Aix-en-Provence, France., 2002.
- [20] P. Braconnot, S. Joussaume, O. Marti, and N. de Noblet. Synergistic feedbacks from ocean and vegetation on the African monsoon response to mid-Holocene insolation. *Geophysical Research Letters*, 26 (16): 2481–2484, 1999.
- [21] P. Bretagnon. Termes à longues périodes dans le système solaire. *Astronomy and Astrophysics*, 30: 141–154, 1974.
- [22] D. Brickman, W. Hyde, and D.G. Wright. Filtering of Milankovitch cycles by the thermohaline circulation. *Journal of Climate*, 12: 1644–1658, 1999.
- [23] W. S. Broecker and J. van Donk. Insolation changes, ice volumes, and  $O^{18}$  record in deep-sea cores. *Review of Geophysics*, 8: 169–198, 1970.
- [24] A. Broström, M. Coe, S.P. Harrison, R. Gallimore, J.E. Kutzbach, J. Foley, I.C. Prentice, and P. Behling. Land surface feedbacks and palaeomonsoons in northern Africa. *Geophysical Research Letters*, 25 (19): 3615–3618, 1998.
- [25] V. Brovkin, A. Ganopolski, and Y. Svirezhev. A continuous climate-vegetation classification for use in climate-biosphere studies. *Ecological Modelling*, 101: 251–261, 1997.

- [26] V. Brovkin, M. Claussen, V. Petoukhov, and A. Ganopolski. On the stability of the atmosphere-vegetation system in the Sahara/Sahel region. *Journal of Geophysical Research*, 103 (D24): 31,613–31,624, 1998.
- [27] Budyko. *Atlas of the Heat Balance of the Earth (in Russian)*. 1963. Glabnaia Geofiz. Observ., A.I. Voeikova.
- [28] N. Calder. Arithmetic of ice ages. *Nature*, 252: 216–218, 1974.
- [29] R. Cheddadi, G. Yu, J. Guiot, S.P. Harrison, and I.C. Prentice. The climate of Europe 6000 years ago. *Climate Dynamics*, 13: 1–9, 1997.
- [30] M. Claussen, A. Ganopolski, V. Brovkin, F.-W. Gerstengarbe, and P. Werner. Simulated global-scale response of the climate system to Dansgaard/Oeschger and Heinrich events. *Climate Dynamics*, 21: 361–370, 2003. doi:10.1007/s00382-003-0336-2.
- [31] M. Claussen, C. Kubatzki, V. Brovkin, and A. Ganopolski. Simulation of an abrupt change in Saharan vegetation in the mid-Holocene. *Geophysical Research Letters*, 26 (14): 2037–2040, 1999.
- [32] M. Claussen and V. Gayler. The greening of the Sahara during the mid-Holocene: Results of an interactive atmosphere-biome model. *Global Ecology and Biogeography Letters*, 6 (5): 369–377, 1997.
- [33] M. Claussen, L.A. Mysak, A.J. Weaver, M. Crucifix, T. Fichefet, M.-F. Loutre, S.L. Weber, J. Alcamo, V.A. Alexeev, A. Berger, R. Calov, A. Ganopolski, H. Goosse, G. Lohmann, F. Lunkeit, I.I. Mokhov, V. Petoukhov, P. Stone, and Z. Wang. Earth system models of intermediate complexity: closing the gap in the spectrum of climate system models. *Climate Dynamics*, 18: 579–586, 2002.
- [34] S. Clemens, W. Prell, D. Murray, G. Shimmield, and G. Weedon. Forcing mechanisms of the Indian Ocean monsoon. *Nature*, 353: 720–725, 1991.
- [35] S. C. Clemens, D.W. Murray, and W.L. Prell. Nonstationary Phase of the Plio-Pleistocene Asian monsoon. *Science*, 274: 943–948, 1996.
- [36] E. R. Cook, R.D. D’Arrigo, and K.R. Briffa. A reconstruction of the North Atlantic Oscillation using tree-ring chronologies from North America and Europe. *The Holocene*, 8 (1): 9–17, 1998.
- [37] A. Cramp, M.B. Collins, and R. West. Late Pleistocene-Holocene sedimentation in the NW Aegan Sea: a paleoclimatic paleoceanographic reconstruction. *Palaeogeography, Palaeoclimatology, Palaeoecology*, 68: 61–77, 1988.
- [38] A. Cramp and G. O’Sullivan. Neogene sapropels in the Mediterranean: a review. *Marine Geology*, 153: 11–28, 1999.
- [39] J. Croll. *Climate and time in their geological relations: A theory of secular changes of the Earth’s climate*, 1875. Appleton, New York.

- [40] M. Crucifix and M. F. Loutre. Transient simulations over the last interglacial period (126-115 kyr BP): feedback and forcing analysis. *Climate Dynamics*, 19: 417–433, 2002.
- [41] M. Crucifix, M.-F. Loutre, P. Tulkens, T. Fichefet, and A. Berger. Climate evolution during the Holocene: a study with an Earth system model of intermediate complexity. *Climate Dynamics*, 19: 43–60, 2002.
- [42] H. M. Cullen and P. B. deMenocal. North Atlantic influence on Tigris-Euphrates streamflow. *International Journal of Climatology*, 20: 853–863, 2000.
- [43] N. de Noblet, P. Braconnot, S. Joussaume, and V. Masson. Sensitivity of simulated Asian and African summer monsoons to orbitally induced variations in insolation 126, 115 and 6 kBP. *Climate Dynamics*, 12: 589–603, 1996.
- [44] G. Digerfeldt, S. Olsson, and P. Sandgren. Reconstruction of lake level changes in lake Xinias, central Greece, during the last 40 000 years. *Palaeogeography, Palaeoclimatology, Palaeoecology*, 158: 65–82, 2000.
- [45] R. Doherty, J. Kutzbach, J. Foley, and D. Pollard. Fully coupled climate/dynamical vegetation model simulations over Northern Africa during the mid-Holocene. *Climate Dynamics*, 16: 561–573, 2000.
- [46] J.-C. Duplessy, C. Lalou, and A.C. Vinot. Differential isotopic fractionation in benthic foraminifera and paleotemperatures reassessed. *Science*, 168: 250–251, 1970.
- [47] C. Emiliani. Pleistocene temperatures. *Journal of Geology*, 63: 538–578, 1955.
- [48] K. Faegri and J. Iversen. *Textbook of Pollen analysis*. John Wiley & Sons, 1989.
- [49] A. Farjon. *Pinaceae, drawings and descriptions of the genera*, volume 121 of *Regnum Vegetabile*. Koeltz Scientific Books, 1990. 330 pp.
- [50] J. A. Foley, J.E. Kutzbach, M.T. Coe, and S. Levis. Feedbacks between climate and boreal forests during the Holocene epoch. *Nature*, 371:52–54, 1994.
- [51] A. M. Forte and J. X. Mitrovica. A resonance in the Earth’s obliquity and precession over the past 20 Myr driven by mantle convection. *Nature*, 390: 676–680, 1997.
- [52] M. R. Frogley, P.C. Tzedakis, and T.H.E. Heaton. Climate variability in North West Greece during the Last Interglacial. *Science*, 285: 1886–1889, 1999.
- [53] R. G. Gallimore and J. E. Kutzbach. Snow cover and sea ice sensitivity to generic changes in Earth orbital parameters. *Journal of Geophysical Research*, 100 (D1): 1103–1120, 1995.
- [54] A. Ganopolski, C. Kubatzki, M. Claussen, V. Brovkin, and V. Petoukhov. The influence of vegetation-atmosphere-ocean interaction on climate during the mid-Holocene. *Science*, 280: 1916–1919, 1998.



- [55] A. Ganopolski, S. Rahmstorf, V. Petoukhov, and M. Claussen. Simulation of modern and glacial climates with a coupled global model of intermediate complexity. *Nature*, 391: 351–356, 1998.
- [56] A. Ganopolski, V. Petoukhov, S. Rahmstorf, V. Brovkin, M. Claussen, A. Eliseev, and C. Kubatzki. CLIMBER-2: a climate system model of intermediate complexity. Part II: model sensitivity. *Climate Dynamics*, 17: 735–751, 2001.
- [57] J. Giraudeau, M. Cremer, S. Manthe, L. Labeyrie, and G. Bond. Cocolith evidence for instabilities in surface circulation south of Iceland during Holocene times. *Earth and Planetary Science Letters*, 179 (2): 257–268, 2000.
- [58] H. Goosse, E. Deleersnijder, T. Fichefet, and M.H. England. Sensitivity of a global coupled model ocean-sea ice model to the parametrization of vertical mixing. *Journal of Geophysical Research*, 104: 13,681–13,695, 1999.
- [59] H. Goosse and T. Fichefet. Importance of ice-ocean interactions for the global ocean circulation: A model study. *Journal of Geophysical Research*, 104 (C10): 23,337–23,355, 1999.
- [60] H. Goosse, F.M. Selten, R.J. Haarsma, and J.D. Opsteegh. Decadal variability in high northern latitudes as simulated by and intermediate-complexity climate model. *Annals of Glaciology*, 33: 525–532, 2000.
- [61] H. Goosse, F.M. Selten, R.J. Haarsma, and J.D. Opsteegh. Large sea-ice volume anomalies simulated in a coupled climate model. *Climate Dynamics*, 20: 523–536, 2003.
- [62] K. Haines and P. Wu. GCM studies of intermediate and deep-waters in the Mediterranean. *Journal of Marine Systems*, 18: 197–214, 1998.
- [63] S. P. Harrison, J.E. Kutzbach, I.C. Prentice, P.J. Behling, and M.T. Sykes. The response of Northern Hemisphere extratropical climate and vegetation to orbitally induced changes in insolation during the last interglaciation. *Quaternary Research*, 43: 174–184, 1995.
- [64] L. D. D. Harvey. Milankovitch forcing, vegetation feedback, and North Atlantic deep-water formation. *Journal of Climate*, 2: 800–815, 1989.
- [65] J. Hays, J. Imbrie, and N.J. Shackleton. Variations in the Earth’s orbit: Pacing-makers of the ice ages. *Science*, 194: 1121–1132, 1976.
- [66] J. D. Hays, T. Saito, N.D. Opdyke, and L.H. Burckle. Pliocene-Pleistocene sediments of the equatorial Pacific: Their paleomagnetic biostratigraphic and climatic record. *Geol. Soc. Am. Bull.*, 80: 1481–1514, 1969.
- [67] A. M. Haywood, P.J. Valdes, and B.W. Sellwood. Global scale palaeoclimate reconstruction of the middle Pliocene climate using the UKMO GCM: initial results. *Global and Planetary Change*, 25: 239–256, 2000.

- 
- [68] C. D. Hewitt and J. F. B. Mitchell. A fully coupled GCM simulation of the climate of the mid-Holocene. *Geophysical Research Letters*, 25 (3): 361–364, 1998.
- [69] F. J. Hilgen. Astronomical calibration of Gauss to Matuyama sapropels in the Mediterranean and implication for the Geomagnetic Polarity Time Scale. *Earth and Planetary Science Letters*, 104: 226–244, 1991.
- [70] F. J. Hilgen, W. Krijgsman, C.G. Langereis, L.J. Lourens, A. Santarelli, and W.J. Zachariasse. Extending the astronomical (polarity) time scale into the Miocene. *Earth and Planetary Science Letters*, 136 (3): 495–510, 1995.
- [71] M. M. Holland, C.M. Bitz, and A.J. Weaver. The influence of sea ice physics on simulations of climate change. *Journal of Geophysical Research*, 106 (C9): 19,639–19,655, 2001.
- [72] F. S. Hu, D. Kaufman, S. Yoneji, S. Nelson, A. Shemesh, Y. Huang, J. Tian, G. Bond, B. Clegg, and T. Brown. Cyclic variation and solar forcing of Holocene climate in the Alaskan Subarctic. *Science*, 301: 1890–1893, 2003.
- [73] T. M. C. Hughes and A. J. Weaver. Multiple equilibria of an asymmetric two-basin ocean model. *Journal of Physical Oceanography*, 24: 619–637, 1994.
- [74] J. W. Hurrell. Decadal trends in the North Atlantic Oscillation: Regional temperatures and precipitation. *Science*, 269: 676–679, 1995.
- [75] J. W. Hurrell and H. van Loon. Decadal variations in climate in climate associated with the North Atlantic Oscillation. *Climatic Change*, 36 (3/4): 301–326, 1997.
- [76] J. Imbrie. Astronomical theory of the Pleistocene ice ages: A brief historical review. *Icarus*, 50: 408–422, 1982.
- [77] J. Imbrie, A. McIntyre, and A. Mix. Oceanic response to orbital forcing in the late Quaternary: Observational and experimental strategies. In A. Berger, S.H. Schneider and J-C. Duplessy, editor, *Climate and Geosciences*, pages 121–164. D. Reidel, Dordrecht, Netherlands, 1989.
- [78] J. Imbrie, E.A. Boyle, S.C. Clemens, A. Duffy, W.R. Howard, G. Kukla, J. Kutzbach, D.G. Martinsson, A. McIntyre, A.C. Mix, B. Molfino, J.J. Morley, L.C. Peterson, N.G. Pisias, W.L. Prell, M.E. Raymo, N.J. Shackleton, and J.R. Toggweiler. On the structure and origin of major glaciation cycles 1. Linear responses to Milankovitch forcing. *Paleoceanography*, 7 (6): 701–738, 1992.
- [79] J. Imbrie and J. Z. Imbrie. Modeling the climatic response to orbital variations. *Science*, 207: 943–953, 1980.
- [80] J. Imbrie and K. P. Imbrie. *Ice Ages, solving the mystery*. Enslow Publishers, 1979. pp. 224.

- [81] J. Imbrie and N. G. Kipp. A new micropaleontological method for paleoclimatology: Application to a late pleistocene caribbean core. In K.K. Turekian, editor, *The late Cenozoic glacial ages*, pages 71–181. Yale University Press, New Haven, Conn., 1971.
- [82] C. S. Jackson and A. J. Broccoli. Orbital forcing of Arctic climate: mechanisms of climate response and implications for continental glaciation. *Climate Dynamics*, 21: 539–557, 2003. DOI 10.1007/s00382-003-0351-3.
- [83] L. Jaeger. Monatskarten des Niederschlags für die ganze Erde. *Bericht des Deutschen Wetterdienstes*, 139, 1976.
- [84] J. G. Johnson. Climate control requires a dam at the Strait of Gibraltar. *EOS*, 78 (27): 277–280/81, 1997.
- [85] P. D. Jones, T. Johnsson, and D. Weeler. Extension to the North Atlantic Oscillation using early instrumental pressure observations from Gibraltar and South West Iceland. *International Journal of Climatology*, 17 (13): 1433–1450, 1997.
- [86] S. A. Josey. Changes in the heat and freshwater forcing of the eastern Mediterranean and their influence on deep water formation. *Journal of Geophysical Research*, 108 (C7): 3237, 2003. doi:10.1029/2003JC001778.
- [87] S. Joussaume and P. Braconnot. Sensitivity of paleoclimate simulation results to season definitions. *Journal of Geophysical Research*, 102 (D2): 1943–1956, 1997.
- [88] S. Joussaume, K.E. Taylor, P. Braconnot, J.F.B. Mitchell, J.E. Kutzbach, S.P. Harrison, I.C. Prentice, A.J. Broccoli, A. Abe-Ouchi, P.J. Bartlein, C. Bonfils, B. Dong, J. Guiot, K. Herterich, C.D. Hewitt, D. Jolly, J.W. Kim, A. Kislov, A. Kitoh, M.F. Loutre, V. Masson, B. McAveny, N. McFarlane, N. de Noblet, W.R. Peltier, J.Y. Peterschmitt, D. Pollard, D. Rind, J.F. Royer, M.E. Schlesinger, J. Syktus, S. Thompson, P. Valdes, G. Vettoretti, R.S. Webb, and U. Wyputta. Monsoon changes for 6000 years ago: Results of 18 simulations from the Paleoclimate Modeling Intercomparison Project (PMIP). *Geophysical Research Letters*, 26 (7): 859–862, 1999.
- [89] M. Kageyama, O. Peyron, S. Pinot, P. Tarasov, J. Guiot, S. Joussaume, and G. Ramstein. The Last Glacial Maximum over Europe and western Siberia: a PMIP comparison between models and data. *Climate Dynamics*, 17: 23–43, 2001.
- [90] R. Kistler, E. Kalnay, W. Collins, S. Saha, G. White, J. Woollen, M. Chelliah, W. Ebisuzaki, M. Kanamitsu, V. Kousky, H. van den Dool, R. Jenne, and M. Fiorino. The NCEP-NCAR 50-Year Reanalysis: Monthly Means CD-ROM and Documentation. *Bulletin of the American Meteorological Society*, 82 (2): 247–267, 2001.

- [91] A. Kitoh, S. Murakami, and H. Koide. A simulation of the Last Glacial Maximum with a coupled atmosphere-ocean GCM. *Geophysical Research Letters*, 28 (11): 2221–2224, 2001.
- [92] M. L. Kloosterboer-van Hoeve. *Cyclic changes in the late Neogene vegetation of northern Greece, a palynological study*. PhD thesis, Utrecht, 2000. 132 pp.
- [93] M. L. Kloosterboer-van Hoeve, H. Visscher, J. Steenbrink, and E. Tuenter. Coupling between orbital precession and atmospheric dynamics of the North Atlantic/European region. *Submitted to Global and Planetary Change*, 2004.
- [94] J. Kondo. Air-sea bulk transfer coefficients in diabatic conditions. *Boundary-Layer Meteorology*, 9: 91–112, 1975.
- [95] W. Köppen and A. Wegener. *Die Klimate der geologischen Vorzeit*. Borntraeger, Berlin, 1924. pp. 255.
- [96] G. Korres and A. Lascaratos. A one-way nested, eddy-resolving model of the Aegean and Levantine basins: Implementation and climatological runs. *Annales Geophysicae*, 21: 205–220, 2003.
- [97] G. Koslowski and R. Glaser. Variations in reconstructed ice winter severity in the west Baltic from 1501 to 1995 and their implications for the NAO. *Climatic Change*, 41 (2): 175–191, 1999.
- [98] W. Krijgsman, F.J. Hilgen, C.G. Langereis, A. Santarelli, and W.J. Zachariasse. Late Miocene magnetostratigraphy, biostratigraphy and cyclostratigraphy in the Mediterranean. *Earth and Planetary Science Letters*, 136: 475–494, 1995.
- [99] C. Kubatzki, M. Montoya, S. Rahmstorf, A. Ganopolski, and M. Claussen. Comparison of the last interglacial climate simulated by a coupled global model of intermediate complexity and an AOGCM. *Climate Dynamics*, 16: 799–814, 2000.
- [100] G. J. Kukla. Loess stratigraphy of central Europe. In K.W. Butzer and G.L. Isaac, editor, *After the Australopithecines*, pages 99–188. Mouton, The Hague, 1975.
- [101] J. Kutzbach, G. Bonan, J. Foley, and S.P. Harrison. Vegetation and soil feedbacks on the response of the African monsoon to orbital forcing in the early to middle Holocene. *Nature*, 384: 623–626, 1996.
- [102] J. E. Kutzbach. Monsoon climate of the early Holocene: Climate experiment with the Earth’s orbital parameters for 9000 years ago. *Science*, 214: 59–61, 1981.
- [103] J. E. Kutzbach and R. G. Gallimore. Sensitivity of a coupled atmosphere/mixed layer ocean model to changes in orbital forcing at 9000 years B.P. *Journal of Geophysical Research*, 93 (D1): 803–821, 1988.

- [104] J. E. Kutzbach and P. J. Guetter. The influence of changing orbital parameters and surface boundary conditions on climate simulations for the past 18 000 years. *Journal of the Atmospheric Sciences*, 43 (16): 1726–1759, 1986.
- [105] J. E. Kutzbach and Z. Liu. Response of the African monsoon to orbital forcing and ocean feedbacks in the middle Holocene. *Science*, 278: 440–443, 1997.
- [106] J. E. Kutzbach and B. L. Otto-Bliesner. The sensitivity of the African-Asian monsoonal climate to orbital parameter changes for 9000 years B.P. in a low-resolution General Circulation Model. *Journal of the Atmospheric Sciences*, 39 (6): 1177–1188, 1982.
- [107] J. E. Kutzbach, R.G. Gallimore, and P. J. Guetter. Sensitivity experiments on the effect of orbitally-caused insolation changes on the interglacial climate of high northern latitudes. *Quaternary International*, 10-12: 223–229, 1991.
- [108] J. E. Kutzbach and F. A. Street-Perrott. Milankovitch forcing of fluctuations in the level of tropical lakes from 18 to 0 kyr BP. *Nature*, 317: 130–134, 1985.
- [109] W. Larcher. Low temperature effects on Mediterranean sclerophylles: an unconventional viewpoint. In N. S. Margaris and H. A. Mooney, editors, *Components of productivity of Mediterranean-Climat regions*, pages 259–267. Dr. W. Junk Publishers, 1981.
- [110] A. Lascaratos, R.G. Williams, and E. Tragou. A mixed-layer study of the formation of Levantine Intermediate Water. *Journal of Geophysical Research*, 98 (14): 14,739–14,749, 1993.
- [111] J. Laskar. Accurate methods in general planetary theory. *Astronomy and Astrophysics*, 144: 133–146, 1985.
- [112] J. Laskar. Secular terms of classical planetary theories using the results of general theory. *Astronomy and Astrophysics*, 157: 59–70, 1986.
- [113] J. Laskar. Secular evolution of the solar system over 10 millions years. *Astronomy and Astrophysics*, 198: 341–362, 1988.
- [114] J. Laskar. A numerical experiment on the chaotic behaviour of the solar system. *Nature*, 338: 237–238, 1989.
- [115] J. Laskar. The chaotic motion of the solar system: A numerical estimate of the size of the chaotic zones. *Icarus*, 88: 266–291, 1990.
- [116] J. Laskar. The limits of Earth orbital calculations for geological time scale use. *Royal Society of London Philosophical Transactions*, 357: 1735–1759, 1999.
- [117] J. Laskar, F. Joutel, and F. Boudin. Orbital, precessional and insolation quantities for the Earth from -20Myr to +10Myr. *Astronomy and Astrophysics*, 270: 522–533, 1993.

- [118] J. Lean. Variations in the Sun's radiative output. *Review of Geophysics*, 29 (4): 505–535, 1991.
- [119] J. Lean and D. Rind. Evaluating sun-climate relationships since the little Ice age. *Journal of Atmospheric and Solar-Terrestrial Physics*, 61 (1-2): 25–36, 1999.
- [120] L. Lourens, F.J. Hilgen, L. Gudjonsson, and W.J. Zachariasse. Late Pliocene to early Pleistocene astronomically forced sea surface productivity and temperature variations in the Mediterranean. *Marine Micropaleontology*, 19: 49–78, 1992.
- [121] L. J. Lourens, A. Antonarakou, F.J. Hilgen, A.A.M. Van Hoof, C. Vergnaud-Grazzini, and W.J. Zachariasse. Evaluation of the Plio-Pleistocene astronomical timescale. *Paleoceanography*, 11 (4): 391–413, 1996.
- [122] L. J. Lourens, R. Wehausen, and H. J. Brumsack. Geological constraints on tidal dissipation and dynamical ellipticity of the Earth over the past three million years. *Nature*, 409: 1029–1033, 2001.
- [123] M. F. Loutre and A. Berger. Marine Isotope Stage 11 as an analogue for the present interglacial. *Global and Planetary Change*, 36: 209–217, 2003.
- [124] L. Martin, J. Bertaux, T. Corrège, M.-P. Ledru, P. Mourguiart, A. Sifeddine, F. Soubiès, D. Wirmann, K. Suguio, and B. Turcq. Astronomical forcing of contrasting rainfall changes in tropical South America between 12,400 and 8800 cal yr B.P. *Quaternary Research*, 47: 117–122, 1997.
- [125] P. A. Mayewski, L.D. Meeker, M.S. Twickler, S. Whitlow, Q. Yang, W.B. Lyons, and M. Prentice. Major features and forcing of high-latitude Northern Hemispheric atmospheric circulation using a 110,000-year-long glaciochemical series. *Journal of Geophysical Research*, 102 (C12): 26,345–26,366, 1997.
- [126] P. T. Meijer, R. Slingerland, and M.J.R. Wortel. Tectonic control on past circulation of the Mediterranean Sea: a model study of the late Miocene. *Paleoceanography*, 19: PA1026, 2004. doi:10.1029/2003PA000956.
- [127] P. T. Meijer and E. Tuenter. The effect on circulation of precession-induced changes in the Mediterranean freshwater budget; The response at shallow and intermediate depth. 2004. in prep.
- [128] K. J. Meissner, A.J. Weaver, H.D. Matthews, and P.M. Cox. The role of land surface dynamics in glacial inception: a study with the UVic Earth System Model. *Climate Dynamics*, 21: 515–537, 2003. DOI 10.1007/s00382-003-0352-2.
- [129] J. J. Mercier, D. Sorel, and P. Vergely. Extensional tectonic regimes in the Aegean basins during the Cenozoic. *Basin Research*, 2: 49–71, 1989.

- [130] U. Mikolajewicz, M. Scholze, and R. Voss. Simulating near-equilibrium climate and vegetation for 6000 cal. years BP. *The Holocene*, 13 (3): 319–326, 2003.
- [131] M. Milankovitch. Théorie mathématique des phénomènes thermiques produits par la radiation solaire. 1920. Académie Yougoslave des Sciences et des Arts de Zagreb, Gauthier-Villars.
- [132] M. Milankovitch. *Kanon der Erdbestrahlung und seine Anwendung auf das Eiszeitenproblem*, volume 33 of *Royal Serbian Academy Special publication 132*. 1941. pp. 633.
- [133] J. F. B. Mitchell, N.S. Grahame, and K.J. Needham. Climate simulations for 9000 years before present: Seasonal variations and effect of the Laurentide Ice Sheet. *Journal of Geophysical Research*, 93 (D7): 8283–8303, 1988.
- [134] J. X. Mitrovica, A.M. Forte, and R. Pan. Glaciation-induced variations in the Earth’s precession frequency, obliquity and insolation over the last 2.6 Ma. *Geophysical Journal International*, 128: 270–284, 1997.
- [135] J. X. Mitrovica and A. M. Forte. Pleistocene glaciation and the Earth’s precession constant. *Geophysical Journal International*, 121: 21–32, 1995.
- [136] H. J. P. M. Mommersteeg, M.F. Loutre, R. Young, T.A. Wijmstra, and H. Hooghiemstra. Orbital forced frequencies in the 975000 year pollen record from Tenage Philippon (Greece). *Climate Dynamics*, 11: 4–24, 1995.
- [137] M. Montoya, H. von Storch, and T.J. Crowley. Climate Simulation for 125 kyr BP with a Coupled Ocean-Atmosphere General Circulation Model. *Journal of Climate*, 13: 1057–1072, 2000.
- [138] P. G. Myers. Flux-forced simulations of the paleocirculation of the Mediterranean. *Paleoceanography*, 17 (1): 1–7, 2002.
- [139] P. G. Myers and K. Haines. Stability of the Mediterranean’s thermohaline circulation under modified surface evaporative fluxes. *Journal of Geophysical Research*, 107 (C3): 3021, 2002. doi:10.1029/2000JC000550.
- [140] P. G. Myers, K. Haines, and E.J. Rohling. Modeling the paleocirculation of the Mediterranean: The last glacial maximum and the Holocene with emphasis on the formation of sapropel S<sub>1</sub>. *Paleoceanography*, 13 (6): 586–606, 1998.
- [141] G. R. North, J.G. Mengel, and D.A. Short. A two-dimensional climate model useful in Ice Age applications. In A.L. Berger et al., editor, *Milankovitch and Climate*, volume 2, pages 513–518. D. Reidel Publishing Company, 1984.
- [142] R. Oglesby and J. Park. The effect of precessional insolation changes on Cretaceous climate and cyclic sedimentation. *Journal of Geophysical Research*, 94 (D12): 14,793–14,816, 1989.

- 
- [143] J. D. Opsteegh, R.J. Haarsma, F.M. Selten, and A. Kattenberg. ECBILT: a dynamic alternative to mixed boundary conditions in ocean models. *Tellus*, 50A: 348–367, 1998.
- [144] T. J. Osborn, K.R. Briffa, S.F.B. Tett, P.D. Jones, and R.M. Trigo. Evaluation of the North Atlantic Oscillation as simulated by a coupled climate model. *Climate Dynamics*, 15: 685–702, 1999.
- [145] R. C. Pacanowski and S. M. Griffies. MOM 3.0 Manual. 1998. NOAA/Geophysical Fluid Dynamics Laboratory, Princeton, USA.
- [146] H. Paeth and A. Hense. Climate change signals in the North Atlantic Oscillation. *CLIVAR Newsletter Exchanges*, 4 (4): 25–29, 1999.
- [147] D. Paillard. Glacial cycles: Toward a new paradigm. *Review of Geophysics*, 39 (3): 325–346, 2001.
- [148] A. Papakonstantiou. Die hydrogeologischen Verhältnisse im Raum der Ptolemais-Senke und des westlichen Vermiongebirges in Griechisch-Mazedonien. *Berliner Geowissenschaften*, 13: 1–79, 1979.
- [149] J. Park and R. J. Oglesby. A comparison of precession and obliquity effects in a Cretaceous paleoclimate simulation. *Geophysical Research Letters*, 17 (11): 1929–1932, 1990.
- [150] J. Park and R. J. Oglesby. Milankovitch rhythms in the Cretaceous: A GCM modelling study. *Palaeogeography, Palaeoclimatology, Palaeoecology*, 90: 329–355, 1991.
- [151] F. Pastor, M.J. Estrela, D. Peñarrocha, and M.M. Millán. Torrential rains on the Spanish Mediterranean coast: Modeling the effects of the sea surface temperature. *Journal of Applied Meteorology*, 40 (7): 1180–1195, 2001.
- [152] S. B. Pavlides and D. M. Mountrakis. Neotectonics of the Florina-Vegorites-Ptolemais Neogene Basin (NW Greece): an example of extensional tectonics of the Greater Aegean Area. *Ann. Geol. Pays. Hellen*, 33 (1): 311–327, 1986.
- [153] W. R. Peltier and X. Jiang. The precession constant of the Earth: Variations through the ice age. *Geophysical Research Letters*, 21: 2299–2302, 1994.
- [154] V. Petoukhov, A. Ganopolski, V. Brovkin, M. Claussen, A. Eliseev, C. Kubatzki, and S. Rahmstorf. CLIMBER-2: a climate system model of intermediate complexity. Part I: model description and performance for present climate. *Climate Dynamics*, 16: 1–17, 2000.
- [155] N. Pinardi and E. Masetti. Variability of the large scale general circulation of the Mediterranean Sea from observations and modelling: a review. *Palaeogeography, Palaeoclimatology, Palaeoecology*, 158: 153–173, 2000.



- [156] E. M. Pokras and A. C. Mix. Earth's precession cycle and Quaternary climatic change in tropical Africa. *Nature*, 326: 486–487, 1987.
- [157] D. Pollard. An investigation of the astronomical theory of the ice ages using a simple climate-icesheet model. *Nature*, 272: 233–235, 1978.
- [158] W. L. Prell. Monsoonal climate of the Arabian Sea during the late Quaternary: A response to changing solar radiation. In A. L. Berger et al., editor, *Milankovitch and Climate*, volume 1, pages 349–366. D. Reidel Publishing Company, Dordrecht, Holland, 1984.
- [159] W. L. Prell and J. E. Kutzbach. Monsoon variability over the past 150,000 years. *Journal of Geophysical Research*, 92 (D7): 8411–8425, 1987.
- [160] T. R. Quinn, S. Tremaine, and M. Duncan. A three million year integration of the Earth's orbit. *Astronomical journal*, 101: 2287–2305, 1991.
- [161] S. Rahmstorf. On the freshwater forcing and transport of the Atlantic thermohaline circulation. *Climate Dynamics*, 12: 799–811, 1996.
- [162] M. E. Raymo, W.F. Ruddiman, J. Backman, B.M. Clement, and D.G. Martinson. Late Pliocene variations in Northern Hemisphere ice sheets and North Atlantic Deep water circulation. *Paleoceanography*, 4 (4): 413–446, 1989.
- [163] G. J. Reichert, L.J. Lourens, and W.J. Zachariasse. Orbital- and suborbital controlled variability in the Oxygen Minimum Zone (OMZ) of the northern Arabian Sea during the last 225,000 yr. *Paleoceanography*, 13 (6): 607–621, 1998.
- [164] E. Rohling and F. J. Hilgen. The eastern Mediterranean climate at the times of sapropel formation: a review. *Geologie en Mijnbouw*, 70: 253–264, 1991.
- [165] M. Rossignol-Strick. African monsoons, an immediate climate response to orbital insolation. *Nature*, 304: 46–49, 1983.
- [166] M. Rossignol-Strick. Mediterranean Quaternary sapropels, an immediate response of the African monsoon to variation of insolation. *Palaeogeography, Palaeoclimatology, Palaeoecology*, 49: 237–263, 1985.
- [167] F. Rostek, E. Bard, L. Beaufort, C. Sonzogni, and G. Ganssen. Sea surface temperature and productivity records for the past 240 kyr in the Arabian Sea. *Deep-Sea Research II*, 44 (6-7): 1461–1480, 1997.
- [168] W. F. Ruddiman. *Earth's climate : past and future*. W.H. Freeman and Company, New York, 2001. pp. 465.
- [169] M. Schaeffer, F.M. Selten, J.D.. Opsteegh, and H. Goosse. The influence of ocean convection patterns on high-latitude climate projections. *Journal of Climate*, 2004. Accepted.

- 
- [170] S. J. Schenau, A. Antonarakou, F.J. Hilgen, L.J. Lourens, I.A. Nijenhuis, C.H. van der Weijden, and W.J. Zachariasse. Organic-rich layers in the Metochia section (Gavdos, Greece): evidence for a single mechanism of sapropel formation during the past 10 My. *Marine Geology*, 153: 117–135, 1999.
- [171] F. M. Selten, R.J. Haarsma, and J.D. Opsteegh. On the mechanism of North Atlantic decadal variability. *Journal of Climate*, 12: 1956–1973, 1999.
- [172] N. Shackleton. Oxygen isotope analyses and Pleistocene temperatures reassessed. *Nature*, 215: 15–17, 1967.
- [173] H. F. Shaw and G. Evans. The nature distribution and origin of a sapropelic layer in the sediments of the Cilicia Basin, north-eastern Mediterranean. *Marine Geology*, 61: 1–12, 1984.
- [174] S.-I. Shin, Z. Liu, B. Otto-Bliesner, E.C. Brady, J.E. Kutzbach, and S.P. Harrison. A simulation of the Last Glacial Maximum climate using the NCAR-CCSM. *Climate Dynamics*, 20: 127–151, 2003.
- [175] D. A. Short, J.G. Mengel, T.J. Crowley, W.T. Hyde, and G.R. North. Filtering of Milankovitch cycles by Earth’s geography. *Quaternary Research*, 35: 157–173, 1991.
- [176] D. A. Short and J. G. Mengel. Tropical climatic phase lags and Earth’s precession cycle. *Nature*, 323: 48–50, 1986.
- [177] F. J. Sierro, J.A. Flores, I. Zamarreño, A. Vázquez, R. Utrilla, G. Francés, F.J. Hilgen, and W. Krijgsman. Messinian pre-evaporite sapropels and precession-induced oscillations in western Mediterranean climate. *Marine Geology*, 153: 137–146, 1999.
- [178] J. Steenbrink. *Orbital signatures in lacustrine sediments*. PhD thesis, University of Utrecht, 2001. 168 pp.
- [179] J. Steenbrink, N. van Vugt, F.J. Hilgen, J.R. Wijbrans, and J.E. Meulenkamp. Sedimentary cycles and volcanic ash beds in the Lower Pliocene lacustrine succession of Ptolemais (NW Greece): discrepancy between  $^{40}\text{Ar}/^{39}\text{Ar}$  and astronomical ages. *Palaeogeography, Palaeoclimatology, Palaeoecology*, 152 (2-3): 283–303, 1999.
- [180] T. F. Stocker, D.G. Wright, and L.A. Mysak. A zonally averaged coupled ocean-atmosphere for paleoclimate studies. *Journal of Climate*, 5: 773–797, 1992.
- [181] K. Stratford, R.G. Williams, and P.G. Myers. Impact of the circulation on sapropel formation in the eastern Mediterranean. *Global Biogeochemical cycles*, 14 (2): 683–695, 2000.
- [182] M. J. Suarez and I. M. Held. The sensitivity of an energy balance climate model to variations in the orbital parameters. *Journal of Geophysical Research*, 84 (C8): 4825–4836, 1979.

- [183] J. P. Suc. Origin and evolution of the Mediterranean vegetation and climate in Europe. *Nature*, 307:429–432, 1984.
- [184] J. P. Suc, A. Bertini, N. Combourieu-Nebout, F. Diniz, S. Leroy, E. Russo-Ermolli, Z. Zheng, E. Bessias, and J. Ferrier. Structure of Western Mediterranean vegetation and climate since 5.3 Ma. *Acta zoologica Cracov*, 38 (1): 3–16, 1995.
- [185] H. E. Suess and T. W. Linick. The  $^{14}\text{C}$  record in bristlecone pine wood of the past 8000 years based on the dendrochronology of the late C.W. Ferguson. *Phil. Trans. R. Soc. Lond.*, A 330: 403–412, 1990.
- [186] R. S. Thompson, K.H. Anderson, and P.J. Bartlein. *Atlas of relations between climatic and distributions of important trees and shrubs in North America, introduction and conifers*. 2000. 1650-A. 269 pp.
- [187] R. M. Trigo, T.J. Osborn, and J.M. Corte-Real. The North Atlantic Oscillation influence on Europe: climate impacts and associated physical mechanisms. *Climate Research*, 20: 9–17, 2002.
- [188] E. Tuenter, S.L. Weber, F.J. Hilgen, and L.J. Lourens. The response of the African summer monsoon to remote and local forcing due to precession and obliquity. *Global and Planetary Change*, 36: 219–235, 2003.
- [189] E. Tuenter, S.L. Weber, F.J. Hilgen, and L.J. Lourens. The influence of precession and obliquity on the Atlantic/European winter climate. 2004. In prep.
- [190] E. Tuenter, S.L. Weber, F.J. Hilgen, L.J. Lourens, and A. Ganopolski. Simulation of climate phase lags in the response to precession and obliquity forcing and the role of vegetation. *Climate Dynamics*, 2004. Under review.
- [191] P. C. Tzedakis. Long-term tree populations in northwest Greece through multiple Quaternary climatic cycles. *Nature*, 364: 437–440, 1993.
- [192] P. C. Tzedakis. Vegetation change through glacial-interglacial cycles: a long pollen perspective. *Phil. Trans. R. Soc. Lond.*, B 345: 403–432, 1994.
- [193] P. C. Tzedakis and K. D. Bennett. Interglacial vegetation succession: a view from southern Europe. *Quaternary Science Reviews*, 14: 967–982, 1995.
- [194] G. Van der Schrier, S.L. Weber, and S.S. Drijfhout. Sea level changes in the North Atlantic by solar forcing and internal variability. *Climate Dynamics*, 19: 435–447, 2002.
- [195] B. van Geel, O.M. Raspopov, H. Renssen, J. van der Plicht, V.A. Dergachev, and H.A.J. Meijer. The role of solar forcing upon climate change. *Quaternary Science Reviews*, 18: 331–338, 1999.

- 
- [196] N. van Vugt, J. Steenbrink, C.G. Langereis, F.J. Hilgen, and J.E. Meulenkamp. Magnetostratigraphy-based astronomical tuning of the early Pliocene lacustrine sediments of Ptolemais (NW Greece) and bed-to-bed correlation with the marine record. *Earth and Planetary Science Letters*, 164: 535–551, 1998.
- [197] W. van Zeist and S. Bottema. Vegetational history of the eastern Mediterranean and the near east during the last 20.000 years. In J. Bintliff and W. van Zeist, editors, *Palaeoclimates, Palaeoenvironments and Human Communities in the Eastern Mediterranean in Later Prehistory*. BAR international series, 1982. pp. 277–321.
- [198] W. van Zeist, H. Woldring, and D. Stapert. Late Quaternary vegetation and climate of southwestern Turkey. *Palaeohistoria*, XVII: 55–142, 1975.
- [199] W. van Zeist, R.T. Timmers, and S. Bottema. Studies of modern and Holocene pollen precipitation in southeastern Turkey. *Palaeohistoria*, XIV: 19–40, 1970.
- [200] S. J. Vavrus. The response of the coupled Arctic sea ice-atmosphere system to orbital forcing and ice motion at 6 kyr and 115 kyr BP. *Journal of Climate*, 12: 873–896, 1999.
- [201] A. D. Vernekar. Long-period global variations of incoming solar radiation. *Meteorological Monographs*, 12, 1972. pp 130.
- [202] L. Verrier. 1856. Ann. Obs. Paris, vol II. Paris: Mallet-Bachelet.
- [203] G. J. M. Versteegh. Recognition of cyclic and non-cyclic environmental changes in the Mediterranean Pliocene; a palynological approach. *Marine Micropaleontology*, 23: 147–183, 1994.
- [204] G. Vettoretti and W. R. Peltier. Post-Eemian glacial inception. Part I: The impact of summer seasonal temperature bias. *Journal of Climate*, 16 (6): 889–911, 2003.
- [205] D. J. Webb. An ocean model code for array processor computers. *Computers & Geosciences*, 22: 569–578, 1996.
- [206] S. L. Weber. The impact of orbital forcing on the climate of an intermediate-complexity coupled model. *Global and Planetary Change*, 30: 7–12, 2001.
- [207] S. L. Weber and J. Oerlemans. Holocene glacier variability: three case studies using an intermediate-complexity model. *The Holocene*, 13 (3): 353–363, 2003.
- [208] S. L. Weber, T.J. Crowley, and G. van der Schrier. Solar irradiance forcing of centennial climate variability during the Holocene. *Climate Dynamics*, 22, 2004. DOI 10.1007/s00382-004-0396-y.
- [209] J. Weertman. Milankovitch solar radiation variations and ice age ice sheet sizes. *Nature*, 261: 17–20, 1976.

- 
- [210] T. A. Wijmstra, R. Young, and H.J.L. Witte. An evaluation of the climatic conditions during the Late Quaternary in northern Greece by means of multivariate analysis of palynological data and comparison with recent phytosociological and climate data. *Geologie en Mijnbouw*, 69: 243–251, 1990.
  - [211] U. Wyputta and B. J. McAvaney. Influence of vegetation changes during the Last Glacial Maximum using the BMRC atmospheric general circulation model. *Climate Dynamics*, 17: 923–932, 2001.
  - [212] P. Xie and P. A. Arkin. Global precipitation: A 17-year monthly analysis based on gauge observations, satellite estimates and numerical model outputs. *Bulletin of the American Meteorological Society*, 78: 2539–2558, 1997.
  - [213] M. Yoshimori, M.C. Reader, A.J. Weaver, and N.A. McFarlane. On the causes of glacial inception at 116 kaBP. *Climate Dynamics*, 18: 383–402, 2002.
  - [214] G. Yu and S. P. Harrison. An evaluation of the simulated water balance of Eurasia and northern Africa at 6000 yr BP using lake status data. *Climate Dynamics*, 12: 723–735, 1996.
  - [215] M. Zavatarelli and G. L. Mellor. A numerical study of the Mediterranean circulation. *Journal of Physical Oceanography*, 25: 1384–1414, 1995.

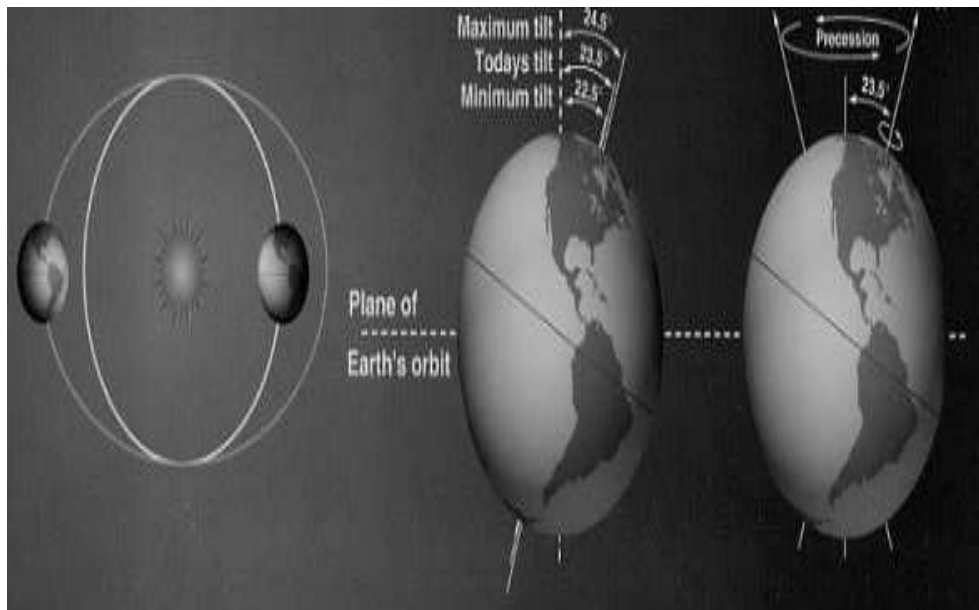


# Samenvatting

Het klimaat op aarde varieert op tijdschalen van enkele jaren tot vele miljoenen jaren. De variaties op tijdschalen van tienduizenden jaren worden veroorzaakt door periodieke schommelingen in de stand van de aardas en in de vorm van de baan van de aarde om de zon. Deze schommelingen zorgen voor een astronomische sturing van het klimaat doordat ze veranderingen veroorzaken in de hoeveelheid zonne-instraling die de aarde ontvangt en in de verdeling van deze instraling over de seizoenen en over het aardoppervlak. De schommelingen worden veroorzaakt door de gravitatiekrachten die de zon, de maan en de andere planeten in ons zonnestelsel op de aarde uitoefenen. De periodieke schommelingen worden ook wel Milankovitch cycli genoemd naar de Servische astronoom Milutin Milankovitch. Milankovitch heeft in de eerste helft van de 20ste eeuw baanbrekend onderzoek verricht naar de relatie tussen de astronomische forcering en het klimaat op aarde. De Milankovitch cycli bestaan uit periodieke veranderingen in de astronomische parameters: excentriciteit van de baan van de aarde om de zon, precessie en obliquiteit.

Excentriciteit is een maat voor de vorm van de baan van de aarde om de zon. Deze varieert van bijna cirkelvormig tot ellipsvorming met periodes van ongeveer 100.000 en 400.000 jaar (Figuur 1). De excentriciteit heeft gevolgen voor de afstand van de aarde tot de zon. Als de baan cirkelvormig is, bevindt de aarde zich altijd even ver van de zon. Als de baan ellipsvormig is, dan bevindt de aarde zich soms dichtbij de zon en soms verder weg. Op dit moment is de baan van de aarde bijna cirkelvormig.

De draaiende beweging van de rotatie-as van de aarde wordt precessie genoemd (Figuur 1). Deze beweging is vergelijkbaar met die van een draaiende tol die scheef hangt. Hierbij staat het middelpunt van de aarde stil terwijl beide polen een cirkel beschrijven. Precessie heeft een periode van ongeveer 20.000 jaar. Het gevolg van precessie is dat zomer en winter op een ander punt van de baan van de aarde om de zon worden bereikt. De huidige situatie is dat het winter is op het noordelijk halfrond als de aarde het dichtst bij de zon staat en zomer als de aarde het verst weg staat. Deze toestand noemen we een precessie maximum. Over ongeveer 10.000 jaar is het precies andersom. Dan is het zomer op het noordelijk halfrond wanneer de aarde het dichtst bij de zon staat en winter als de afstand zon-aarde het grootst is. Dit wordt een precessie minimum genoemd. Nog eens 10.000 jaar later zal de huidige toestand opnieuw bereikt worden tijdens het volgende precessie maximum. Precessie wordt versterkt en verzwakt door excentriciteit. Als de excentriciteit heel klein is, is het verschil tussen de grootste en kleinste afstand tussen de aarde en de zon ook



Figuur 1: Een schematisch overzicht van de astronomische parameters. Het linkerdeel laat de excentriciteit zien. Het middelste deel geeft de obliquiteit (of tilt) weer samen met de maximum en minimum obliquiteit over de laatste 1 miljoen jaar en de huidige obliquiteit. Het rechterdeel geeft de precessie beweging weer.

heel klein. Dan is dus ook het verschil tussen een precessie minimum en een precessie maximum minimaal (wanneer de baan van de aarde om de zon cirkelvormig is, is er zelfs helemaal geen effect van precessie). Wanneer de excentriciteit juist heel groot is, is het verschil tussen een precessie minimum en een precessie maximum ook heel groot.

De laatste astronomische parameter is obliquiteit. Obliquiteit wordt gedefinieerd als de hoek tussen de rotatie-as van de aarde en de loodlijn op het vlak waarin de aarde om de zon draait (Figuur 1). Deze hoek veroorzaakt de seizoenen en varieert met een periode van ongeveer 41.000 jaar. Gedurende de laatste miljoen jaar varieerde de hoek van ongeveer 22 graden tot ongeveer 24,5 graden. De huidige hoek is 23,45 graden. Veranderingen in de astronomische parameters veroorzaken veranderingen in de hoeveelheid instraling die de aarde ontvangt en in de verdeling van de instraling over de seizoenen en het aardoppervlak. Excentriciteit op zichzelf heeft een hele kleine invloed op de totale hoeveelheid instraling die de aarde jaarlijks ontvangt. Een belangrijker effect van excentriciteit is dat het precessie versterkt en verzwakt. Tijdens een precessie minimum is de instraling tijdens de zomer op het noordelijk halfrond op alle breedtegraden groter dan tijdens een precessie maximum (Figuur 2a). Tijdens de winter op het noordelijk halfrond is het precies omgekeerd (Figuur 2b). Tijdens een precessie minimum heeft het noordelijk halfrond dus een extra warme zomer en

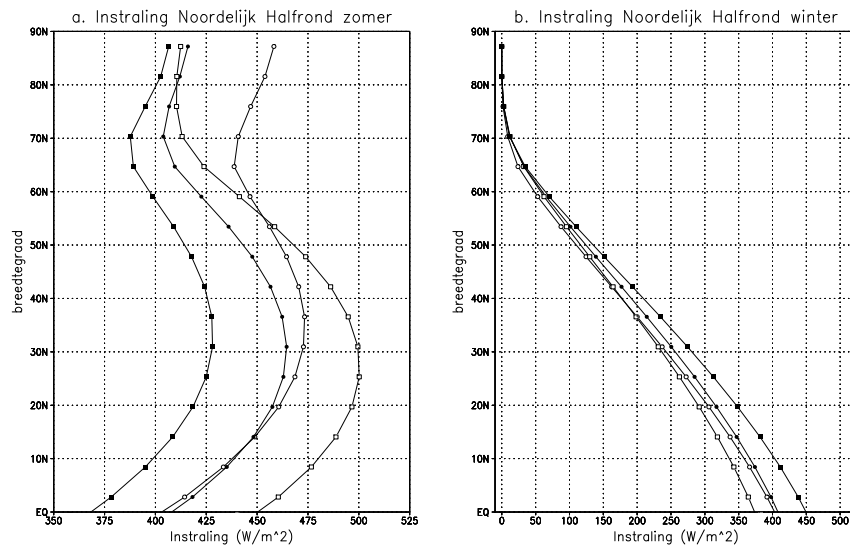


een extra koude winter terwijl tijdens een precessie maximum het verschil tussen de winter en de zomer juist kleiner wordt. Wanneer de obliquiteit van een minimum naar een maximum gaat, wordt de instraling op het noordelijk halfrond in de zomer sterker en in de winter juist zwakker (Figuur 2a-b). Met andere woorden, tijdens een obliquiteit maximum heeft het noordelijk halfrond een extra warme zomer en een extra koude winter terwijl tijdens een obliquiteit minimum de zomer relatief koel is en de winter relatief warm. Een belangrijk verschil tussen precessie en obliquiteit is dat het precessiesignaal in de instraling op alle breedtes sterk is. Het obliquiteitssignaal is echter alleen sterk op hoge breedtes terwijl het op lage breedtes (in de subtropen en tropen) zwak is (Figuur 2a-b).

De astronomisch gestuurde klimaatvariaties worden zowel in de oceaan als op het land vastgelegd in sedimentaire afzettingen. De ijstijden van de afgelopen 2,5 miljoen jaar die in afzettingen zijn terug gevonden zijn de bekendste klimaatvariaties. Een ander voorbeeld vinden we in afzettingen uit de Middellandse Zee (Figuur 3). De sedimenten in Figuur 3 bevinden zich nu op het land maar ze zijn oorspronkelijk afgezet op bodem van de Middellandse Zee. Door tektoniek is het land dat vroeger onder water lag nu boven water gekomen. De afzettingen bestaan uit afwisselend donkere en lichte lagen met een duidelijk patroon. De lichte lagen bestaan vooral uit mergel en de donkere lagen zijn zogenaamde sapropelen. Het belangrijkste kenmerk van sapropelen is dat ze erg veel organisch materiaal bevatten. Uit dateringen blijkt dat sapropelen worden gevormd tijdens precessie minima (Figuur 3). Het voorkomen van sapropelen in groepen wordt veroorzaakt door de excentriciteit die immers de sterkte van precessie bepaalt. Hoewel de vorming van sapropelen gedomineerd wordt door precessie, is ook de invloed van obliquiteit in de sapropel patronen te herkennen. Dit obliquiteitssignaal bestaat uit een afwisseling van dikke, duidelijke sapropelen en dunne en minder duidelijke sapropelen (Figuur 3). De meest geaccepteerde verklaring voor sapropelen is dat ze gevormd worden doordat het oppervlaktewater in de Middellandse Zee niet meer naar de diepte zakt. Dit heeft als gevolg dat het diepe water niet meer wordt ververst, waardoor zuurstof opraakt. Het organisch materiaal dat naar de bodem zakt wordt daardoor niet meer geoxideerd en blijft liggen. Dit leidt tot de vorming van een sapropel. Het stoppen van diep water vorming zou worden veroorzaakt door een sterkere afvoer van de Nijl tijdens een precessie minimum. Deze versterkte Nijlafvoer wordt weer veroorzaakt door een sterkere Afrikaanse zomermoesson. De aanvoer van meer zoet water zorgt ervoor dat het oppervlaktewater van de Middellandse Zee lichter wordt waardoor het niet meer naar de bodem zinkt en de vorming van diep water stopt.

Alhoewel de afzetting van sapropelen een robuust signaal is en duidelijke cycli laat zien, zijn er nog veel onzekerheden. Enkele van deze onzekerheden zijn in dit proefschrift onderzocht:

1. Als de vorming van sapropelen wordt bepaald door de sterkte van de Afrikaanse moesson via de afvoer van de Nijl, dan moet de Afrikaanse moesson beïnvloed worden door obliquiteit. Immers, de sapropel patronen laten ook de invloed van obliquiteit zien (Figuur 3). Op het eerste gezicht is dit niet logisch want obliquiteit beïnvloedt de instraling op lage breedtes nauwelijks. De eerste vraag is dus hoe het astronomisch gestuurde signaal in de Afrikaanse zomermoesson eruit ziet. Een specifieke vraag



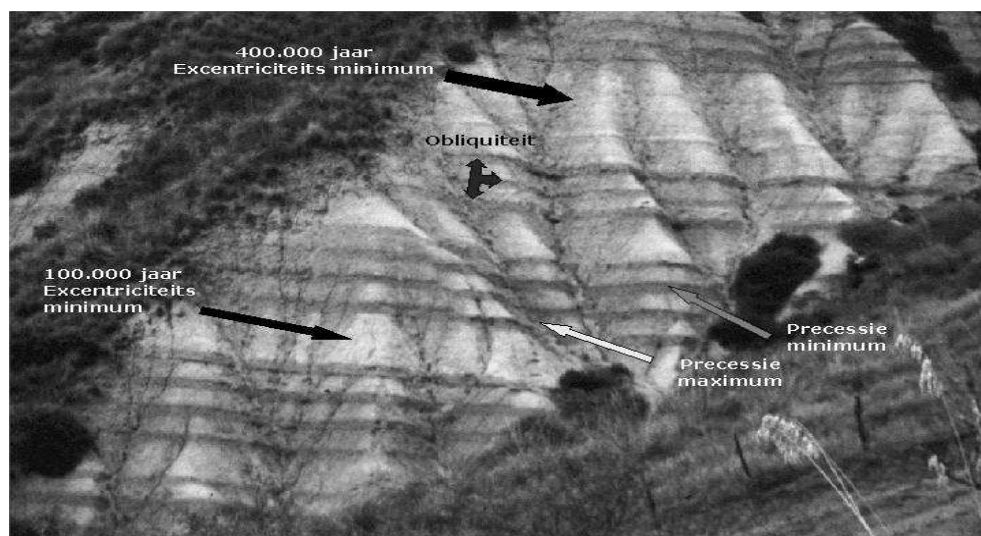
Figuur 2: De hoeveelheid binnenkomende zonne-instraling (in  $\text{Watt/m}^2$ ) aan de top van de atmosfeer gemiddeld over juni, juli en augustus (figuur a) en over december, januari en februari (figuur b). De instraling wordt per breedtegraad getoond (vertikale as). De lijnen met de open vierkantjes gelden voor een precessie minimum, de lijnen met de dichte vierkantjes gelden voor een precessie maximum, de lijnen met de open bolletjes gelden voor een obliquiteit maximum en de lijnen met de dichte bolletjes voor een obliquiteit minimum. De schalen op de horizontale assen zijn niet gelijk.

daarbij is of obliquiteit de intensiteit van de Afrikaanse moesson beïnvloedt.

2. Met nauwkeurige dateringsmethoden is gebleken dat de jongste sapropel (die ongeveer 10.000 jaar geleden is gevormd) zo'n 3000 jaar na het laatste precessie minimum is afgezet. Het is niet duidelijk of alle sapropelen achterlopen of dat de laatste sapropel een uitzondering is en dat de andere sapropelen wel in fase lopen met precessie. Dit geeft aanleiding tot de tweede vraag: kunnen er faseverschillen voorkomen tussen de astronomische forcering en veranderingen in het klimaat?

3. De Nijl is niet de enige rivier die uitmondt in de Middellandse Zee. Vanaf het noorden wordt zoet water aangevoerd door verschillende rivieren dat ook belangrijk zou kunnen zijn voor de vorming van sapropelen. De derde vraag is dan ook: hoe ziet het astronomisch gestuurde signaal in het Atlantisch/Europees gebied er uit?

4. Wanneer de astronomisch gestuurde signalen in het klimaat rondom en boven de Middellandse Zee bekend zijn, is het nog steeds niet duidelijk hoe de circulatie in de Middellandse Zee daarop reageert. De vierde vraag luidt dan ook: hoe reageert



Figuur 3. *Sapropelen op Sicilië (Italië) die ruim 9 miljoen jaar geleden zijn gevormd op de bodem van de Middellandse Zee.*

de circulatie in de Middellandse Zee op de astronomisch gestuurde veranderingen in rivierafvoer, neerslag en verdamping?

Voor het beantwoorden van de vragen 1-3 zijn in dit proefschrift verschillende 3-dimensionale klimaatmodellen gebruikt. Deze modellen hebben een atmosfeer, een oceaan, zeeijs en soms een vegetatiemodel en ze kunnen het klimaat over de hele wereld berekenen. Ze hebben een lage resolutie wat wil zeggen dat het aardoppervlak in grote stukken van typisch 500 bij 500 kilometer of zelfs nog groter wordt verdeeld. Voor elk stuk berekent het model dan verschillende klimaatvariabelen zoals temperatuur, neerslag en circulatie. Voor de circulatie in de Middellandse Zee is zo'n resolutie veel te laag omdat de circulatie voor een groot deel bestaat uit kleine wervels die niet kunnen worden opgelost door deze klimaatmodellen. Daarom is voor de beantwoording van vraag 4 een model van de Middellandse Zee met een hoge resolutie (ongeveer 25 bij 25 kilometer) gebruikt.

Vraag 1 komt in **hoofdstuk 2** van dit proefschrift aan bod. Met het klimaatmodel ECBilt zijn zowel het precessie- als het obliquiteitssignaal gemodelleerd. Voor het precessiesignaal is dit gedaan door twee modelsimulaties uit te voeren: een simulatie voor een precessie minimum en een simulatie voor een precessie maximum waarbij de waarde van precessie niet verandert tijdens de simulaties. Voor deze precessiesimulaties hebben we dezelfde obliquiteit gebruikt. Voor het obliquiteitssignaal hebben we simulaties voor een obliquiteit maximum en een obliquiteit minimum uitgevoerd met een constante precessie. Op deze manier worden het obliquiteitssignaal en het precessiesignaal gescheiden. De resultaten laten zien dat de Afrikaanse moesson zowel door precessie als door obliquiteit wordt beïnvloed. Zowel tijdens een precessie

minimum als een obliquiteit maximum is de Afrikaanse moesson sterker en schuift de neerslag verder naar het noorden dan tijdens respectievelijk een precessie maximum en een obliquiteit minimum. We vinden dus toch een obliquiteitssignaal in de Afrikaanse moesson, ondanks het zwakke obliquiteitssignaal in de instraling op lage breedtes. Dit doet vermoeden dat de Afrikaanse moesson voor een deel wordt gecontroleerd door instralingveranderingen op hogere breedtes die wel door obliquiteit worden beïnvloed. Extra simulaties laten inderdaad zien dat het astronomisch gestuurde signaal in de Afrikaanse moesson gesplitst kan worden in een lokaal geforceerd signaal (d.w.z. door instralingveranderingen ten zuiden van  $30^\circ\text{N}$ ) en een op afstand geforceerd signaal (d.w.z. door instralingveranderingen ten noorden van  $30^\circ\text{N}$ ). Het lokaal geforceerde signaal veroorzaakt een sterke verwarming van de lucht boven land, terwijl de lucht boven de oceaan veel minder sterk opwarmt. Dit contrast in temperatuur veroorzaakt een groot luchtdrukverschil tussen land en oceaan met de laagste druk boven land. Hierdoor komt er een sterke stroming van de oceaan naar het land op gang die veel vocht naar het land transporteert. Boven land regent het vocht uit wat resulteert in een sterke moesson. Het op afstand geforceerde signaal kan verklaard worden door 2 mechanismen. Het eerste mechanisme is het opwarmen van het Aziatisch continent. Hierdoor ontstaat een sterk lagedrukgebied boven Azië waardoor er sterkere winden vanaf de Atlantische Oceaan over het Afrikaanse moessongebied naar Azië ontstaan. Net als bij het lokale signaal brengen deze winden veel vocht naar het moessongebied wat leidt tot een sterkere Afrikaanse moesson. Het tweede mechanisme voor het op afstand geforceerde signaal is een toename van het vochttransport vanaf Europa richting Afrika. Dit wordt veroorzaakt door het extra opwarmen van Europa in de zomer. Warme lucht bevat meer vocht en deze extra hoeveelheid vocht wordt naar het moessongebied getransporteerd en regent daar uit. Het op afstand geforceerde signaal laat de invloed van zowel precessie als obliquiteit zien terwijl het lokale signaal uitsluitend door precessie gestuurd wordt omdat, zoals eerder genoemd, obliquiteit de instraling op lage breedtes nauwelijks beïnvloedt.

In **hoofdstuk 3** zijn modelsimulaties beschreven die als doel hebben vraag 2 (faseverschillen tussen de astronomische forcering en het klimaat) te beantwoorden. Om te kijken naar faseverschillen tussen de astronomische forcering en de daarmee samenhangende klimaatveranderingen hebben we zeer lange (130.000 jaar) simulaties uitgevoerd met het klimaatmodel CLIMBER. Dit model is eenvoudiger en heeft een lagere resolutie dan ECBilt waardoor we heel lange simulaties kunnen uitvoeren. Met ECBilt zouden zulke lange simulaties teveel rekentijd kosten. Voor het precessiesignaal hebben we obliquiteit weer vast gehouden en voor het obliquiteitssignaal hebben we precessie niet verandert. Een verschil met de simulaties in hoofdstuk 2 is dat de precessie en obliquiteit niet constant blijven maar ze worden gedurende de simulaties gevarieerd. Bovendien doen we de simulaties voor het precessie- en het obliquiteitssignaal twee keer. Een keer met een vegetatie die niet verandert tijdens de simulatie en een keer met een vegetatiemodel. Dit model berekent aan de hand van de hoeveelheid neerslag en de temperatuur het soort en de hoeveelheid vegetatie. Vegetatie beïnvloedt het klimaat omdat het het albedo (de mate van reflectie) van het aardoppervlak bepaalt en vegetatie versterkt de verdamping. Met deze simulaties kunnen we zien of vegetatie belangrijk is voor het optreden van faseverschillen tussen

de astronomische forcing en de klimaatveranderingen. We zullen ons concentreren op de moesson, de temperatuur op hoge breedtes en de circulatie in de Atlantische Oceaan.

Er zijn faseverschillen tussen de maandelijksse moesson neerslag en precessie. Echter, zowel voor de simulatie met constante vegetatie als voor de simulatie met het vegetatiemodel heffen de maandelijksse faseverschillen elkaar op waardoor de jaarlijkse neerslag van de moesson precies in fase verloopt met precessie. Wat geldt voor de neerslag geldt ook voor de rivierafvoer naar de Middellandse Zee. Er is geen faseverschil tussen de jaarlijkse rivierafvoer en precessie.

De sterkte van de moesson wordt door vegetatie beïnvloedt. De moesson wordt namelijk sterker in de simulatie met variërende vegetatie dan in de simulatie met constante vegetatie. Dit komt omdat de toename van vegetatie het albedo van het aardoppervlak verkleint waardoor er meer zonnestraling geabsorbeerd wordt. Hierdoor wordt het land warmer waardoor het temperatuurverschil tussen land en oceaan groter wordt en de moesson dus sterker. Een tweede effect van de toename van vegetatie is dat de verdamping toeneemt. Het verdampte water regent gedeeltelijk weer uit wat zorgt voor een sterkere moesson.

De wintertemperaturen boven land op hoge noordelijke breedtes lopen zo'n 1000 jaar en 5000 jaar achter op precessie in respectievelijk de simulaties met een vaste en een veranderlijke vegetatie. De faseverschillen tussen de luchttemperaturen in de winter en precessie hebben gevolgen voor de circulatie in de Atlantische Oceaan. In de winter koelt de atmosfeer het oceaanooppervlak sterk af op hoge breedtes waardoor het water zwaarder wordt en zinkt. Deze vorming van diep water is de motor voor de circulatie in de hele Atlantische Oceaan. De faseverschillen tussen de luchttemperaturen in de winter en precessie veroorzaken dezelfde faseverschillen tussen precessie en de sterkte van de circulatie in de Atlantische Oceaan.

Voor het obliquiteitssignaal zijn de hierboven beschreven klimaatvariabelen precies in fase of precies uit fase met obliquiteit. Dit geldt zowel voor de simulatie met constante vegetatie als voor de simulatie met variërende vegetatie.

In **hoofdstuk 4** wordt vraag 3 (astronomisch gestuurde klimaatveranderingen in het Atlantisch/Europees gebied) onderzocht. In dit hoofdstuk wordt dezelfde werkwijze als in hoofdstuk 2 gebruikt maar nu wordt gekeken naar het astronomisch gestuurde signaal boven en rondom Europa. Het blijkt dat het precessie- en obliquiteitssignaal in de neerslag het sterkst zijn in het najaar. Zowel tijdens een precessie minimum als een obliquiteit maximum is de neerslag boven en rondom de Middellandse Zee sterker dan tijdens respectievelijk een precessie maximum en een obliquiteit minimum. Het mechanisme is voor obliquiteit en precessie hetzelfde. Door de sterke instraling tijdens een precessie minimum en een obliquiteit maximum wordt het Middellandse Zeewater sterk opgewarmd in de zomer. In het najaar koelt de lucht boven het water al af, maar doordat water langzamer afkoelt is het water nog relatief warm. Koude lucht boven warm water leidt tot vorming van depressies waardoor de neerslag toeneemt.

Sapropelen zijn niet de enige geologisch data waarmee de modelresultaten vergeleken kunnen worden. In **hoofdstuk 5** wordt een pollen record uit meerafzettingen in Griekenland met een ouderdom van ruim 5 miljoen jaar beschreven. Aan de hand

van het aantal pollen en welke soorten er voorkomen kan iets gezegd worden over de hoeveelheid neerslag. Het blijkt dat er een sterk precessiesignaal in de pollen record aanwezig is. De neerslag tussen oktober en maart is sterker tijdens een precessie minimum dan tijdens een precessie maximum. Dit is in overeenstemming met de sterkere neerslag tijdens het najaar zoals beschreven in hoofdstuk 4. De pollen record is te kort om met zekerheid iets over het obliquiteitssignaal te kunnen zeggen.

In **hoofdstuk 6** wordt vraag 4 (astronomisch gestuurd signaal in de Middellandse Zee) met een circulatiemodel van de Middellandse Zee bestudeerd. Er zijn twee locaties in de Middellandse Zee belangrijk voor vorming van sapropelen omdat daar diep water gevormd wordt. De locaties zijn de Golf van Lyon en de Adriatische Zee die beiden in het noorden van de Middellandse Zee liggen. Uit de modelresultaten beschreven in hoofdstuk 2 en 4 blijkt dat we twee kandidaten hebben die het Middellandse Zeewater zoeter (en dus lichter) kunnen maken en dus diep water vorming kunnen voorkomen. Dit zijn de toename van Nijlafvoer vanaf het zuiden naar de Middellandse Zee en de toename van neerslag in het najaar boven de Middellandse Zee. In hoofdstuk 6 hebben we geprobeerd om te achterhalen welke van deze processen het grootste effect op het zoutgehalte van het oppervlaktewater heeft (en daarmee op de vorming van diep water). Uit de resultaten blijkt dat een grotere Nijl afvoer alleen het water in het uiterste oosten van de Middellandse Zee zoeter maakt. Dit is niet belangrijk voor de vorming van diep water want dat gebeurt in het noorden van de Middellandse Zee. Versterkte (najaars)neerslag maakt bijna het hele bekken zoeter, dus ook op plaatsen waar de vorming van diep water plaats vindt. Versterkte rivierafvoer vanaf het noorden zorgt alleen voor een verzoeting vlakbij de riviermondingen. Deze liggen echter wel vlakbij de plaatsen waar diep water wordt gevormd en de toename van de rivierafvoer vanaf het noorden kan dus belangrijk zijn voor het stoppen van diepwater vorming.

In **hoofdstuk 7** zijn enkele conclusies getrokken. Er zijn geen faseverschillen tussen obliquiteit/precessie en de jaarlijkse Afrikaanse moesson neerslag gevonden. Het is dus niet waarschijnlijk dat het faseverschil tussen de laatste sapropel en precessie veroorzaakt wordt door rivierafvoer vanaf het zuiden. Het zou kunnen dat de laatste sapropel een uitzondering is (door welke oorzaak dan ook) en dat de andere sapropelen wel in fase verlopen met precessie. Het is echter niet uitgesloten dat het mechanisme voor het faseverschil dat gevonden werd tussen de vorming van diep water in de Atlantische Oceaan en precessie ook geldt voor de diep water vorming in de Middellandse Zee.

Simulaties met klimaatmodellen geven aanwijzingen dat de rivierafvoer (zowel van het noorden als vanaf het zuiden) naar de Middellandse Zee en de neerslag (in het najaar) boven de Middellandse Zee sterker is tijdens een precessie minimum dan tijdens een precessie maximum. Simulaties met een Middellandse Zee model laten zien dat de rivierafvoer vanaf het noorden en de neerslag in het najaar effectiever zijn in het verzoeten van de Middellandse Zee rondom de plaatsen waar diepwater wordt gevormd. Al met al kan geconcludeerd worden dat de vorming van sapropelen eerder wordt veroorzaakt door toename van de (najaars)neerslag en rivierafvoer vanaf het noorden en dan door de afvoer van de Nijl. Dit is in tegenstelling tot de meest algemeen geaccepteerde hypothese.

# Dankwoord

Het is een ontzettend cliché en ik heb eigenlijk een hekel aan clichés, maar promoveren doe je niet alleen. Er zijn een heleboel mensen aan wie ik dank ben verschuldigd. Een paar daarvan wil ik speciaal noemen.

Allereerst een van mijn co-promotoren, Nanne Weber. Ondanks dat onze manier van werken niet overeenkomt ('Wanneer ruim je je bureau nou eens op') heb ik onze samenwerking als uitermate plezierig ervaren. Je was altijd enthousiast en zelfs toen je afdelingshoofd werd bleef je veel tijd voor me houden. Ik heb van jou ontzettend veel over modellen en (paleo)klimatologie geleerd en daarvoor ben ik je erg dankbaar. Dan mijn andere co-promotor, Frits Hilgen. Als rasechte 'dataman' heb jij het lef gehad om in het diepe van de modellenwereld te springen. Het kostte veel moeite om elkaars taal te leren spreken ('ik heb die rare commando's van L<sup>A</sup>T<sub>E</sub>X maar weg gehaald') maar je hebt er toch altijd vertrouwen in gehad. Ik wist heel weinig tot niets van geologie maar ik heb veel geleerd van onze discussies, al dan niet onder het genot van een biertje. Frits, dankjewel. Mijn promotor, Johan Meulenkamp, bedank ik voor de vrijheid die hij me steeds heeft gegeven. Je hebt je niet bemoeid met details maar wel de grote lijnen in de gaten gehouden, wat minstens zo belangrijk is.

Gerard van der Schrier wil ik graag bedanken voor de talrijke discussies (wetenschappelijk en niet-wetenschappelijk) en voor de hulp bij (numerieke) problemen. Gerard, jouw aandeel in dit proefschrift is veel groter dan je kunt vermoeden en ik ben dan ook blij dat jij mijn paranimf wilt zijn. Ik dank ook Lucas Lourens voor zijn niet aflatende enthousiasme en belangstelling voor de modelresultaten. Luc, ik heb genoten van onze discussies ondanks (of misschien wel, dankzij) dat we het vaak niet met elkaar eens waren. Ik ben dankbaar voor het vertrouwen dat je in me hebt gesteld en dat jij nu mijn 'baas' bent.

Uiteraard ben ik veel dank verschuldigd aan mijn mede-auteurs, Marloes Kloosterboer - van Hoeve, Paul Meijer en Andrey Ganopolski. Marloes, jouw drang naar kennis over de NAO en de niet aflatende stroom (soms lastige) vragen heb ik altijd zeer gewaardeerd. Je hebt me een beetje wegwijs gemaakt in de pollenwereld en ik ben erg blij met hoofdstuk 5 in mijn proefschrift. Paul, ik ben van mening dat hoofdstuk 6 het proefschrift compleet maakt. Ik ben mij ervan bewust dat ik heel veel druk op je heb gelegd om het hoofdstuk voor de deadline klaar te hebben. Desondanks bleef je altijd enthousiast en geduldig en dat waardeer ik zeer. Ik hoop dat onze samenwerking de komende tijd net zo goed blijft. Andrey, thank you very much for the code of CLIMBER and for your (technical) support. I enjoyed our discussions and the time

I spent with you in Cambridge. I really hope that our collaboration will continue.

Er zijn altijd mensen waarvan het niet meteen duidelijk is dat ze meegeholpen hebben aan het tot stand komen van een proefschrift. Mensen die ooit een proefschrift hebben geschreven weten echter dat zonder hun hulp het proefschrift er nooit gekomen was. Daarom wil ik graag Brigitta, Greet en Marjolein bedanken voor hun hulp. Ondanks mijn steeds terugkerende vragen bleven ze altijd geduldig en behulpzaam wat me erg geholpen heeft. Het KNMI bedank ik voor de geboden faciliteiten tijdens mijn promotie-onderzoek. Ook mijn collega's op het KNMI ben ik dankbaar voor alles wat ze gedaan hebben. Ik heb in ruim vier jaar op het KNMI veel kamergenoten zien komen en gaan. Twee daarvan wil ik graag apart noemen. Thijs, wij zaten in hetzelfde schuifje en ik heb veel van je geleerd over Unix maar ook heel veel lol gehad. Roberto, muito obrigado pela sua ajuda com L<sup>A</sup>T<sub>E</sub>X e o nosso interesse comun pelo Calvin e Hobbes. En dan mijn medepioniers: Erwin, Frank en Julia. Ik heb de (te zeldzame) gesprekken over wetenschap en niet-wetenschap altijd erg leuk gevonden. Dankzij jullie ben ik een rijker mens geworden op het gebied van geologie maar ook op het gebied van muziek.

En dan komt er hier weer een cliché: Er bestaat ook nog een leven naast het promoveren. Met het risico dat ik mensen ga vergeten en daarmee misschien beledigen, wil ik mijn vriendjes en vriendinnetjes graag bedanken om de sapropel-problematiek even uit mijn hoofd te zetten met diepgaande en vooral minder diepgaande E-mails, gesprekken en activiteiten. Bink, Catelijne, Coen, de dames van Protos (nu Majella), Ellen, Gijs, Inge, Jasper, Jose, Laura, Nienke, Robert, Taco en Ylva: Bedankt. Dan zijn daar ook nog Jop, Gosse en Martin. Ondanks dat de beste klaverjasser nog steeds niet is komen bovendrijven, heb ik meestal erg veel plezier gehad tijdens de klaverjasavonden en andere bezigheden. Mijn dank is redelijk.

Als laatste wil ik graag mijn ouders en Lianne bedanken. Ondanks een moeilijke periode bleven ze me steunen en zich interesseren voor mijn werk, ook al was het soms ver van hun bed. Dankzij mijn ouders kon ik überhaupt gaan studeren en ook daar ben ik ze erg dankbaar voor. En dan Astrid, mijn dank en liefde gaan veel verder dan voor het doorlezen van de Engelse en Nederlandse samenvattingen.



# Curriculum Vitae

Erik Tuenter is op 21 februari 1975 geboren te Doetinchem. In deze plaats doorliep hij het VWO op het Ulenhof College waar het diploma werd gehaald in 1993. In hetzelfde jaar begon hij aan de studie meteorologie & fysische oceanografie aan de Universiteit Utrecht. Deze studie was toen nog een bovenbouw studie van natuurkunde. Zijn interesse ging uit naar het klimaat wat onder andere tot uiting kwam in zijn afstudeerproject bij Cor Schuurmans over verschillende aspecten van de Noord Atlantische Oscillatie. Het doctoraaldiploma behaalde hij in februari 1999. Van februari tot november 1999 heeft hij werkcollege gegeven bij de natuurkunde cursus van het James Boswell instituut in Utrecht en gewerkt bij FIDES studiebegeleiding in Baarn. In november 1999 is hij begonnen als promovendus bij de faculteit aardwetenschappen van de Universiteit Utrecht. Het promotiewerk werd verricht in het deelproject 'modeling of astronomically forced variations in (circum-)Mediterranean climate' van het PIONIER-programma 'Late Neogene climate variability in annual to Milankovitch frequency bands. An integrated Mediterranean approach' van Frits Hilgen. Het deelproject was een samenwerking tussen de Universiteit Utrecht en het KNMI. Het onderzoek werd uitgevoerd op de afdeling klimaatvariabiliteit van het KNMI. Het promotiewerk resulteerde in een proefschrift dat u nu onder ogen heeft. Vanaf april 2004 is Erik Tuenter werkzaam als postdoc onderzoeker bij de faculteit Geowetenschappen van de Universiteit Utrecht. Dit postdoc project is een onderdeel van het VIDI-programma 'Milankovitch climate forcing and the Earth's rate of rotation' van Lucas Lourens in samenwerking met Nanne Weber van het KNMI. Dit project is een vervolg op het promotie-onderzoek en wordt weer uitgevoerd op het KNMI.



# Publications

Based on chapter 2:

Tuenter, E., S.L. Weber, F.J. Hilgen and L.J. Lourens, 2003. The response of the African summer monsoon to remote and local forcing due to precession and obliquity. *Global and Planetary Change*, 36: 219-235.

Based on chapter 3:

Tuenter, E., S.L. Weber, F.J. Hilgen, L.J. Lourens and A. Ganopolski. Simulation of climate phase lags in the response to precession and obliquity forcing and the role of vegetation. *Climate Dynamics*, under review.

Based on chapter 4:

Tuenter, E., S.L. Weber, F.J. Hilgen and L.J. Lourens. The influence of precession and obliquity on the Atlantic/European winter climate. In preparation.

Based on chapter 5:

Kloosterboer-van Hove, M.L., H. Visscher, J. Steenbrink and E. Tuenter. Coupling between orbital precession and long-term dynamics in the North Atlantic/European region. Submitted to *Global and Planetary Change*.

Based on chapter 6:

Meijer, P. Th. and E. Tuenter. The effect of precession-induced changes in the Mediterranean freshwater budget on circulation at shallow and intermediate depth. In preparation.

